HELLENIC REPUBLIC
National and Kapodistrian University of Athens

SCHOOL OF SCIENCE

DEPARTMENT OF GEOLOGY AND GEOENVIRONMENT

SEASONAL ASSESSMENT OF CLIMATE CONDITIONS FAVOURING DROUGHT WITH THE USE OF DOWNSCALING METHODS UNDER DIFFERENT EMISSION SCENARIOS FOR GREECE

Ph.D. Thesis

KONSTANTINA POLITI

ATHENS 2023

ΕΛΛΗΝΙΚΗ ΔΗΜΟΚΡΑΤΙΑ
Εθνικόν και Καποδιστριακόν Πανεπιστήμιον Αθηνών

ΣΧΟΛΗ ΘΕΤΙΚΩΝ ΕΠΙΣΤΗΜΩΝ

ΤΜΗΜΑ ΓΕΩΛΟΓΙΑΣ ΚΑΙ ΓΕΩΠΕΡΙΒΑΛΛΟΝΤΟΣ

ΕΠΟΧΙΚΗ ΕΚΤΙΜΗΣΗ ΤΩΝ ΚΛΙΜΑΤΙΚΩΝ ΣΥΝΘΗΚΩΝ ΠΟΥ ΕΥΝΟΟΥΝ ΤΗΝ ΞΗΡΑΣΙΑ ΜΕ ΧΡΗΣΗ ΜΟΝΤΕΛΩΝ ΔΥΝΑΜΙΚΗΣ ΥΠΟΚΛΙΜΑΚΩΣΗΣ ΓΙΑ ΔΙΑΦΟΡΕΤΙΚΑ ΣΕΝΑΡΙΑ ΚΛΙΜΑΤΙΚΗΣ ΑΛΛΑΓΗΣ ΓΙΑ ΤΗΝ ΕΛΛΑΔΑ

Διδακτορική Διατριβή

της

ΚΩΝΣΤΑΝΤΙΝΑΣ ΠΟΛΙΤΗ

ΑΘΗΝΑ 2023

Three Member Advisory Committee

Supervisor: **Panagiotis Nastos**
(Professor, Department of Geology and Geoenvironment, NKUA)

Nikolaos Dalezios
(Professor, University of Thessaly)

Diamando Vlachogiannis
(Senior Researcher, NCSRD)

Seven Member Examination Committee

Supervisor: **Panagiotis Nastos**
(Professor, Department of Geology and Geoenvironment, NKUA)

Diamando Vlachogiannis
(Senior Researcher, NCSRD)

Nikolaos Dalezios
(Professor, University of Thessaly)

Athanasios Sfetsos
(Senior Researcher, NCSRD)

Maria Xatzaki
(Assistant Professor, Department of Geology and Geoenvironment, NKUA)

Konstantinos Eleftheratos
(Associate Professor, Department of Geology and Geoenvironment, NKUA)

Emmanouil Vassilakis
(Associate Professor, Department of Geology and Geoenvironment, NKUA)

Examination date: 16-06-2023

Τριμελής Συμβουλευτική Επιτροπή

Επιβλέπων: **Παναγιώτης Νάστος**
(Καθηγητής, Τμήμα Γεωλογίας και Γεωπεριβάλλοντος, ΕΚΠΑ)

Νικόλαος Δαλέζιος
(Καθηγητής, Πανεπιστήμιο Θεσσαλίας)

Διαμάντω Βλαχογιάννη
(Διευθύντρια Ερευνών, ΕΚΕΦΕ Δημόκριτος)

Επταμελής Εξεταστική Επιτροπή

Επιβλέπων: **Παναγιώτης Νάστος**
(Καθηγητής, Τμήμα Γεωλογίας και Γεωπεριβάλλοντος, ΕΚΠΑ)

Διαμάντω Βλαχογιάννη
(Διευθύντρια Ερευνών, ΕΚΕΦΕ Δημόκριτος)

Νικόλαος Δαλέζιος
(Καθηγητής, Πανεπιστήμιο Θεσσαλίας)

Αθανάσιος Σφέτσος
(Διευθυντής Ερευνών, ΕΚΕΦΕ Δημόκριτος)

Μαρία Χατζάκη
(Επίκουρη Καθηγήτρια, Τμήμα Γεωλογίας και Γεωπεριβάλλοντος, ΕΚΠΑ)

Κωνσταντίνος Ελευθεράτος
(Αναπληρωτής Καθηγητής, Τμήμα Γεωλογίας και Γεωπεριβάλλοντος, ΕΚΠΑ)

Εμμανουήλ Βασιλάκης
(Αναπληρωτής Καθηγητής, Τμήμα Γεωλογίας και Γεωπεριβάλλοντος, ΕΚΠΑ)

Ημερομηνία Προφορικής Εξέτασης: 16-06-2023

Η παρούσα Διδακτορική Διατριβή εκπονήθηκε στον Τομέα Γεωγραφίας και Κλιματολογίας της Σχολής Θετικών Επιστημών του Τμήματος Γεωλογίας και Γεωπεριβάλλοντος. Το ερευνητικό έργο πραγματοποιήθηκε στο Εργαστήριο Περιβαλλοντικών Ερευνών του Ινστιτούτου Πυρηνικών και Ραδιολογικών Επιστημών και Τεχνολογίας, Ενέργειας και Ασφάλειας του Ε.Κ.Ε.Φ.Ε. «Δημόκριτος».

This Thesis was prepared in the Department of Climatology of the School of Sciences in the Faculty of Geology and Geoenvironment. The research project was carried out at the Environmental Research Laboratory of the Institute of Nuclear and Radiological Sciences and Technology, Energy and Safety of the E.K.E.F.E. "Demokritos".

.

Ευχαριστίες

Φτάνοντας αυτός ο μακροχρόνιος στόχος της ολοκλήρωσης του διδακτορικού στο τέλος του θα ήθελα να ευχαριστήσω με όλη μου την καρδιά όλους τους ανθρώπους που με υποστήριξαν. Δεν ήταν καθόλου εύκολο ταξίδι αλλά είχα τους καλύτερους συνοδοιπόρους.

Αρχικά θα ήθελα να ευχαριστήσω θερμά την τριμελή επιτροπή μου, τον κύριο Παναγιώτη Νάστο, την κυρία Διαμάντω Βλαχογιάννη και τον κύριο Νικόλαο Δαλέζιο, για την υποστήριξη, τις ιδέες και την συνεχή καθοδήγηση που προσέφεραν. Θα ήθελα να ευχαριστήσω ιδιαιτέρως τον επιβλέποντα καθηγητή κύριο Παναγιώτη Νάστο για την άριστη συνεργασίας μας, καθοδήγηση και την υποστήριξη του σε όλη την διάρκεια της εκπόνησης της έρευνας.

Στη συνέχεια, θα ήθελα αρχικά να πω ένα μεγάλο ευχαριστώ στην κυρία Διαμάντω Βλαχογιάννη, που με την αμέριστη κατανόηση, υπομονή και καθοδήγηση με βοήθησε στο να μπορέσω να φέρω εις πέρας το στόχο μου, να κάνουμε άριστες δημοσιεύσεις αφού ήταν πάντα η σύμμαχος μου σε κάθε τρόπο βελτίωσης των άρθρων που προετοίμαζα και να μου δίνει αυτοπεποίθηση να συνεχίζω όταν προκύπταν προβληματισμοί. Να ευχαριστήσω φυσικά και τον κύριο Αθανάσιο Σφέτσο όχι μόνο για την καθοδήγηση και τις συμβουλές του άλλα που ήταν η κινητήριος δύναμη της ιδέας και της απόφασης μου να ξεκινήσω διδακτορικό. Θα ήθελα να ευχαριστήσω ξεχωριστά τους συναδέλφους στο εργαστήριο του Δημόκριτου που έχουν δημιουργήσει ένα άριστο εργασιακό ερευνητικό περιβάλλον. Φυσικά να ξεχωρίσω τον κύριο Στέλιο Καρόζη και τον ευχαριστώ πολύ, που με την πολύτιμη βοήθεια του με έβαλε στην λογική του προγραμματισμού και της υπολογιστικής μηχανικής (όσο ήταν εφικτό), στην ολοκλήρωση των προσομοιώσεων με το WRF με επιτυχία, και ήταν πρόθυμος να συζητήσουμε ό,τι πρόβλημα παρουσιαζόταν. Να ευχαριστήσω επιπλέον τον κύριο Νίκο Γούναρη για ένα σημαντικό δημιουργικό απεικονιστικό τμήμα των αποτελεσμάτων στο GIS, καθώς και τον κύριο Γιάννη Καψωμενάκη από την Ακαδημία Αθηνών για τα εισαγωγικά βήματα στον προγραμματισμό με την γλώσσα R.

Special thanks to professors Rita Margarida Antunes de Paula Cardoso and Pedro Suarez from Instituto Dom Luiz of the University de Lisbon, for providing the EC-EARTH global models dataset and sharing their knowledge during my stay in Lisbon for the 15-days training in climate simulation with WRF model. I would also like to thank them for their guidance and their support during those years.

I would also like to kindly acknowledge the Greek Research and Technology Network (GRNET) where this work was supported by computational time granted in the

National High-Performance Computer (HPC) facility ARIS to perform the long-term climate simulations using WRF model under projects ID HRCOG (pr004020) and HRPOG (pr006028).

Ολοκληρώνοντας θα ήθελα ιδιαιτέρως να ευχαριστήσω θερμά τους γονείς μου και κυρίως τον αγαπημένο μου σύζυγο Μίνω και την κόρη μου Κατερίνα που την αμέριστη κατανόηση, υποστήριξη και αγάπη τους συνετέλεσαν ανυπολόγιστα στην ολοκλήρωση αυτής της έρευνας.

Abstract

During the last decades, Greece is experiencing an increasing number of various extreme events such as heat waves, drought, wildfires and floods, with serious environmental and socio-economic impacts, which could be attributed to climate change due to global warming. Focusing on drought problem, several regions of Greece are currently facing severe drought conditions that are affecting agriculture, putting availability of water resources at risk and threatening agriculture production. As the area of Greece is characterized by complex topography and climate variability, the investigation of climate change impact assessment in the topic of drought, requires the existence of historical and projected timeseries of meteorological variables, such as precipitation and temperature at regional or local scales for different future scenarios. In this thesis, the dynamical downscaling technique was selected to perform high resolution climate change projections of drought over Greece, using the Weather Research and Forecasting model (WRF). Historical and future simulations were performed at a spatial resolution of 5 km, to produce downscaled datasets, aiming to capture the complex topographical characteristics of this country. The WRF model was driven by the global model EC-EARTH. However, it was important initially to investigate the capability of the model, to reproduce the long-term climate characteristics, in such a high resolution, for the historical period using reanalysis ERA-Interim data. To obtain reliable historical climate simulations of high spatial resolution, it was mandatory to investigate the WRF model's performance through continuous validation of sensitivity tests for short periods of time to select the optimal setup that best capture the climate of Greece. Thus, a series of preliminary studies were conducted, examining the effect of parent coarse domain resolution (European domain) and seven different combinations of model parameterization schemes on high resolution (5 km) (domain of Greece) and initialization times, on simulation ability during different periods (1-year for 2002 and 5-years 2000-2004), encouraging further evaluation for long historical climate study. Such an approach was computationally intensive but provided valuable insights into the model's behavior and performance. Although, none of the configurations performed clearly better than the others over the study area, regarding surface variables, the key selection was influenced by the effect of precipitation compared to observations provided by the Hellenic National Meteorological Service (HNMS).

Afterward, WRF optimal model configuration was applied for a long-term climatological period driven by ERA-Interim reanalysis and EC-EARTH model, to detect uncertainties associated with RCM or inherited by the GCM. Both WRF outputs were used to quantify the 5 km resolution model performance in a detailed validation effort at various spatial and temporal scales for the minimum and maximum temperatures (TX and TN) and precipitation (PR). These meteorological variables are commonly employed in climate model validation and are the primary parameters for obtaining climate indices for climate assessment impact studies. Overall, the statistical analysis of the results showed evidence of the capability of the WRF model to represent the main characteristics of the climate of Greece, along with their extremes and the climate indices of extremes. Furthermore, downscaled results highlighted the added value of the downscaling methodology compared to reanalysis and global fields to represent the climate characteristics of the study area.

Further to the evaluation of the model performance with reanalysis, high-resolution dynamical downscaling was applied with WRF, driven by the global EC-EARTH for two different future emission scenarios (RCP4.5 and RCP8.5) and two 25-year future time slices (2025–2049 and 2075–2099). The downscaled results aimed to investigate the climate change signal of the regional climate, regarding the mean minimum and maximum temperatures and total precipitation as well as the projected changes on the indices of extremes. The analysis was based on the delta-change approach (Hay et al. 2000), by comparing the future model output to the results of the historical reference period. Model's results projected a noticeable magnitude of warming regarding both temperatures with the most pronounced changes up to 5°C mostly over the eastern parts of the country (TX) and over the western part of the mainland, the Ionian Islands, and in some plains of central and northern mainland and southern Crete (TN) under the RCP8.5 in the far future period. The climate change signal of precipitation revealed a general decrease of the annual precipitation all over the eastern part of the country (with islands included) with the most dramatic reductions (above 40%).

Then, the investigation of drought characteristics in Greece focused on predicted changes in temperature and precipitation using appropriate indicators, which can provide a comprehensive interpretation of drought events. For the determination of spatial and temporal drought characteristics in terms of severity, intensity and duration, model daily outputs datasets were converted to monthly values to compute two drought

indices, the Standardized Precipitation Index (SPI) and the Standardized Precipitation Evapotranspiration Index (SPEI) for the examined period and scenarios. The present study indicated that Greece will face relatively severe drought conditions in the upcoming years. It was found that the drought conditions will be more severe in the lowland areas (plain areas), such as Thessaly, Crete, etc. where all the agricultural activity takes place. This research also revealed a shift of drought in the western parts of the country, by the end of the 21st century, under both scenarios. Moreover, owing to the high spatial resolution used, substantial differences in drought characteristics were found in future projections between areas, highly varying in temporal and spatial terms under the two emission scenarios. It was deduced that the study of drought events is not a straightforward task for areas of complex topography that present climatic variations and the corresponding spatial and temporal characteristics may depend on the choice of the index. Within this context, the produced high resolution projected changes of the present study can serve as a firm and reliable basis for climate change impact assessments based on drought characteristics for the area of Greece.

Περίληψη

Τις τελευταίες δεκαετίες, η Ελλάδα βιώνει έναν αυξανόμενο αριθμό διαφόρων ακραίων γεγονότων, όπως κύματα καύσωνα, ξηρασία, πυρκαγιές και πλημμύρες, με σημαντικές περιβαλλοντικές και κοινωνικοοικονομικές επιπτώσεις, που θα μπορούσαν να αποδοθούν στην κλιματική αλλαγή λόγω της υπερθέρμανση του πλανήτη. Εστιάζοντας στο πρόβλημα της ξηρασίας, αρκετές περιοχές της Ελλάδας αντιμετωπίζουν σήμερα σοβαρές συνθήκες ξηρασίας που επηρεάζουν τη γεωργία, θέτοντας σε κίνδυνο τη διαθεσιμότητα των υδάτινων πόρων και απειλώντας τη γεωργική παραγωγή καθώς και άλλους τομείς. Καθώς η περιοχή της Ελλάδας χαρακτηρίζεται από πολύπλοκη τοπογραφία και μεταβλητότητα του κλίματος, η διερεύνηση της εκτίμησης επιπτώσεων της κλιματικής αλλαγής στο θέμα της ξηρασίας απαιτεί την ύπαρξη ιστορικών και προβλεπόμενων χρονοσειρών μετεωρολογικών μεταβλητών, όπως βροχόπτωση και θερμοκρασίες σε τοπική κλίμακα για διαφορετικά μελλοντικά σενάρια. Σε αυτή την διατριβή, επιλέχθηκε η τεχνική δυναμικής υποκλιμάκωσης για την εκτίμηση των μελλοντικών αλλαγών της ξηρασίας σε υψηλή ανάλυση στην ευάλωτη περιοχή της Ελλάδας, χρησιμοποιώντας το μοντέλο Έρευνας και Πρόβλεψης Καιρού (WRF, Weather Research and Forecasting). Για την παραγωγή δεδομένων, πραγματοποιήθηκαν λοιπόν, ιστορικές και μελλοντικές προσομοιώσεις οριζόντιας χωρικής ανάλυσης 5 km προκειμένου να αποτυπωθούν τα πολύπλοκα τοπογραφικά χαρακτηριστικά αυτής της χώρας. Το μοντέλο WRF, που χρησιμοποιήθηκε ως περιοχικό κλιματικό μοντέλο τροφοδοτήθηκε από το παγκόσμιο μοντέλο EC-EARTH. Ωστόσο, αρχικά ήταν σημαντικό να διερευνηθεί η ικανότητα του μοντέλου να αναπαράγει τα μακροπρόθεσμα χαρακτηριστικά του κλίματος, στην ανάλυση 5 km, για την ιστορική περίοδο χρησιμοποιώντας δεδομένα επανανάλυσης (Reanalysis) ERA-Interim. Για την απόκτηση αξιόπιστων ιστορικών κλιματικών προσομοιώσεων υψηλής χωρικής ανάλυσης, διερευνήθηκε η απόδοση του μοντέλου WRF μέσω συνεχούς επικύρωσης δοκιμών ευαισθησίας για σύντομο χρονικό διάστημα, προκειμένου να επιλεχθεί η βέλτιστη ρύθμιση που αποτυπώνει καλύτερα το κλίμα της Ελλάδας. Έτσι, διεξήχθη μια σειρά προκαταρκτικών μελετών, που εξέτασαν την επίδραση του αρχικού πεδίου (Ευρωπαϊκό πεδίο) και επτά διαφορετικών συνδυασμών σχημάτων παραμετροποίησης μοντέλων σε υψηλή ανάλυση (5 km) (τομέας Ελλάδας) και διαφορετικούς χρόνους αρχικοποίησης, στην ικανότητα προσομοίωσης κλιματικών παραμέτρων, κατά τη διάρκεια διαφορετικές περιόδους (1 έτος για το 2002 και 5ετία

2000-2004). Μια τέτοια προσέγγιση ήταν υπολογιστικά εντατική, αλλά παρείχε πολύτιμες πληροφορίες για τη συμπεριφορά και την απόδοση του μοντέλου, ενθαρρύνοντας περαιτέρω αξιολόγηση για μακροχρόνια ιστορική μελέτη του κλίματος. Παρόλο που καμία από τις διαμορφώσεις δεν απέδωσε σαφώς καλύτερα από τις άλλες στην περιοχή μελέτης, όσον αφορά τις μεταβλητές της επιφάνειας, η βασική επιλογή παραμετροποίησης του μοντέλου επηρεάστηκε κυρίως από την επίδραση της βροχόπτωσης σε σύγκριση με τις παρατηρήσεις της Εθνικής Μετεωρολογικής Υπηρεσίας (ΕΜΥ).

Στη συνέχεια, η διαμόρφωση του βέλτιστου μοντέλου WRF εφαρμόστηκε για μια μακροπρόθεσμη κλιματολογική περίοδο που καθοδηγείται από την ERA-Interim reanalysis και το μοντέλο EC-EARTH, για τη συγκεκριμένη γεωγραφική περιοχή, για τον εντοπισμό αβεβαιοτήτων που σχετίζονται με το RCM ή που κληρονομήθηκαν από το GCM. Τα αποτελέσματα του WRF των δύο ιστορικών προσομοιώσεων, χρησιμοποιήθηκαν για την ποσοτικοποίηση της επίδοσης του μοντέλου ανάλυσης 5 km σε μια λεπτομερή προσπάθεια επαλήθευσης σε διάφορες χωρικές και χρονικές κλίμακες των ελάχιστων και μέγιστων θερμοκρασιών (TX και TN) και της βροχόπτωσης (PR). Αυτές οι μετεωρολογικές μεταβλητές χρησιμοποιούνται συνήθως στην επαλήθευση του κλιματικού μοντέλου και είναι οι κύριες παράμετροι για τη λήψη κλιματικών δεικτών για μελέτες εκτίμησης επιπτώσεων του κλίματος. Συνολικά, η στατιστική ανάλυση των αποτελεσμάτων έδειξε την ικανότητα του μοντέλου WRF να αναπαραστήσει τα κύρια χαρακτηριστικά του κλίματος της Ελλάδας, τις ακραίες τιμές τους και τους κλιματικούς δείκτες των ακραίων. Επιπλέον, τα υψηλής ανάλυσης αποτελέσματα τόνισαν την συμβολή και την προστιθέμενη αξία της μεθοδολογίας δυναμικής υποκλιμάκωσης σε σύγκριση με τα αρχικά δεδομένα των παγκόσμιου μοντέλου reanalysis για την αναπαράσταση των κλιματικών χαρακτηριστικών της περιοχής μελέτης.

Περαιτέρω της αξιολόγησης της επίδοσης του μοντέλου με reanalysis, εφαρμόστηκε δυναμική υποκλιμάκωση υψηλής ανάλυσης με χρήση του WRF, με αρχικές και πλευρικές συνθήκες από το παγκόσμιο EC-EARTH για δύο διαφορετικά μελλοντικά σενάρια εκπομπών (RCP4.5 και RCP8.5) και δύο μελλοντικά χρονικά τμήματα 25 ετών (2025–2049 και 2075–2099). Τα υψηλής ανάλυσης αποτελέσματα αποσκοπούσαν στη διερεύνηση της κλιματικής ανωμαλίας βασικών κλιματικών παραμέτρων, όπως είναι οι μέσες εποχιακές και ετήσιες ελάχιστες και μέγιστες θερμοκρασίες, η συνολική

βροχόπτωση καθώς και οι προβλεπόμενες αλλαγές όσον αφορά στους δείκτες των ακραίων τιμών. Η ανάλυση βασίστηκε στην προσέγγιση μεταβολής δέλτα, συγκρίνοντας τα αποτελέσματα του μελλοντικού μοντέλου με τα αποτελέσματα της ιστορικής περιόδου αναφοράς. Τα αποτελέσματα του μοντέλου προέβλεψαν ένα αξιοσημείωτο μέγεθος θέρμανσης και στις δύο θερμοκρασίες με τις πιο έντονες αλλαγές έως και 5°C κυρίως στα ανατολικά τμήματα της χώρας (ΤΧ) και στο δυτικό τμήμα της ηπειρωτικής χώρας, τα Ιόνια νησιά και σε ορισμένες πεδιάδες κεντρική και βόρεια ηπειρωτική και νότια Κρήτη (ΤΝ) στο πλαίσιο του RCP8.5 στο μακρινό μέλλον. Η μεταβολή των βροχοπτώσεων στο μέλλον λόγω κλιματικής αλλαγής, αποκάλυψε γενική μείωση της ετήσιας βροχόπτωσης με τις πιο δραματικές μειώσεις (πάνω από 40%), σε όλη την ανατολική περιοχή της χώρας (και των νησιών).

Στη συνέχεια, η διερεύνηση των χαρακτηριστικών της ξηρασίας στην Ελλάδα, επικεντρώθηκε στις προβλεπόμενες αλλαγές της θερμοκρασίας και της βροχόπτωσης με την χρήση κατάλληλων δεικτών, οι οποίες μπορούν να παρέχουν μια ολοκληρωμένη ερμηνεία των γεγονότων ξηρασίας. Για τον προσδιορισμό των χαρακτηριστικών ξηρασίας που περιγράφονται από τη σοβαρότητα, την ένταση και τη διάρκεια, τα ημερήσια δεδομένα των προσομοιώσεων μετατράπηκαν σε μηνιαίες τιμές για τον υπολογισμό δύο δεικτών ξηρασίας, του Standardized Precipitation Index (SPI) και του Standardized Precipitation Evapotranspiration Index. (SPEI) για τις εξεταζόμενες περιόδους και τα σενάρια. Γενικότερα, η παρούσα μελέτη έδειξε ότι η Ελλάδα θα αντιμετωπίσει σχετικά σοβαρές συνθήκες ξηρασίας τα επόμενα χρόνια. Διαπιστώθηκε ότι οι συνθήκες ξηρασίας θα είναι πιο έντονες στις πεδινές περιοχές, όπως η Θεσσαλία, η Κρήτη κ.λπ. όπου λαμβάνει χώρα η μέγιστη αγροτική δραστηριότητα. Αυτή η έρευνα αποκάλυψε επίσης μια μετατόπιση της ξηρασίας στις δυτικές περιοχές της χώρας, μέχρι το τέλος του 21ου αιώνα, και στα δύο σενάρια. Επιπλέον, λόγω της υψηλής χωρικής ανάλυσης που χρησιμοποιήθηκε, βρέθηκαν σημαντικές διαφορές στα χαρακτηριστικά της ξηρασίας στο μέλλον, μεταξύ περιοχών, που ποικίλλουν σε μεγάλο βαθμό χωροχρονικά στα δύο σενάρια εκπομπών. Συμπερασματικά, η μελέτη των γεγονότων ξηρασίας δεν είναι μια απλή εργασία, ειδικά για περιοχές που λόγω πολύπλοκων τοπογραφικών χαρακτηριστικών παρουσιάζουν κλιματικές διακυμάνσεις και άρα τα αντίστοιχα χωροχρονικά χαρακτηριστικά τους μπορεί να εξαρτώνται από την επιλογή του δείκτη. Στο πλαίσιο αυτό, οι μελλοντικές αλλαγές υψηλής χωρικής ανάλυσης που παρήχθησαν στην παρούσα διατριβή, μπορούν να χρησιμεύσουν ως σταθερή και

αξιόπιστη βάση δεδομένων για τις εκτιμήσεις επιπτώσεων της κλιματικής αλλαγής με βάση τα χαρακτηριστικά της ξηρασίας για την περιοχή της Ελλάδας.

Contents

ACRONYMS

IPCC	Intergovernmental Panel on Climate Change
SSP	Shared Socioeconomic Pathways
NAO	North Atlantic Oscillation
WGII AR6	Sixth Assessment Report
CMIP	Coupled Model Intercomparison Project
RCM	Regional Climate Model
CORDEX	Coordinated Regional Climate Downscaling Experiment
RCPs	Representative Concentration Pathways
ETCCDI	Expert Team on Climate Change Detection and Indices
SRES	Special Report on Emissions Scenarios
UHI	Urban Heat Island
PET	Physiologically Equivalent Temperature
UTCI	Universal Thermal Climate Index
PSDI	Palmer Drought Severity Index
SPI	Standardized Precipitation Index
RDI	Reconnaissance Drought Index
SPEI	Standardized Precipitation Evapotranspiration Index
AI	Aridity Index
GCM	General Circulation Models
HNMS	Hellenic National Meteorological Service
WRF-ARW	Weather Research and Forecasting Advanced Research
GHG	greenhouse gases
ECMWF	European Centre for Medium Range Forecasts
PBL	planetary boundary layer
ECAD	European Climate Assessment and Data
WRCP	World Climate Research Program
C3S	European Copernicus Climate Change Service
NCEP	National Centers for Environmental Prediction
FAA	Federal Aviation Administration
NCAR	National Center for Atmospheric Research
MMM	Mesoscale and Microscale Meteorology Division
GRIB	Gridded Binary
RRTMG	Rapid Radiative Transfer Model
LSM	land surface model

PET	potential evapotranspiration
LU	Land Use
ERA-Interim	European Re-Analysis
HPC	High Performance Computing
GRNET	Greek Research and Technology Network
HRCOG	High Resolution Climatology Over Greece
HRPOG	High Resolution Projections Over Greece
NCSR	National Center for Scientific Research
POD	Probability of Detection
CSI	Critical Success index
FAR	False alarm ratio
SR	Success ratio
UTC	Coordinated Universal Time
PP	Physics Parameterizations
YSU	Yonsei University
MYJ	Mellor–Yamada–Janjic
TKE	Turbulent Kinetic Energy
WSM-6	WRF single-moment six-class
RMSE	Root Mean Square Error
MAE	Mean Absolute Error
COR	Correlation Coefficient
CRMSE	Centered Root Mean Square Error
PBIAS	Percent Bias
BMJ	Betts-Miller-Janjic
TX	Maximum Temperature
TN	Minimum Temperature
PR	Precipitation
PDF	Probabilities Density Function
NSE	Nash–Sutcliffe model efficiency coefficient
MIA	Modified index of agreement
Q-Q plots	Quantile-quantile plot
WMO	World Meteorological Organization
GWP	Global Water Partnership

LIST OF FIGURES

LIST OF TABLES

Chapter 1 Introduction

This chapter provides a brief overview of the background of climate modelling in the context of global climate warming with the evolution of global and regional models and the benefit of the use of high resolution up to nowadays. Our discussion includes previous research and its limitations on how climate change generally affects the Euro-Mediterranean region and especially the area of Greece focusing on the study of drought. Through the historical review, the need for accurate historical and future climate simulations was highlight at sufficiently high resolution to estimate spatially and in more detail the projective changes of drought and its characteristics in the entire Greek area, which is characterized by complex topography. This effort has never been done before for the whole country in the high resolution of 5 km and is very important for the development of adequate mitigation and adaptation strategies for water management. The deployment of water management strategies is imperative to improve the resilience of society and avoid water scarcity problems, which can cause considerable impacts on the local population well-being and agricultural crops and yields.

1.1 Climate models

General circulation models (GCMs) are the primary numerical tools nowadays to simulate large-scale properties, for the investigation of the response of the climate system to climate change perturbations. On the other hand, the understanding of local effects and their impacts can be directly studied through regional climate models (RCMs), which are able to capture physically consistent regional and local circulations (Leung et al. 2003; Wang et al. 2004; Laprise 2008).

GCMs can be used by climate scientists to study the physical mechanisms of climate, and how these mechanisms are modified due to the increased emissions of Green House Gases (GHG) and pollutants, and other changes in the Earth system like changes in land use, causing the observed climate changes. GCMs are also used extensively for the simulation of future climate projections since the industrial revolution, in view of global climate change for the application of mitigation and adaptation measures. One of the main goals for their use is to study the climatic impacts through extensive

intercomparison exercises. Thus, successive CMIP (Coupled Model Intercomparison Project) initiatives based on GCMs have been able to provide large ensembles that showed some consistent signals over the European region (Cattiaux et al. 2013; Basharin et al. 2015). CMIP3 simulations have preceded with an average grid mesh larger than 2.5° and adopted the Special Report on Emissions Scenarios (SRES) (Nakicenovic et al. 2000), while the CMIP5 (Lionello and Scarascia 2018) simulations employed grids with approximately twice finer resolution than in CMIP3 under different Representative Concentration Pathways (RCPs) (van Vuuren et al. 2011) adopted by the IPCC fifth Assessment Report (AR5) in 2014. The new generation of Earth system models provides the opportunity to assess the latest ensemble (CMIP6) that underpins the 6th Intergovernmental Panel on Climate Change, with much higher climate sensitivity e.g. (Forster et al. 2019) related to the improved representation of clouds and changes in the model physics (Zelinka et al. 2020) following the combined pathways of Shared Socioeconomic Pathway (SSP) and Representative Concentration Pathway (RCP) on climate projections.

However, the coarse resolution of these models of approximately 80 to 300 km prevents detailed analysis of climate change at regional and local scales, such as changes in climate extremes, water resources, and various other elements crucial for future planning (Gutowski Jr et al. 2020). According to (El-Samra et al. 2018) a number of physical mechanisms (e.g. convection, clouds and precipitation, heterogeneity of surface fluxes, and planetary boundary layer (PBL) turbulence) are not accurately represented in the GCMs for the simulation of physically consistent regional and local circulations, particularly for the regions characterized by complex topographical features due to the rather coarse spatial resolution e.g., (Henderson-Sellers et al. 1995; Déqué et al. 2007; Jacob et al. 2014; White et al. 2018; Vergara-Temprado et al. 2020). Comprehensive analysis of regional impacts, therefore, requires higher-resolution climate variables that cannot be obtained directly from coarse-resolution models. In addition, the anthropogenically-induced regional atmospheric circulation changes are not easy to detect using global simulations due to high internal variability and low signal-to-noise ratio (Palmer 2013; Horton et al. 2015; Zhou et al. 2020). Thus, the human-induced dynamic contribution to regional extremes should be assessed by enhancing regional signals using a regional atmospheric model. In late years, downscaling methodologies, such as dynamical downscaling using a regional climate model (RCM), have been proposed to produce the high-resolution climate variables that

are much needed. A recent study on the biases of the GCMs and RCMs indicated that RCMs could help to systematically reduce the biases of the driving GCMs (Sørland et al. 2018). According to Ke et al. (2013), RCMs with high spatial resolution: (1) resolve better physical processes of regional, mesoscale and local scale circulation effects (surface fluxes, breezes, convection, and heavy precipitation) and (2) improve the representation of surface characteristics and their spatial variability in case of the complex topography of the region with mountainous features and rough coastlines.

Additionally, the increase in spatial resolution of RCM simulations over the last decades has resulted in the comprehension of regional climate processes including important ensemble assessments of climate change effects over Europe. Past projects such as the European project Prediction of Regional Scenarios and Uncertainties for Defining European Climate change risks and Effects (PRUDENCE) (Christensen and Christensen 2007; Christensen et al. 2007); and ENSEMBLES (Hewitt 2005) provided regional climate simulations for the region of Europe at rather high resolutions of about 50 km and 25 km, respectively. More recently, through the international CORDEX (Coordinated Regional Climate Downscaling Experiment) initiative, which is a program sponsored by the World Climate Research Program (WRCP) to organize an internationally coordinated framework to produce improved regional climate change projections for all land regions worldwide, the EURO-CORDEX (Jacob et al. 2014; Dosio 2016; Vautard et al. 2021) (http://www.euro-cordex.net/), and MED-CORDEX (Ruti et al. 2016; Colmet-Daage et al. 2018) multi-model ensemble projects have been enhanced as part of the European Copernicus Climate Change Service (C3S), resulting in a high-resolution ensemble of unprecedented size produced higher resolution climate studies of about 12,5 km (0.11°). The latter two, through some meticulous studies on the benefits of increased spatial resolution in model skills of RCMs, have significantly contributed toward our understanding of regional climate processes and their response to climate change (Knist et al. 2016; Bartók et al. 2017; Cavicchia et al. 2018; Colmet-Daage et al. 2018; Lhotka et al. 2018; Coppola et al. 2020; Jacob et al. 2020). CORDEX program used the output of global simulations with RCMs from CMIP5, however, projections of the latest global CMIP6 phase simulations with RCMs remain unavailable at high spatial resolution.

1.1.1 Added value of high resolution.

Regions for which RCM nesting is expected to provide substantial added value are areas characterized by complex topographical features varying at scales smaller than the resolution of GCMs. EURO-CORDEX experiments also included the evaluation of regional models, in which the lateral boundary forcing for the RCMs, was provided by ERA-Interim reanalysis data (Berrisford et al. 2009; Dee et al. 2011), from the European Centre for Medium Range Forecasts (ECMWF) and the National Centers for Environmental Prediction, NCEP/NCAR, (Kalnay et al. 1996). The added value of the 0.11° models becomes even more obvious by better representing surface characteristics (e.g., orography and coastlines) and by more accurately solving the equations of motion (Prein et al. 2016). Statistical analysis of different daily precipitation indices in ensembles of Med-CORDEX and EURO-CORDEX experiments reported that 0.11° simulations show remarkable performance in reproducing the spatial patterns and seasonal cycle of mean precipitation over all regions, with a consistent and marked improvement compared to the 0.44° resolution ensemble and the ERA-Interim reanalysis (Prein et al. 2016; Fantini et al. 2018). In terms of sub-daily scales of a subset of the EUROCORDEX 0.11° ensemble, (Berg et al. 2019) showed that the spatial patterns over Germany were reproduced at least partly at a 12 h duration but not for shorter periods. Yet, in a systematic analysis of climate classifications with GCMs and RCMs, Tapiador et al. (2019) concluded that "the modeling of precipitation remains the Achilles' heel of models and thus of multidimensional indices, which are very sensitive to this variable". However, a high RCM resolution can help reduce model uncertainties, better represent topographic effects, and improve precipitation simulations (Sylla et al. 2010; Cardoso et al. 2013b; Warrach-Sagi et al. 2013; Warscher et al. 2019; Tian et al. 2020) . In addition, due to their enhanced spatial resolution, they are expected to provide added value in the simulation of the frequency distribution of weather events and extremes (Torma et al., 2015). According to Expósito et al. (2015), this fact is especially relevant in climate studies on islands with a complex orography, where regional models should have a resolution of a few kilometers (Zhang et al. 2009, 2012). For example, Pérez et al. (2014) showed that for the Canary Islands, the model resolution should be of at least 5 km resolution to reproduce the observed geographical distribution of temperature and, particularly, of precipitation.

Moreover, several studies reported an improvement in simulated climate variables through the use of high-resolution modeling, such as rainfall amount (Jung 2006; Vigaud et al. 2012; Berg et al. 2013; Prein et al. 2013; Wagner et al. 2013), and precipitation intensity (Frei et al. 2003; Boberg et al. 2010). Olsson et al. 2015 found that using a high resolution (6 km) RCM (RCA3), low-frequency sub-daily extremes were in good agreement with the values found in point observations in Sweden. A similar study for Denmark revealed that RCM simulations at higher spatial resolution (8 km and 12 km) represent extreme precipitation events better and future projections depend on the combination of GCM-RCM, the spatial resolution and the temporal aggregation (Sunyer et al. 2017). Nevertheless, for local scales where the climate is mainly controlled by large-scale external features, the increase in spatial resolution of the RCMs does not improve the simulated results (Giorgi and Gutowski 2015; Pieri et al. 2015). Consequently, the technique of dynamical downscaling constitutes one of the main tools to produce high-resolution climate variables from global simulations, using regional climate models.

1.1.2 Climate change signal in Euro-Mediterranean region

Large parts of Europe, including the region of the Mediterranean basin, are particularly responsive to global climate change (Giorgi 2006). The Mediterranean Basin, located in a transition zone between mid-latitude and subtropical atmospheric circulation regimes, with large topographic gradients, is very sensitive to changes in the global mean climate state. In this context, previous IPCC reports have shown that the Mediterranean region faces a number of climate risks, specially included in the literature published since AR5, such as heat waves, droughts, desertification, wildfire, soil and coastal erosion, and flooding (IPCC 2022). According to this latest report, over the last decades, mean surface temperature has increased more rapidly in the Mediterranean region than the global mean, and temperature extremes (heat waves, peak temperatures) have increased (high confidence). Moreover, although observed trends of precipitation are generally negative (low confidence) and vary strongly between regions and for different seasons, droughts have become more frequent. Recently, the global average temperature has been rising and is projected to increase up to around 2°–5°C by the end of the twenty-first century based on different emissions

scenarios and socio-economic pathways (Shared Socioeconomic Pathways, SSP) (European Environment Information and Observation Network (Eionet) 2022).

Research studies based on the physical processes related to projecting future changes (Giorgi and Lionello 2008; Mariotti and Dell'Aquila 2012; Barcikowska et al. 2018; Lionello and Scarascia 2018) found that the important factors that influence the response of the future regional atmospheric circulation and are responsible for the effect of global warming are the increase of barotropic sea-level pressure (with NAO climate variability) and geopotential height at the 500 hPa level in the central Mediterranean, along with the thermal inertia of the large water mass of the Mediterranean Sea among continents at these latitudes. The increasing anticyclonic circulation over the region would lead to a reduction of precipitation over most parts of the region, and intensification at the sub-regional scale in the northwestern areas. On the other hand, during summer, the circulation change is associated with the intensification of the Azores anticyclone (reduction of weather regimes producing precipitation events in the northern part of the basin) and increased advection of warm dry continental air masses towards the central and eastern Mediterranean. Also, NAO variability associated with high positive values explains (in winter) up to 30% of the decadal precipitation changes in the Mediterranean region.

Focusing on the phenomenon of drought, according to the latest IPCC WGII AR6 report (Ali et al. 2022), climate change is projected to intensify throughout the Mediterranean region and its impacts include longer and/or more intensive droughts that will become in the future more prevalent in many areas. Drought causes a cascade of effects that will affect many different environmental systems in a region, through direct and indirect natural processes (Vicente-Serrano et al. 2020). It is a recurring, inevitable feature of climate that results in serious economic, environmental, and social impacts (Wilhite and Pulwarty 2017). For those reasons, the recognition of drought as a climate hazard is becoming an urgent priority in a warming world (IPCC 2022).

Previous modelling studies on drought projection from the Coupled Model Intercomparison Project (CMIP) of phase three (e.g., CMIP3; (Dai 2011; Orlowsky and Seneviratne 2012) and five (CMIP5; (Christel et al. 2014; Cook et al. 2014; Touma et al. 2015; Polade et al. 2017; Ukkola et al. 2018; Sharafati et al. 2020; Salman et al. 2021)) revealed similar results, in which droughts were more frequent and severe in the 21st century over identified drought hotspots like the Mediterranean basin and some adjacent areas. In the global scale study of Li et al. (2021), the results indicate that the

magnitude and extent of droughts are projected to increase significantly with increasing SSPs and warming in some regions of the world by the late 21st century.

At the regional scale, several studies (Ozturk et al. 2015; Marcos et al. 2017; Daliakopoulos et al. 2017; Turkes et al. 2020; Spinoni et al. 2020) agree on the increase in droughts over the past decades and on projected increases in the duration and intensity of droughts for most parts of the Mediterranean basin, based on future climate scenarios. The latest emission scenarios RCP4.5 and RCP8.5 simulations within the CORDEX initiative indicate a reduced northwards shift of Mediterranean drying evolution and slightly stronger mean precipitation increases over most of Europe as well as a large decrease in surface water resources mostly during the wet season (Tramblay et al. 2013; Jacob et al. 2014). Mathbout et al. (2021) emphasized that droughts are not spatially coherent in the Mediterranean basin, demonstrating different spatial patterns even at the regional scale or between eastern and western regions. Drought conditions are established in the southern and eastern regions of the Mediterranean Basin (Nastos et al. 2013a), however, recent studies also report, in high confidence, that the North Mediterranean areas experience more frequent and intense drought events (Ali et al. 2022).

1.2 Greece under climate change

As a northeastern Mediterranean country, Greece is highly vulnerable to the impact of climate change (Barros 2014). Greece is characterized as a semi-arid region, experiencing an increasing number of various extreme events during the last decades that could be attributed to climate change directly or indirectly (e.g., fires, floods, heat waves, dry episodes, etc.). Kostopoulou and Jones (2005) analysed extreme precipitation indices that showed negative trends indicating drier conditions (from 1958 to 2000) for the eastern Mediterranean. Founda et al. (2004) analysed the 105-year (1897–2001) surface air temperature record of the National Observatory of Athens (NOA) revealing a tendency towards warmer years, with significantly warmer summer and spring periods. Yet, the first comprehensive climate impact study was published in 2011 by an interdisciplinary committee set up by the Bank of Greece. According to the findings of this report, based on the two extreme climate change scenarios B2 and A2

of IPCC Working Group III, it is expected that by the end of the 21st century, the decrease in precipitation levels due to anthropogenic factors would range between 5% and roughly 19% countrywide, depending on the scenario, while mean temperature would increase by 3.0ºC to 4.5ºC, respectively. Heavy rainfall is projected to become more frequent in eastern and central Greece and in northwestern Macedonia, while drought would increase for the eastern mainland and northern Crete (Zerefos et al. 2011). Previous studies, that analysed the potential seasonal (winter and summer) future changes in temperature and precipitation conditions over the Greek area, were conducted by Tolika and Zanis (2012), Zanis et al. (2009), during PRUDENCE and ENSEMBLES projects, but in coarse resolution (50 to 25 km, respectively). More specifically, the warming during winter was in the range of about 2.5–4.5 °C and generally, it increased from the coastal areas to the central and northern continental interiors based on the scenarios. The warming was even higher during summer with an increase from 3.5 to 6 °C. A decrease of precipitation was estimated in the study of Zanis et al. (2009), for the future climate for both winter and summer along with the increasing mean temperature for the majority of nine RCMs from PRUDENCE projects for the period 2071–2100 under the A2 emission scenario. These two latest studies also noted that Greece would experience a persisting absence of rainfall. Winters were estimated to be drier by the end of the twenty-first century with a decrease of up to − 30% in southern Greece, while the expected changes of summer precipitation showed a prevailing decrease or rainfall heights up to − 60% with respect to the reference period (mainly in the areas of Peloponnese and the eastern Aegean Sea). Moreover, a high-resolution simulation was carried out with RegCM3 over the period 1960−2100 under the A1B scenario, with 10 km spatial resolution for Greece by Zanis et al. (2015), indicating small changes in the near period and larger by the end of the 21st century for mean temperature and precipitation.

Apart from trends estimation and relative or absolute changes in climate variables, climate change is also estimated based on the calculation of a number of indices. More specifically, to gain a uniform perspective on observed changes in weather and climate extremes, Expert Team on Climate Change Detection and Indices (ETCCDI) has defined a core set of descriptive indices of extremes that describe particular characteristics of extremes and involve the calculation of the number of days in a year exceeding specific thresholds (Tank et al. 2009).

According to Giannakopoulos et al. (2011) for IPCC SRES A1B scenario and during the midcentury period, the largest increases derived from the ENSEMBLES models simulations (0.25deg) were found in 'summer' days (>25°C) and 'tropical' nights (>20°C), while urban areas would face warmer temperatures, which was translated into more days with maximum temperature above 35°C. The increase was also found to be greater in summer maximum temperatures compared with the winter minimum temperatures. Kostopoulou et al. (2014) also estimated that the warmer future of the area would also include a strong increase in the occurrence of tropical nights, summer and hot days and a decrease of frost days and wet days based on the SRES A1B for the late century. Recently, Founda et al. (2019) highlighted the expansion in hot extremes' season by ~3–10 days/decade since the mid-1970s based on observational data for 10 Greek stations along with their projected increase according to EU-CORDEX climate models under RCP8.5. Similarly, Georgoulias et al. (2022) indicated that as a consequence of warming, the number of hot days and tropical nights in a year is projected to increase significantly and the number of frost days to decrease, while the number of consecutive dry days in a year to increase by 15.4 days (30%) under RCP8.5 at the end of the century, as derived from the ensemble of eleven EU-CORDEX climate simulations.

Moreover, recent research studies have contributed to the investigation of different sectors that climate change affects (e.g. forests, land, health, energy), under different RCPs scenarios in Greece, mostly in the country's specific areas, and not necessarily at a high resolution below 12.5 km (EU-CORDEX resolution). For example, a large increase in the future frequency of extremely hot nights was observed in the National Observatory of Athens under all Urban Heat Island (UHI) regimes and climate scenarios for the area of Athens, in the study of van der Schriek et al. (2020) that assessed future variability in summer temperatures under different UHI intensity regimes. With respect to thermal risk in the tourism sector, related studies analyzed the present and future climate-tourism conditions in Milos Island interpreted by the Physiologically Equivalent Temperature (PET) (Nastos and Matzarakis 2019) and Santorini Island, based on the advanced Universal Thermal Climate Index (UTCI) (Katavoutas et al. 2021) using regional climate models. Regarding the energy sector, climate change impacts on wind resources and the wind energy potential in Greece were assessed by Katopodis et al. (2019) and buildings' heating and cooling demand and energy use by Droutsa et al. (2021) derived from regional climate models (RCMs).

(Varela et al. 2020) presented a methodology for the estimation of fire weather indicators of the current fire weather and for the near future applied in touristic areas in Greece, based on (EURO-CORDEX) climate model data under RCP4.5 and RCP8.5. Under the same scenarios, the future thermal feeling, estimated by Kambezidis et al. (2021) showed an insignificant shift in the class of the thermal (dis)comfort index for the 33 locations in Greece as derived from 33 stations and two EURO-CORDEX climate models. Land degradation was also assessed by Kairis et al. (2022) in three representative study sites of Thessaly, based on RCP4.5 and RCP8 from (EURO-CORDEX) climate models, yielding that the desertification risk in the future is expected to increase in comparison to the reference period. In the context of forest fire danger, using the same climate models, Rovithakis et al. (2022) studied the changes in future fire danger conditions for the different regions of Greece using the Canadian fire weather index (FWI), under three RCPs, highlighting the progressively increased fire danger, especially in the southern and eastern regions of Greece in the future, due to the ongoing climate change.

1.2.1 Drought

Referring to drought, considerable drought incidents have been noted during the late 50 years (e.g., 1989-2003, 2007-2008) in Greece and a number of studies have contributed to the assessment of drought conditions in Greece. Dalezios et al. (1991) applied the Palmer Drought Severity Index (PSDI) based on station data, in the central and northern regions of Greece. Severity-duration-frequency (SDF) relationships of droughts and wet periods over Greece for hydroclimatic and agroclimatic design and planning were also developed by Dalezios et al. (2000). Anagnostopoulou et al. (2003) studied the drought phenomenon through the spatiotemporal analysis of the dry spells. Vasiliades et al. (2009) indicated that long persistent droughts over Greece are related to large scale atmospheric circulation patterns, such as the extension of the subtropical anticyclone of the Atlantic (Azores) up to the central Mediterranean, characterized by a high positive anomaly of geopotential height of 500mb over North-Eastern Europe or high positive North Atlantic Oscillation (NAO) index. Tsakiris and Vangelis (2004) presented SPI for characterising drought, while (Livada and Assimakopoulos 2007; Karavitis et al. 2011, 2012; Tsesmelis et al. 2022) used SPI to detect and study important drought events on a spatiotemporal basis based on station data. In addition,

Tsakiris et al. (2007), proposed a new index, as "Reconnaissance Drought Index-RDI" which includes, apart from precipitation, an additional meteorological parameter, the potential evapotranspiration. A few studies have applied statistical analysis to obtain spatiotemporal parameters of drought episodes in Greece (Nastos and Zerefos 2008, 2009). Vangelis et al. (2013) calculated Reconnaissance Drought Index using different PET methods from two reliable meteorological stations in Greece. Paparrizos S et al. (2016) estimated the Aridity Index (AI) for three selected areas in Greece based on local observations data and interpolation methods. Extensively previous studies of Dalezios et al. (2012, 2014, 2017a, 2017b, 2017c, 2018a, 2018b, 2018c, 2021) have also give valuable insights on risk identification of agricultural drought, including assessment of composite drought indices and using remotely sensed information in drought analysis. More recently, Alpanakis et al. (2022), performed drought analysis using satellite-based SPI index for the spatial variability in the region of Thessaly.

Other studies used datasets derived from global or regional models to assess the historical and projected changes in drought. Loukas et al. (2007) examined the changes in spatiotemporal drought characteristics of the Thessaly region using SPI through GCM output and under SRES scenarios. Vasiliades et al. (2009) applied statistical downscaling method in the outputs of the Global Circulation Model for the assessment of climate change on hydrological, agricultural and water resources droughts in Thessaly. Vrochidou et al. (2013b, a) assessed drought in Platis basin and for the island of Crete based on bias-corrected historical and future GCM output data under RCPs scenarios. Nastos et al. (2013b) studied the spatial and temporal variability of the Aridity Index (AI) in Greece, derived from 8 regional models within the ENSEMBLES European Project under SRES A1B, showing that drier conditions are expected to become established in regions of Greece. Anagnostopoulou (2017) showed the projected effects of climate change on meteorological drought in the Greek region using five RCMs from the ENSEMBLES European Project. Paparrizos et al. (2018) estimated projected changes of drought based on SPI using simulated data from the ENSEMBLES European Project for three agricultural areas widespread in Greece. More recently, Georgoulias et al. (2022) studied the consecutive dry days only for the end-of-the-century period under RCP8.5 based on an ensemble of eleven EU-CORDEX models simulations. These simulations under three RCPs, were also used in the study of Mavromatis et al. (2022), for crop-specific temperature- and precipitation-related

indices assessment that showed that the increased heat stress and water deficit are expected to have negative crop impacts.

As it is presented here, a number of studies have contributed to the investigation of drought conditions in Greece to assess the drought dimensions based on meteorological, water supply and demand information, for the estimation and quantification of drought conditions in the country's hydrographic basin or specific areas, but not in the entire country. In high spatial resolution simulations, the more detailed patterns can be related to better-resolved physical processes and characteristics of regional/local circulation effects like surface fluxes, breezes, convection and heavy precipitation. Im et al. (2010) reported that for mountainous regions, even 10 km can be considered a coarse resolution because a higher resolution is needed to provide useful information for input into basin hydrology studies. Therefore, the resolution of 12.5 km (in EU-CORDEX) is still not fine enough to sufficiently resolve mesoscale systems, valley flows and therefore the spatial temperature pattern. In addition, such high spatial resolution simulations are imperative when the topography of the region is rather complex with mountainous features and rough coastlines, because of the improved representation of surface characteristics and their spatial variability (Loukas et al. 2007). The significant impact of orography on the convective precipitation distribution in the mountainous area of the Mediterranean region, as it is mostly affected by lightning and convective precipitation, was also confirmed by Khodayar et al. (2016). Paparrizos et al. (2018) highlighted the importance of the influence of elevation and broadly the topography in the generation of different climatic conditions in different basins which in turn affect the spatial analysis of droughts.

Therefore, taking into account the previously commented considerations and the added value that RCM provides, there has been limited effort to explicitly examine the potential impacts of future climate change on droughts across Greece at higher spatial resolution. More specifically, this presumption is attributed to the use of output data from global models or of the commonly used horizontal resolutions ranges between 50 and 25 km (usually RCMs from ENSEMBLES project), 12.5km from EU-CORDEX or application of interpolation methods with limited stations' numbers. The need for high–resolution climatology - drought analysis studies is highly linked to the geomorphological complexity of the country due to 1) the orographic chain along the central part together with the moisturized air masses coming from the central Mediterranean Sea, 2) the extended coastal zones and numerous scattered islands,

creating an inhomogeneous geographical distribution of climatic variables (rainfall, temperature, etc.). Thus, given the country's vulnerability, the need for updated and reliable information on climate change projections based on more recent IPCC emission scenarios and higher resolution data for the country is profound. As these topographic features influence the local climate characteristics of parts of the country, providing many different climatic variations across it (Eleftheriou et al. 2018), it is imperative to study in higher detail drought characteristics that are expected to vary spatially. Also, the benefit of spatial resolution increase from 12.5 km to 5 km is potentially very useful for climate impact local studies. Taking also into consideration 1) the lack of reliable observational gridded dataset covering the entire country, except that of satellite precipitation data (CHIRPS, Duan et al 2016), which is mandatory for fine resolution studies (1-4 km) in case of convection-permitting models, and 2) computational cost and storage, the high horizontal resolution of 5 km used in our study, produces high-resolution climate information that is computationally affordable and suitable for the climate.

In conclusion, the study of future drought events recommends the use of regional models which are capable of capturing the different processes associated with drought events more precisely at a high-resolution spatial scale.

1.3 Objectives of the thesis

The general scope of the presented research is to investigate the future changes in drought characteristics in Greece due to climate change, at a very high resolution through a regional model and the application of a dynamical downscaling technique. To achieve this, it was also important to establish the following:

- 1) benefits of high-resolution dynamic downscaling at 5 km
    - Quantify the high-resolution model performance regarding the spatial and temporal distribution of three meteorological variables, the minimum temperature, the maximum temperature at 2m, and total precipitation.
    - Evaluate downscaled results and ERA-Interim reanalysis datasets with the historical observations from the HNMS based on statistical metrics.

- Prove/establish the added value of the downscaling methodology regarding the reanalysis fields.

- 2) suitability of WRF under different configurations
  - Examine the performance of the Weather and Forecasting Model (WRF) optimal setup to dynamically downscale the coarse-resolution reanalysis ERA-Interim datasets to the high spatial resolution of 5 km grid over the area of Greece.
  - High-resolution downscaling (5 km) with WRF driven by the GCMEC model for two different future emission scenarios (RCP4.5 and RCP8.5), with 25-year historical data (1980–2004) and two 25-year future time slices (2025–2049 and 2075–2099), to carry out a very detailed assessment of future changes in the minimum and maximum temperatures and the precipitation conditions for the Greek area.
- 3) spatial and temporal change of indicators
  - Assess the spatial and temporal change of climate indices based on ETCCDI for extreme temperatures and precipitation.
  - Assess the spatial and temporal change of drought characteristics (severity, duration, and intensity), which are thoroughly investigated using two drought indices, the Standardized Precipitation Index (SPI) and the Standardized Precipitation Evapotranspiration Index (SPEI) in different timescales (6 and 12 months).

1.4 Research Innovation

The innovation in this work lies in the production and validation of new and reliable high-resolution datasets of climate variables and pertinent indices taking into consideration the complex topography of Greece. Overall, this work aims to provide driving data for impact assessment models that require high spatial details and to study the potential climate risks in a region characterized as a "climate hot spot" in IPCC AR6 (Ali et al. 2022).

The 5 km resolution describes the Greek territory with significantly higher detail than lower resolved RCM simulations, e.g., of the EURO-CORDEX ensemble. Within

its limitations, this work advocates that a specific model setup is suitable for high-resolution climate modeling studies (hindcast and future climate scenario runs) for the domain of Greece as the specific parameterization schemes simulate better the temperature and precipitation fields compared to the rest of the investigated setups. To our knowledge, this is the first time that a comprehensive high-resolution WRF model evaluation effort is presented, based on reanalysis and observational datasets, for this geographical region and long-term, climatological historical and future periods. In addition, the extended high-resolution datasets derived for the region by downscaling EC-EARTH GCM data to 5 km for Greece are unique so far.

By leveraging the added value of the dynamic downscaling process to simulate as accurately as possible the regional climate and future changes in Greece and to achieve an improved characterization of the expected changes in temperature and precipitation as well as their extremes, an important task in view of the pronounced warming projected in the vulnerable to climatic hazards Mediterranean region. These meteorological variables are commonly employed in climate model validation and are useful for obtaining climate indices and studies of climate change impact assessment. The added value of the downscaled main climate variables also provides high confidence to further study spatially the projective changes in ETCCDI indices.

The final motivation of this dissertation lies not only in the aforementioned statements but also in the characterization in high detail of the future drought conditions over the whole area using two drought indices, the SPI and the SPEI in different timescales. In addition, the spatiotemporal changes of drought characteristics, i.e., severity, duration, and intensity, are thoroughly investigated as they could contribute to the coordination of efficient climate change adaptation and mitigation strategies among different sectors/areas for drought risk management.

This document consists of eight chapters, in total. Chapter 2 begins with the description of the developed research methodology and continues with the application of the dynamical downscaling technique, along with the description of the observational datasets for evaluation purposes. It also provides a general description of the Weather and Forecasting (WRF) model and basic model setup. Chapter 3 analyses the investigation of the WRF model configuration through escalating sensitivity experiments for the decision of the optimal model setup. Chapter 4 demonstrates the evaluation of long-term high-resolution historical simulations derived from reanalysis and global datasets by comparison to observations. Chapter 5 presents the derived

results of the future changes in downscaled climate projections. Chapter 6 describes the investigation of the changes in extreme climate indices. Furthermore, the work escalates with the computations of drought indices and the analysis of future projections on drought characteristics along with the concluding remarks which are included in Chapter 7. Finally, Chapter 8 summarises the main key findings and presents future recommendations based on the research performed. this work in Chapter 8.

Chapter 2 Working Methodology and Models description

This chapter includes the description of the working methodology and climate models that are used, along with the development and application of the downscaling methodology to achieve high-resolution climate products for the study area of Greece. Downscaling is a method for obtaining high-resolution climate or climate change information from relatively coarse-resolution global climate models (GCMs). Dynamical downscaling uses a limited-area, high-resolution model (a regional climate model, or RCM) driven by boundary conditions from a GCM to derive smaller-scale climate information. The description also includes details of the study area, the observational and reanalysis datasets, the global circulation and regional models, and the two emission scenarios (RCP 4.5 and 8.5),) and the basic WRF model configuration and parameters that remain consistent during the investigation for the optimal setup.

The investigation of climate change impact assessment studies based on different future scenarios requires projected future timeseries of meteorological variables such as precipitation and temperatures at the regional or local scales. To satisfy the main objective of the thesis, the development and application of the dynamical downscaling technique (Figure 2.1 below) is required using a suitable regional model and input datasets from a global circulation model.

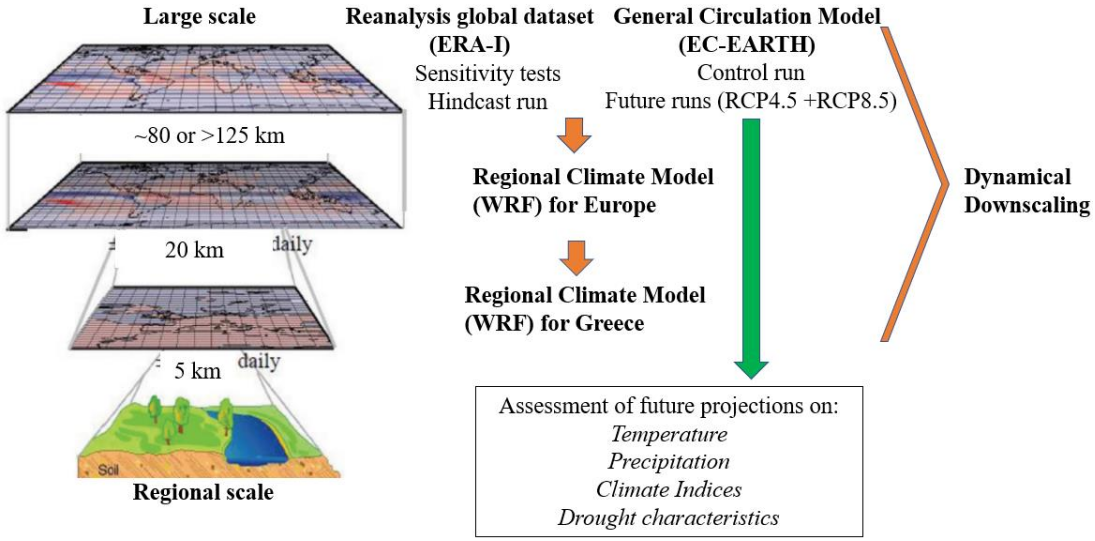

Figure 2.1 Schematic presentation of the dynamical downscaling technique for climate simulations in the area of Greece.

2.1 Working Methodology

For the estimation of projected changes in the study area, it is important initially to investigate the capability of the model to reproduce the long-term climate characteristics, in 5 km resolution, for the historical period using reanalysis and global model data. To obtain reliable historical climate simulations of high spatial resolution, the WRF model's performance was investigate through continuous validation of sensitivity tests for a short period of time in order to select the optimal setup.

WRF model has been developed as a research and operational numerical weather prediction model but is increasingly used as an RCM, because it allows users to choose among a large combination of different configurations, according to the needs of each study. Recent studies, many of these realized in the framework of the CORDEX project, have focused on the performance of the Advanced Research WRF (ARW) model as RCM to represent extreme events of temperature or precipitation, climate indicators, and drought variability at high spatial resolutions. Generally, these studies, with rather fine spatial resolution simulations (10 to 7 km) over Europe, have indicated an improved description of simulation results by accurately reproducing climate features at several time scales, climate patterns, extreme events and drought characteristics as the WRF model allows to easily choose among a large number of physical parameterizations, focusing on country level domains over Europe (Argüeso et al. 2011, 2012; Soares et al. 2012; Berg et al. 2013; Wagner et al. 2013; Cardoso et al. 2013a; Gao et al. 2015; García-Valdecasas Ojeda et al. 2015, 2017; Sun et al. 2016; Prein et al. 2017; Ojrzyńska et al. 2017; Hu et al. 2018; Tian et al. 2020). These studies showed an improved description of temperature spatial and temporal variability and precipitation extremes, due to a better representation of regional processes, related to orographic and coastal forcing. Drought studies also indicated that WRF generally captures reasonably well the drought temporal evolutions with reliable temporal correlations. Komurcu et al. (2018) reported that the improvement obtained with higher resolution dynamical downscaling is dependent on the region simulated and the choice of parameterizations and model setup used in the regional model.

Thus, a series of preliminary studies were performed to examining the effect of parent coarse domain resolution (European domain) and different combinations of model parameterization schemes on high resolution (5 km) (domain of Greece) and initialization times, on simulation ability during different periods, encouraging further

evaluation for this long historical climate study. Such an approach can be computationally intensive, but it can provide valuable insights into the model's behavior and performance. Those research works included firstly sensitivity tests with seven different combinations of physics parameterizations for one year (Politi et al. 2018), examining the performance of the model to simulate surface variables, to select the four best setups, and then sensitivity tests for a period of 5 years with the selected schemes to arrive at the optimal model configuration (Politi et al. 2020). After selecting the best setup, the effects of reinitializing the model were investigated with three different types of time integration approaches for the decision of the final model configuration. The detailed statistical analysis and the results of sensitivity tests are included in Chapter 3.

Afterward, the optimal model configuration was applied, and the model ran for a long-term, climatological period of 30 years, over the period 1980–2010, for the specific geographical region. Then, the WRF output was used to quantify the 5 km resolution model performance in a detailed validation effort at various spatial and temporal scales for the minimum and maximum temperatures (TX and TN) and precipitation (PR). These meteorological variables are commonly employed in climate model validation and are useful for obtaining climate indices and studies of climate change impact assessment. The performed statistical analysis involved the comparison of the results from WRF output of the high-resolution domain, (hereafter WRF_5) and the driver data ERA-Interim (hereafter ERA-I) with the available for Greece observational data.

Further to the evaluation of the model performance with reanalysis, high-resolution dynamical downscaling was applied with WRF, driven by the global EC-EARTH (hereafter GCMEC) model data for the area of Greece and for two different future emission scenarios (RCP4.5 and RCP8.5), with 25-year historical data (1980–2004), as control run, and two 25-year future time slices (2025–2049 and 2075–2099). The downscaled results (hereafter WRFEC) aimed to investigate: (1) the model performance in the historical period compared to observational data; and (2) the projected changes of the regional climate, regarding the mean minimum and maximum temperatures and total precipitation as well as the indices of extremes. For the investigation of drought characteristics, output data were converted to monthly values to compute drought indices of the Standardized Precipitation Index (SPI) and the Standardized Precipitation Evapotranspiration Index (SPEI) for two time periods in the future and under two emission scenarios (RCP4.5 and RCP8.5). Both indices were

calculated over the land grid cells of the nested domain for each grid point and for each time period. In a final step, the analysis was performed to determine the modifications in spatial and temporal drought characteristics in terms of severity, intensity and duration under a changing climate. That approach followed the methodological steps applied in other studies e.g., (Spinoni et al. 2018, 2019; Raymond et al. 2019; Turkes et al. 2020; García-Valdecasas Ojeda et al. 2021)

The working methodology is presented schematically in the Figure 2.2 below:

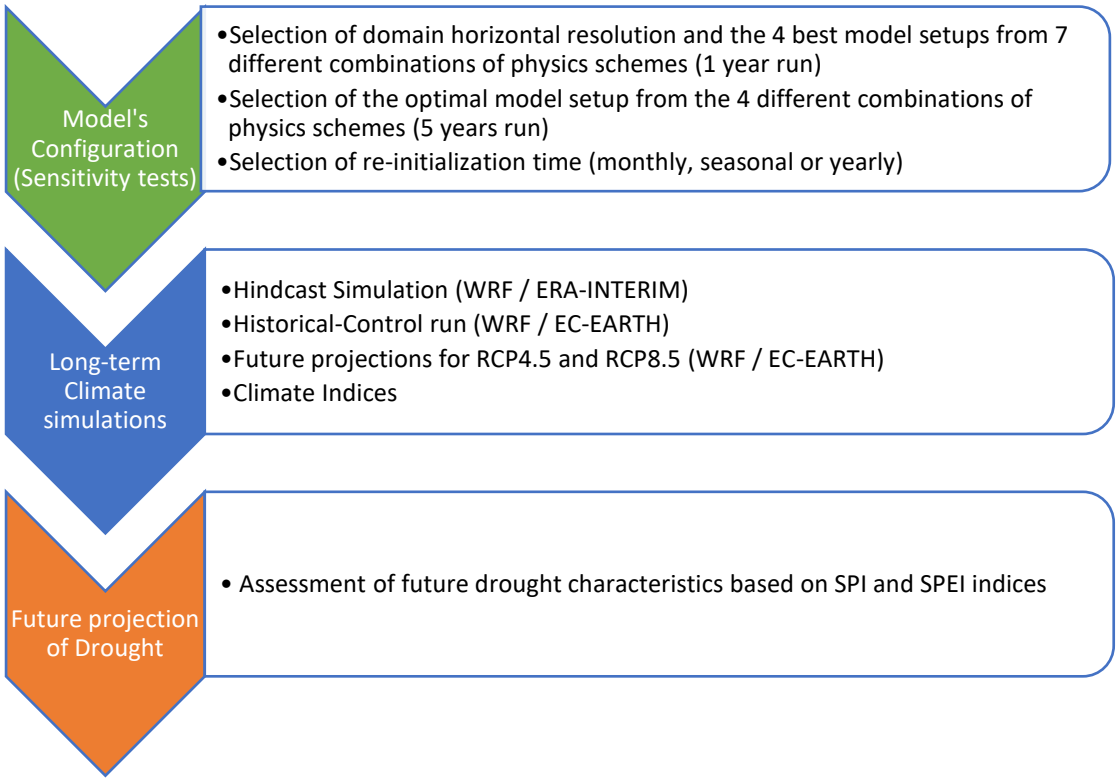

Figure 2.2 Description of the working methodology adopted in this research.

2.2. Study area

Greece is a southern European country in the Mediterranean region, that is bordering the Ionian Sea, the Aegean Sea and the Mediterranean Sea, between 34°00′N to 42°00′N latitude and 19°00′E to 28°30′E longitude. The mainland of Greece and its approximately 1,500 islands extend from the European continent southward to the Mediterranean, Ionian, Cretan, Aegean, and Thracian seas. It is a mostly mountainous country (circa 80%), making Greece one of the most mountainous nations among the European countries, with mountain heights up to 2900 m (Mount Olympus). Greece

includes an extended coastal line (measuring 15,021 km), encompassing many peninsulas and numerous islands.

The climate in Greece is typical of the Mediterranean climate: mild and rainy winters, relatively warm and dry summers and, generally, extended periods of sunshine throughout most of the year. However, a great variety of climate subtypes, always in the Mediterranean climate frame, are encountered in several regions of Greece due to the influence of topography. These topographic features influence some local climate characteristics for each region, as great mountain chains along the central part and other mountainous bodies on the air masses coming from the moisture sources of the central Mediterranean Sea, providing many different climatic variations across the country (Eleftheriou et al. 2018). As a result, the various climatic characteristics and meteorological parameters can alter the local climate, even within a few kilometers' distance (Spyridi, Dimitra, Vlachokostas et al. 2015) in a way that the country presents an inhomogeneous geographical distribution of climatic variables.

2.3 Models and Observational Datasets

For the comparison of model output data against observed data, the present research focused on model evaluation against real points and only validated observations by the formal meteorological organization of Greece, the Hellenic National Meteorological Service (HNMS).

2.3.1 Observational datasets

For the sensitivity experiments analysed in the present chapter, the available observations were examined for continuity and consistency, retaining 28 temperature stations, and 23 precipitation, relative humidity and wind speed stations for evaluation, initially for the selected year 2002 and then for the 5-year period from 2000 to 2004. The datasets were obtained from the https://www.ecad.eu/download/ensembles/download.php) ECA&D station dataset.

Moreover, continuous observations covering the long-term simulations of 30 years, analysed in Chapter 4, were not available due to the lack of formally validated data by HNMS. The HNMS validated temperature dataset covered the period of 1980–2004 with measurements from 32 stations. On the other hand, the HNMS network of 66

stations provided continuous precipitation observations for the period of 1980–2000. The names of the stations and the location are included in the Appendix. Thus, the model assessment was realized during those specific time ranges as dictated by the validated data availability. Figure 2.3 illustrates the spatial distribution of the HNMS stations for a) precipitation and b) minimum and maximum temperatures. The geographical distribution of the available observational stations reveals, also, the limited number of measurements over mountainous, mainland areas that might disrupt the evaluation process over such regions.

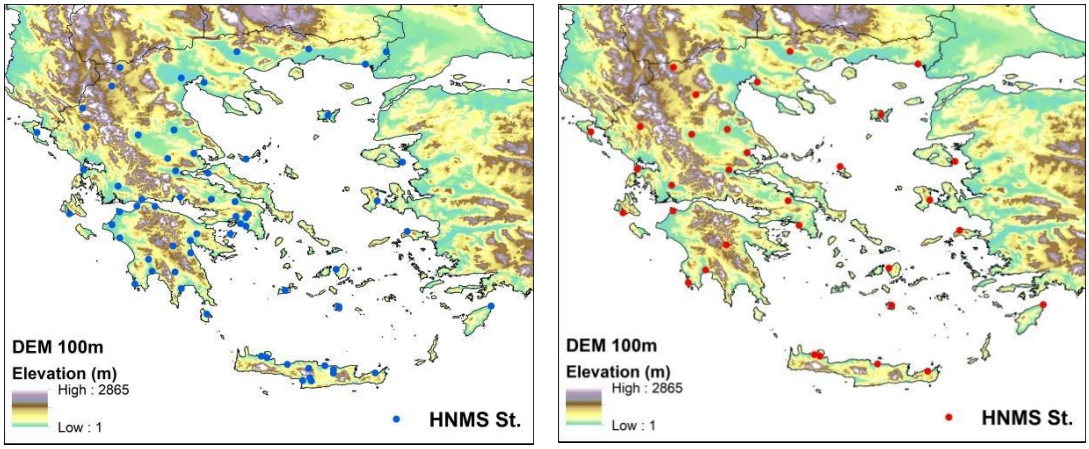

Figure 2.3 The observational stations used for the validation of the model results: a. precipitation (blue dots) and b. temperature (red dots)

2.3.2 EC-EARTH model and RCPs

The selected GCM for this work was the EC-Earth model. EC-Earth is both a model and a consortium that develops and applies the model. EC-Earth is a full physics seamless atmosphere–ocean sea-ice coupled earth system prediction model (Hazeleger et al. 2010) developed from the operational Integrated Forecast System (IFS) cycle 31r of ECMWF. EC-Earth has been developed to a state-of-the-art model system and as such contributed significantly to CMIP5, the model intercomparison project that fed into the 5th IPCC report and more recently in CMIP6 (Vautard et al. 2021). The EC-Earth climate simulations and projections have been widely used for climate studies. In a global scale, (Hazeleger et al. 2010) indicated that the EC-Earth model demonstrates very good forecasting skills from daily up to interannual time scales (interannual variability must be well represented for successful seasonal-to-decadal predictions) and

for the long-term mean climate. (Hazeleger et al. 2013) have shown that the EC-Earth model simulates well the tropospheric fields and the dynamic variables, but not as good the surface temperature and fluxes. Additionally, the EC-Earth model (v2.3) simulates well the Arctic climate according to the study of (Koenigk et al. 2013). More recently, the model was also downscaled to a regional scale in the Framework of Coordinated Regional Downscaling Experiment (CORDEX) over different CORDEX domains at a spatial resolution of 50 km and 12 km e.g., (Jacob et al. 2014; Prein et al. 2016). (Soares et al. 2017; Cardoso et al. 2019) denoted that WRF at 9-km high resolution driven by EC-Earth results were in good agreement with EUROCORDEX and observational data for Portugal.

The set-up of the atmospheric model in the EC-Earth version 2.3 corresponds to the use of a horizontal spectral resolution of T159 (triangular truncation at wavenumber 159), roughly 125 km, and a vertical grid with vertical 62 levels of a terrain-following mixed sigma-pressure hybrid coordinates, of which about 15 are within the planetary boundary layer (PBL) and 1 degree in the ocean with 42 vertical layers. The historical and future projected (RCP4.5 and RCP8.5) datasets used for this study, were already transformed into the appropriate (grib) format which is needed as input in the WRF model.

During the working out of the thesis, four RCPs pathways were used for long-term climate modeling and research for the IPCC Fifth Assessment Report (AR5) in 2014 (IPCC 2014). Note that a Representative Concentration Pathway (RCP) is a greenhouse gas concentration (not emissions) trajectory. The pathways describe different climate futures, all of which are considered possible depending on the volume of greenhouse gases (GHG) emitted in the years to come. The two most frequently RCPs used by almost all modeling groups (as well for the scope of this thesis), are RCP4.5 and RCP8.5. The later RCP8.5, regarded as the most severe scenario, is built on the assumption that the emissions rise throughout the twenty-first century (Riahi et al. 2011) implying at its end a radiative forcing of 8.5 W/m2 relative to the pre-industrial era. On the other hand, RCP4.5 (Clarke L. et al. 2007; Moss et al. 2010) scenario is representing an increase of 4.5 W/m2 in radiative forcing relative to the pre-industrial era. It is a scenario according to which emissions peak around 2049 and stabilize until 2099 by the employment of a range of technologies and strategies for reducing greenhouse gas emissions. By the year 2099, the corresponding RCP4.5 and RCP8.5

greenhouse gas concentrations become equivalent to 650 and more than 1370 parts per million (ppm) carbon dioxide (CO2), respectively, (Moss et al. 2010).

2.3.3 ERA-Interim Reanalysis Datasets

ERA-Interim global reanalysis (Dee et al. 2011) output is used as initial and boundary conditions over limited area domains, in order to obtain high-resolution information to reflect how global patterns influence regional weather conditions. According to Dulière et al. (2011), the reanalysis data can be used for the evaluation of regional models as they sufficiently represent the large-scale forcing necessary for the models to simulate the physical processes and surface interactions. As agreed in CORDEX (Giorgi et al. 2008), ERA-Interim reanalysis dataset has been used as a "perfect" GCM to downscale in the evaluation simulations (García-Díez et al. 2015). The data assimilation system used to produce ERA-Interim is based on a 2006 release of the IFS (Cy31r2). The system includes a 4-dimensional variational analysis (4D-Var) with a 12-hour analysis window. ERA-Interim dataset has a coarse horizontal resolution, around 80 km on 60 vertical levels from the surface up to 0.1 hPa, covering the global atmosphere in a T255 spectral. ERA reanalysis is good enough to reproduce climate conditions on large scale but not sufficient for representing regional or local climate variability, extreme events, particularly in the cases of pronounced topography, complex orography, irregular coastlines and surface heterogeneity. Finally, the ERA-Interim datasets are available from January 1979 to 31 August 2019. Public access to this dataset will be closed on June 1st, 2023. It has been superseded by the ERA5 reanalysis.

It should be mentioned that in this work, the ERA-Interim reanalysis datasets were used instead of ERA-5 for downscaling, since the latter reanalysis dataset covering the total period 1979-near present became publicly available in January 2019, and our work (testing various regional model configurations and validations) had started in 2016. In addition, Rita M. Cardoso and Pedro M. M. Soares from the Insituto Dom Luiz of the University of Lisbon (Portugal) provided us ERA-Interim reanalysis datasets for the entire historical period along with the EC-EARTH model input data for historical and future periods in (grib) format and 6-hour timescale.

2.4 Weather Research and Forecast model (WRF)

This section describes the Weather Research and Forecasting (WRF) Model (Skamarock et al. 2008), the importance of using it as a regional climate model as highlighted in previous studies and how in the current research the model had to be configured to curry out historical and future climate simulations.

2.4.1 WRF model

The (WRF) Model is a state-of-the-art mesoscale numerical weather prediction system designed for both atmospheric research and operational forecasting applications. It features two dynamical cores, a data assimilation system, and a software architecture supporting parallel computation and system extensibility. The model serves a wide range of meteorological applications across scales from tens of meters to thousands of kilometers. The effort to develop WRF began in the latter 1990s and was a collaborative partnership of the National Center for Atmospheric Research (NCAR), the National Oceanic and Atmospheric Administration (represented by the National Centers for Environmental Prediction (NCEP) and the Earth System Research Laboratory), the U.S. Air Force, the Naval Research Laboratory, the University of Oklahoma, and the Federal Aviation Administration (FAA).
For researchers, WRF can produce simulations based on actual atmospheric conditions (i.e., from observations and analyses) or idealized conditions. WRF offers operational forecasting as a flexible and computationally efficient platform while reflecting recent advances in physics, numerics and data assimilation contributed by developers from the expansive research community. WRF is currently in operational use at NCEP and other national meteorological centers as well as in real-time forecasting configurations at laboratories, universities, and companies. The WRF Software Framework (WSF) accommodates two Dynamics solvers:

a. Advanced Research WRF (ARW), and the b. Non hydrostatic Mesoscale Model (NMM).

The Preprocessing System (WPS) (see Figure 2.4) consists of three programs with the purpose of providing input data to the WRF real program for real data simulations (NCAR (National Center for Atmospheric Research) and MMM (Mesoscale and Microscale Meteorology Division) 2016):

1. Geogrid – It defines the simulation domains and interpolates various terrestrial data sets to the model domains.

2. Ungrib – It reads GRIB (Gridded Binary) files, 'degribs' the data, and writes the data in a simple format.

3. Metgrid – It takes the output data from ungrib and horizontally interpolates it to the simulation domains defined by geogrid. The vertical interpolation is performed by the WRF real program.

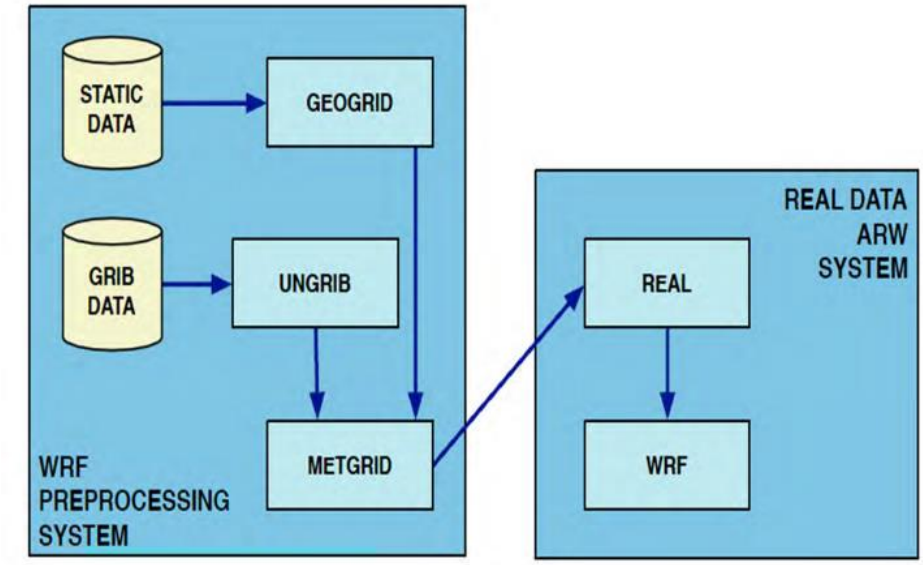

Figure 2.4 Schematic representation of the WRF preprocessing and processing system.

2.4.2 Basic WRF Model setup

As Greece is influenced by many mesoscale and synoptic systems and therefore, in what concerns domain design, which is determining the area of interest, the parent domain has to be large enough to take into account the large-scale dynamical patterns that affect the region of the study. At first, two spatial configurations of the model were composed of two nested grids. The spatial set-up of the first model was at 20 km horizontal resolution outer (parent) domain (Europe) with 265 × 200 grid points and the second at 25 km with 214 × 162 grid points, centered in the Mediterranean basin at 42.5 N and 16.00E. The high-resolution inner (child) domains of each model were set up at 5 km (D02—Greece) of horizontal grid spacing 185 × 185 and 174 × 174 grid points, respectively, named D02(25) and D02(20), according to their coarse domain from where they were produced (Fig 2.5). The set-up of both models has used 40

vertical levels arranged according to terrain-following hydrostatic pressure vertical coordinates, and one-way nesting has been applied to avoid possible noise during feedback from the inner domain to the coarse domain. As the simulations evolve, the internal solution computed by the RCM drifts away from the driving analysis, thus spectral nudging is applied above the PBL and only over the coarse domain. According to Argüeso et al. (2011), spectral nudging reduces the effects of domain location and geometry and prevents any inconsistencies along boundaries over an open system during long-term simulations. The spectral nudging was applied for temperature, winds, and geopotential height but not for humidity. In addition, the simulation was nudged using wave numbers 5 and 4 in the x and y direction, respectively.

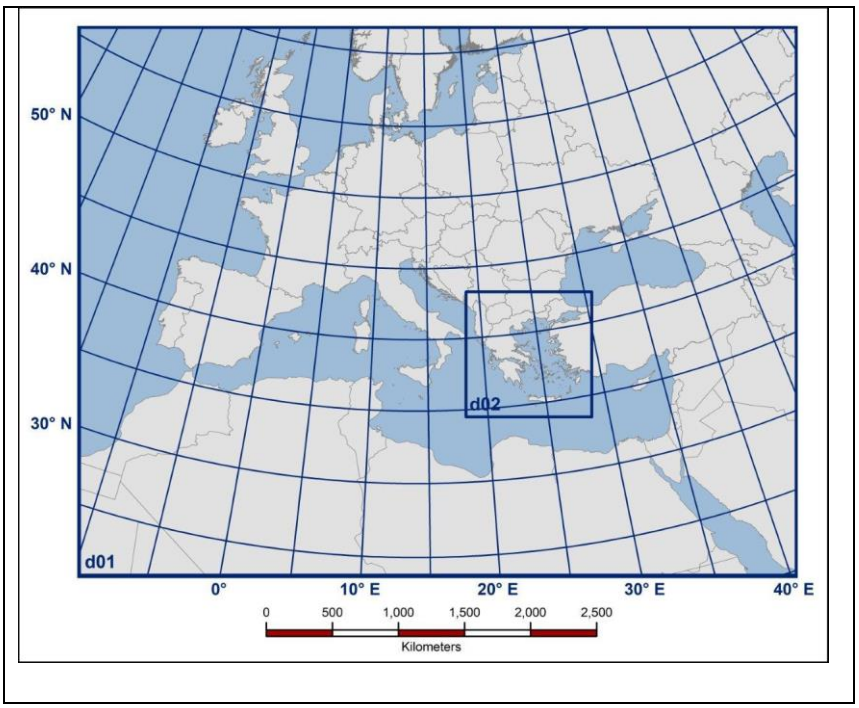

Figure 2.5 Modelling Domains: d01 refers to the outermost domain and d02 to the nested domain of 5 km (region of Greece).

Table 2.1 Model's version, horizontal grid spacing (Δx; in kilometers), initial and boundary conditions, simulation period, number of vertical levels and pressure of the highest level.

Model: ***WRF-ARW Version 3.6.1***	
DOMAINS	**WRF1**
D01(EU)	20km
D02(GR)	5km

Initial and boundary conditions:	*ERA - INTERIM 6hourly reanalysis (~80km)* *EC-EARTH model 6hourly (~125km)*
Vertical levels	*40 sigma levels (up to 50 hPa)*

For each simulation, the last four days of the previous month were regarded as model spin-up for the following month and were discarded, thus the model was re-initialized every month. The frequent re-initialization of the runs retains sufficient long-term forcing, outperforms the continuous simulation runs and distinguishes model errors that develop quickly from those over a long period (Lo et al. 2008; Menendez et al. 2014; García-Díez et al. 2015). However, this way of re-initialization is going to be further investigated in Chapter 3.4.

In what concerns the physics schemes, the radiation scheme was set to the newer version of the Rapid Radiative Transfer Model, RRTMG; (Iacono et al. 2008) for both longwave and shortwave radiation. Only the Noah LSM was employed as the land surface model (LSM), as it is widely adopted for climate studies (Chen et al. 1996, 2001; Zhang et al. 2009). According to Cavan and Hare (2016) the scheme allows the simulation of soil and land surface temperature, snow depth and snow water equivalent, both water and energy fluxes, among others e.g., (Chen et al. 2001; Ek 2003; Feng et al. 2008) . The Noah Scheme has four distinct soil layers (0.1, 0.3, 0.6 and 1.0 m) that reach a total depth of 2 m, and one vegetation canopy layer. For the estimation of potential evapotranspiration (PET), the Penman equation is used, while 16 soil and vegetation parameters are utilized for the estimation of soil temperature, soil moisture, snow cover and atmospheric feedbacks (Evans et al. 2005). Finally, the IGBP Modified MODIS 20-category Land Use Categories was selected as the land use dataset, which should only be used with the WRF Noah land surface model (Wang and Kotamarthi 2015).

For the evaluation and the validation of the WRF model, the European Centre for Medium-Range Weather Forecasts (ECMWF) Re-Analysis (ERA-Interim) fields of 0.75° × 0.75° horizontal resolution were downscaled to the region of Greece. Thus, the ERA-Interim reanalysis dataset was used to provide initial and boundary conditions. The lateral boundary conditions and the sea surface temperature were both updated every 6 h, from ERA-Interim. Respectively, regarding the historical and future simulations, initial and boundary conditions were provided by the EC-EARTH model.

In addition, for future projections, the equivalent-CO2 concentration was updated every year according to the emission scenario in the WRF simulations.

2.4.3 Computing Resources

The short-term simulations of sensitivity tests were carried out using the WRF model in SLURM Batch system in the HPC infrastructure (18x E3-1271v3 @ 3.6 GHz, GBit ethernet, NFS) of the Environmental Research Laboratory of NCSR "Demokritos", using homemade bash scripts. A one-day simulation run needs approximately 1 hour (55'), so one month (of 35 days) simulation time needs 1.3 days which corresponds to 16 days for one simulation year (12 simulation months). In order to run simultaneously and efficiently in different years, 48 CPUs were used.

The available computer power and resources in our laboratory that summed up to 96 nodes of 3TB RAM (45.5 TFlops) were not enough at all to carry out such kind of simulations. Due to offered limited processing capacity, the work of the long-term climate historical and projection experiments was supported by computational time granted from the Greek Research and Technology Network (GRNET) in Athens, in the National high-performance computing HPC facility (https://hpc.grnet.gr/en/), ARIS, under projects ID HRCOG (pr004020) and HRPOG (pr006028), with the minimum requested number of cores (240), as the optimal solution for the implementation of this research. For the simulations, 80 cores were requested using 4 nodes as each node has 20 cores.

The methodology developed for the deduction of the optimal setup and thus the final model configuration to proceed with long-term climate simulations, is detailed in the following Chapter 3.

Chapter 3 Sensitivity tests and selection of optimal model setup

For the decision of the model setup, it is important to consider many aspects, such as the physics parameterizations, the domain resolution and the re-initialization time. For the determination of the optimal model configuration, different sensitivity tests for shorter and longer periods were conducted to establish high-resolution dynamical downscaling climate simulations over the complex topography of Greece. This chapter includes the description of the methodology and the results derived from each sensitivity test. The objectives of the first sensitivity test concerned the selection of the appropriate horizontal resolution of the first domain (at European scale) through the performance of seven different combination of physics parameterizations of the model at high resolution to simulate surface variables, along with the choice of the four best setups, for one year simulation time. In addition, the second set of sensitivity tests was carried out for a period of 5 years with the four selected schemes to arrive at the optimal configuration for the model setup. In the third set of sensitivity tests, the effects of reinitializing the model with three different types of time integration approaches were examined using the best set-up for the decision of the final model configuration.

The examined parameterization schemes were selected in accordance with the findings of previous studies for climate forecasting applications performed for specific regions in Greece and others in the continent of Europe with the WRF model. Efstathiou et al. (2013) studied the sensitivity of WRF to boundary layer parameterizations in simulating heavy rainfall, and to different parameterizations according to microphysics, boundary layer and convective schemes. Kartsios et al. (2015) and Pytharoulis et al. (2014) worked on the characteristics of convective activity over central Greece, Plexousakis (2013) performed a study of extreme weather events over Greece and Giannaros et al. (2013) tested the urban heat island over Athens as well as the predicting lightning activity in Greece (Giannaros et al. 2016). Matsangouras et al. (2011) made the first attempt to model a tornado event. Considering convection schemes, Sindosi et al. (2012) indicated that for the terrain of the Epirus region, north-west of the country, the activation of a convective parameterization scheme in high resolution appears necessary as the results were considerably improved; except for mountainous areas where results with or without convective schemes were comparable. Similar results were noted by Kotroni and Lagouvardos (2004) and Mazarakis et al. (2009), who

studied summer thunderstorm activity forecasts over the urban area of Athens and convective parameterization during a warm period, respectively. The setup of the WRF model has been applied for operational and seasonal forecasting purposes (Vlachogiannis et al. 2013; Eleftheriadou et al. 2016) in the Environmental Research Laboratory of NCSR Demokritos.

For evaluation purposes, the results derived from the sensitivity tests were compared with the observational data of HNMS, described in the previous chapter, through detailed statistical analysis. As there were no available high-resolution observational gridded datasets, the comparison of the simulations was realized through the closest model grid point of the inner domain to the station e.g., (Zittis et al. 2016; El-Samra et al. 2018)

The results of the model simulations of the sensitivity tests were validated with all available Greek station measurements by utilizing the following statistical metrics shown in **Table 3.1.** according to each sensitivity study. Further information and statistical formulas for statistical metrics are available in APPENDIX.

Table 3.1 Description of statistical tools for the validation process for each sensitivity tests

SENSITIVITY TESTS	STATISTICAL METRICS
SENSITIVITY TEST 1	BIAS (or Pbias), RMSE, MAE (or MAPE), COR, STDE, Taylor Diagrams
SENSITIVITY TEST 2	BIAS (or Pbias), RMSE, MAE (or MAPE), COR, Taylor diagrams Statistical scores of Contingency Table: probability of detection (POD), critical success index (CSI) and false alarm ratio (FAR) for four distinct threshold values of precipitation for low rainfall (>1mm), medium rainfall (>2.5 mm), heavy rainfall (>10 mm) and extremely heavy rainfall days (>20 mm)
SENSITIVITY TEST 3	BIAS (or Pbias), RMSE, MAE (or MAPE), COR Statistical scores of Contingency Table: Probability of detection (POD), success ratio (SR), bias and critical success index (CSI)

The approach to evaluating our model setup and the downscaling methodology included the analysis of coarse resolution original data and the simulated downscaled high resolution datasets. Thereupon, the statistical analysis involved the comparison of the output fields of the inner (nested) domain and driver data ERA-Interim with the

available observational data. WRF downscaled temperatures were converted to daily maximum and minimum variables, derived from the 6-h data simulations. The minimum and maximum temperatures of the ERA-Interim data were derived from the processing of the 00 and 12 UTC forecasts.

Height differences between model topography and stations were observed because of the complexity of the topography and coastlines of the area. Thus, before proceeding with the statistical analysis for temperature, a constant lapse-rate elevation correction of 6°C/km was applied (Barstad et al. 2009; Heikkilä et al. 2011; Soares et al. 2012) to both minimum and maximum temperatures.

3.1. Sensitivity test 1

To obtain reliable climate simulations of high spatial resolution with the future RCP scenarios, a preliminary investigation of the effect of parent coarse domain resolution and different combinations of model parameterization schemes on high resolution (5 km) regional climatology studies were performed over the domain of Greece, downscaling ERA-Interim reanalysis data. The two spatial configurations of the model were composed of two nested grids. The spatial set up of the first model was at 20 km resolution outer (parent) domain (Europe) with 265 × 200 grid points and the second at 25 km with 214 × 162 grid points, centered in the Mediterranean basin at 42.5 N and 16.00E (Fig 3.1c- up). The high-resolution inner (child) domains of each model were set up at 5 km (D02—Greece) of horizontal grid spacing 185 × 185 and 174 × 174 grid points, respectively, named D02(25) and D02(20), according to their coarse domain from where they were produced (Fig 3.1c-down). Fig. 3.1 shows the Greek topography for each of the models' setups in order to highlight the need of the higher spatial resolution due to the irregular terrain and coastline of Greece.

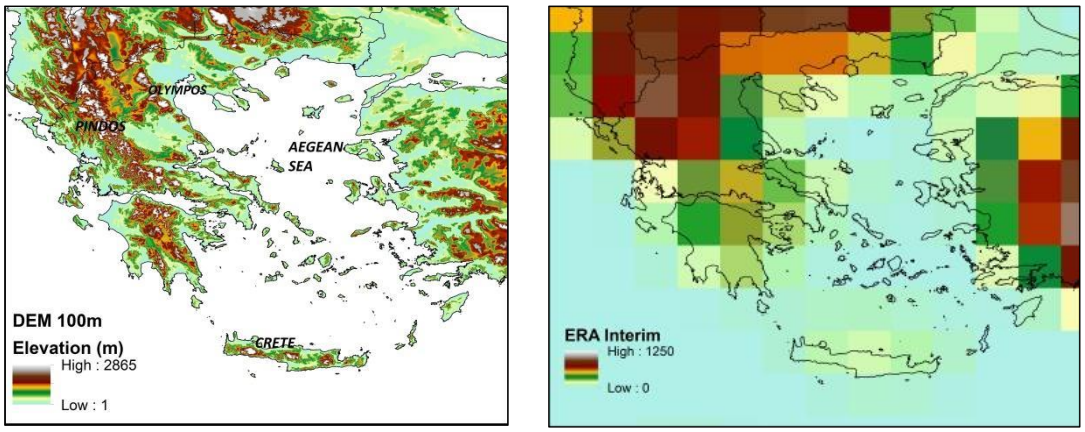

(a) **(b)**

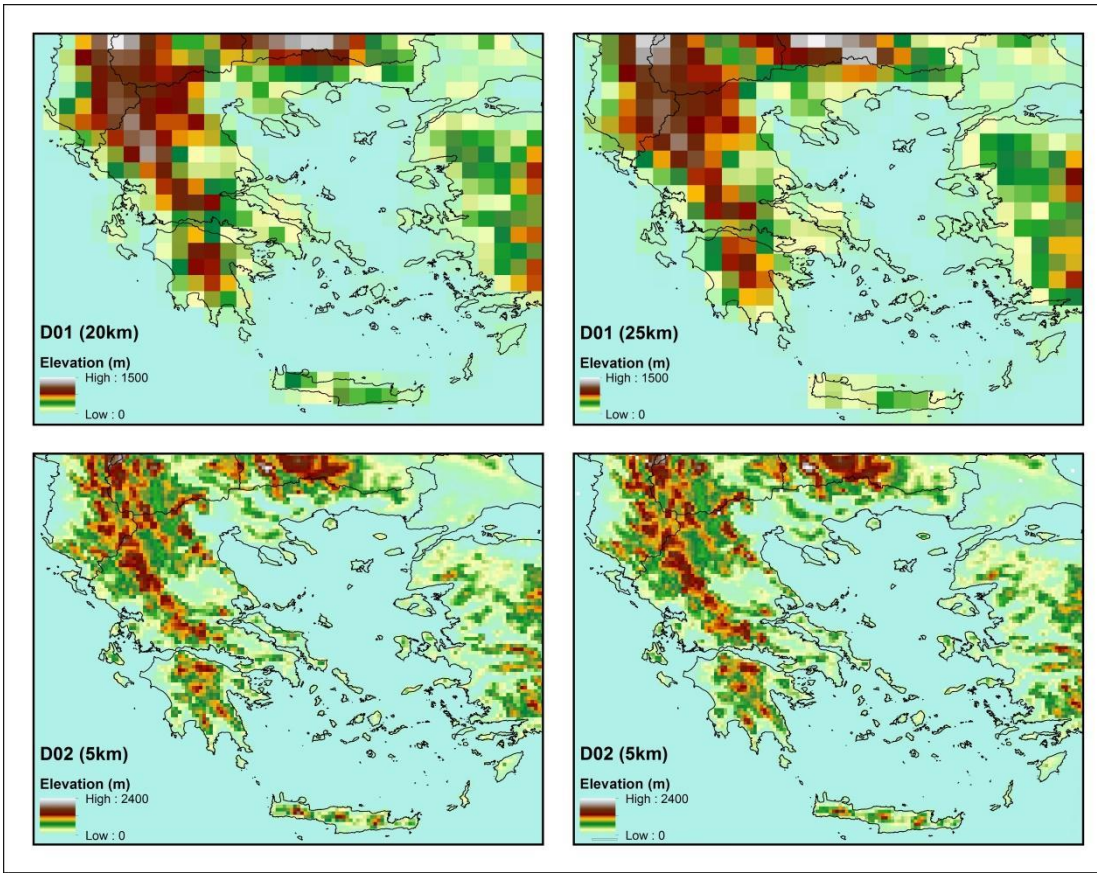

(c)

Figure 3.1 Real topography of the study area for Greece (a) ERA-Interim reanalysis topography (b), and models' topography according to their horizontal resolution for the area of Greece (c).

For the first sensitivity test, the evaluation of the simulation period of the run starts from 0000 UTC January 1, 2002, to 1800 UTC December 31, 2002. This year was selected based on the maximum number of high quality available observational data, uniformly distributed over the country.

Table 3.2 summarizes the way the different physical schemes were combined for each of the seven simulations (PP1, PP2, PP3, PP4, PP5, PP6, and PP7). The cumulus convection scheme controls the sub-grid scale effects of convective clouds. In our study, the following options were mainly used, taking into consideration the gray zone between 5 and 10 km for cumulus option (Skamarock and Dudhia 2011):

- Kain–Fritsch (KF);(Kain and Kain 2004),

- Grell-3D (G3D),

- Grell-Freitas (GF),

- Betts–Miller–Janjic (BMJ); (Janjić 2001) or none in the high-resolution domains.

Table 3.2 Configuration of the Physics Parameterizations (PP) schemes for each of the seven simulations.

D01(EUROPE)							
SIM.ID/ SCHEMES	**PP1**	**PP2**	**PP3**	**PP4**	**PP5**	**PP6**	**PP7**
MP	WSM6	WSM6	WSM6	WSM6	WSM6	WSM6	FE (new Eta)
SFL	MM5	MO	MO	MM5	MM5	MO	MO
PBL	YSU	MYJ	MYJ	YSU	YSU	MYJ	MYJ
CUM	KF	G3D	BMJ	KF	BMJ	GF	G3D
RAD	RRTMG						
LSM	NOAH						
D02(GREECE)							
MP	WSM6	THOM	WSM6	THOM	THOM	WSM6	FE (new Eta)
SFL	MM5	MO	MO	MM5	MM5	MO	MO
PBL	YSU	MYJ	MYJ	YSU	YSU	MYJ	MYJ
CUM	-	G3D	BMJ	KF	BMJ	GF	G3D
RAD	RRTMG						
LSM	NOAH						

Concerning the Planetary Boundary Layer (PBL) schemes, Yonsei University (YSU); (Hong et al. 2006) and Mellor–Yamada–Janjic (MYJ); (Level and Closure 1998) were involved, associated with the corresponding surface layers schemes, which provide the surface fluxes of momentum, moisture and heat to PBL scheme. The MYJ scheme is a local closure model which applies a local approach to determine eddy diffusion coefficients, based on the local turbulent kinetic energy (TKE) equation. No information from lower or higher levels directly influences these terms. In this scheme, the entrainment develops only from local mixing. In contrast, the YSU scheme is a non-local closure scheme, where the critical Richardson number that describes the top of the PBL is set to 0.25 over land for enhancing mixing in the stable boundary layer. In this case, entrainment is explicitly treated.

The three following cloud microphysics schemes were used: WRF single-moment six-class (WSM6) containing ice, snow and graupel processes (Hong and Lim 2006),

Ferrier (FE) and Thompson (THOM), which includes six classes of moisture for ice as prognostic variables (Thompson et al. 2008).

The analysis did involve comparisons of the WRF model simulations with available measurements from the various stations of the inner (nested) domain. To evaluate the WRF downscaling results and model performance, daily statistics are derived from the 6-h data simulations.

Table 3.3 Number of stations according to their location on Dominant IGBP- Modifies 20-category Land Use, for high resolution domains D02(20) and D02(25).

WRF LU CATEGORY		Number of Stations D02(20) /D02(25)	
17	WATER	6	7
21	INLAND LAKES	0	1
12	CROPLANDS	11	10
8	WOODY SAVANNAS	4	3
13	URBAN	4	3
1	EVERGREEN NEEDLEAF FOREST	0	1
7	OPEN SHRUBLANDS	3	3

a) Analysis of the two 5 km domains over Greece

The first analysis involves the investigation of the discrepancies in the characteristics as station/model elevation and land use (LU) category at the locations of the observational stations and the centers of the grid cells between the two high inner resolution domains (D02). Due to the difficult topography and the complexity of the coastlines of the area, height differences between models-stations are observed. As it was noticed in Figure 3.2, overall, 14 stations show a difference in height ranging from 50 m to 240 m, while seven stations present significant differences of 110 m to 240 m in both high resolution domains, at Hellinikon, Samos, Thessaloniki, Tripoli, Milos, Kithira and Tanagra locations. These discrepancies are possible to cause different evolution of observational precipitation totals from model results, and therefore false statistical results. These discrepancies are possible to cause different evolution of precipitation totals from model results, and therefore false statistical results. In total, six stations from D02(20) and eight stations from D02(25) parent domains are the

stations belonging to the grid described as water (id 17) in a percentage of 40% to 83% and 40–100%, respectively. Table 3.3 shows in detail the total number of stations and the LU category of the model in which they are found in the two high resolution domains. Corfu, Heraklion, Methoni, Argostoli, Mitilini, Kithira, Naxos and Ierapetra are some of the weather stations that are located close to the coastal zone, but their model point is characterized by the water LU category. In the following analysis it will be indicated how their position may affect the statistical results.

As it was mentioned in the introduction, dynamical downscaling can add value to the modelling process by using local information through the interaction with mesoscale atmospheric features, particularly in regions with complex topography like Greece. The difference in the elevation between the reanalysis orography of the outer and inner model domains of WRF was quite significant throughout the domain, while an improvement was obtained with the higher resolution as can be deduced from the plotted data in Figure 3.2.

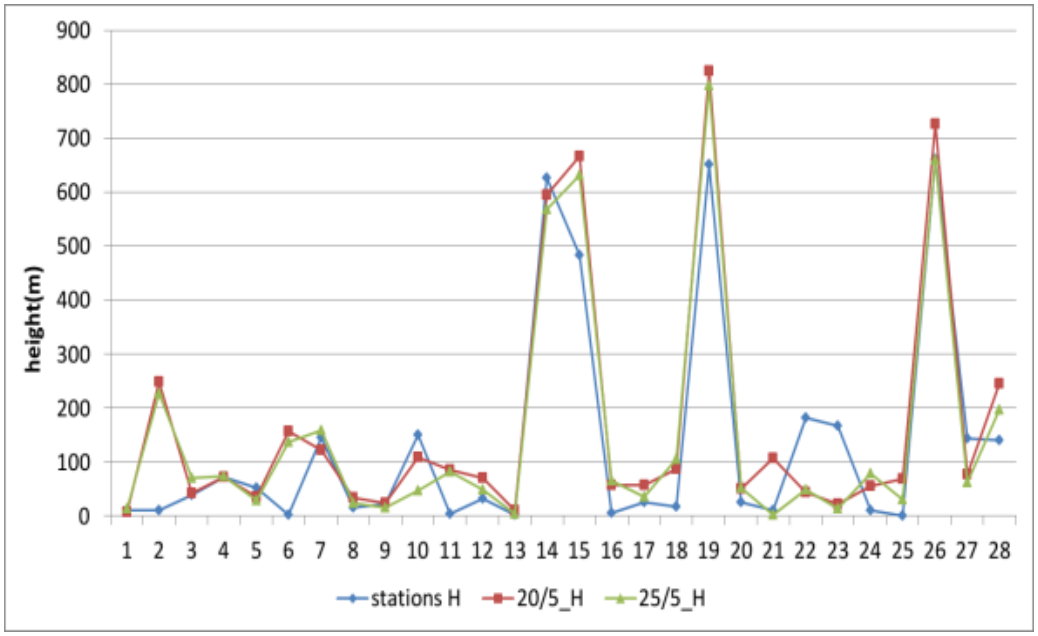

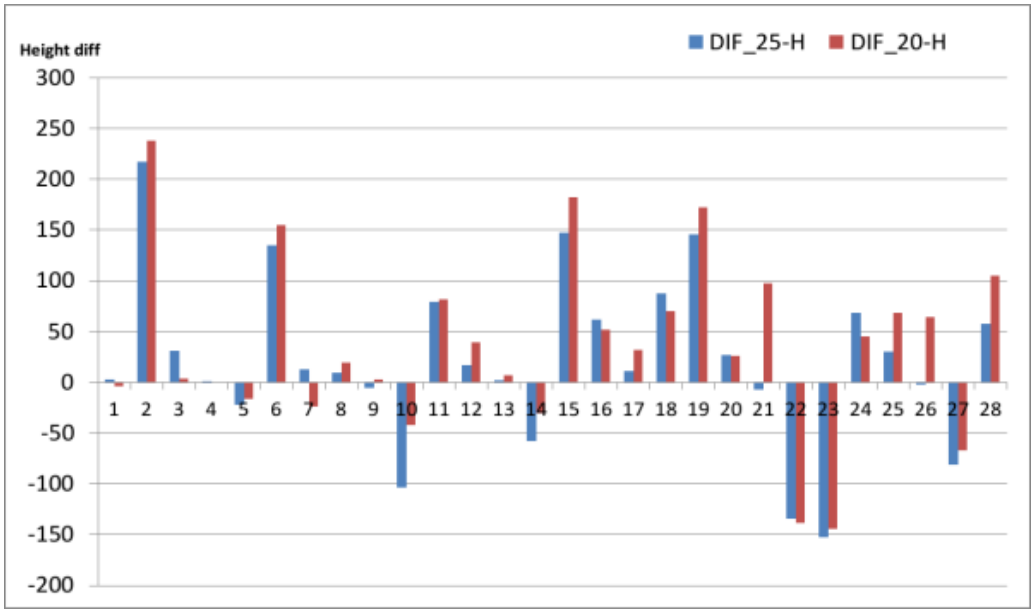

Figure 3.2 Elevation of the models (red – green lines) for high resolutions D02(20), D02(25) respectively and HNMS stations with blue line (left). Height differences between HNMS stations and models (right), for D02(25) on blue bars and D02(20) on red bars.

The resolution elevation of the ERA-I orography improved from the outer to the inner WRF model domains by increasing the spatial resolution. More specifically, as depicted in detail Fig 3.1, the mountains reached in the ERA-I up to 1,250 m of elevation, in the WRF D01 up to 1,500 m, marking a significant deviation from the highest peak of mountain Olympus (of around 2,900 m height), whereas in the higher resolution domain d02, the maximum elevation reached up to 2,400 m. Also, the topography of Pindos, the major mountain range of the country, as well as the higher mountains of the Peloponnese and Crete are resolved very realistically in d02. Similarly, the lower elevation features of the topography (valleys) resolved better in d02. These differences occurred due to the smoothing of the topography caused by the weaker description in the lower resolution domains. According to those findings, the aforementioned improved topography of the study area obtained with D01 and d02 resolutions was not possible to attain with the ERA-I coarse resolution. However, it was further evaluated against observations to derive the degree of agreement between the two datasets in an attempt to quantify the benefit of downscaling the reanalysis dataset.

b) Validation of physics parameterizations over the domain of Greece for D02(25) and D02(20)

3.1.1. Maximum Temperature and Minimum Temperature

The results of minimum and maximum temperatures yield overall small differences not only between the inner domains but also between the seven simulation setups. Figure 3.3 represents the seasonal cycle of the observed and simulated mean daily minimum and maximum values of temperature by month for the total number of grid points. The dashed black lines indicate observational data and colored lines the models' results.

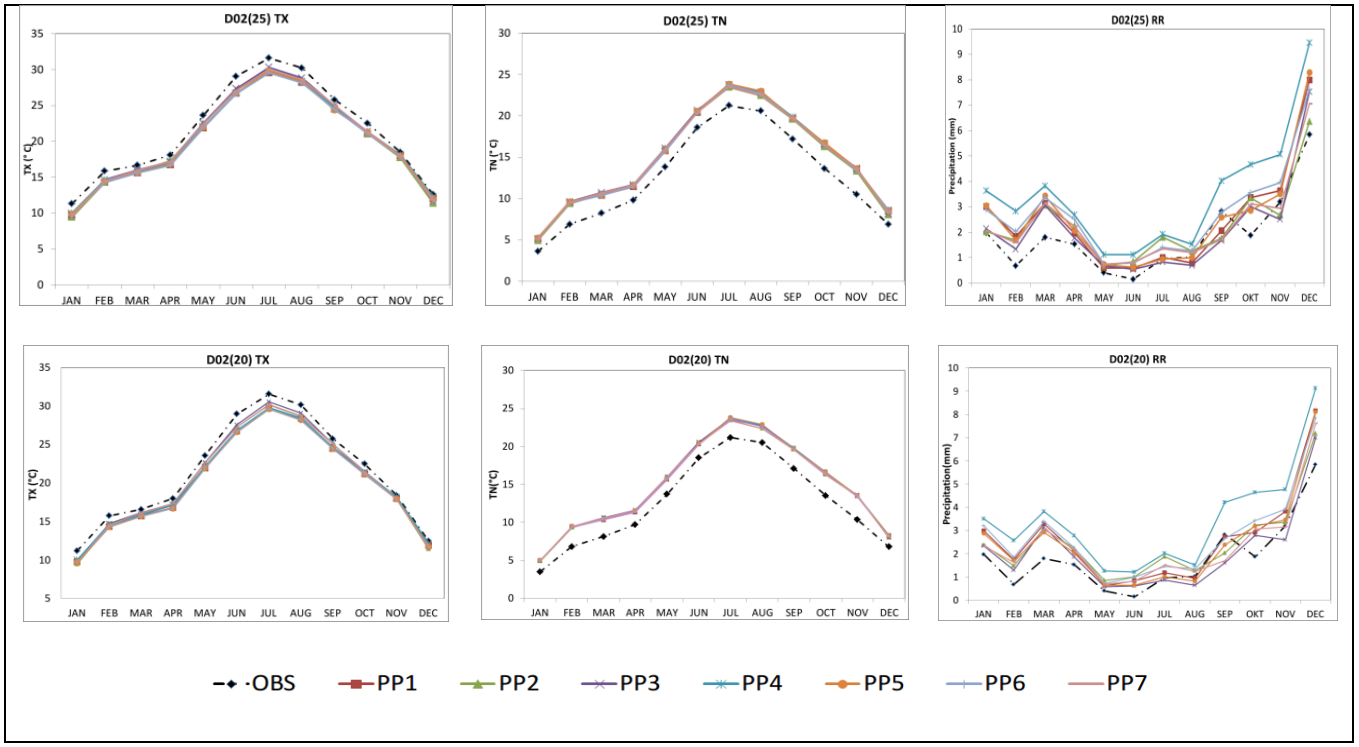

Figure 3.3 Observed and simulated mean daily TX and TN values, on the total grid points by month, for the seven different simulations (PP1, PP2, PP3, PP4, PP5, PP6, PP7), for the high-resolution domains (left and centered). Similarly, daily precipitation values (RR) by month, for 2002 over Greece (on the right)

Similar representation and behavior of temperatures are observed for all physical schemes. There is a consistent overestimation of the minimum temperature TN and slightly consistent underestimation of TX for both inner domains. Table 3.4 summarizes the statistical metrics found in daily values for WRF's high resolution domains derived from the different resolution coarse domains. The correlation coefficients between the observed and the simulated maximum temperature TX are 0.95–0.96 with an overall negative BIAS from −0.92 to −1.33 for D02(20) and −1.1 to −1.5 °C for D02(25), indicating a slightly better performance of the model for the PP3

simulation scheme of D02(20). The RMSE and MAE errors range close to 2–2.5 °C, with similar values found for all simulations. The correlation coefficients of minimum temperature reveal lower values (0.92–0.93) for high resolution domains, for all simulations, a finding in accordance to other studies (Zhang et al. 2009; Soares et al. 2012). The model performs better for TN with the PP2 scheme with positive BIAS near 2 °C for both high resolution domains.

Table 3.4 Statistical metrics of the seven simulations in the total grid points for daily minimum temperature (TN), daily maximum temperature (TX), daily precipitation (RR), daily relative humidity (RH) and daily wind speed (WS) for 2002, over the area of Greece. The best performing configuration for each metric and variable is in bold.

2002	sim ID #	PP1		PP2		PP3		PP4		PP5		PP6		PP7		OBS
		D02(20)	D02(25)	D02(20)	D02(25)	D02(20)	D02(25)	D02(20)	D02(25)	D02(20)	D02(25)	D02(20)	D02(25)	D02(20)	D02(25)	
	BIAS(°C)	-1.33	-1.44	-1.1	-1.32	**-0.92**	**-1.1**	-1.15	-1.26	-1.23	-1.37	-1.4	-1.5	-1.04	-1.21	
	RMSE(°C)	2.53	2.58	2.55	2.58	2.49	**2.50**	**2.45**	**2.50**	2.46	2.52	2.56	2.59	2.52	2.54	
TX	MAE(°C)	2	2.06	1.99	2.05	1.93	**1.96**	**1.92**	1.98	1.93	2	2.03	2.07	1.96	2	**Mean**
	COR	0.96	0.96	0.95	0.96	0.95	0.95	0.96	0.96	0.96	0.96	0.96	0.96	0.95	0.95	21.2
	STDE(°C)	7.15	7.1	**7.43**	7.37	7.5	7.41	7.08	7.03	7.17	7.11	7.13	7.09	7.38	7.3	7.47
	BIAS(°C)	2.16	2.19	**2.14**	**2.08**	2.27	2.29	2.27	2.27	2.28	2.29	2.14	2.16	2.16	2.19	
	RMSE(°C)	3.43	3.4	3.42	**3.32**	3.54	3.51	3.49	3.46	3.52	3.49	3.39	3.37	3.44	3.41	
TN	MAE(°C)	2.71	2.7	**2.67**	**2.6**	2.78	2.78	2.78	2.76	2.79	2.78	2.67	2.68	2.69	2.68	**Mean**
	COR	0.93	0.93	0.93	0.93	0.92	0.93	0.93	0.93	0.93	0.93	0.93	0.93	0.93	0.93	12.5
	STDE(°C)	6.92	6.89	6.84	6.85	6.9	6.89	6.95	6.93	6.95	6.92	6.92	6.89	6.81	6.81	7.01
	pBIAS(%)	40.6	34.4	34.6	24.3	**13.7**	**15.8**	85.6	87.2	33.7	38	48.3	47.3	30.3	25.4	
	RMSE(mm)	8.13	7.8	7.03	6.95	**6.66**	**7.14**	8.27	8.87	7.04	7.36	7.45	7.36	7.07	7.21	
RR	MAE	2.71	2.62	2.57	2.46	**2.26**	**2.28**	3.15	3.24	2.46	2.52	2.7	2.63	2.49	2.48	
	MAPE(%)	75.8	64.3	64.5	45.4	**25.6**	**29.5**	159.8	162.8	62.9	71.0	90.1	88.4	56.5	47.5	**Mean**
	COR	0.39	0.4	0.42	0.42	**0.46**	0.41	0.45	0.42	**0.44**	0.43	0.43	**0.45**	0.43	0.4	1.87
	STDE(mm)	8.02	7.55	6.51	6.34	6.23	6.6	8.63	9.14	**6.77**	7.19	7.25	7.35	6.63	6.59	6.53
	BIAS(%)	-1.47	-0.62	-1.25	-0.08	-1.84	-0.27	-2.11	-1.36	-1.4	-0.52	**-1.2**	-0.3	-1.43	**-0.03**	
	RMSE(%)	12.37	12	13.05	13.2	12.68	12.6	12.47	12.1	**12.1**	**11.7**	12.5	12.03	13.1	13.1	
RH	MAE(%)	9.58	9.3	10.19	10.4	9.86	9.91	9.67	9.36	**9.35**	**9.07**	9.7	9.38	10.21	10.34	**Mean**
	COR	0.61	0.62	0.58	0.57	0.60	0.59	0.60	0.60	**0.62**	**0.63**	0.60	0.61	0.58	0.57	
	STDE(%)	14.42	14.01	14.86	14.92	14.57	14.39	14.08	13.6	14.23	13.74	14.51	**14.05**	14.82	14.72	13.3
	BIAS(m/s)	0.72	0.81	1.16	1.33	1.18	1.19	0.73	0.82	0.71	0.8	**0.7**	**0.79**	1.15	1.17	
	RMSE(m/s)	**2.03**	**2.03**	2.24	2.41	2.26	2.27	2.05	2.04	**2.03**	**2.03**	**2.03**	**2.03**	2.23	2.24	
WS	MAE(m/s)	1.57	1.58	1.76	1.87	1.78	1.79	1.57	1.58	1.57	1.58	**1.56**	1.57	1.76	1.77	**Mean**
	COR	0.63	0.65	**0.64**	0.62	**0.64**	0.64	0.62	**0.65**	0.62	**0.65**	0.63	**0.65**	**0.64**	**0.65**	
	STDE(m/s)	1.91	2	2.11	2.23	2.09	2.12	1.93	2.01	1.91	2	1.93	2.02	2.1	2.13	2.37

Additionally, the analysis of the correlation coefficients of TN for each station (not shown), showed values close to 0.75, while the correlation coefficients of TX appeared to have a more dispersed behavior that varied from 0.5–0.7. An overall performance of the simulations is illustrated in Figure 3.4 by Taylor plots were computed for yearly and seasonal (winter, spring, summer and autumn) time periods of 2002 only for TN, TX and RR. The white circle represents the standard deviation of precipitation station data, while the black circle and black triangle represent the standard deviation of minimum and maximum temperatures station data.

For TX, the results present minute differences during all seasons for both high resolution domains. In particular, in winter, spring and autumn seasons lower RMSE errors (around 2 °C) and better correlations (0.9–0.95) are calculated than in summer period where the RMSE value is around 2.5 °C and the coefficient correlation is equal to 0.8. This probably occurs due to the more intense thermal instability during summer in combination with the fact that some of the model points are not located on land - like the observation stations – but on sea cells. Thus, there is stronger sea-land interaction due to the greater differences in temperature during the summer period.

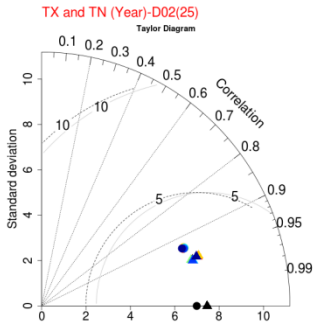

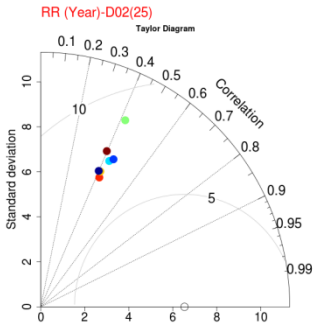

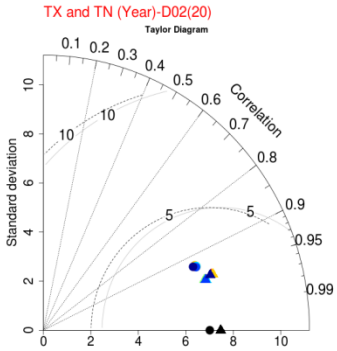

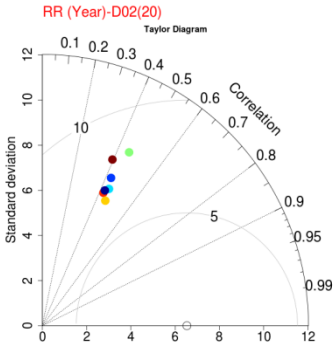

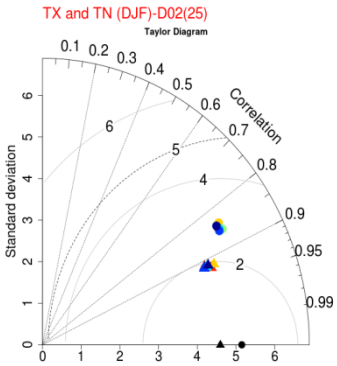

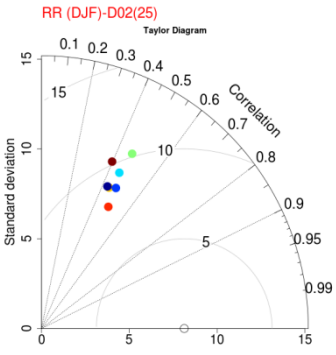

TX and TN (DJF)-D02(20)

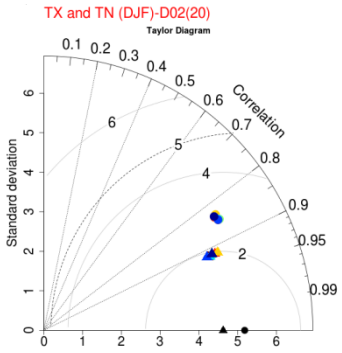

RR (DJF)-D02(20)

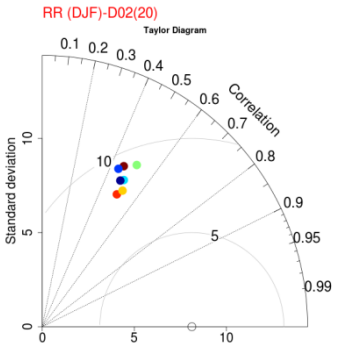

PP1 PP2 PP3 PP4 PP5 PP6 PP7

TX and TN (JJA)-D02(25)

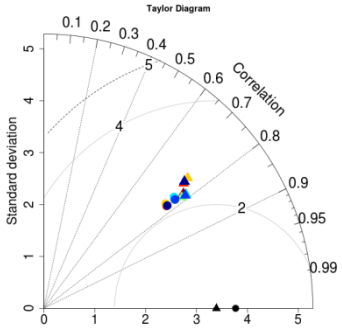

RR (JJA)-D02(25)

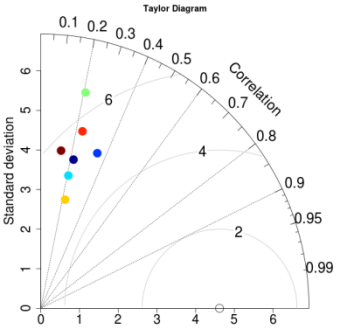

TX and TN (JJA)-D02(20)

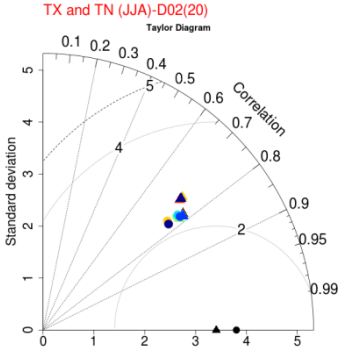

RR (JJA)-D02(20)

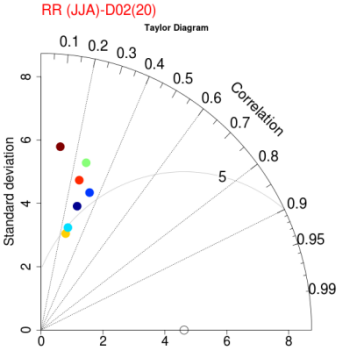

TX and TN (MAM)-D02(25)

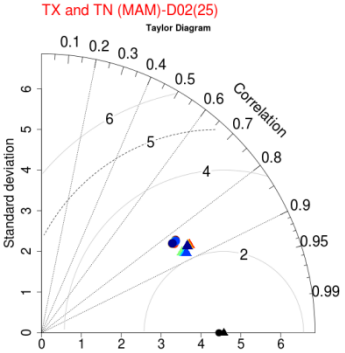

RR (MAM)-D02(25)

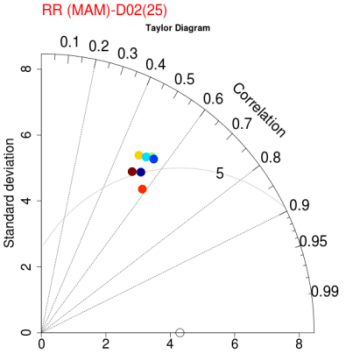

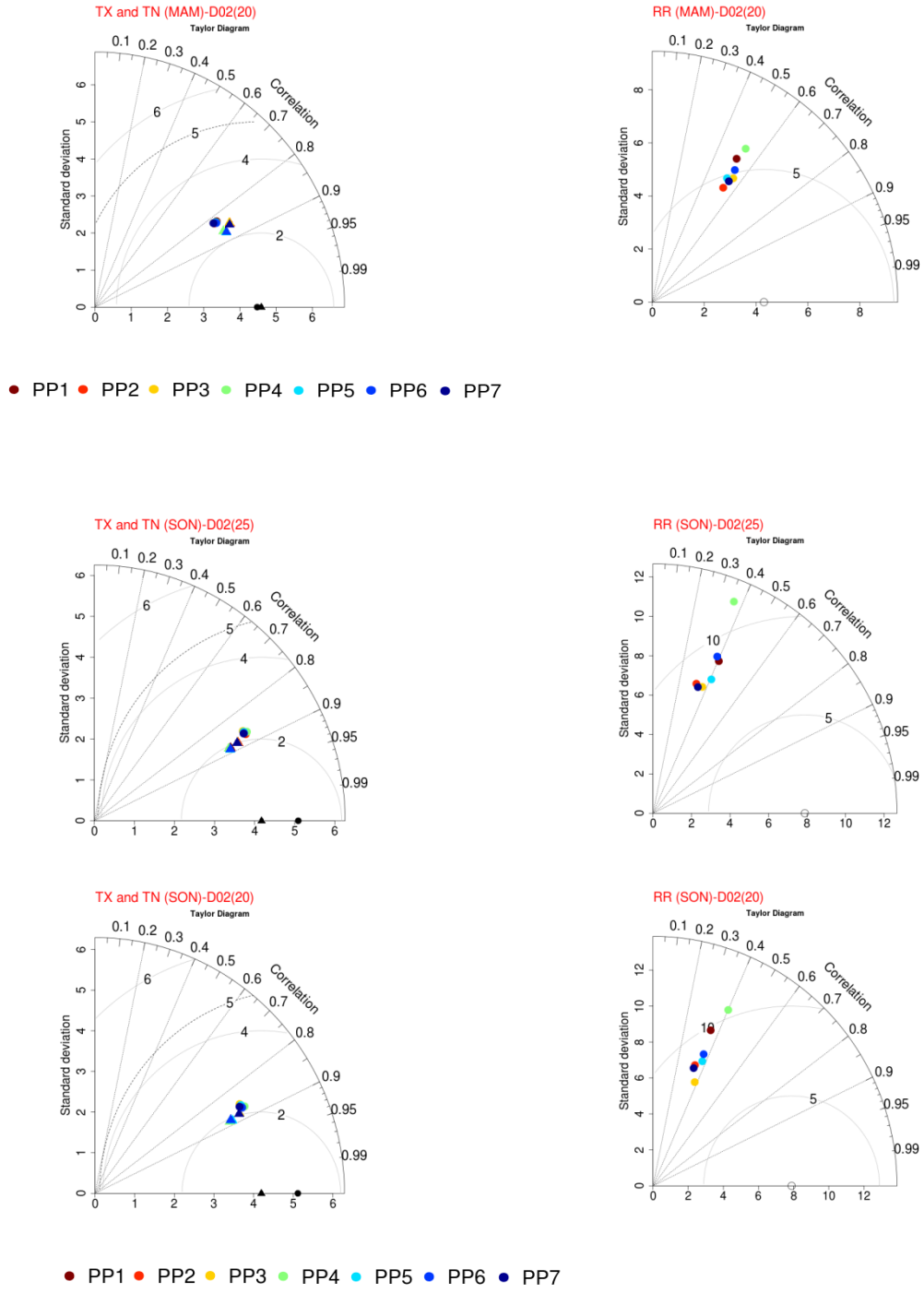

Figure 3.4 Annual and seasonal Taylor plots of maximum temperature (TX, on triangle), minimum temperature (TN, on circle) and precipitation (RR, on circle) for the seven different physics parameterizations (PP1, PP2, PP3, PP4, PP5, PP6, PP7), for high resolution domains D02(20) and D02(25).

This explanation is also justified in Fig. 3.5, where these stations are found to have the higher RMSE values of about 3.5 °C. Same representation follows the TN with highest

statistical errors (near 2.5–3 °C and 0.75–0.8, of RMSE and COR values respectively), noticing a tendency of perceptible discrepancies, among the different parameterization schemes during summer. As good agreement with observations is found and no significant statistical differences are yielded among PPs schemes for TN and TX temperatures, for both domain configurations, with slightly smaller errors for D02(20), the selection of the two PBL schemes is not considered as critical.

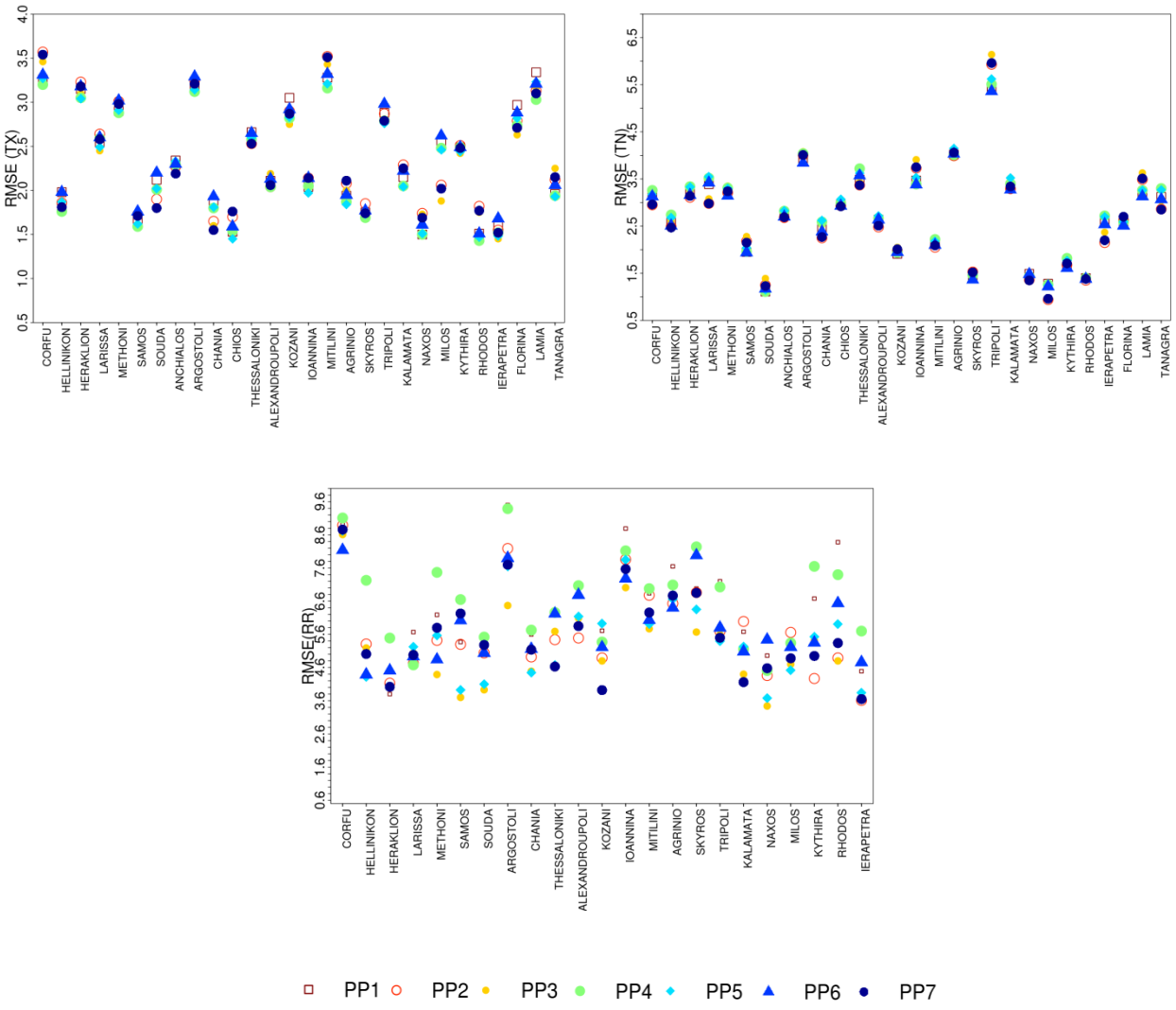

Figure 3.5 Root mean square error of modeled fields, maximum temperature (TX), minimum temperature (TN) and precipitation (RR) for each of the HNMS stations, for the seven different physics parameterisations schemes (PP1, PP2, PP3, PP4, PP5, PP6, PP7) for 2002.

3.1.2. Precipitation

A general overview of precipitation's statistical analysis doesn't show satisfactory results in either physical schemes, or in high resolution domains. In Figure 3.3 (on the right-hand plots) the seasonal cycle of the observed and simulated mean daily values for precipitation is illustrated by month for the total grid points and stations, over the area of Greece for the inner domains D02(20) and D02(25). The black dashed lines of observations yield a seasonal variability of daily precipitation, which is noticed on the models' results. The model calculations of the seven simulation setups resulted in overestimated precipitation values compared to observations, for both high resolution domains, during the rainy months. These current findings are aligned with the fact that WRF overestimates precipitation at higher spatial resolutions (Kotlarski et al. 2014). A clear topographical dependency is revealed on the spatial distribution of total precipitation (Fig. 3.8) with maximum values of annual precipitation found in the West part of the country, related to fronts passage with orographic enhancement. However, the seasonal pattern of daily precipitation is well captured by the majority of the schemes during the year 2002, showing highest precipitation during winter and lowest during summer. It is also concluded that the highest overestimation is noticed with the PP4, while the lowest with PP3 simulation. This result is confirmed with the statistical errors depicted on Table 3.4, with indicative values of positive percentage BIAS for PP4 and PP3 of about 86% and 15% respectively. Figure 3.5 represents the RMSE error of daily precipitation by station. It is probable that high values of RMSE for some stations (Argostoli, Tripoli, Skyros) could be related to the difference in the locations between the closest model point and station due to the mountainous or coastal topography. (Kioutsioukis et al. 2016) reported better matching at stations located in the continental Europe than those that had closer proximity to the Mediterranean. Such overestimation in precipitation is caused by a combination of different factors reported as gauge undercatchment (Frei et al. 2003; Kotlarski et al. 2014), overestimation of the frequency of light rain events and biases in the atmospheric circulations (García-Díez et al., 2015). PP3 that shows the best performance in both high resolution domains, uses WSM6 for microphysics, the Betts-Miller-Janjic cumulus parameterization, as PBL scheme the Mellor–Yamada–Janjic and Monin-Obukhov similarity theory. PP4, on the other hand, uses Thomson, Kain–Fritsch for convection and Yonsei University (YSU) scheme. According to the seasonal Taylor plots, a small variation among seasons and

simulations is deduced with more dispersed results and without significant differences between the two high resolution domains.

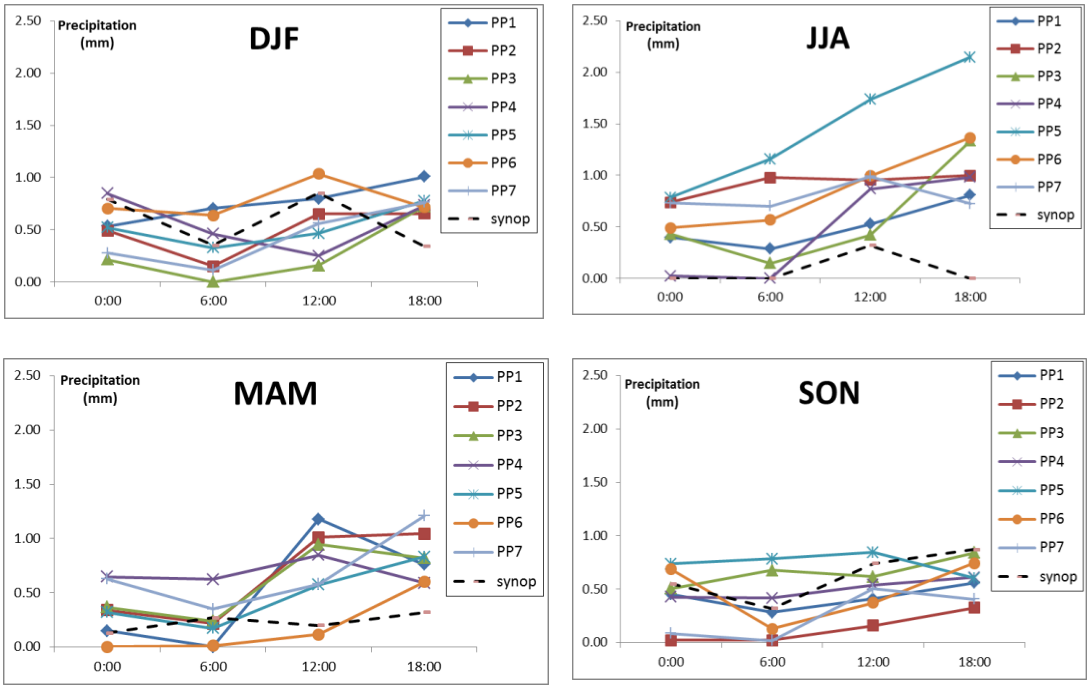

a.

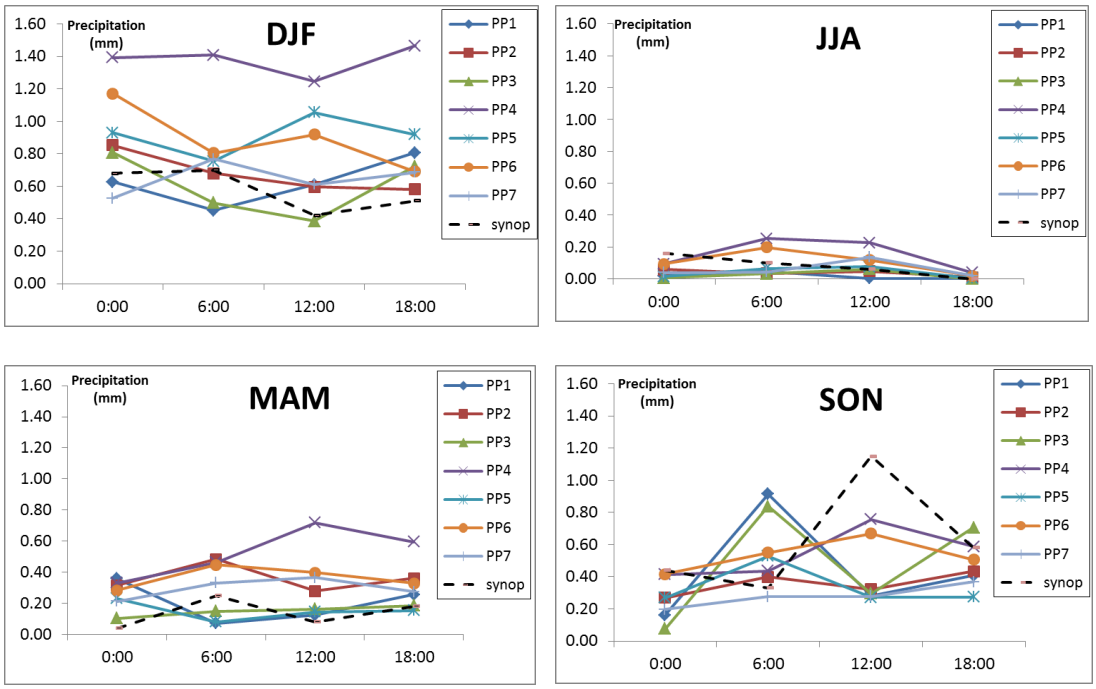

b.

Figure 3.6 a. Mean daily precipitation cycle on 6 h temporal resolution for each season for the selected year 2002 from Hellinikon SYNOP station data compared to the seven models. b. Mean daily precipitation cycle on 6 h temporal resolution and each season, for the selected year 2002 from Heraklion SYNOP station data, compared to the seven models.

A similar pattern is noticed for each season. Moreover, lower RMSE errors and better correlation (around 5 mm and 0.6, respectively) appear during spring, with PP2 configuration presenting the best performance in that season. The PP3 simulation shows the best performance with respect to the statistical errors during the other seasons and mostly during summer and autumn where the RMSE marks the lowest values of about 5 and 8 mm on both domains. PP2 and PP3 physical schemes are associated with the MYJ PBL scheme and different convective schemes. MYJ and YSU parameterizations are related with different ability to transfer moisture to the free troposphere. YSU that uses the Richardson number to characterize instability and turbulence produces highest latent heat and vertical velocity at mid-levels, resulting in transferring moisture at upper levels, while MYJ, with increased vertical stability, doesn't produce sufficient vertical mixing, yielding highest relative humidity at lower levels. One of the concluding remarks, reported on by most of multi-physics studies, examining parameterization combinations, is that although precipitation is more sensitive than temperature to the choice of cumulus and planetary boundary layer parameterizations, there is no combination clearly better than others (Fernández et al. 2007; Argüeso et al. 2011; García-Díez et al. 2013). These findings are observed in minimum and maximum temperatures (see Table 3.4), where differences among the statistical errors of the seven simulations appear mainly in the first or second decimal digit (e.g., RMSE errors between PP1 and PP7 are 2.53 and 2.52, respectively). Additionally, almost identical representations on Taylor plots were deduced (see Fig. 3.4). Regarding precipitation, 5 out of 7 simulation setups have similar but not satisfactory results for statistical errors, of about 40% of PBIAS and Correlation Coefficient close to 0.42.

Considering the mean precipitation daily cycle on 6 h temporal resolution and each season, depicted on Figures 3.6a and 3.6b, for the case of Hellinikon and Heraklion stations, graphical representations are not satisfactory. However, similar patterns of mean daily cycle were detected during winter and autumn for Hellinikon station as well as for winter, spring and summer in the majority of simulations for Heraklion station.

As by definition wet days are those days when daily precipitation is above 0.1 mm (Barstad et al. 2009), dry days are defined as those with daily precipitation below 0.1 mm. Table 5 represents the ratio percentage of the number of dry days in WRF to observations for each model setup and station. WRF simulations overall underestimate the number of dry days in the range [1–50] % among the different stations. Concerning the 99th percentile of rainfall (Table 3.5), many of the stations strongly overestimate extreme precipitation events for all simulations but others underestimate them. This fact probably indicates the importance of locations. In the final processing, a ranking procedure was carried out between simulations and each station based on their statistical metrics of RMSE and MAE in order to find which configuration was the most representative in the majority of the stations for precipitation. Results are presented in percentages in Figure 3.7.

Table 3.5 Ratios (WRF/OBS) of Dry days and 99th percentile for rainfall, according to each station and to each model's simulation. Figures in parenthesis concern number of dry days and 99th percentile values.

	Dry Days								99th percentile							
	WRF/OBS								WRF/OBS							
Stations	PP1	PP2	PP3	PP4	PP5	PP6	PP7	# Dry days OBS	PP1	PP2	PP3	PP4	PP5	PP6	PP7	99th OBS
CORFU	0.86 (222)	0.73 (188)	0.85 (219)	0.75 (194)	0.81 (207)	0.81 (209)	0.79 (203)	*257*	0.49 (28.6)	0.47 (27.5)	0.42 (24.3)	0.62 (36.1)	0.54 (31.3)	0.61 (35.5)	0.4 (23.5)	*58.1*
HELLINIKON	0.84 (248)	0.72 (213)	0.83 (245)	0.69 (203)	0.74 (219)	0.77 (225)	0.78 (230)	*294*	1.55 (34.2)	1.14 (25)	1.17 (25.8)	2.03 (44.6)	0.9 (19.9)	1 (21.9)	1.23 (27.1)	*22*
HERAKLION	0.91 (257)	0.85 (240)	0.99 (278)	0.72 (203)	0.96 (270)	0.86 (243)	0.89 (251)	*282*	0.64 (16.4)	0.91 (23.5)	0.79 (20.4)	1.26 (32.4)	0.74 (19.1)	0.87 (22.4)	0.76 (19.6)	*25.7*
LARISSA	0.86 (239)	0.74 (207)	0.75 (208)	0.74 (207)	0.7 (195)	0.74 (205)	0.83 (232)	*278*	1.01 (27.1)	0.69 (18.4)	0.67 (17.9)	0.9 (24.1)	0.9 (24.1)	0.85 (22.8)	0.76 (20.2)	*26.7*
METHONI	0.64 (216)	0.62 (211)	0.71 (242)	0.52 (178)	0.6 (205)	0.56 (191)	0.62 (211)	*340*	2.22 (42.6)	2.03 (38.9)	1.45 (27.9)	2.42 (46.4)	1.76 (33.8)	1.48 (28.4)	2.26 (43.3)	*19.2*
SAMOS AIRPORT	0.85 (260)	0.8 (247)	0.89 (274)	0.76 (234)	0.83 (255)	0.79 (244)	0.82 (251)	*307*	1.26 (39.5)	1.3 (40.7)	0.98 (30.6)	1.73 (54.1)	1.41 (44.2)	1.41 (44.2)	1.1 (34.4)	*31.3*
SOUDA AIRPORT	0.81 (230)	0.81 (229)	0.9 (254)	0.67 (189)	0.87 (245)	0.79 (224)	0.84 (237)	*283*	1.81 (40.4)	1.77 (39.5)	1.26 (28)	1.67 (37.3)	1.32 (29.4)	1.55 (34.5)	1.46 (32.5)	*22.3*
ARGOSTOLI	0.86 (220)	0.75 (193)	0.9 (231)	0.74 (189)	0.79 (201)	0.73 (188)	0.82 (210)	*256*	1.07 (46.2)	1.1 (47.2)	0.74 (31.8)	1.18 (50.9)	1.14 (49.2)	0.8 (34.6)	1.25 (53.9)	*43.1*
CHANIA	0.79 (235)	0.78 (232)	0.85 (255)	0.64 (190)	0.84 (251)	0.75 (225)	0.8 (239)	*299*	1.67 (38.8)	1.31 (30.4)	1.27 (29.5)	1.77 (41)	1.28 (29.6)	1.52 (35.3)	1.48 (34.3)	*23.2*
THESSALONIKI	0.83 (225)	0.7 (188)	0.77 (209)	0.72 (194)	0.75 (202)	0.67 (180)	0.72 (195)	*270*	2.02 (46.1)	1.59 (36.3)	1.75 (39.8)	1.86 (42.3)	1.3 (29.7)	2.15 (49.1)	1.27 (28.9)	*22.8*
ALEXANDROUPOLI	0.86 (251)	0.73 (215)	0.77 (226)	0.67 (195)	0.76 (223)	0.75 (219)	0.79 (232)	*293*	1.52 (38.1)	1.13 (28.3)	1.76 (44.1)	1.62 (40.6)	1.58 (39.7)	1.7 (42.7)	1.16 (29.2)	*25.1*
KOZANI	0.75 (201)	0.6 (160)	0.59 (158)	0.52 (140)	0.56 (151)	0.63 (168)	0.63 (170)	*268*	1.5 (29)	1.21 (23.3)	1.26 (24.4)	1.46 (28.2)	1.71 (33)	1.59 (30.6)	0.92 (17.8)	*19.3*
IOANNINA	0.77 (185)	0.61 (145)	0.6 (144)	0.55 (132)	0.62 (148)	0.69 (164)	0.64 (154)	*239*	1.48 (52.1)	0.92 (32.4)	0.87 (30.6)	1.49 (52.3)	0.94 (33)	0.96 (33.8)	0.91 (32.1)	*35.2*
MITILINI	0.96 (279)	0.86 (249)	0.96 (278)	0.84 (244)	0.92 (266)	0.89 (258)	0.89 (258)	*290*	0.95 (35.9)	0.86 (32.6)	0.97 (36.6)	1.23 (46.2)	0.99 (37.5)	0.66 (24.7)	0.69 (26)	*37.7*
AGRINIO	0.86 (233)	0.64 (174)	0.73 (197)	0.58 (158)	0.69 (186)	0.61 (166)	0.73 (197)	*271*	0.78 (36.4)	0.6 (27.9)	0.61 (28.5)	0.64 (29.7)	0.62 (29.1)	0.56 (26.2)	0.66 (30.6)	*46.6*
SKYROS	0.86 (243)	0.71 (202)	0.84 (238)	0.63 (178)	0.77 (219)	0.7 (198)	0.74 (211)	*284*	0.87 (34.8)	0.95 (38.1)	0.83 (33.3)	1.17 (47.1)	0.55 (22.2)	1.14 (45.8)	0.85 (33.9)	*40.1*
TRIPOLI	0.65 (178)	0.62 (170)	0.59 (161)	0.44 (121)	0.59 (162)	0.65 (178)	0.63 (173)	*274*	1.73 (38.9)	1.21 (27.2)	1.32 (29.6)	1.8 (40.5)	1.63 (36.6)	1.45 (32.7)	1.22 (27.4)	*22.5*
KALAMATA	0.82 (221)	0.75 (203)	0.85 (228)	0.61 (164)	0.77 (207)	0.7 (189)	0.81 (219)	*269*	1.21 (40.2)	0.92 (30.5)	0.83 (27.7)	1.03 (34.3)	0.87 (29)	1.2 (39.8)	0.86 (28.7)	*33.2*
NAXOS	0.91 (270)	0.77 (229)	0.95 (282)	0.68 (201)	0.87 (257)	0.78 (231)	0.82 (245)	*297*	1.53 (35.7)	1.05 (24.6)	0.8 (18.7)	1.09 (25.5)	0.68 (15.9)	1.37 (32)	0.92 (21.6)	*23.4*
MILOS	0.84 (255)	0.72 (219)	0.85 (257)	0.69 (208)	0.79 (238)	0.73 (222)	0.78 (236)	*303*	0.92 (34.9)	0.83 (31.6)	0.58 (22)	0.96 (36.4)	0.65 (24.8)	0.85 (32.1)	0.67 (25.4)	*37.9*
KYTHIRA	0.82 (240)	0.79 (229)	0.85 (246)	0.71 (207)	0.79 (230)	0.75 (217)	0.81 (236)	*291*	1.64 (51.3)	1.34 (41.8)	1.58 (49.4)	1.94 (60.8)	1.47 (46)	1.56 (48.7)	1.16 (36.4)	*31.3*
RHODOS	0.91 (274)	0.86 (260)	0.96 (291)	0.84 (253)	0.91 (275)	0.8 (241)	0.88 (267)	*302*	2.23 (67.7)	1.23 (37.3)	1.34 (40.6)	2.12 (64.5)	2.29 (69.5)	1.96 (59.5)	1.5 (45.5)	*30.4*
IERAPETRA	0.91 (274)	0.89 (270)	0.92 (278)	0.74 (223)	0.87 (264)	0.86 (259)	0.95 (288)	*302*	1.26 (28.4)	0.97 (22)	0.76 (17.1)	1.78 (40.2)	0.87 (19.7)	1.65 (37.4)	0.97 (22)	*22.6*

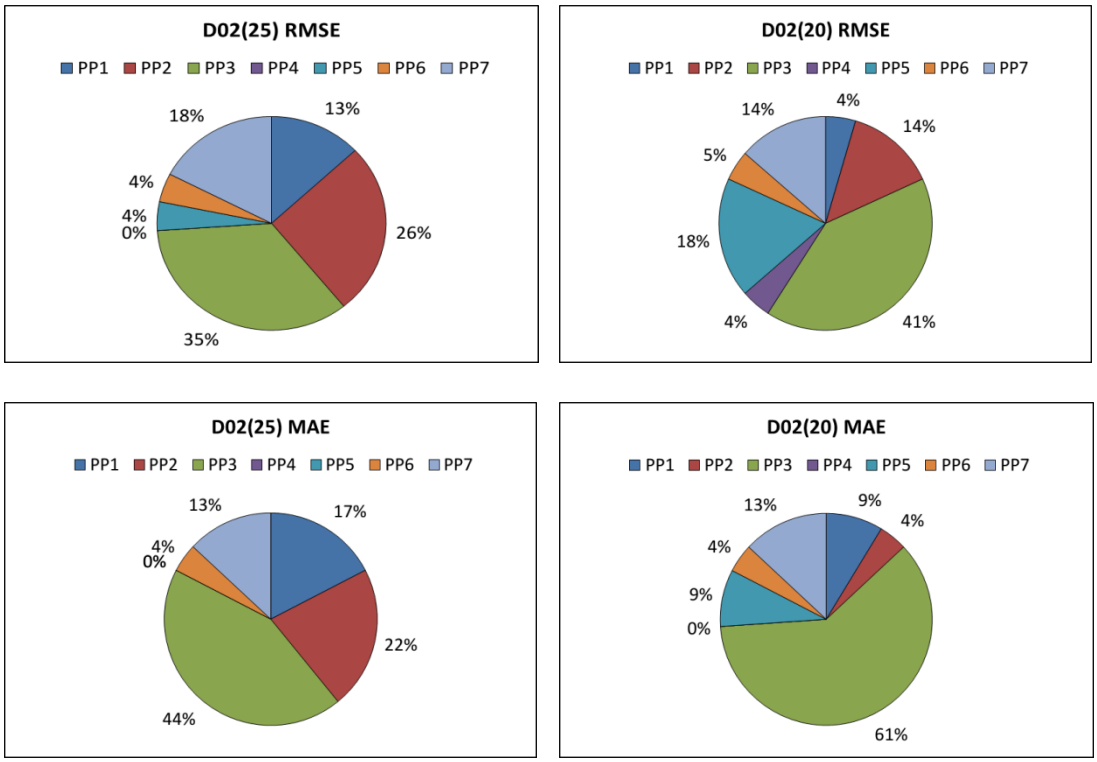

Figure 3.7 Percentage of stations representing physical schemes based on RMSE and MAE. The highest percentage represents the parameterization scheme (PP1, PP2, PP3, PP4, PP5, PP6, PP7) which has the best score of statistical metrics (RMSE and MAE) for precipitation, on the total number of stations.

For precipitation, PP3 was found to perform better in the majority of the stations yielding percentages of lower RMSE and MAE of 35% and 41%, and 44% and 61%, for the high resolution domains D02(25) and D02(20), respectively. Many studies have reported the difficulty to model precipitation with WRF model configurations, yet more when it is related to difficult topography and extended coastal complexity, such as in the case of Greece.

However, the PP3 configuration (WSM6 with MYJ and BMJ) appeared to perform better in the majority of the stations with the percentage of 40–60% combined with lower statistical metrics RMSE and MAE. According to (Zittis et al. 2014), maximum and minimum temperatures with WSM6 scheme-driven simulations showed closer agreement with the observational datasets/stations and also these simulations were able to capture the annual precipitation cycle adequately. Other studies have also supported these options of physical schemes (PP3 WRF setup) for climate applications, having more balanced overall behavior for both surface variables (Argüeso et al. 2011; Soares

et al. 2012; Katragkou et al. 2015). Efstathiou et al. (2013) indicated that WSM6 in conjunction with MYJ for hourly rain rates provided better statistical scores for light to moderate precipitation over eastern Chalkidiki.

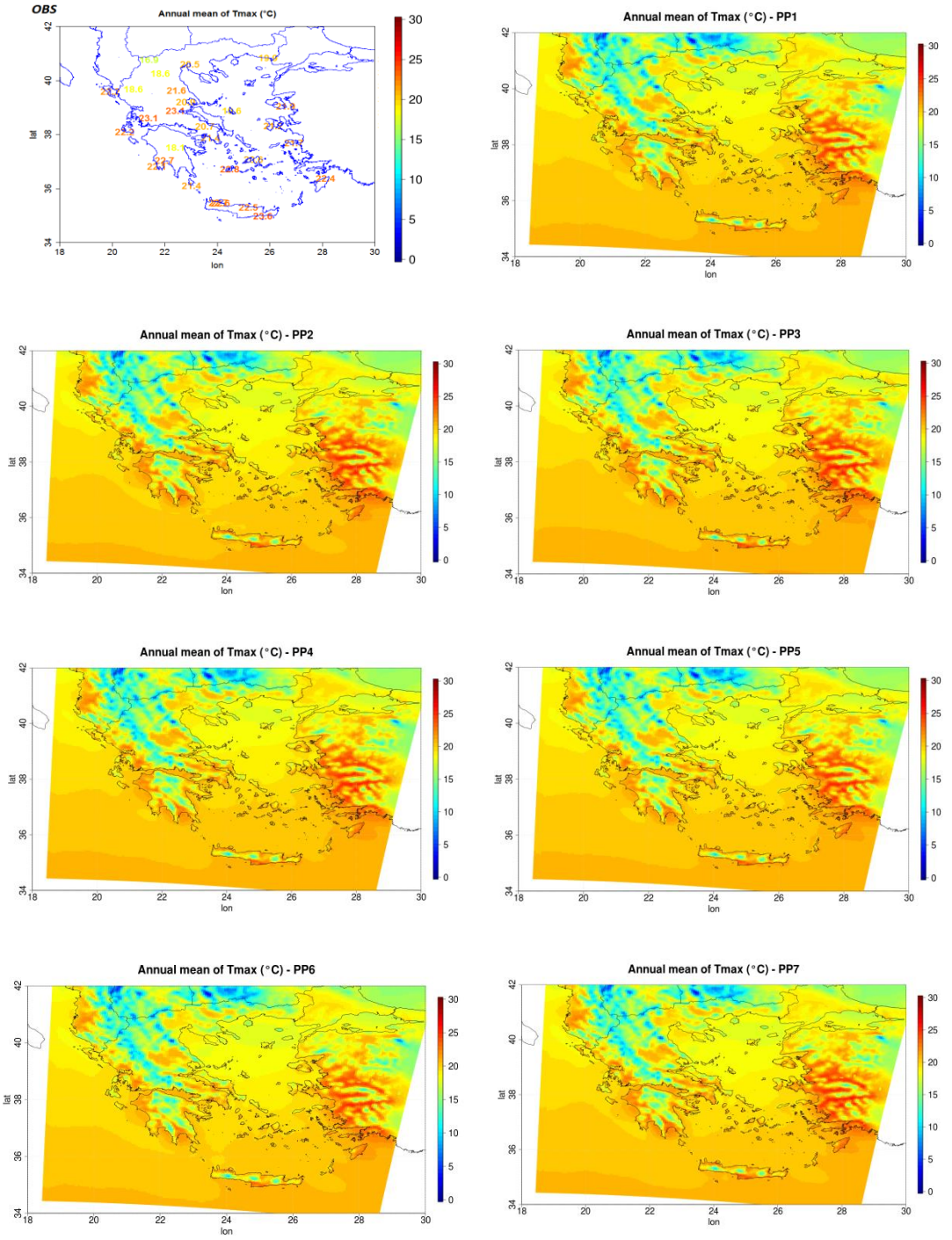

a.

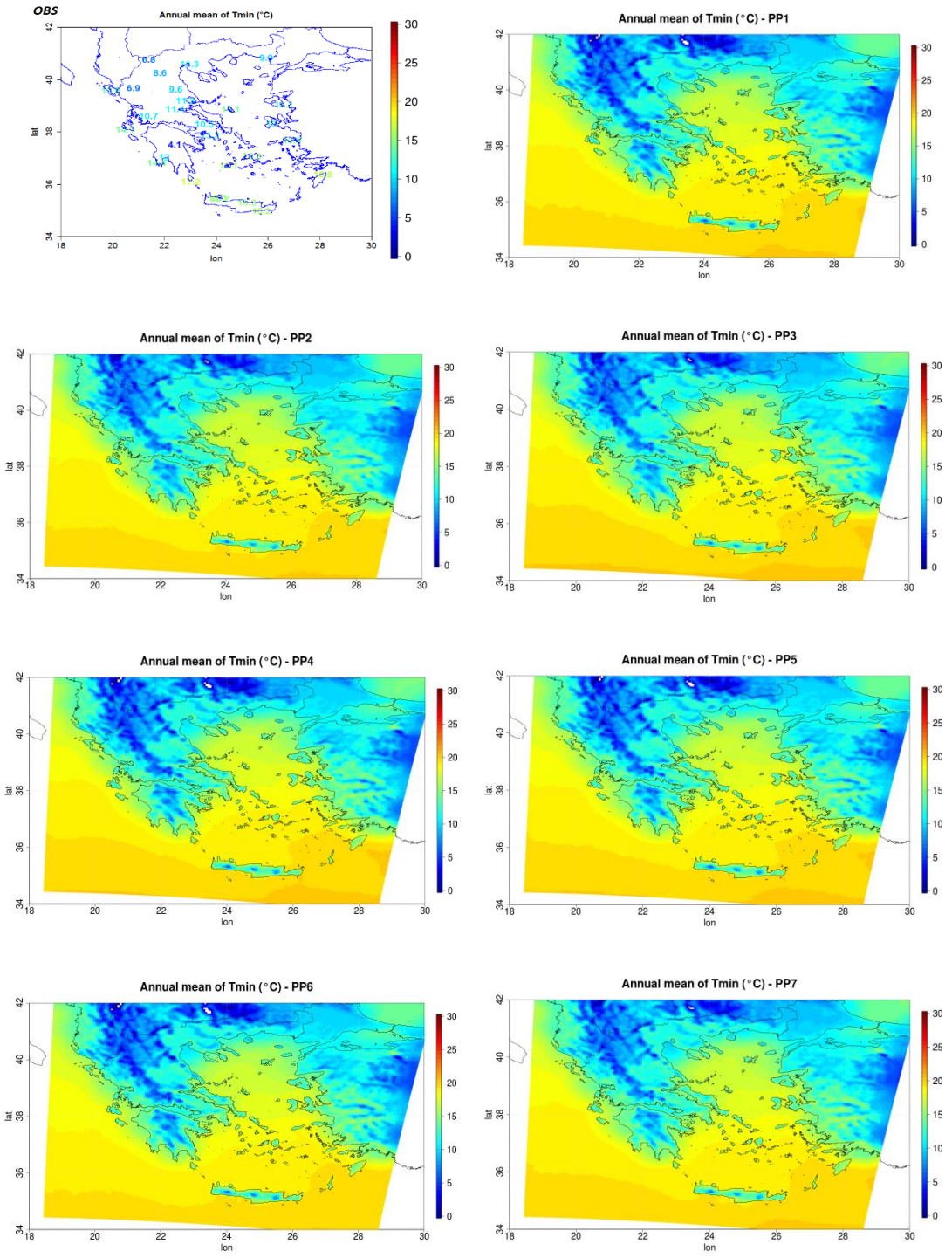
OBS
Annual mean of Tmin (°C)
Annual mean of Tmin (°C) - PP1
Annual mean of Tmin (°C) - PP2
Annual mean of Tmin (°C) - PP3
Annual mean of Tmin (°C) - PP4
Annual mean of Tmin (°C) - PP5
Annual mean of Tmin (°C) - PP6
Annual mean of Tmin (°C) - PP7
lat
lon

b.

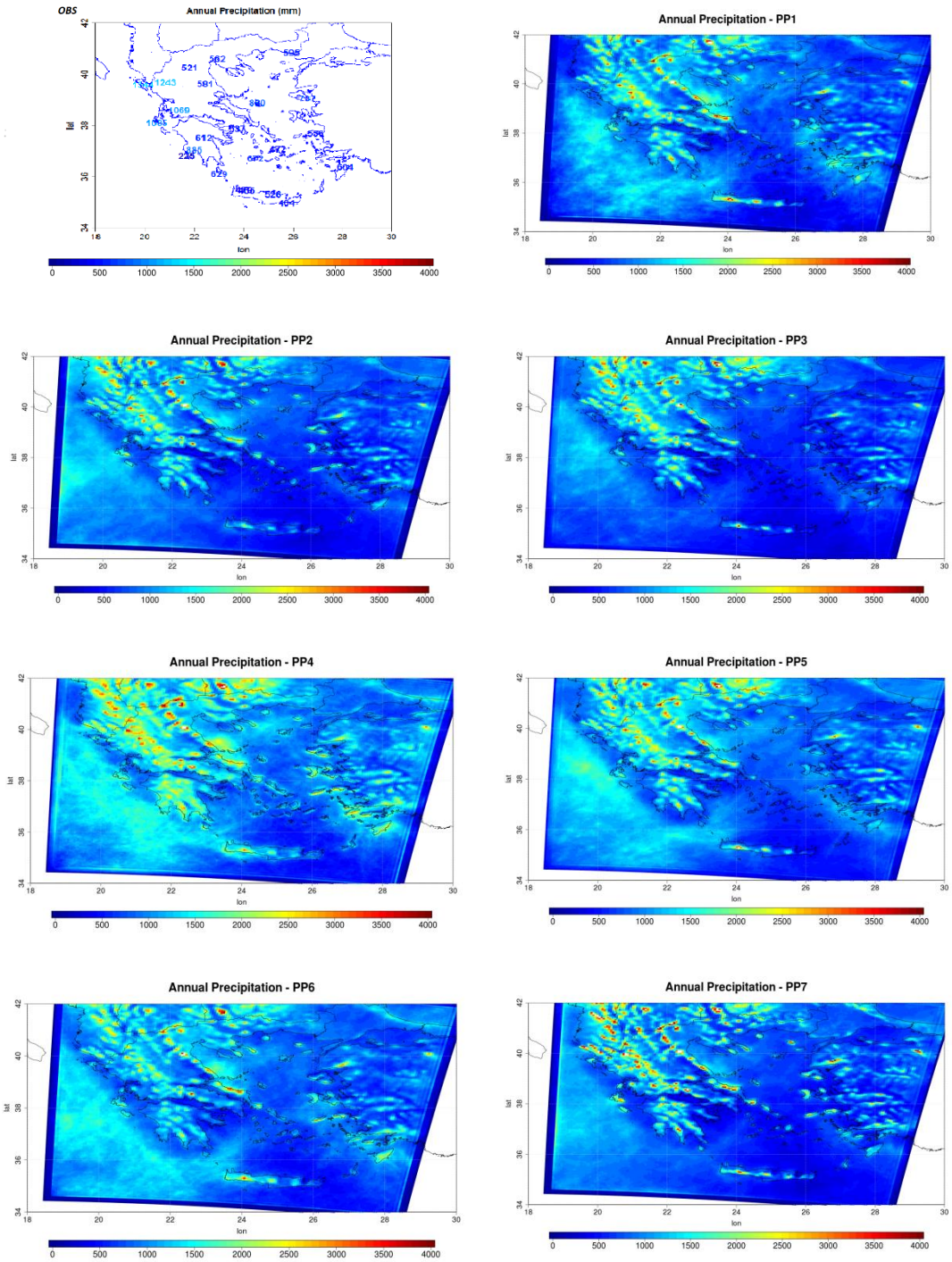

c.

Figure 3.8 Spatial distribution of a) annual mean maximum (Tmax) and b) annual mean minimum temperature (Tmin) in °C and c) the annual precipitation (in mm) for the 5-km region of Greece D02(20), for the selected year 2002.

3.1.3. Relative humidity and wind speed

The results of relative humidity (Table 3.4) revealed a consistent underestimation of RH for both inner domains. Statistical errors yield overall small differences not only in both high resolution domains but also between the seven simulation set ups. The RMSE and MAE errors range close to 12 and 9% respectively, with similar values found for all simulations. The correlation coefficients between the observed and the simulated RH are around 0.60 with an overall negative BIAS from−1.2 to −2.1% for D02(20) and −0.03 to −1.36% for D02(25). The overall score indicates a slightly better performance of the model for the PP5 simulation scheme (lowest errors in bold). On the other hand, the statistical errors of wind speed (Table 3.4 also) showed a consistent overestimation of WS for both inner domains, with similar values found for all simulations. The RMSE and MAE errors range close to 2.2 and 1.5 m/s respectively, the correlation coefficients between the observed and the simulated WS are around 0.64–0.65. A positive BIAS is observed from 0.7 to 1.18 m/s for D02(20) and 0.79 to 1.33 m/s for D02(25) indicating a slightly better performance for the PP6 model set up.

The statistical errors of relative humidity and wind speed yield overall small differences not only on both high-resolution domains but also between the seven simulation setups. A consistent underestimation of RH was observed, followed by a consistent overestimation of WS for the sum of grid point stations. The representation of the statistical errors by stations was just made to indicate the variety of results among stations caused by the difference in the distance between the station and the nearest model grid point due to the complex topography of the area. Thus, direct comparisons were avoided with other studies considering the differences in locations.

This study was a first step towards obtaining high resolution climatology in Greece, with some limitations due to the rather short time of the examined period (one year) and the limited number of observational data. To investigate further, the effect of the choice of physics schemes combinations, more simulations of 5-years run along with statistical analysis are analysed in the next Section 3.3 through the second sensitivity test. These sensitivity studies will assist in the identification of the likely best set of physics parameterization schemes exhibiting the most skill in the area of Greece to advance efforts for consistent high resolution climate simulations and a more robust assessment of future climate impacts in the country.

Key Remarks

- ***Lower errors were obtained with 20 km grid resolution than the 25 km of the parent (European) domain considering the downscaled results of the examined parameters.***
- ***No significant statistical differences found between the two studied domains D02(25) and D02(20) by means of statistical errors in the observed and simulated data for the seven simulation set ups.***
- ***Underestimation of simulated maximum temperature and overestimation of the minimum temperature compared to station data.***
- ***Overestimation of simulated precipitation with good representation of spatial patterns.***
- ***For precipitation, PP3 was found to perform better in the majority of the stations yielding percentages of lower statistical errors.***
- ***Consistent underestimation of relative humidity was observed, followed by a consistent overestimation of WS for the sum of grid point stations.***
- ***The 20 km spatial resolution grid will be preferably selected for historical and future climate simulations.***

3.2 Sensitivity test 2

Following the results of the previous sensitivity test, 5 years of high-resolution dynamical downscaling experiments were performed, from 2000 to 2004 inclusive, with the use of the WRF model and 5 km spatial resolution. The period for the evaluation of all the WRF simulations spans from 1 January 2000 until 31 December 2004. This period was selected based on the satisfactory number of high quality available observational data. The simulations have run independently of each other with parallel integration to decrease the total time needed to complete the 5-year climatology. The objective of this work is to validate the high-resolution downscaling simulations with the use of the available observed values of minimum and maximum daily temperature and daily precipitation, in order to select among different physics parameterizations (e.g., cloud microphysics, boundary layer and cumulus), the sufficient setup to investigate the overall model's performance over the area of interest for subsequent high resolution historic and future climate model experiments.

In the current study, four WRF simulations have been performed, using different combinations of physics parameterizations, in order to investigate their effects on temperature and precipitation fields in the inner domain of Greece. These different experiments were finally selected considering previous results for the same area, employing a larger set of WRF simulations covering 1-year period and more variables, such as relative humidity and surface wind speed (Politi et al. 2018). For convenience and link to this previous research, the names of the four best selected combinations of physics parameterizations (as PP2, PP3, PP5, PP7) were kept. The simulations have run independently of each other with parallel integration in order to decrease the total time needed to complete the 5-year climatology. Table 3.6 summarizes the different physical schemes combinations for each of the four simulations.

Table 3.6 Parameterization combinations of WRF model. The four different simulations are named as PP2, PP3, PP5 and PP7.

Schemes →	**Microphysics**		**PBL/SLP**		**Cumulus**	
Sim.ID ↓	*D01*	*D02*	*D01*	*D02*	*D01*	*D02*
PP2	WSM6	THOM	MYJ/MO		Grell-3D	
PP3	WSM6	WSM6	MYJ/MO		BMJ	

PP5	WSM6	THOM	YSU/MM5	BMJ
PP7	FE	FE	MYJ/MO	Grell-3D

Focusing on precipitation verification, the accuracy of the simulated precipitation was also determined by statistical scores of a contingency table using four distinct threshold values of precipitation (for further information, see Table A.2 of the Appendix), precipitation for low rainfall (>1mm), medium rainfall (>2.5 mm), heavy rainfall (>10 mm) and extremely heavy rainfall days (>20 mm) (Lagouvardos and Kotroni 2005; Kryza et al. 2013; Dasari and Challa 2015), to evaluate small and large rainfall events, for the location of each station separately.

3.2.1 Maximum Temperature and Minimum Temperature

Annual and seasonal changes in the daily minimum (TN) and maximum (TX) temperatures for the selected period have been analyzed. In general, it was found that physics parameterizations appear to have less noticeable effect on temperature than on precipitation [56].

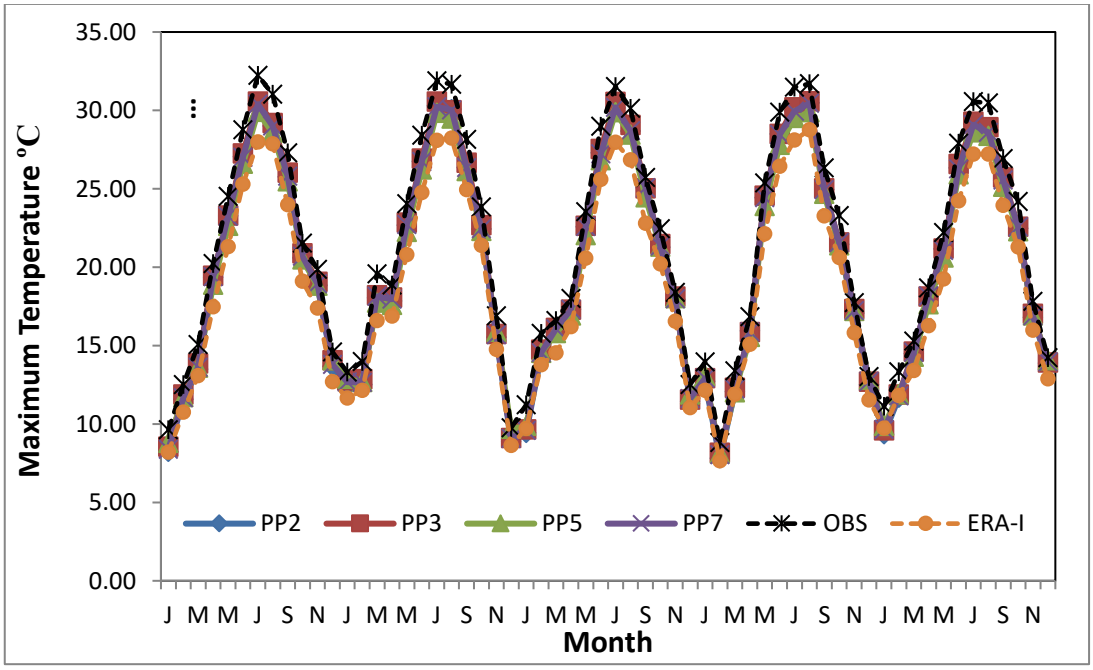

(a)

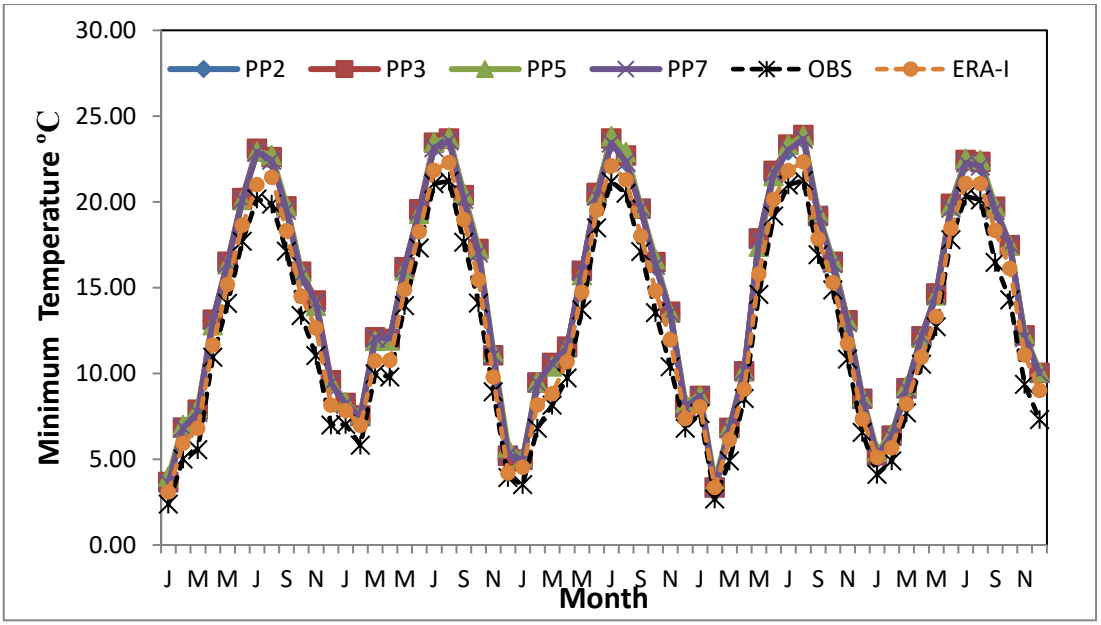

(b)

Figure 3.9 Observed and simulated mean daily TX (a) and TN values (b), on the total grid stations' points by month, for the four different simulations (PP2, PP3, PP5, PP7), for the high-resolution domain of Greece (D02) during 2000–2004.

In Figure 3.9, the inter-annual cycle of daily-average minimum and maximum values of temperature by month is displayed for the total number of grid stations' points for the whole region of the study. The colored lines show the results of the simulations, and the dashed, black lines indicate observational data. In general, the observational seasonality is precisely captured during 2000–2004, while the summer/winter peaks are clearly identified as well. Similar representation and behavior of temperatures are observed regarding all physical schemes. Both temperature measures are in agreement over the study period, but WRF TX results are consistently colder, while TN is much warmer than observational data for all physical schemes. This bias appears to result mainly from the summertime over-prediction of daily-minimum temperature and summertime under-prediction of TX; daily maximum biases tend to be smaller in magnitude and seasonally invariant, while the warm bias is mainly confined to the maximum temperatures. Additionally, the spatial distribution (Figure 3.10) of the simulated 5-years mean that the daily TX is characterized normally by a warm decreasing gradient from the coasts and low altitudes regions to mountainous chains, verified by the weather station values in spite of the limited number of observational data. Similar results are observed for minimum temperature as well (Figure 3.11).

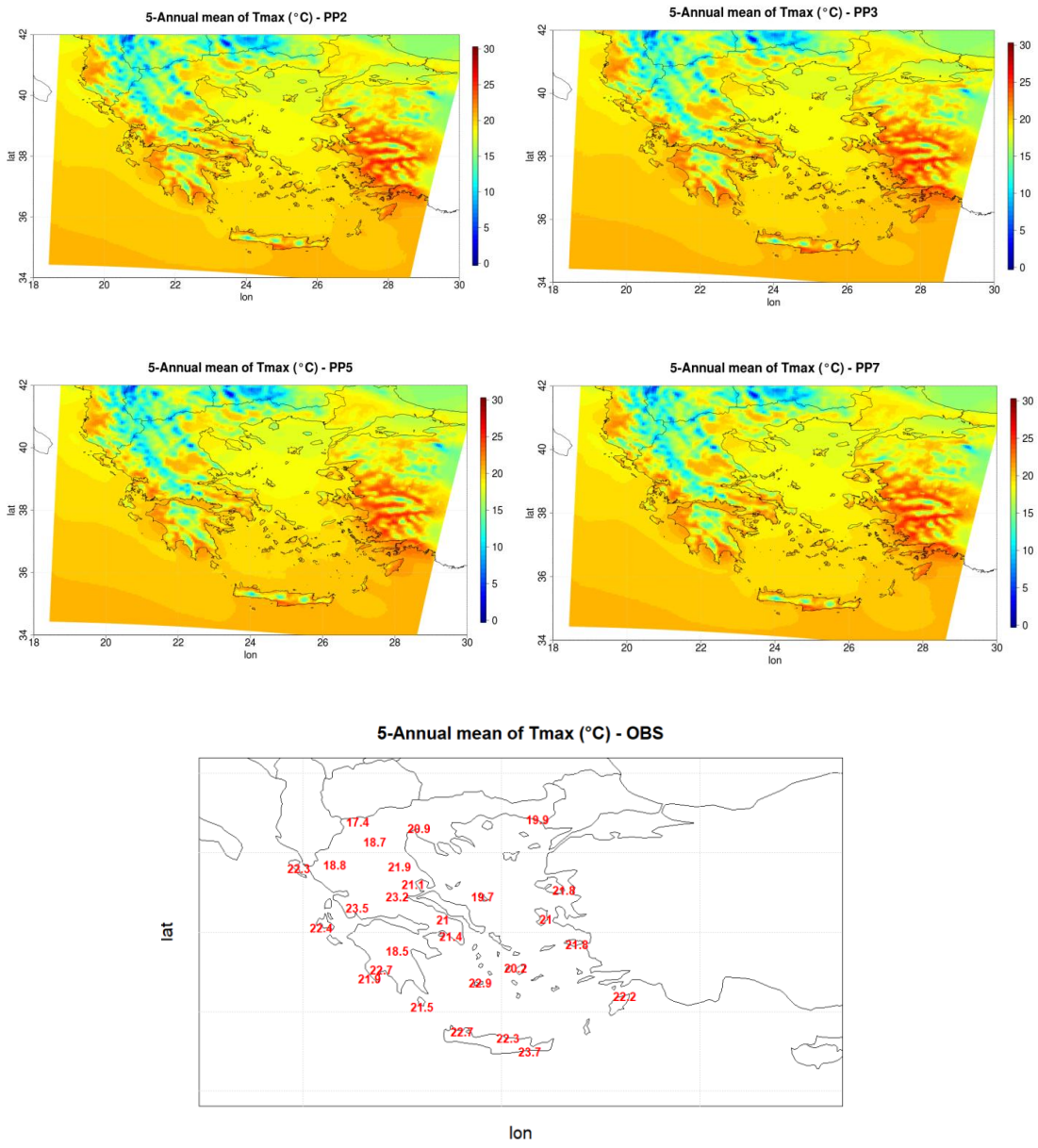

Figure 3.10 Spatial distribution of 5-annual mean maximum temperature (TX) for the 5-km region of Greece (D02), for the selected period 2000-2004.

ERA-interim also performed well the inter-annual cycle for both temperatures, indicating lower values than the observed and modeled values during summer maximum values in the case of maximum temperature. Table 3.7 presents the statistical metrics calculated for daily values. A high correlation coefficient of 0.96 is observed between the station and the simulated daily maximum temperature TX, with an overall negative BIAS from −1.1 to −1.4 °C, indicating a slightly better performance of the model for the PP3 (−1.06 °C) simulation.

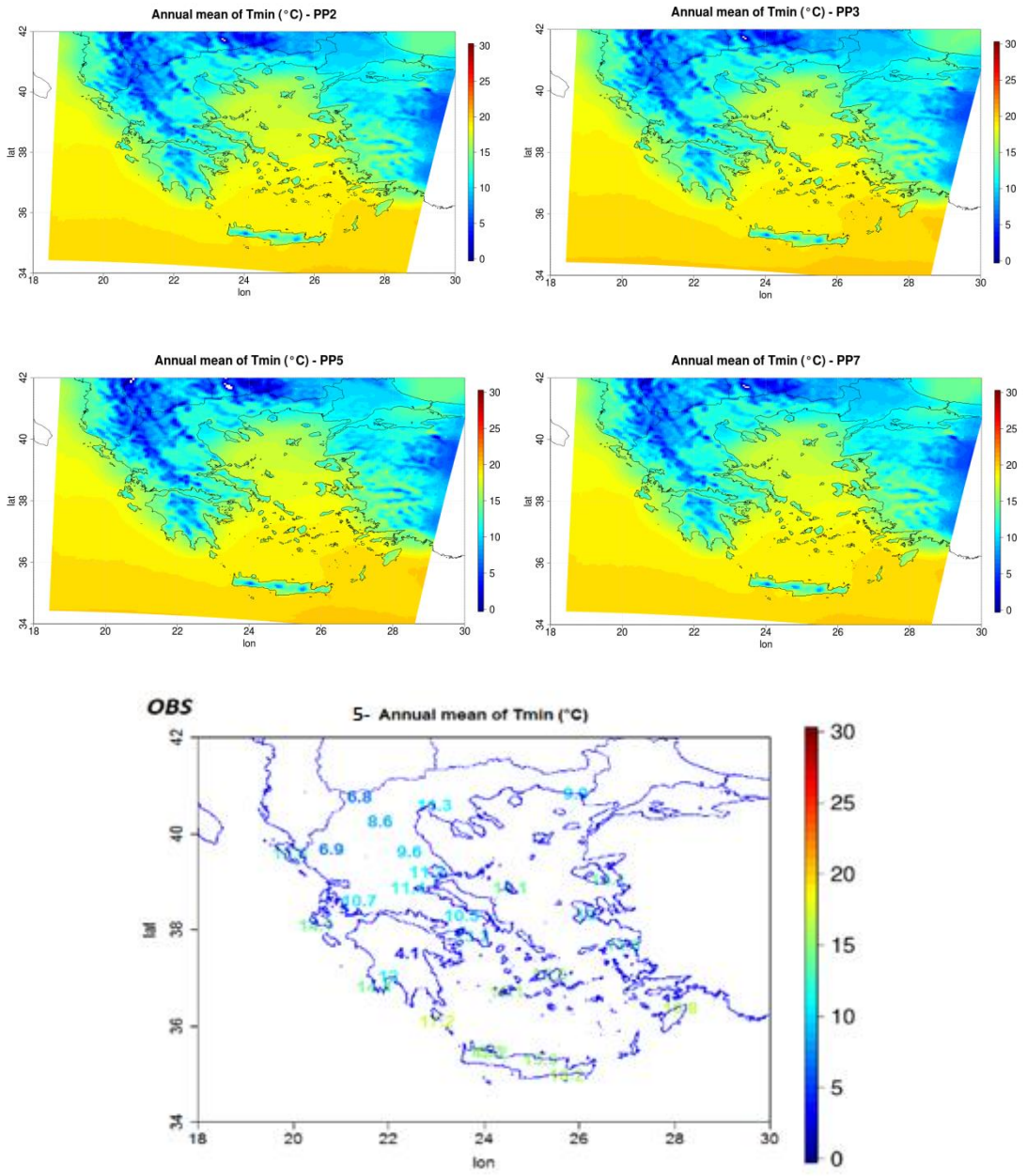

Figure 3.11 Spatial distribution of 5-annual mean minimum temperature (TN) for the 5-km region of Greece (D02), for the selected period 2000-2004.

Table 3.7 Statistical metrics of the four simulations in the total grid points for daily minimum temperature (TN), daily maximum temperature (TX) for 2000–2004, over the area of Greece.

	ID	PP2	PP3	PP5	PP7	ERA-I
	BIAS(°C)	-1.24	**-1.06**	-1.39	-1.18	-2.64
TX	**RMSE**(°C)	2.66	**2.60**	2.62	2.64	3.95

	MAE(°C)	2.08	**2.01**	2.06	2.06	3.18
	COR	0.96	0.96	0.96	0.96	0.93
	BIAS(°C)	**2.08**	2.21	2.22	2.11	0.77
TN	**RMSE**(°C)	**3.53**	3.64	3.61	3.55	3.36
	MAE(°C)	**2.68**	2.78	2.78	2.70	2.58
	COR	0.92	0.92	0.92	0.92	0.90

The RMSE and MAE errors have values close to 2.6 °C and 2 °C, respectively, with similar values found for all simulations. Regarding the daily TN, a high correlation coefficient of 0.92 is observed between observations and model data, with a consistent positive bias of around 2 °C, ~3.5 °C RMSE and ~ 2.7 °C MAE values. These findings are in good agreement with high resolution climate analysis for temperature by Berg et al. [4] for Germany, and little higher values regarding RMSE/MAE values, (especially in the case of TX BIAS, which is found negligible −0.4 °C) in a similar study of Soares et al. 2012 for Portugal. The results showed an improvement in maximum temperature with respect to the ERA-Interim dataset, and higher bias regarding minimum temperature, but without significant discrepancies on the other statistical errors. An overall performance of the simulations is illustrated in Figure 3.12, by Taylor plots, for seasonal periods (winter, spring, summer and autumn - 7a) and annual (7b) during 2000–2004.

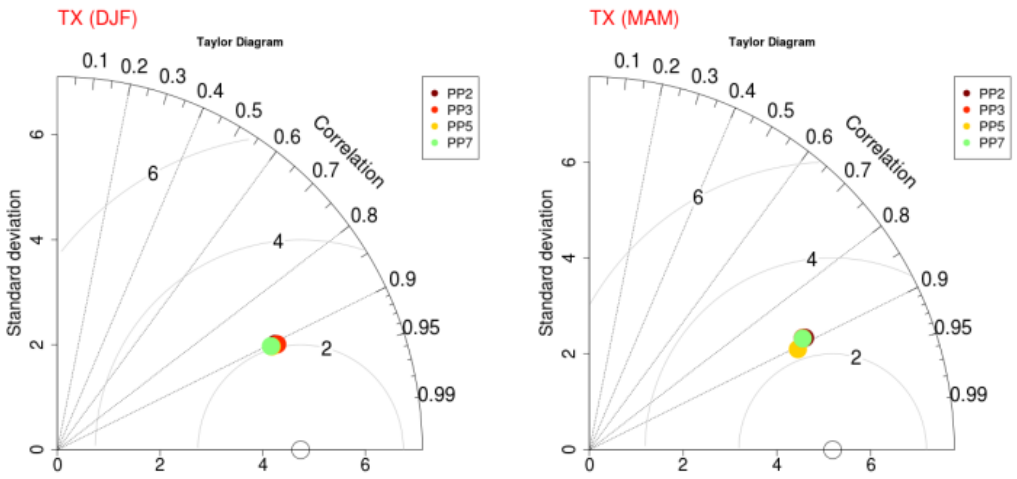

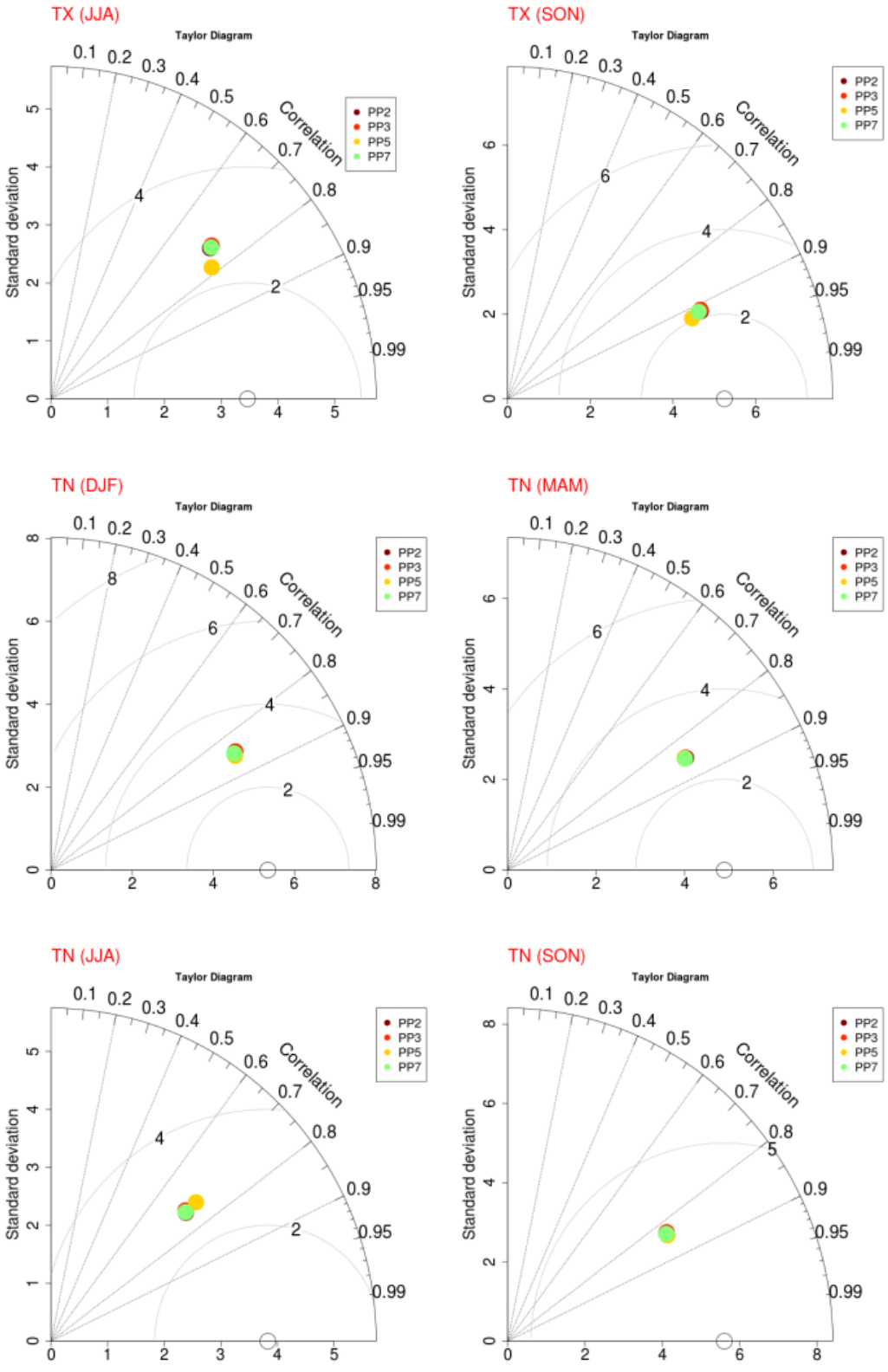

Annual Taylor Plots of TX and TN

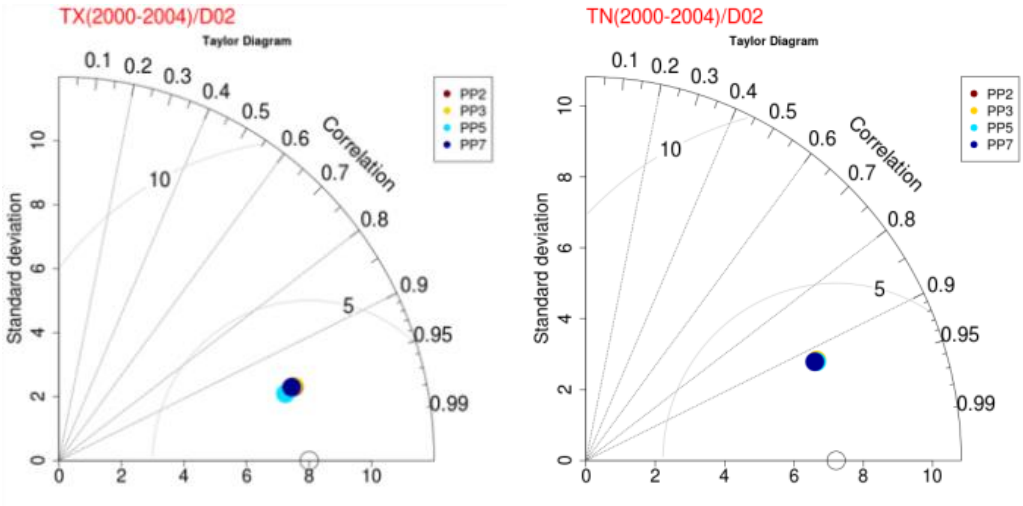

Figure 3.12 Seasonal and annual Taylor diagrams of the four WRF simulations (PP2, PP3, PP5, PP7) with respect to observed daily maximum (TX) and minimum temperatures (TN) for the high resolution domain of Greece (D02).

The diagrams for maximum temperature showed a good match between model results and observations at seasonal time scales. The lowest performance was obtained during the summer months, with correlations close to 0.75 that increase to 0.8 for PP5 simulation results. In addition, in the representation of metrics by station in Table 5, high RMSE values are observed, of about 3–3.5 °C for several stations. It was found in the initial study Politi et al. 2018 that the cell of the certain model points that correspond to the location of the observed stations is characterized by the sea dominant land use category (e.g., Corfu, Heraklion, Mitilini, Argostoli etc.), and consequently during summer period could affect the results, with higher differences in temperature leading to stronger sea-land interaction in combination with the appearance of more intense thermal instability. The correlations in the other seasons are much higher in the range of 0.9–0.95, and lower errors are observed with very similar values for all models. The Taylor diagram in a yearly time scale showed a very good agreement of models' performance, with no distinct differences among them during the 5-year period. The correlation coefficient results showed a good match with values above 0.9 arising in the climatological study of (Marta-Almeida et al. 2016) for seasonal time scales in Spain.

Minimum temperatures showed a slightly lower performance than TX, with correlation values around 0.85 during spring, autumn and winter regarding all simulations results, while during summer months, a correlation lower than 0.8 is observed with no significant changes with respect to errors. A good agreement with

observations is also found, and no significant statistical differences are yielded among PPs models for TN, as illustrated in the Taylor plot of Figure 3.12 with respect to the annual timescale. The values of the correlations are higher than 0.9, as an increasing number of days were averaged. It is noticed that for all simulations the correlation coefficients of TN yield lower values (0.92–0.93) for high resolution domains, which is in agreement with other works (Zhang et al. 2009, Soares et al. 2012). It could be deduced that the model performs better for TN with the PP2 scheme with positive BIAS near 2 °C. Table 3.8 depicts the best setup based on the daily values of statistical metrics, RMSE, MAE and for the daily maximum temperature separately for each of the 28 stations, during the 5 years and the four different experiments. These same calculations were derived as well as for TN. Some exceptions in Table 3.8, concern 6–7 stations, that their BIAS is in the range of 2–3.5 °C, and probably is related to the selection of the nearest model point to a station that is not located in a land cell or displays a significant height difference. From this analysis, it is evident that the setup that statistically outperforms with the lowest errors among stations is PP3, showing a significant improvement regarding the others, and thus representing the majority of the stations in Greece.

Table 3.8 Values of statistical metrics of root mean squared error (RMSE) and mean absolute error (MAE), regarding TX for the four different setups classified by station. The final column indicates the best setup by station.

Stations	PP2	PP3	PP5	PP7	PP2	PP3	PP5	PP7	BEST SETUP
	RMSE (ºC)				MAE (ºC)				
CORFU	3.87	3.8	3.58	3.87	3.45	3.38	3.18	3.45	**PP5**
HELLINIKON	1.92	1.82	1.94	1.85	1.51	1.42	1.55	1.46	**PP3**
HERAKLION	3.38	3.28	3.23	3.37	2.89	2.77	2.72	2.87	**PP5**
LARISSA	2.53	2.49	2.69	2.5	2.01	1.95	2.14	1.98	**PP3**
METHONI	3.09	2.98	2.99	3.05	2.7	2.57	2.56	2.66	**PP3**
SAMOS AIRPORT	1.95	1.88	1.74	1.92	1.53	1.46	1.39	1.5	**PP5**
SOUDA AIRPORT	2	1.85	2.3	1.97	1.57	1.4	1.82	1.53	**PP3**
ANCHIALOS	2.45	2.39	2.57	2.38	1.86	1.8	2.01	1.8	**PP3/PP7**
ARGOSTOLI	3.58	3.49	3.49	3.56	3.04	2.93	2.93	3.01	**PP3/PP5**
CHANIA	1.82	1.75	2.1	1.79	1.42	1.35	1.67	1.4	**PP3**
CHIOS	2.09	2.09	1.73	2.07	1.63	1.62	1.33	1.61	**PP5**

THESSALONIKI	2.73	2.68	2.76	2.71	2.26	2.2	2.33	2.24	**PP3**
ALEXANDROUPOLI	2.22	2.2	2.19	2.17	1.72	1.68	1.72	1.68	**PP3/PP7**
KOZANI	2.9	2.81	2.97	2.84	2.36	2.26	2.45	2.32	**PP3**
IOANNINA	2.25	2.15	2.22	2.25	1.73	1.64	1.74	1.7	**PP3**
MITILINI	3.98	3.92	3.64	3.99	3.38	3.31	3.09	3.38	**PP5**
AGRINIO	2.07	1.96	1.98	2.08	1.59	1.48	1.54	1.59	**PP3**
SKYROS	1.89	1.81	1.85	1.84	1.42	1.32	1.4	1.37	**PP3**
TRIPOLI	3.1	3.06	3.11	3.1	2.49	2.45	2.54	2.46	**PP3**
KALAMATA	2.28	2.22	2.08	2.23	1.82	1.77	1.66	1.79	**PP5**
NAXOS	1.91	1.93	1.56	1.87	1.49	1.52	1.2	1.45	**PP5**
MILOS	2.51	2.33	3.04	2.48	2.06	1.87	2.48	2.01	**PP3**
KYTHIRA	3.2	3.15	3.13	3.2	2.46	2.41	2.4	2.46	**PP5**
RHODOS	2.01	2.03	1.63	2.02	1.59	1.59	1.27	1.59	**PP5**
IERAPETRA	1.66	1.61	1.58	1.63	1.3	1.24	1.25	1.28	**PP3**
FLORINA	3.34	3.26	3.41	3.32	2.69	2.63	2.82	2.69	**PP3**
LAMIA	3.28	3.22	3.36	3.18	2.75	2.66	2.85	2.65	**PP7**
TANAGRA	2.08	2.08	1.95	2.05	1.56	1.54	1.47	1.54	**PP5**

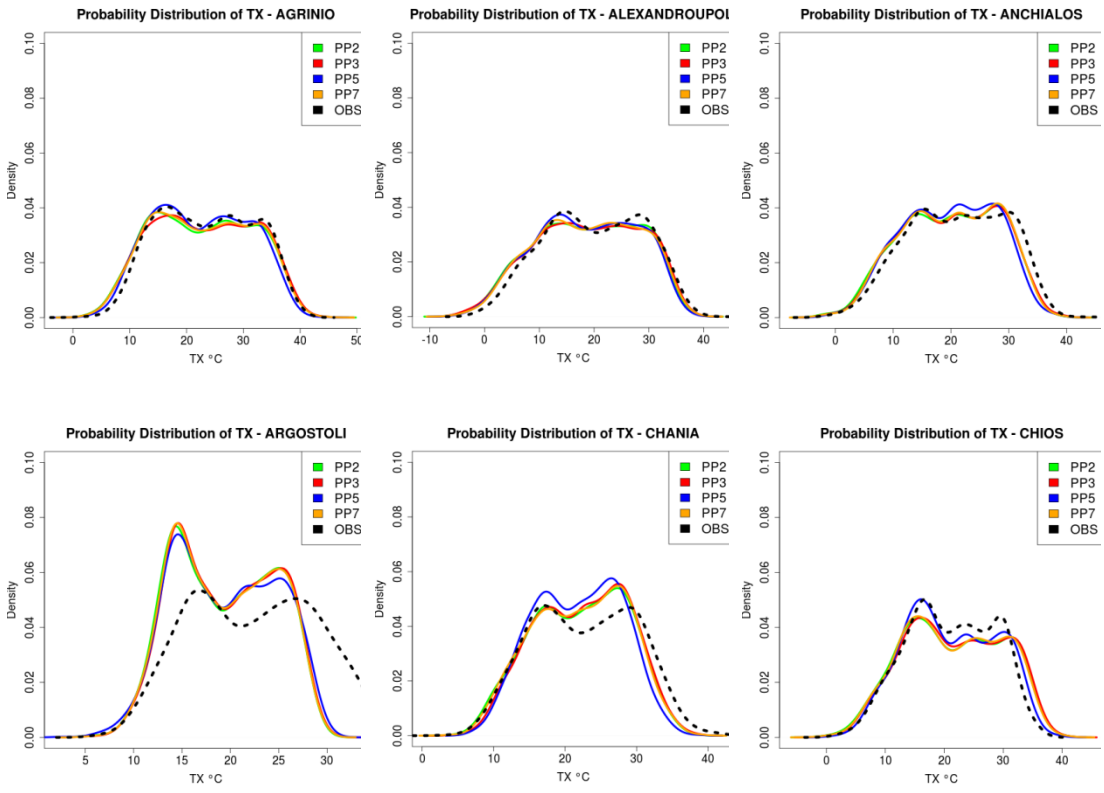

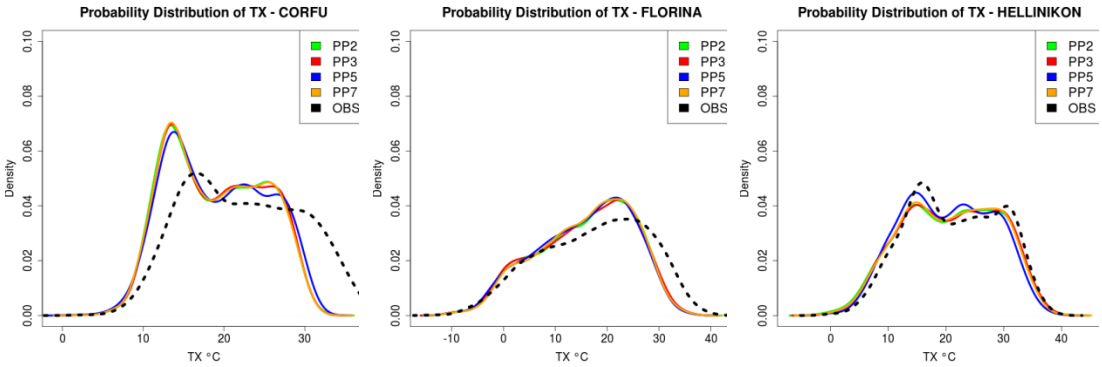
Probability Distribution of TX - CORFU
Probability Distribution of TX - FLORINA
Probability Distribution of TX - HELLINIKON
PP2
PP3
PP5
PP7
OBS
Density
TX °C

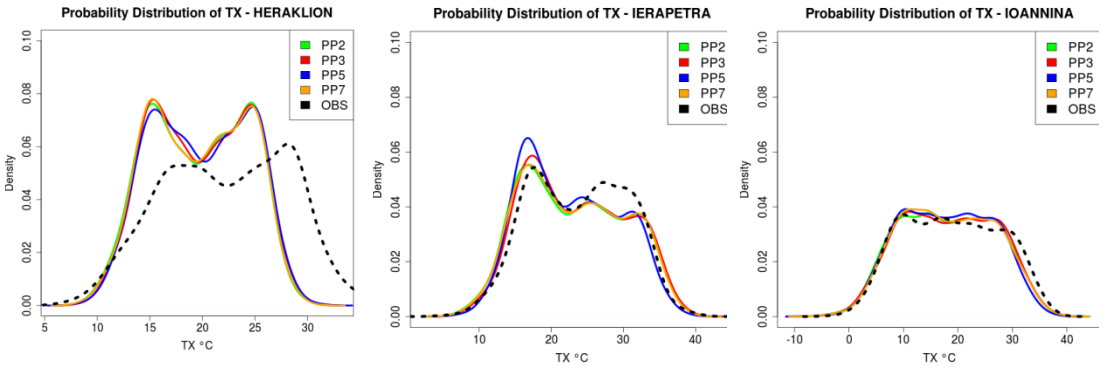
Probability Distribution of TX - HERAKLION
Probability Distribution of TX - IERAPETRA
Probability Distribution of TX - IOANNINA
PP2
PP3
PP5
PP7
OBS
Density
TX °C

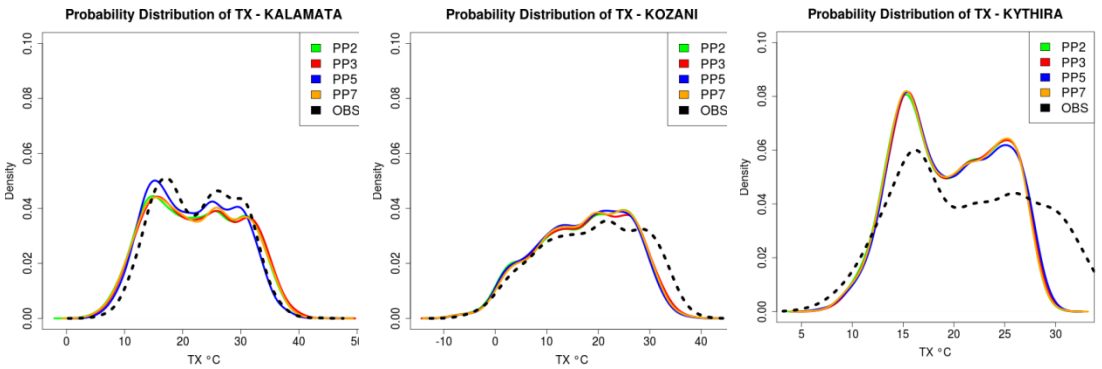
Probability Distribution of TX - KALAMATA
Probability Distribution of TX - KOZANI
Probability Distribution of TX - KYTHIRA
PP2
PP3
PP5
PP7
OBS
Density
TX °C

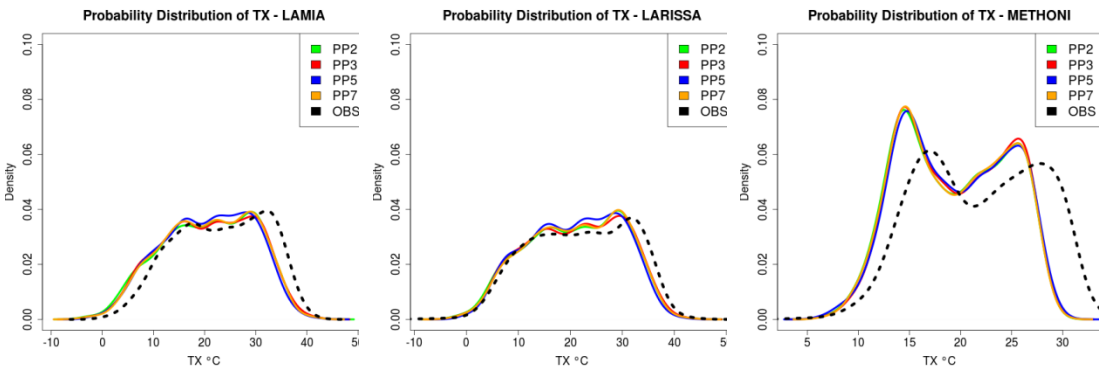
Probability Distribution of TX - LAMIA
Probability Distribution of TX - LARISSA
Probability Distribution of TX - METHONI
PP2
PP3
PP5
PP7
OBS
Density
TX °C

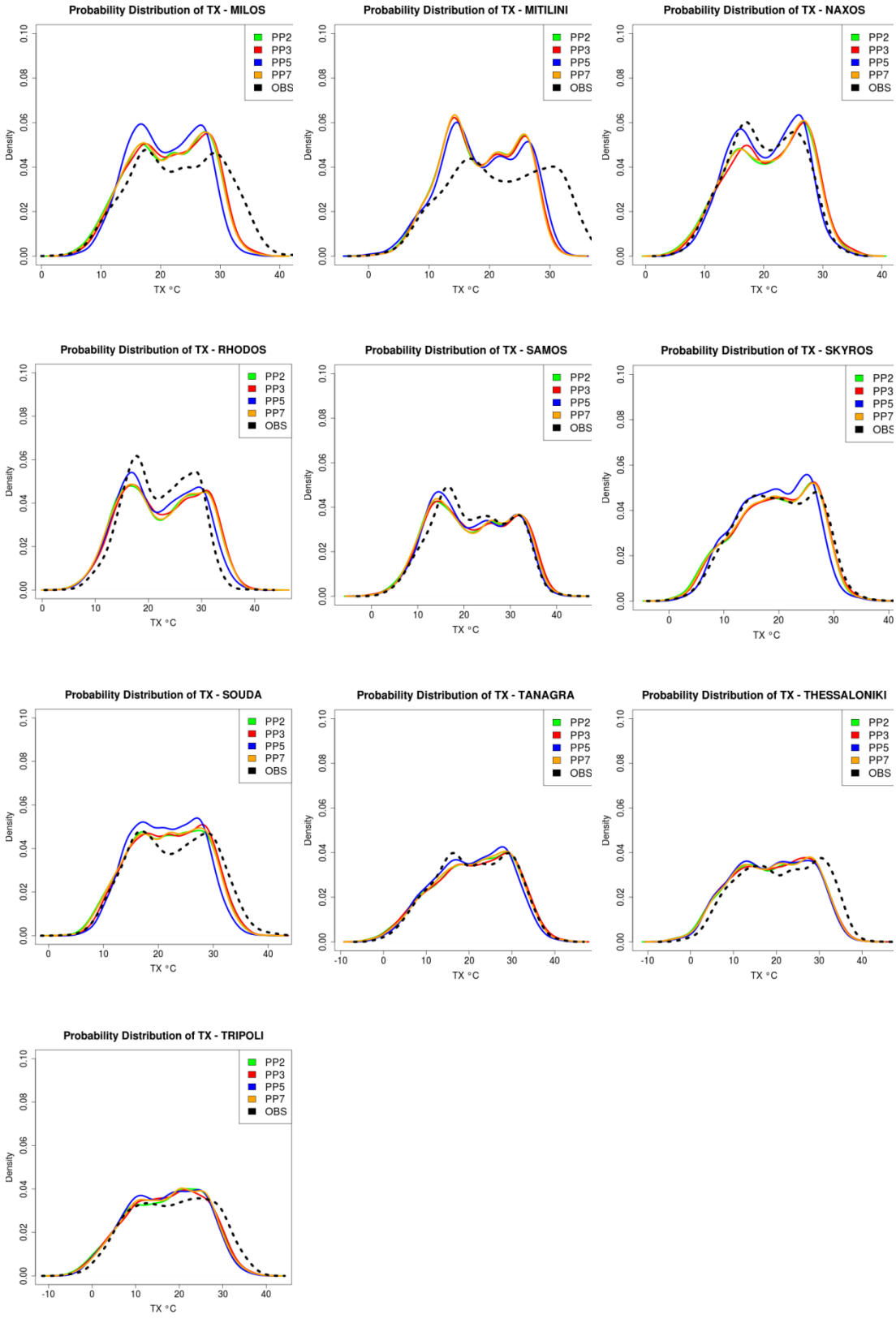

Figure 3.13 Comparison of the observed maximum temperatures by indicative weather stations, and the four simulated results in terms of probability distributions. The dashed line indicates the probability distribution of the observations.

The comparison of model results and observations in terms of probability distribution (see Figure 3.13) for all stations shows satisfied agreement for the majority of the stations for the 5-year period daily TX, as all WRF simulations follow the pattern distribution of observed data without having distinct differences among setups. In a few stations, a lower model - observations correspondence is found. More specifically, the Argostoli, Corfu, Florina, Heraklion, Kithira, Methoni, Milos and Mitilini stations illustrate a large shift towards colder values in the medium temperature range with higher density values. In Chania station all simulations appear to have higher density values for hotter temperatures, while in Ierapetra, the opposite behavior is observed. On the other hand, the TN probability distributions of WRF simulations (Figure 3.14), appear to have a large shift towards hotter values in the temperature range corresponding to either higher or lower density. This behavior justifies the consistent model's overestimation, especially during the summer period. Percentiles of TX and TN (the 1st, 5th, 25th, 75th, 95th and 99th) of daily values for the 28 stations, as well as for the total region of Greece were calculated, in order to focus on the examination of extremes described by the different simulations.

Percentiles for the WRF simulations versus observational percentiles are shown indicatively in Figure 3.15 and Figure 3.16, for TX and TN for several stations, and their average through the domain of Greece. As in the case of precipitation, the over- or underestimation of the simulations is indicated by the blue line, which represents the perfect description. It is evident that the maximum temperature is very well reproduced by WRF, with no significant differences between the different simulations, and with slight underestimation mostly for percentiles higher than 50%.

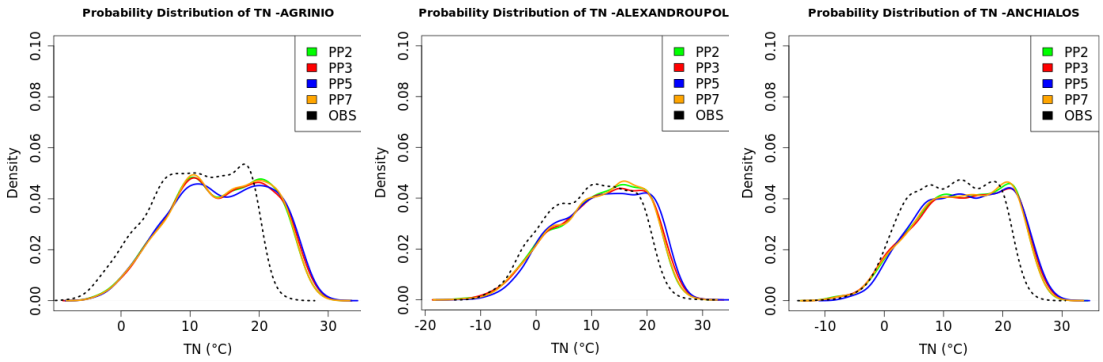

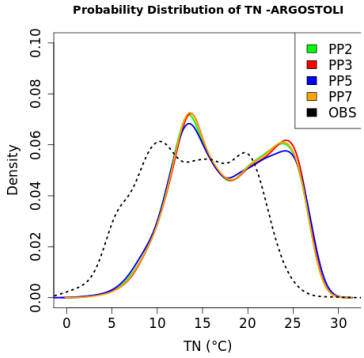
Probability Distribution of TN -ARGOSTOLI
PP2
PP3
PP5
PP7
OBS
Density
TN (°C)

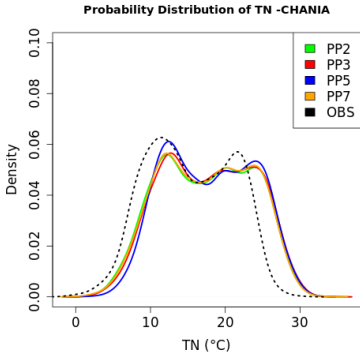
Probability Distribution of TN -CHANIA
PP2
PP3
PP5
PP7
OBS
Density
TN (°C)

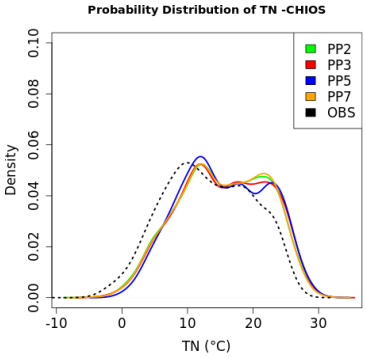
Probability Distribution of TN -CHIOS
PP2
PP3
PP5
PP7
OBS
Density
TN (°C)

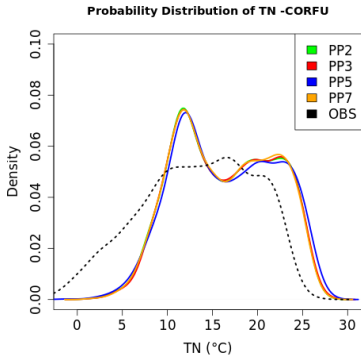
Probability Distribution of TN -CORFU
PP2
PP3
PP5
PP7
OBS
Density
TN (°C)

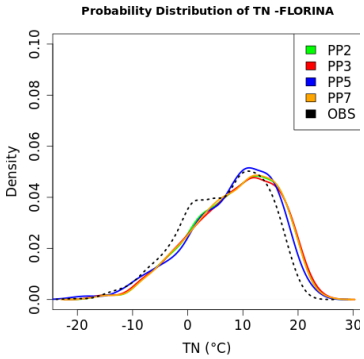
Probability Distribution of TN -FLORINA
PP2
PP3
PP5
PP7
OBS
Density
TN (°C)

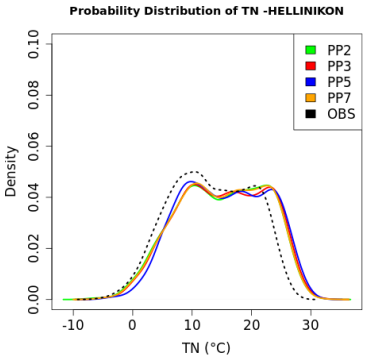
Probability Distribution of TN -HELLINIKON
PP2
PP3
PP5
PP7
OBS
Density
TN (°C)

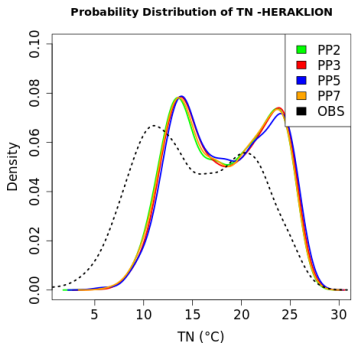
Probability Distribution of TN -HERAKLION
PP2
PP3
PP5
PP7
OBS
Density
TN (°C)

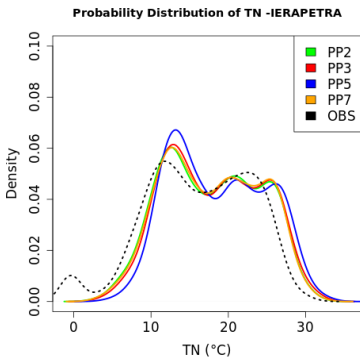
Probability Distribution of TN -IERAPETRA
PP2
PP3
PP5
PP7
OBS
Density
TN (°C)

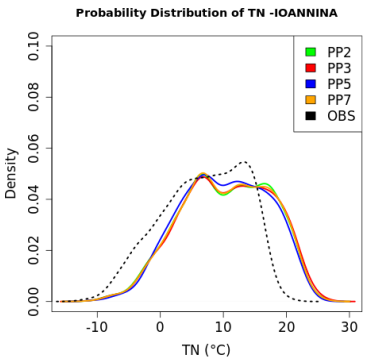
Probability Distribution of TN -IOANNINA
PP2
PP3
PP5
PP7
OBS
Density
TN (°C)

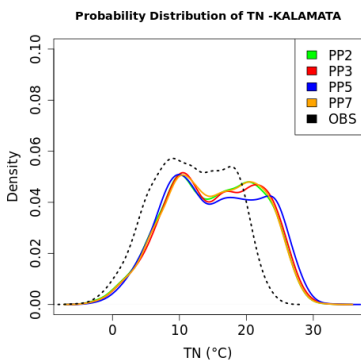
Probability Distribution of TN -KALAMATA
PP2
PP3
PP5
PP7
OBS
Density
TN (°C)

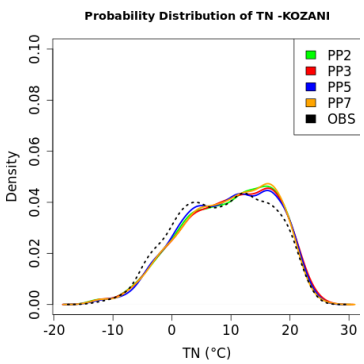
Probability Distribution of TN -KOZANI
PP2
PP3
PP5
PP7
OBS
Density
TN (°C)

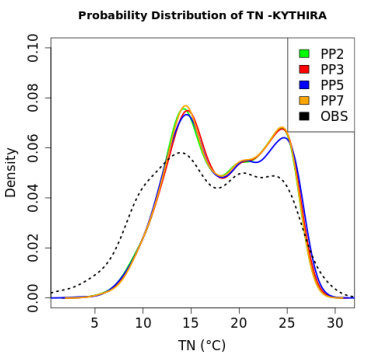
Probability Distribution of TN -KYTHIRA
PP2
PP3
PP5
PP7
OBS
Density
TN (°C)

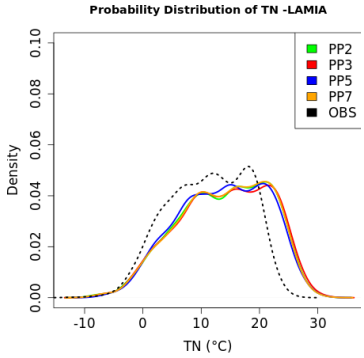
Probability Distribution of TN -LAMIA
PP2
PP3
PP5
PP7
OBS
Density
TN (°C)

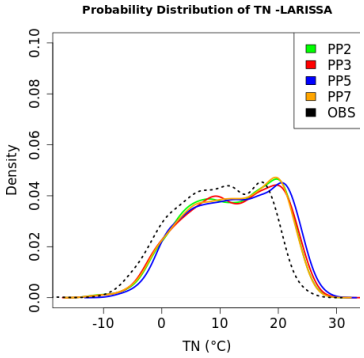
Probability Distribution of TN -LARISSA
PP2
PP3
PP5
PP7
OBS
Density
TN (°C)

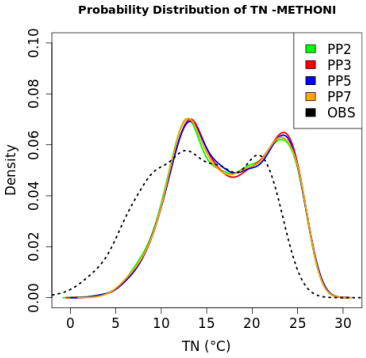
Probability Distribution of TN -METHONI
PP2
PP3
PP5
PP7
OBS
Density
TN (°C)

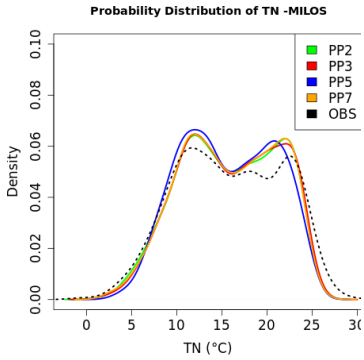
Probability Distribution of TN -MILOS
PP2
PP3
PP5
PP7
OBS
Density
TN (°C)

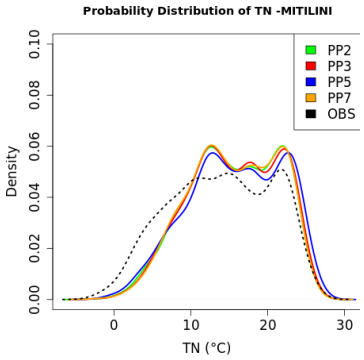
Probability Distribution of TN -MITILINI
PP2
PP3
PP5
PP7
OBS
Density
TN (°C)

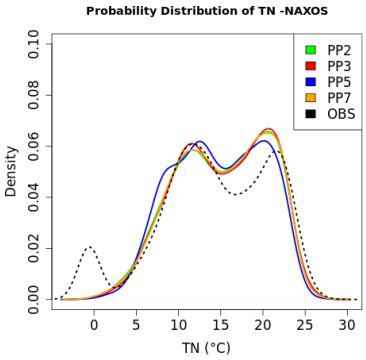
Probability Distribution of TN -NAXOS
PP2
PP3
PP5
PP7
OBS
Density
TN (°C)

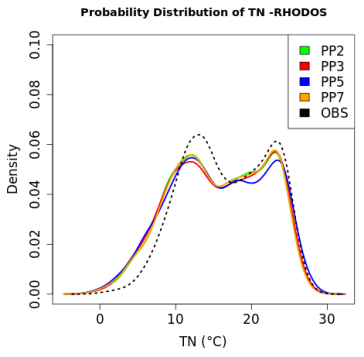
Probability Distribution of TN -RHODOS
PP2
PP3
PP5
PP7
OBS
Density
TN (°C)

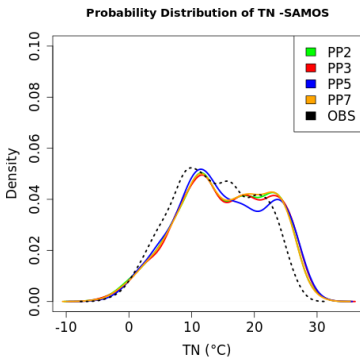
Probability Distribution of TN -SAMOS
PP2
PP3
PP5
PP7
OBS
Density
TN (°C)

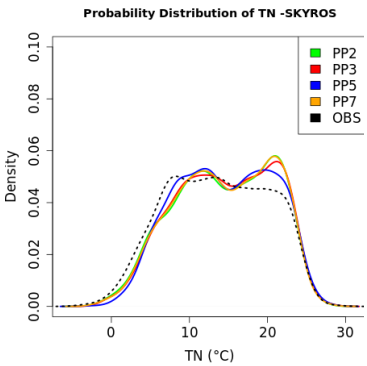
Probability Distribution of TN -SKYROS
PP2
PP3
PP5
PP7
OBS
Density
TN (°C)

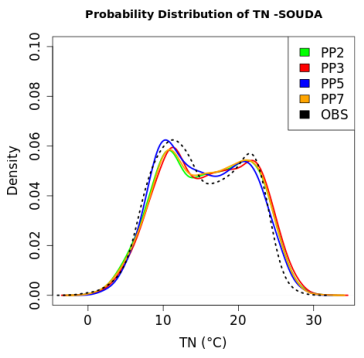
Probability Distribution of TN -SOUDA
PP2
PP3
PP5
PP7
OBS
Density
TN (°C)

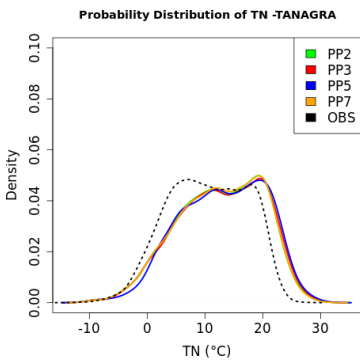
Probability Distribution of TN -TANAGRA
PP2
PP3
PP5
PP7
OBS
Density
TN (°C)

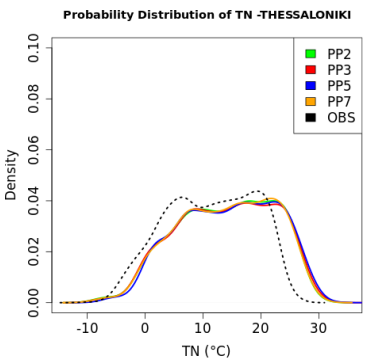
Probability Distribution of TN -THESSALONIKI
PP2
PP3
PP5
PP7
OBS
Density
TN (°C)

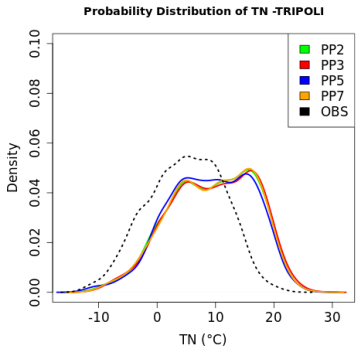

Figure 3.14 Comparison of the observed minimum temperatures by indicative weather stations, and the four simulated results in terms of probability distributions. The dashed line indicates the probability distribution of the observations.

There are some stations, e.g., Argostoli or Mitilini, that appear to have larger deviations in the extreme percentiles, and others like Naxos that show very good performances in predicting the extremes. In accordance, regarding the minimum temperature, all models' setups indicate no significant differences in simulating percentiles as well, however in what concerns their behavior an almost systematic overestimation is observed overall. Probably, as (Pérez et al. 2014) point out in the case study of the Canary Islands, these deviations could be due to the insufficient temperature correction on the representation of mountainous areas, because the altitude difference between the model and stations points has strong influence.

TX

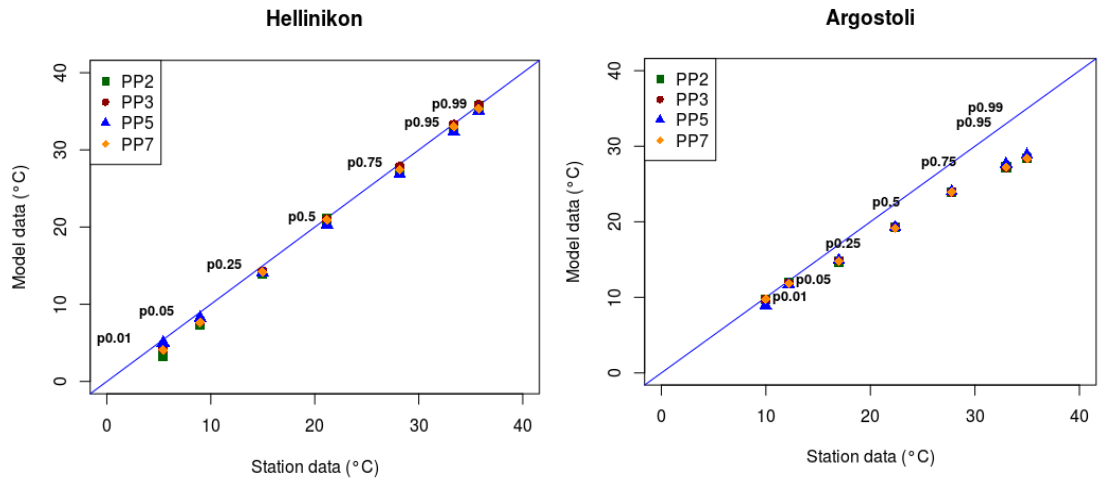

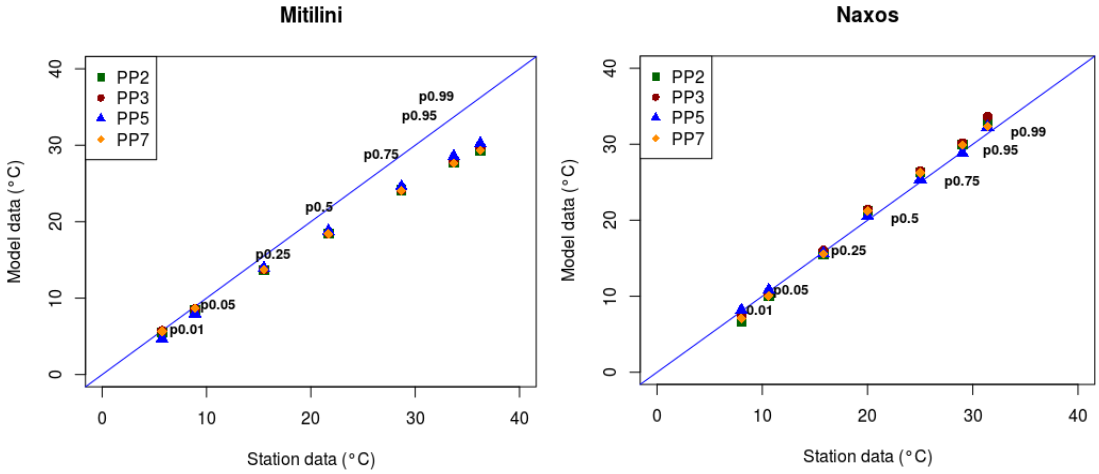
Mitilini
PP2
PP3
PP5
PP7
p0.99
p0.95
p0.75
p0.5
p0.25
p0.05
p0.01
Model data (°C)
Station data (°C)
0
10
20
30
40

Naxos
PP2
PP3
PP5
PP7
p0.99
p0.95
p0.75
p0.5
p0.25
p0.05
p0.01
Model data (°C)
Station data (°C)
0
10
20
30
40

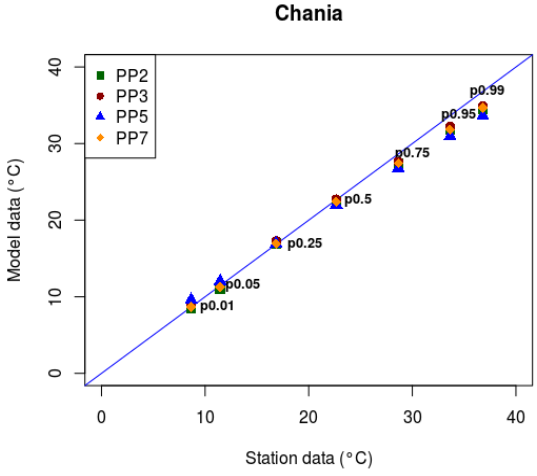
Chania
PP2
PP3
PP5
PP7
p0.99
p0.95
p0.75
p0.5
p0.25
p0.05
p0.01
Model data (°C)
Station data (°C)
0
10
20
30
40

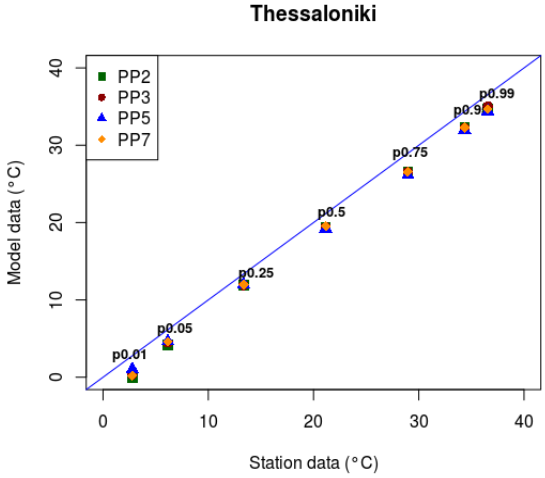
Thessaloniki
PP2
PP3
PP5
PP7
p0.99
p0.95
p0.75
p0.5
p0.25
p0.05
p0.01
Model data (°C)
Station data (°C)
0
10
20
30
40

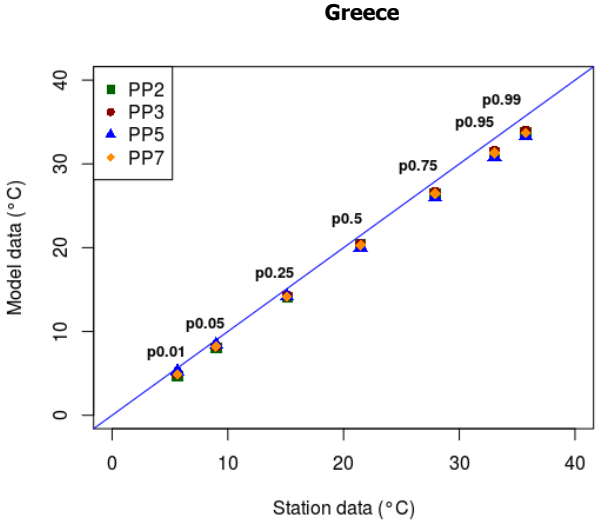
Greece
PP2
PP3
PP5
PP7
p0.99
p0.95
p0.75
p0.5
p0.25
p0.05
p0.01
Model data (°C)
Station data (°C)
0
10
20
30
40

Figure 3.15 Percentiles of daily maximum temperature for the four WRF simulations vs. observational percentiles for some indicative stations and their average for the region of Greece (D02). Straight line represents the perfect performance.

TN

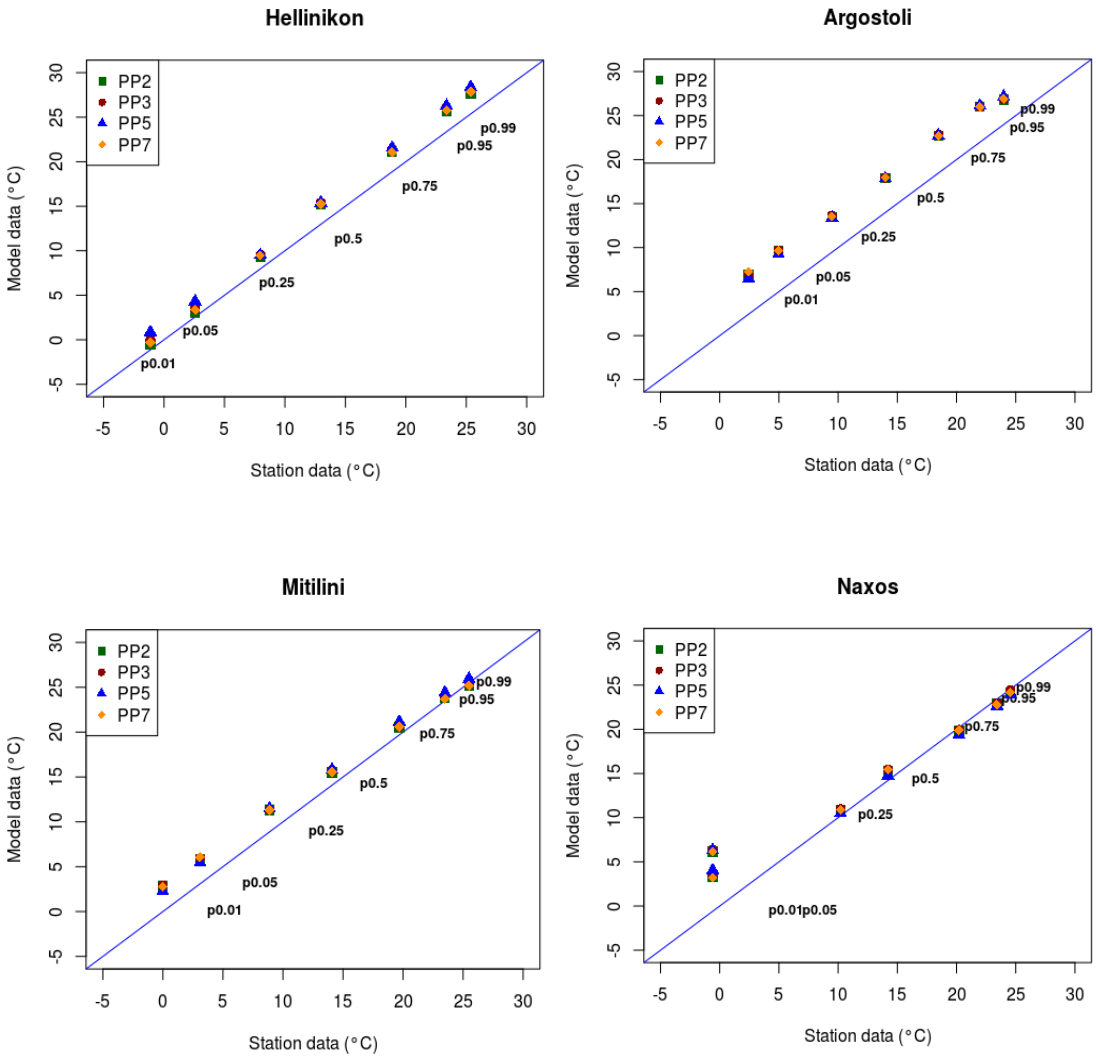

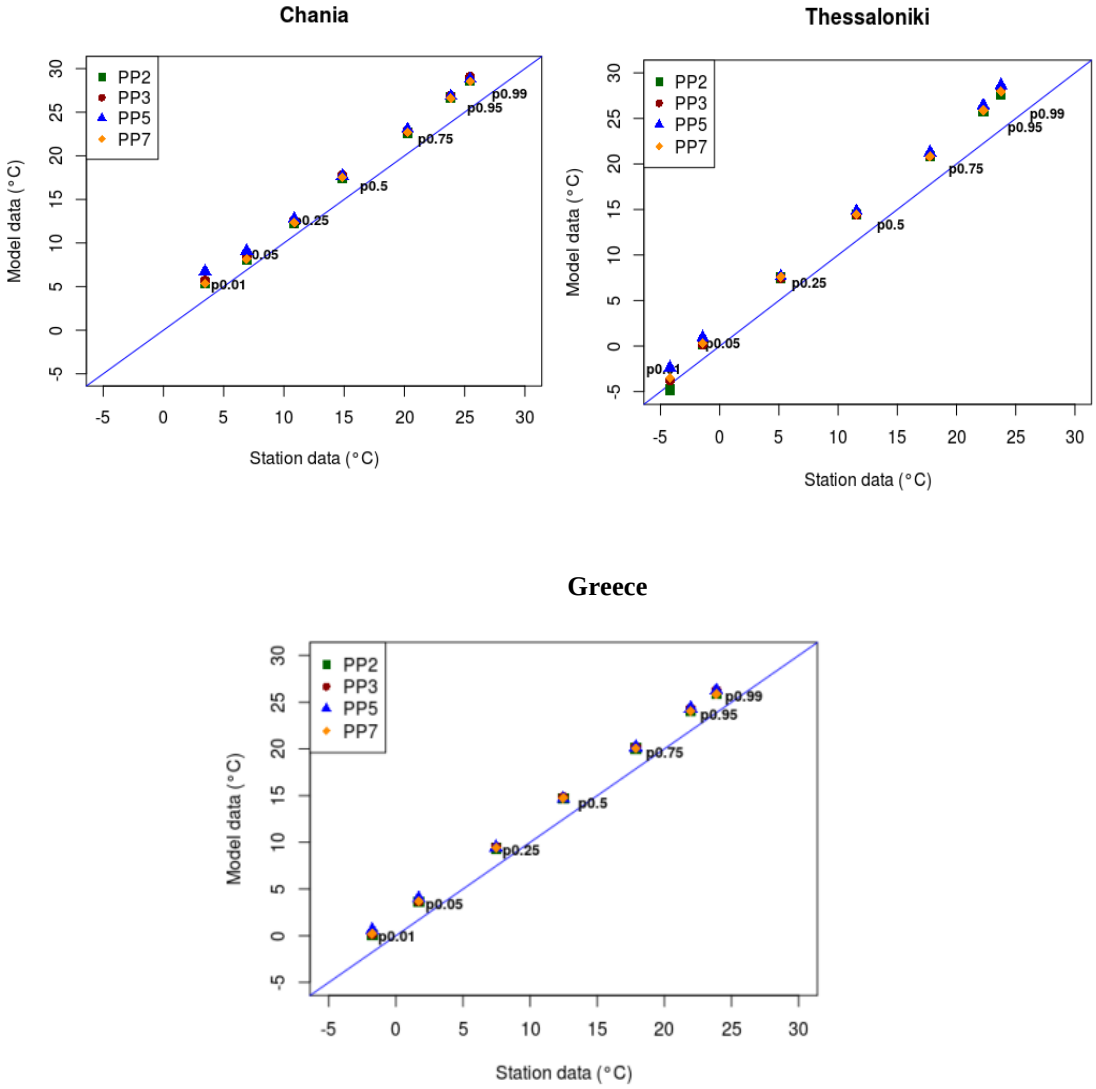

Figure 3.16 Percentiles of daily minimum temperatures for the four WRF simulations vs. observational percentiles for some indicative stations and their average for the region of Greece (D02). Straight line represents the perfect performance.

3.2.2 Precipitation

Monthly precipitation time-series are illustrated in Figure 3.17. The seasonal pattern of monthly precipitation is well captured by the majority of the schemes, also observed in the study of García-Díez et al. 2015, remarking the highest precipitation during winter and lowest during summer. The black, dashed line illustrates the seasonal variability of monthly precipitation derived from the average values of the available stations, which is noticed on the models' results. There are obvious similarities in the precipitation patterns among all experiments and observed data for the 5 years of

comparison, yielding smoothly the precipitation's inter-annual variability, especially during the wettest months and summer periods characterized by limited rainfall. Some differences show that in general, there is an overestimation of precipitation compared to ground data for all setups, and this probably is caused by excessive wintertime precipitation (Caldwell 2010). On the other hand, ERA-Interim appears to underestimate winter precipitation from November to January. Some cases of precipitation's underestimation are related to the PP3 setup during the study period, and as this simulation appears to have the less overestimation among setups.

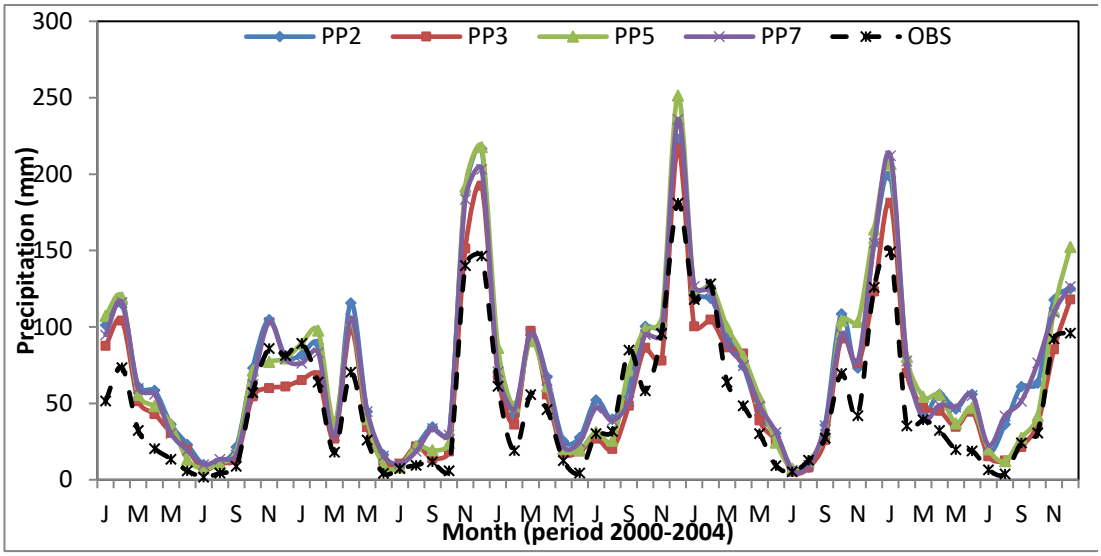

Figure 3.17 Observed and simulated mean monthly cumulative precipitation values on the total grid stations' points, for the four different simulations (PP2, PP3, PP5, PP7), for the high-resolution domain of Greece during 2000–2004.

This fact is also confirmed with the 5-yearly estimation of statistical errors based on daily precipitation values in Table 3.9, where PP3 shows the best performance, with positive percentage BIAS of about 19%, while the other models have values of over 40%. As being observed, RMSE, MAE and COR results as well show slightly better performance for PP3 compared to the other simulations. It is worthy to note that PP3 bias (19%) is significantly smaller than the ±50% reported in the Third Assessment Report of the Intergovernmental Panel on Climate Change by (Giorgi et al. 2001) for RCMs, and while not small, it is close to the range of the best performing RCMs shown in several studies (Zhang et al. 2009; Rauscher et al. 2010; Heikkilä et al. 2011; Soares et al. 2012). PP3 uses the Betts–Miller–Janjic cumulus parameterization, WSM6 for microphysics, the Mellor–Yamada–Janjic as PBL scheme and Monin-Obukhov

similarity theory (Table 3.7). Statistical metrics between ERA-Interim and the WRF results indicate some loss of performance in the WRF model, with an underestimation of 5.5% PBIAS value in the total of stations' grid points.

Table 3.9 Precipitation Statistical metrics of the four simulations for all stations daily precipitation (RR) for 2000–2004, over the area of Greece

		PP2	PP3	PP5	PP7	ERA-I
RR	PBIAS (%)	44.2	19.1	42.3	41.2	-5.53
	RMSE (mm)	7.1	6.4	6.9	7.1	5.46
	MAE (mm)	2.31	2.01	2.22	2.27	1.66
	COR	0.43	0.48	0.45	0.46	0.53

The study of the spatial distribution of 5-annual mean precipitation in WRF simulations and observations shows a clear topographical dependency (Figure 3.18). The analysis of the amount of precipitation yields large differences between plain areas and higher elevations, with maximum values of annual precipitation found in the western part of the country, related to fronts passages with increased vertical lift due to orographic enhancement in mountainous locations. All simulations depict similarly the spatial pattern of precipitation, with excessive rain being observed only in mountainous locations; however, there are no representative stations to validate such precipitation amounts.

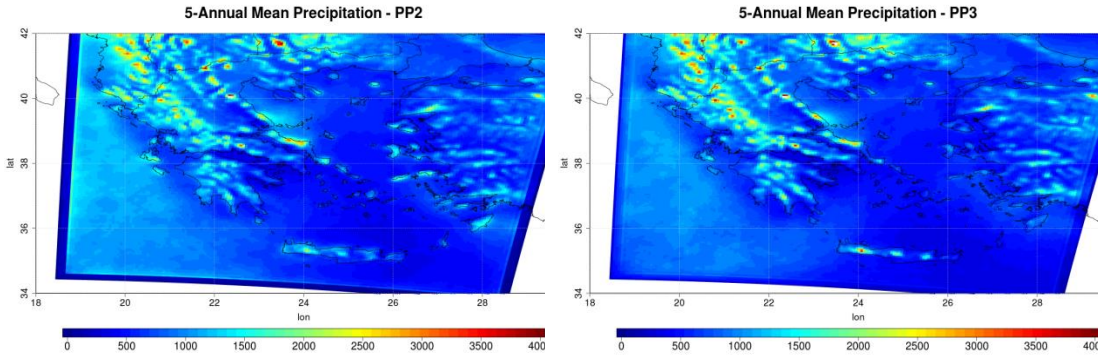

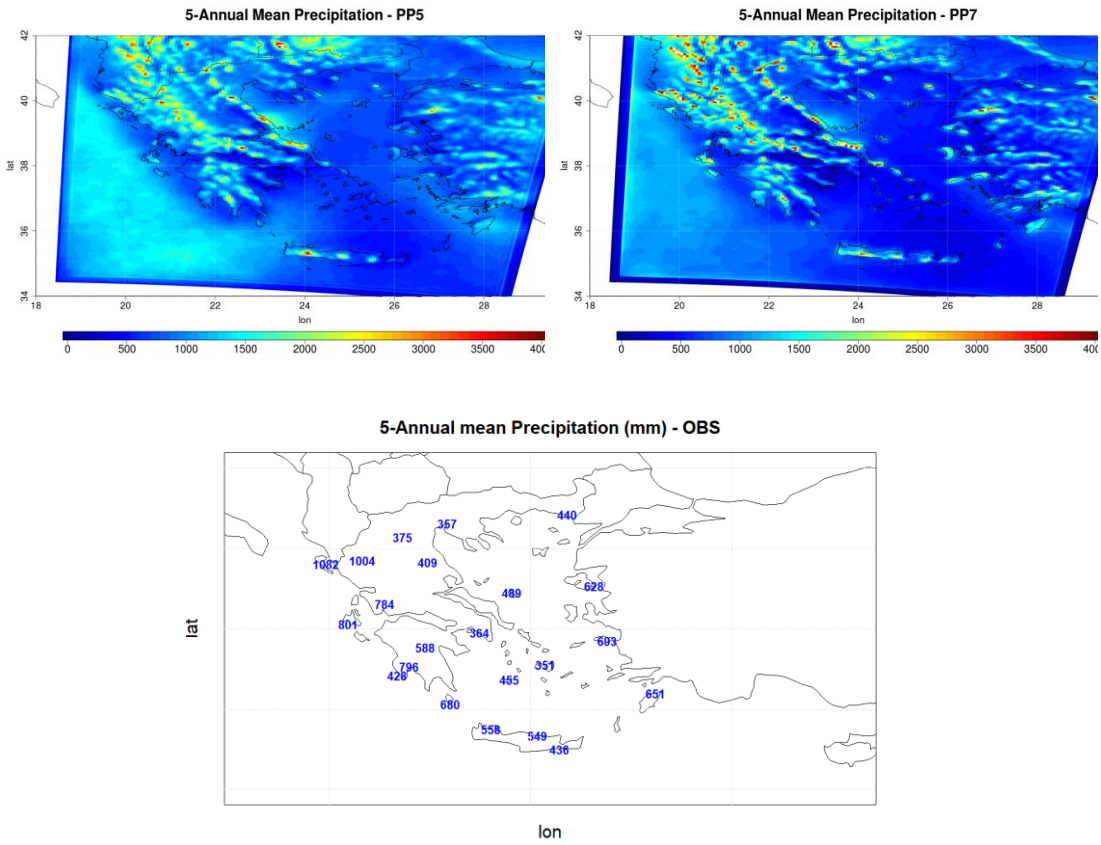

Figure 3.18 WRF Spatial distribution of the annual precipitation (in mm) for the 5-km resolution of the region of Greece (D02), for the selected period 2000-2004.

The same behavior is observed for all model setups, although PP7 seems to produce higher amounts of precipitation during the examined 5-year period than PP2 and PP3. This fact could be related to the interaction of the microphysical scheme with the association of PBL (MYJ) scheme, which is in line with other studies with higher precipitation totals and more convective precipitation (Schwartz et al. 2010; Kioutsioukis et al. 2016). Additionally, for precipitation over areas of complex topography, wet bias is particularly found to be common to several RCMs (Gao et al. 2015; Guo et al. 2018), and is probably caused by an overestimation of orographic precipitation enhancement (Gerber et al. 2018), and/or to an inaccurate PBL simulation (Gao et al. 2015; Xu and Yang 2015; Xu et al. 2019).

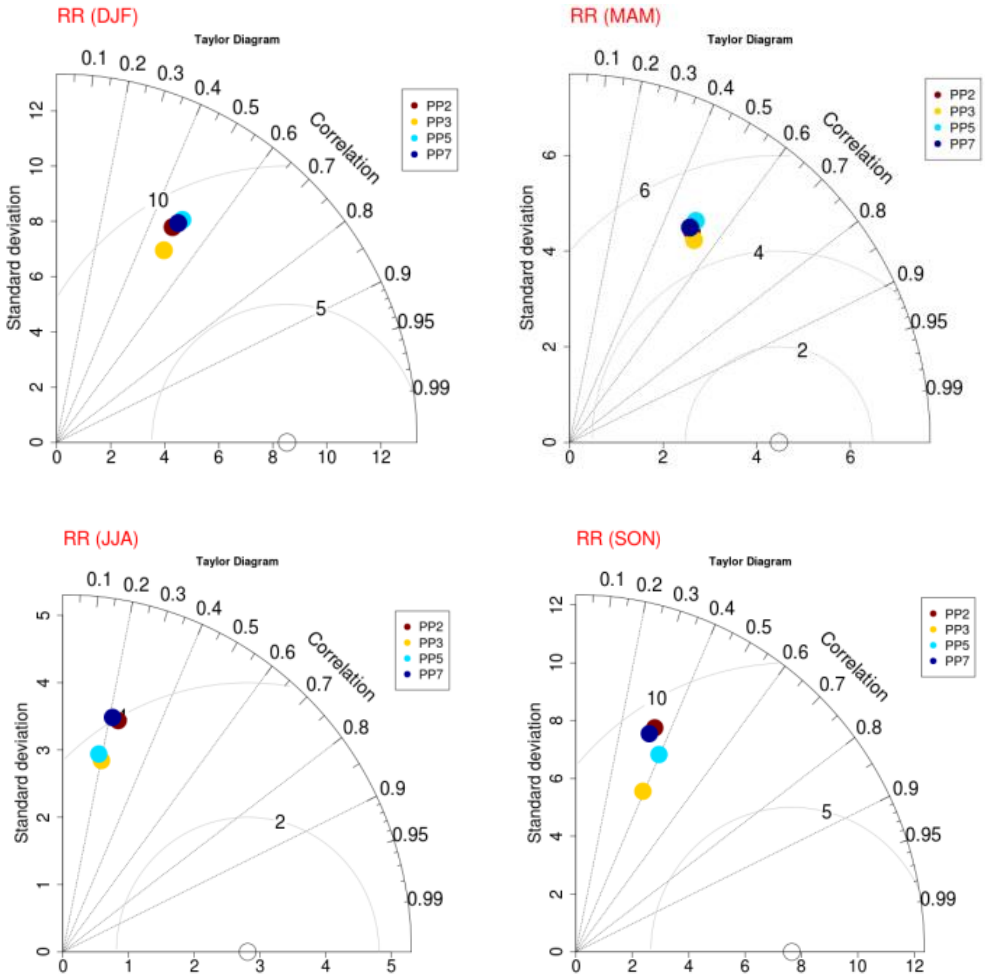

Figure 3.19 Seasonal Taylor diagrams of the four WRF simulations (PP2, PP3, PP5, PP7) with respect to observed daily precipitation (RR) for the high-resolution domain of Greece (D02).

The Taylor diagrams shown in Figure 3.19 provide the comparative assessment of the four different model experiments to the choice of the physical parameterizations, to simulate the seasonal spatial pattern of daily precipitation during the examined period. The simulated results are compared to all observational data from 23 stations. The best simulation is marked by the largest correlation, smaller CRMSE and being closer to the observed standard deviation. It is found that the highest correlation in the range of 0.5–0.6 is observed during the winter and spring seasons, with the poorest correlation in summer, resulting though in the lowest centered RMSE values (~3.5 mm). It is well-known that the satisfied representation of summer precipitation is a demanding field for any model, and as the convective processes prevail, it is not easy to determine confidently the appropriate cumulus scheme. The poor performance of model setups is observed during winter and autumn, where the highest CRMSE values are displayed.

All models' simulations seem to have similar performance; however, PP3 appears to have slightly lowest errors during all seasons, thus yielding a better performance compared to the rest of the setups. Because of the heterogeneous spatial pattern of precipitation in Greece, which is strongly associated with the orography, the extended coastline (see Figure 3.1) and the limited number of stations for comparison, statistical errors are also displayed per station in detail in Figure 3.20:

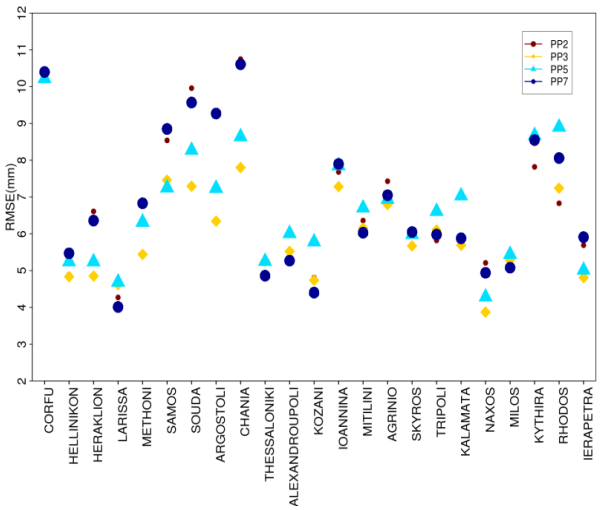

(a)

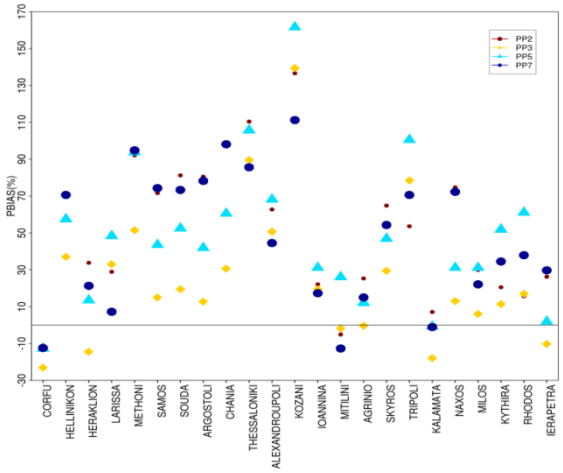

(b)

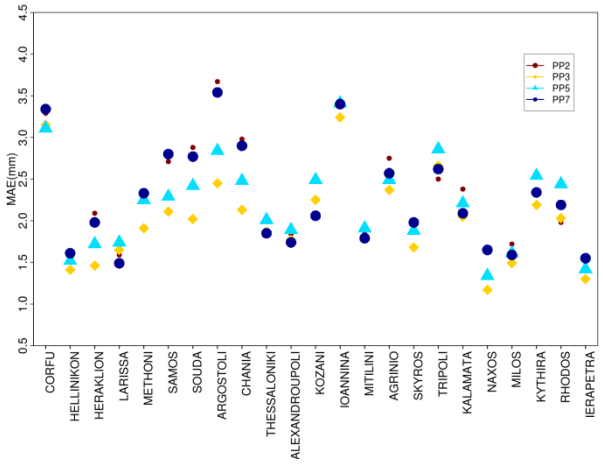

(c)

Figure 3.20 (a) Root mean square error, (b) pbias and (c) correlation coefficient of precipitation (RR) per HNMS station, for the four different physics parameterisations schemes (PP2, PP3, PP5, PP7) for 2000-2004.

This analysis allows also exploring which of the simulations outperforms by station, which of the stations statistically is better validated from the WRF model, and finally

which setup represents outmost the majority of the stations in Greece. It is evident that the prevailing simulation with the lowest errors among stations is represented by PP3, showing a significant improvement regarding the others.

Precipitation

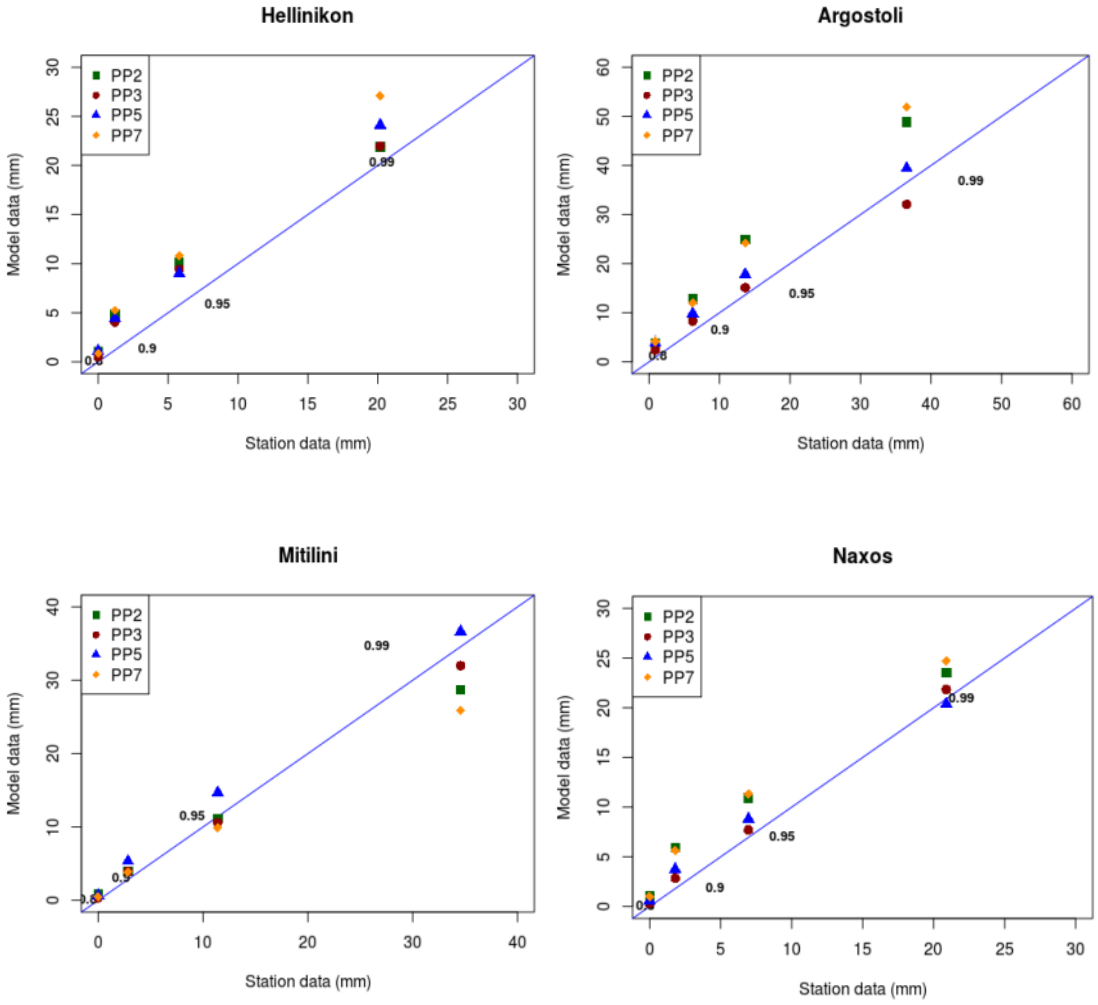

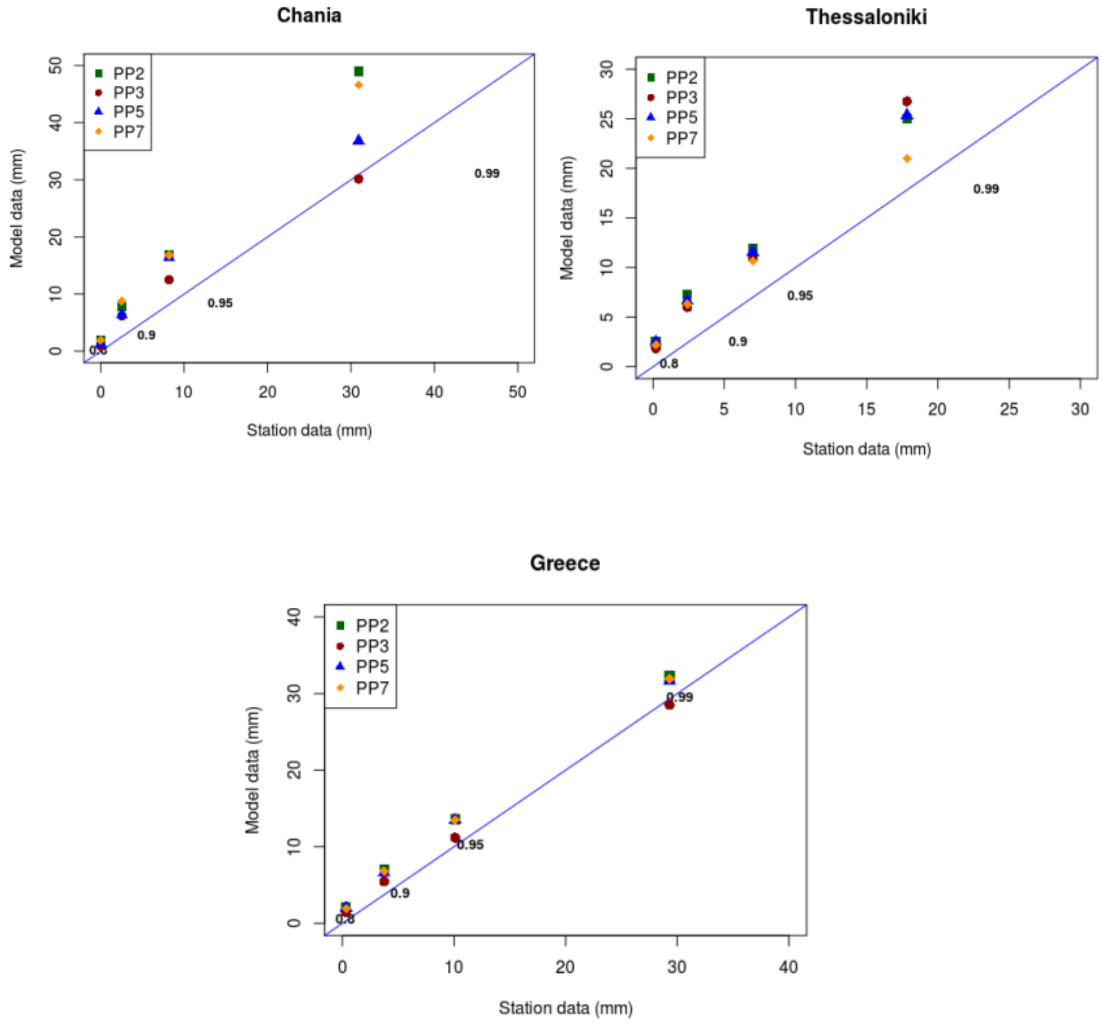

Figure 3.21 Percentiles of daily precipitation for the four WRF simulations vs. observational percentiles for the region of Greece and some indicative stations. Straight (blue) line represents the perfect performance.

In general, regional models still misrepresent daily precipitation and precipitation extremes because of resolution or/and parameterization deficiencies (Soares et al. 2012). The precipitation analysis was extended on studying the intensity of daily precipitation; thus, the 80th, 90th, 95th and 99th higher ranking percentiles were calculated. This analysis is very important for climate change assessment related to extreme weather events, drought and flooding events, that have significant socioeconomic impacts on the global community. The results are shown in Figure 3.21, where the WRF percentiles distribution is plotted versus the observational data for the domain of Greece and several indicative stations distributed all over Greece during

these 5 years. The straight (blue) line depicts a perfect performance, indicating the over- or under-estimation of the simulated values compared to the observations.

The percentiles, obtained for the area of Greece, show that all WRF simulations follow the observational percentiles very well. The PP3 model setup outperforms remarkably well the extreme percentile 99%, while the other setups tend to slightly overestimate rainfall for 90% and 95% extremes. A general inspection of the percentiles results by station shows that WRF dynamical downscaling simulations overestimate extreme precipitation events, with few exceptions regarding the 99% percentile, and also that PP3 model simulation tends to reproduce rainfall extremes better. than the other setups.

In Table 3.10, precipitation verification statistics are presented in the contingency table for four distinct threshold values of precipitation compared to the 5-year observational data. This table depicts the results by station, only for the best performed simulation PP3. The forecasts show reasonable skills for both low and medium intensity rainfall days, as the model runs show POD values of (0.7–0.86) and (0.6–0.85), respectively. Regarding extreme rainfall events, the majority of the stations indicate POD values close to 0.5–0.6, followed by FAR values of (0.5–0.7), meaning that a very low percentage of these rain events (observed and/or predicted) were correctly forecast. Probably the rare episode of convective precipitation is often missed or underestimated by the model and the convective scheme.

Table 3.10 Probability of detection (POD), false alarm ratio (FAR) and critical success index (CSI), are based on the contingency table, described on Table A.2 (APPENDIX), for four thresholds calculated for each station separately, only for PP3.

PP3 sim	1mm/day			2.5mm/day			10mm/day			20mm/day		
STATIONS	POD	FAR	CSI	POD	FAR	CSI	POD	FAR	CSI	POD	FAR	CSI
CORFU	0.74	0.43	0.46	0.69	0.44	0.45	0.45	0.51	0.31	0.29	0.61	0.20
HELLINIKON	0.79	0.58	0.43	0.75	0.63	0.33	0.44	0.70	0.22	0.32	0.79	0.14
HERAKLION	0.71	0.43	0.54	0.63	0.46	0.41	0.51	0.60	0.29	0.32	0.63	0.21
LARISSA	0.69	0.59	0.40	0.62	0.62	0.31	0.37	0.71	0.19	0.08	0.94	0.03
METHONI	0.71	0.65	0.30	0.65	0.66	0.29	0.49	0.76	0.19	0.36	0.79	0.16
SAMOS AIRPORT	0.86	0.45	0.49	0.85	0.43	0.51	0.71	0.53	0.40	0.47	0.68	0.24
SOUDA AIRPORT	0.74	0.47	0.49	0.72	0.49	0.42	0.55	0.68	0.25	0.61	0.73	0.23
ARGOSTOLI	0.77	0.50	0.47	0.75	0.51	0.43	0.55	0.61	0.30	0.40	0.61	0.25

CHANIA	0.72	0.53	0.39	0.67	0.57	0.35	0.53	0.72	0.23	0.50	0.75	0.20
THESSALONIKI	0.70	0.65	0.36	0.64	0.67	0.28	0.52	0.71	0.23	0.09	0.97	0.03
ALEXANDROUPOLI	0.72	0.54	0.39	0.69	0.57	0.36	0.58	0.61	0.30	0.35	0.81	0.14
KOZANI	0.76	0.66	0.35	0.69	0.70	0.26	0.47	0.82	0.15	0.14	0.98	0.02
IOANNINA	0.81	0.54	0.44	0.76	0.56	0.39	0.46	0.62	0.26	0.37	0.60	0.24
MITILINI	0.79	0.43	0.53	0.76	0.46	0.46	0.62	0.49	0.39	0.46	0.66	0.24
AGRINIO	0.73	0.51	0.42	0.64	0.52	0.38	0.50	0.50	0.34	0.28	0.70	0.17
SKYROS	0.76	0.53	0.42	0.71	0.52	0.40	0.47	0.72	0.21	0.39	0.71	0.20
TRIPOLI	0.78	0.59	0.40	0.71	0.62	0.33	0.60	0.71	0.24	0.37	0.85	0.12
KALAMATA	0.74	0.42	0.49	0.66	0.45	0.43	0.47	0.46	0.34	0.27	0.59	0.20
NAXOS	0.73	0.51	0.45	0.69	0.50	0.41	0.38	0.71	0.20	0.17	0.79	0.10
MILOS	0.81	0.50	0.42	0.75	0.52	0.42	0.44	0.64	0.25	0.21	0.77	0.12
KYTHIRA	0.86	0.47	0.44	0.81	0.50	0.44	0.55	0.63	0.29	0.48	0.71	0.22
RHODOS	0.84	0.43	0.51	0.80	0.43	0.50	0.54	0.64	0.28	0.44	0.69	0.22
IERAPETRA	0.65	0.52	0.42	0.58	0.55	0.34	0.35	0.59	0.23	0.22	0.67	0.15

Given the small discrepancies between the results of these two setups in temperatures and taking into account the noticeable difference in the results of PP3 for precipitation, PP3 was recommended as a good choice for the upcoming climate simulations. Several studies have supported the PP3 WRF setup (MYJ, WSM6, RRTMG, NOAH, BMJ) for climate or forecasting applications as overall, more balanced behavior is displayed for both surface variables; the annual precipitation cycle is captured adequately, and closer agreement with the observational datasets is found regarding temperatures and their extreme values [2,37-39,44,88,94,95]. It should be mentioned that this study was based on previous research that has already examined a combination of physics parameterizations, and performed sensitivity tests for the area of interest, analyzing the effect of the chosen schemes; therefore, an in-depth analysis of physical scheme inter-comparison was not in the scope of the current work. The use of RCMs for the simulation of historical, current and future climate, particularly in view of the warming climate, is continuously increasing, as it is considered important for studying regional climate changes. It is considered important to emphasize that the current study aimed at identifying an appropriate WRF model set up in order to perform in the future high-resolution historical climatology simulation, by downscaling ERA-interim reanalysis to the domain of Greece.

Key Remarks

- ***Obvious similarities were found in the precipitation patterns among simulations and observations during the 5-yr period, verifying smoothly the precipitation's inter-annual variability.***
- ***The lowest positive percentage BIAS of about 19% was calculated for the selected combination of physics parameterizations PP3 while for the rest of the setups, values of over 40% were obtained.***
- ***PP3 model simulation reproduced rainfall extremes better than the other setups, even though the model overestimated extreme precipitation events with few exceptions regarding the 99% percentile.***
- ***A good match between modeled and observed data for the maximum and minimum temperatures for all tested simulations with high correlation above 0.9, negative bias around 1–1.5 °C, and a positive bias of around 2 °C, respectively.***
- ***Good performance was deduced with regards to the examination of extreme percentiles for temperatures and precipitation.***
- ***PP3 showed a slightly better performance for the maximum temperature in the majority of the stations, while PP2 for the minimum temperature***
- ***The study advocates that the PP3 model setup, which corresponds to the combination of physics schemes, including WSM6, MYJ, and BMJ, is suitable for high resolution climate modeling studies for the domain of Greece, as the specific parameterization schemes simulate better the temperature and precipitation fields compared to the rest of the investigated setups.***

3.3 Sensitivity test 3

In this section, sensitivity experiments were performed in order to investigate the impact of different initializations of input data on WRF model output variables with different types of time integration approaches, focusing on high resolution integrations for the area of Greece. This final sensitivity test included three types of experiments: The first experiment involved re-initialization from the driving reanalysis data on a monthly basis while the last 4 days of the previous month were regarded as model spin-up for the following month, as an overlap period. In the second experiment, the model was initialized every 6 months, with one month spin-up period, and the third experiment was a long-term continuous run with a single initialization. The evaluation period was from 0000 UTC 1 January 2002 to 31 December 2002. Again, the ERA-Interim reanalysis dataset was used to provide initial conditions. Lateral boundary conditions and sea surface temperature were both updated every 6 hours, from ERA-Interim. The choices of the parameterization schemes were motivated by previous WRF tests studied in the previous sections.

3.3.1 Maximum Temperature and Minimum Temperature

The statistical metrics are illustrated on Table 3.11. The different integration approaches do not appear to have a significant effect on the skill of regional dynamical downscaling and show a good representation for both temperatures. The errors of monthly and seasonal re-initialization runs, averaged over the total station-points, are almost identical for both temperatures (TN and TX), with negative bias around 0.9°C of TX and positive bias of around 2.2°C of TN. Smaller biases of TX are found for the continuous run, however RMSE and MAE result in higher values for TX and TN.

Table 3.11 Statistical errors for daily maximum and minimum temperatures (TX and TN) and precipitation (PR) during 2002 in the total grid points, over the area of Greece.

SimID		1M	6M	1Y
VARS	Metrics			
TX	BIAS (°C)	-0.91	-1	**-0.81**
	RMSE (°C)	**2.49**	2.51	2.83
	MAE (°C)	**1.93**	1.96	3.22
	COR	**0.95**	**0.95**	0.93
TN	BIAS (°C)	2.27	**2.22**	2.84

	RMSE (°C)	3.54	**3.5**	4.19
	MAE (°C)	2.78	**2.75**	3.22
	COR	0.92	**0.93**	0.9
PR	**PBIAS(%)**	15.5	13.7	**6.7**
	RMSE (mm)	**6.64**	7.17	6.72
	MAPE(%)	**121**	122	122
	COR	**0.46**	0.43	0.41

3.3.2 Precipitation

Regarding precipitation results (PR), a less reduced statistical error is observed for the daily precipitation PBIAS (6.7%), in the case of continuous run, although the overall performance for precipitation simulation is not satisfactory. It was also noticed that the model in all experiments notably overestimates the quantity of precipitation between 0.1 and 1mm.

The results of the performance for the three model simulation approaches are summarized on Table 3.12, derived from contingency (Table A.3, APPENDIX) for the three different thresholds. The statistics were calculated for each station separately and the mean values of the total of stations are illustrated in the table. The best value calculated for a station is also indicated in parenthesis. It is observed that all simulations appear to have similar results. The systematic overestimation of precipitation is also verified by the bias in all experiments. Considering the verification for precipitation for the 0.1mm threshold, the POD index of the average of the total station points resulted in higher values, around 0.8 for the cases of the monthly and seasonal simulations. Similar behavior of the POD index is seen for the other two thresholds as well. It is noted that the continuous simulation (1Y) shows slightly lower performance than the other two types of experiments.

Table 3.12 Statistical errors for precipitation (PR) based on contingency table, during 2002 in the total station grid points, over the area of Greece.

Sim ID		**1M**	**6M**	**1Y**
thresholds				
0.1mm	**POD**	0.81 (0.92)	0.79 (0.94)	0.68 (0.88)
	SR	0.53 (0.69)	0.52 (0.69)	0.49 (0.59)
	BIAS	1.66 (0.97)	1.62 (0.97)	1.51 (0.97)
	CSI	0.46 (0.58)	0.45 (0.60)	0.39 (0.47)
1mm	**POD**	0.71 (0.90)	0.71 (0.90)	0.61 (0.86)
	SR	0.52 (0.68)	0.53 (0.71)	0.51 (0.67)

	BIAS	1.47 (0.97)	1.45 (0.98)	1.32 (1.00)
	CSI	0.42 (1.05)	0.43 (0.55)	0.38 (0.50)
10mm	**POD**	0.43 (0.65)	0.49 (0.71)	0.35 (0.75)
	SR	0.40 (0.74)	0.38 (0.63)	0.39 (0.69)
	BIAS	1.16 (1.00)	1.12 (1.00)	0.97 (1.00)
	CSI	0.26 (0.47)	0.24 (0.48)	0.23 (0.50)

Figure 3.22 illustrates the performance of soil moisture for the three different initialization simulations (here for 4 stations shown) in order to determine the effect of interruption on frequent restarts. Soil moisture behavior has also been examined but not validated, due to lack of observations. A similar pattern was observed in the variation of soil moisture between 0.15-0.45 m3/m3 for all experiments, with some slight deviations occurring during the annual cycle. According to Qian et al. (2002), comparing the effect of changing soil moisture to that of updating atmospheric conditions, the rainfall differences are small among those soil-moisture re-initialization experiments, suggesting the secondary importance of soil-moisture memory for regional climate modeling in monthly timescales.

The sensitivity test showed that all simulations do not appear to have a significant impact on the skill of regional dynamical downscaling and show overall a good representation for daily minimum (TN) and maximum (TX) temperatures. Regarding the results of precipitation (PR), a slight improvement is observed for the daily precipitation pbias (6.7%), under the case of continuous run, although precipitation is consistently strongly overestimated. A similar pattern was observed in the variation of soil moisture between 0.15-0.45 m3/m3 for all experiments, with small deviations found in the annual cycle. The similarity between modeled soil moisture suggests that monthly re-initialization does not affect the simulated surface temperature and precipitation fields. Contingency tables and probability density function (pdf) analysis from indicative stations (depicted in figure 3.23) showed that the results were almost indistinguishable between the three simulations. Based on these results, it was workable to proceed to the use of monthly re-initialization of model runs, as none of the three experiments introduced significant impact on the examined variables; moreover, it was more efficient computationally to perform simultaneous runs (in parallel). This procedure was also followed to avoid possible climatic shifts that may result from long-term continuous simulations (Tian et al. 2020).

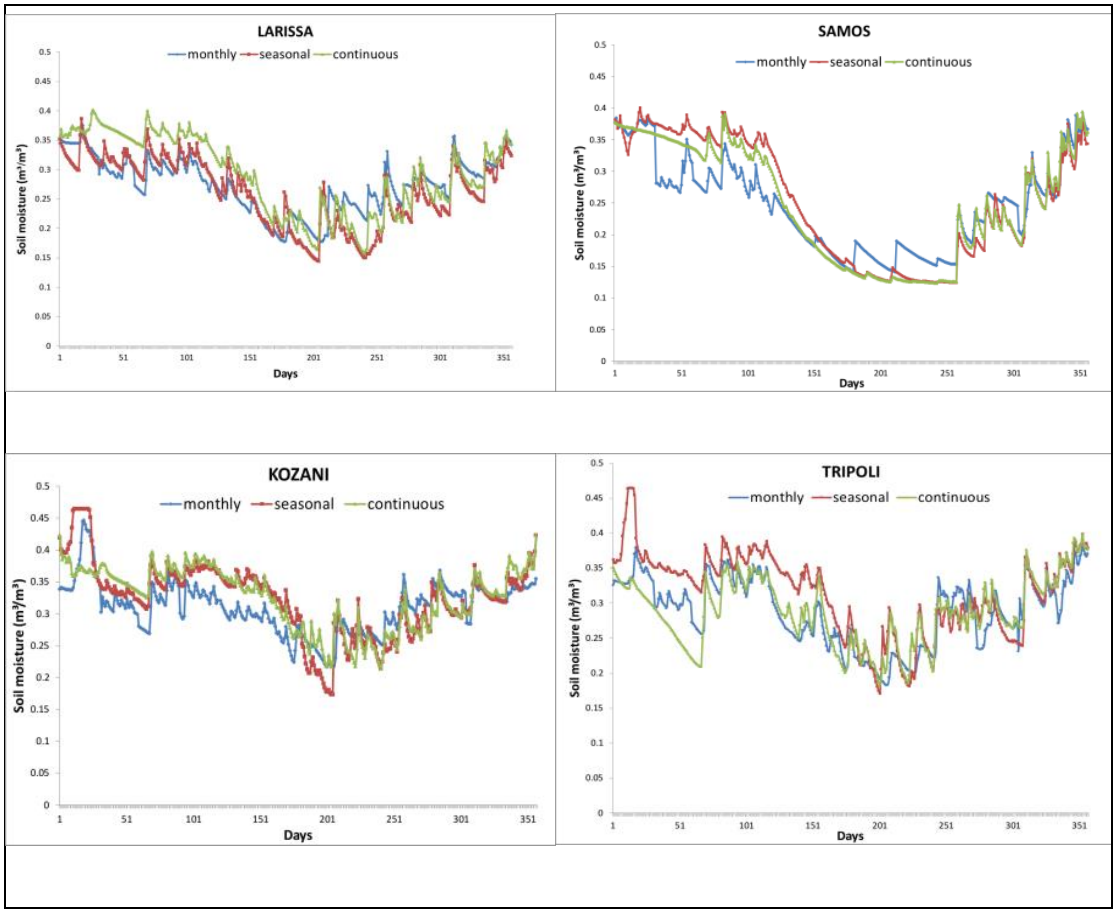

Figure 3.22 Annual cycle of soil moisture of Larissa, Samos, Kozani and Tripoli stations, during 2002 for monthly, seasonal and continuous run.

Methoni	Alexandroupolis
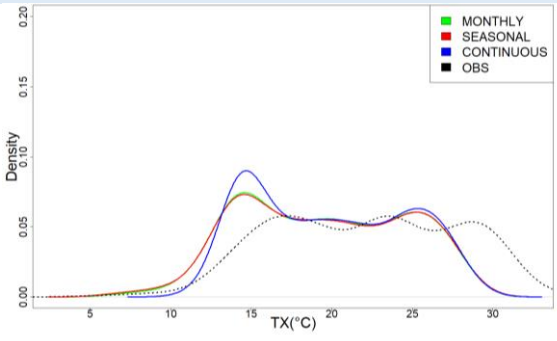	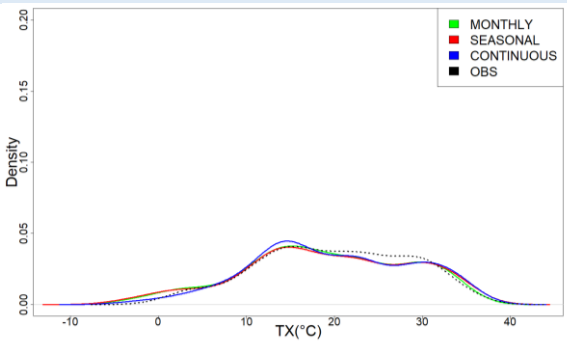

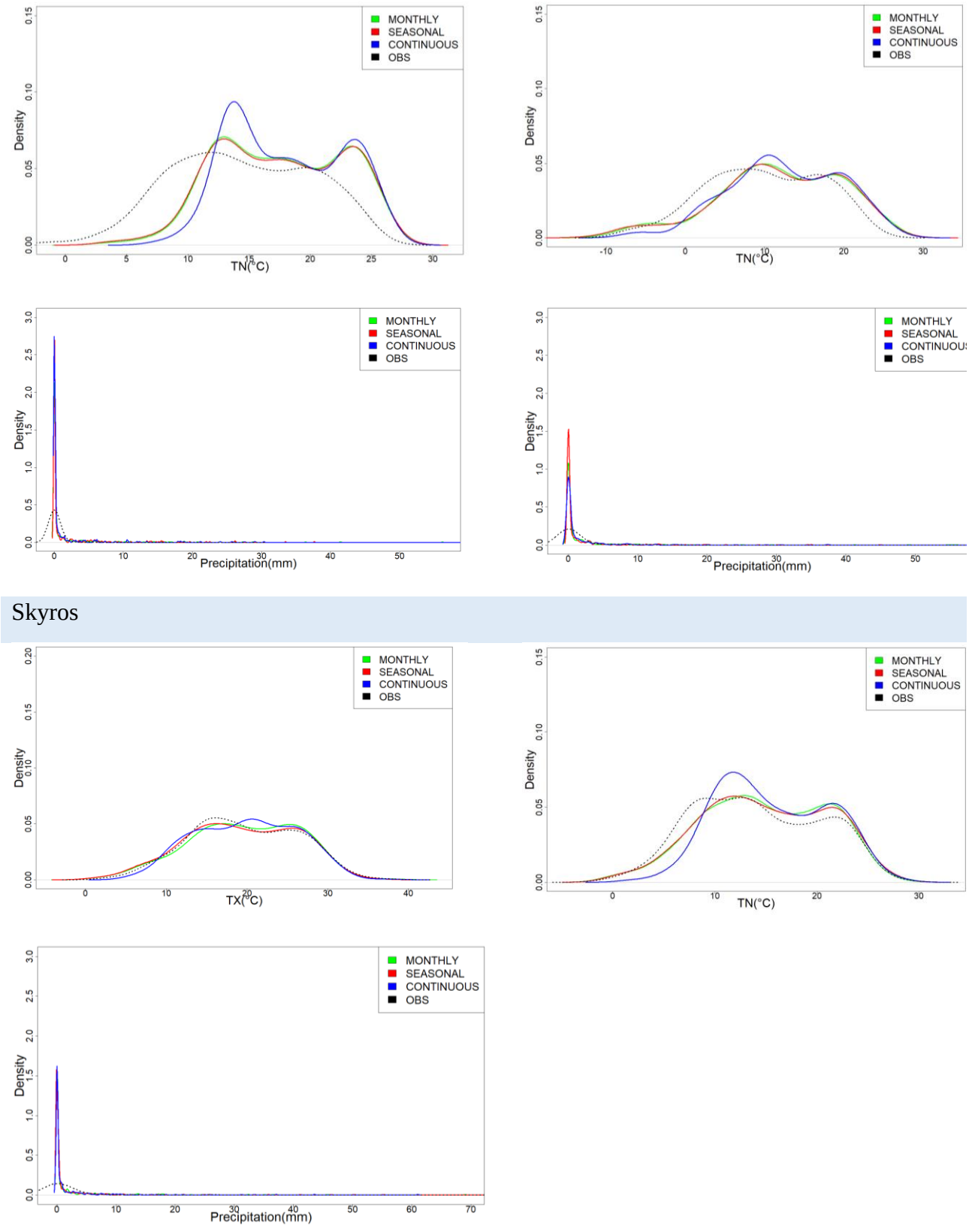

Figure 3.23 Probability density function (pdf) analysis of daily TX, TN and precipitation from indicative stations of Methoni, Alexandroupolis and Skyros for the three examined types of re-initialization compared to observations.

Key Remarks

- ***Different integration approaches do not appear to have a significant effect on the skill of regional dynamical downscaling.***
- ***Smaller bias of maximum temperature and precipitation is found for the continuous run, however RMSE and MAE result in higher values for TX and TN.***
- ***Noticeable overestimation of the quantity of precipitation between 0.1 and 1mm.***
- ***Continuous simulation (1Y) shows slightly lower performance than the other two types of experiments on precipitation verification.***
- ***More efficient computationally to perform simultaneous monthly runs (in parallel) and avoid possible climatic shifts from long-term continuous simulations.***

3.4 The selection optimal model setup

In the final section a summary of the overall optimal model configuration was presented for the historical and future simulations based on the previous studies of sensitivity tests.

The WRF model configuration applied in this study includes a one-way nested domain, with a spatial resolution of 20 km × 20 km in the outermost domain (D01, 265 × 200 grid cells), centered in the Mediterranean basin, and 5 km × 5 km in the innermost one (d02, 184 × 184 grid cells). Both domains have 40 vertical layers. The model domains share the same options of physics for radiation, microphysics, boundary layer scheme, and convection. More specifically, the Mellor–Yamada–Janjic scheme (MYJ) was employed, associated with the corresponding surface layers (SLP) scheme. In this scheme, the entrainment develops only from local mixing. Regarding cloud microphysics, the WRF single-moment six-class scheme (WSM-6) was used to simulate six classes of water mass processes. The Betts–Miller–Janjić scheme was chosen for the cumulus parameterization, taking into consideration the grey zone between 5 and 10 km in the vertical for the cumulus option. The radiation scheme was set to the newer version of the Rapid Radiative Transfer Model, RRTMG, for both longwave and shortwave radiation. Finally, the Noah LSM was employed as the land surface model (LSM), as it is used widely for climate studies. For each simulation, the

last four (4) days of the previous month were regarded as model spin-up for the following month and were discarded, thus, the model was re-initialized every month.

Chapter 4 Evaluation of high-resolution Historical simulations

In this chapter, the analysis of the performance of the WRF model to represent the historical climatology was analysed over the area of Greece, by dynamically downscaling the coarse-resolution ERA-Interim reanalysis and EC-EARTH datasets to the high spatial resolution of 5 km x 5 km grid.

The analysis aimed: (1) to show that our downscaling of ERA-Interim reanalysis to the Greek area produces comparable results to the available observational products and (2) to demonstrate the improvement in downscaled fields (WRF_5) compared to reanalysis dataset and the added value of the downscaling methodology. In addition, the investigation included the ability of the regional model WRFEC historical simulation to represent historical climate through the comparison with the available HNMS observational data.

In this chapter, the validation procedure which includes the statistical and spatial analysis of the historical climate variables, involved initially the representation of temperatures (subchapter 4.1) with WRF_5 *(section 4.1.1)* and WRFEC *(section 4.1.2)* and then that of precipitation (subchapter 4.2) with each of the models. Statistical metrics were calculated for the total number of available stations and then separately by grid point to check the spatial distribution of the errors as well. The following standard error statistics and other statistical methods estimated in this study are included in table 4.1 and are described in the APPENDIX.

Table 4.1 Statistical metrics for the validation of historical simulations.

HISTORICAL SIMULATION	STATISTICAL METRICS
HINDCAST RUN WITH ERA-INTERIM	BIAS (or Pbias), RMSE, MAE, COR, MIA, NSE PDFs, q-q plots
CONTROL-RUN WITH EC-EARTH	BIAS (or Pbias), RMSE, MAE, COR, MIA, NSE PDFs

Additionally, a two-sided student test was performed to identify the areas with no significant differences between observed and model data at the 95% confidence level.

4.1 Maximum (TX) and minimum temperatures (TN)

4.1.1 Evaluation of high-resolution Hindcast simulations with ERA-I

a) Analysis of Spatial and Temporal Climatology

In this subsection, the 5-km WRF high resolution simulations for maximum and minimum temperatures are analyzed and compared against ERA-Interim reanalysis (ERA-I) and station data (OBS) to verify the added value of the increase of the horizontal resolution.

The calculated mean maximum and mean minimum temperature monthly cycles, averaged over the historical period 1980-2004, are presented in Figures 4.1(a) and 4.1(b), respectively, along with the corresponding values of the standard deviation. The monthly mean values were calculated for each dataset at the grid-point location of each station and then, were averaged over the total number of points (stations). Likewise, Figures 4.1(c) and 4.1(d) show the calculated mean inter-annual variability of maximum and minimum temperatures.

Overall, the monthly cycle patterns of TX and TN were well represented with WRF_5 and highly correlated to the climatology of the country. Greece has a typical Mediterranean climate with summers characterized by long hot and dry spells (T>30ºC), peaking between end-July and August, and rather cold winter months particularly, in its northern parts between end-January and February. However, milder winter months experience the southern parts of the country and the islands (Zerefos et al. 2011). The WRF_5 TX followed the typical pattern of monthly variation by displaying lower values in the winter months and higher ones during the summer. Besides, their comparisons to OBS revealed a very good agreement, slightly underpredicted, but within the calculated error range (Fig. 4.1 (a)). On the other hand, ERA-I simulations did not present a better comparison with OBS and systematically were underestimated throughout all months. The same conclusions were drawn for the inter-annual cycle of TX as depicted in Fig 4c, where WRF_5 simulations were in impressive agreement with OBS, in contrast to ERA-I results, which were underestimated persistently.

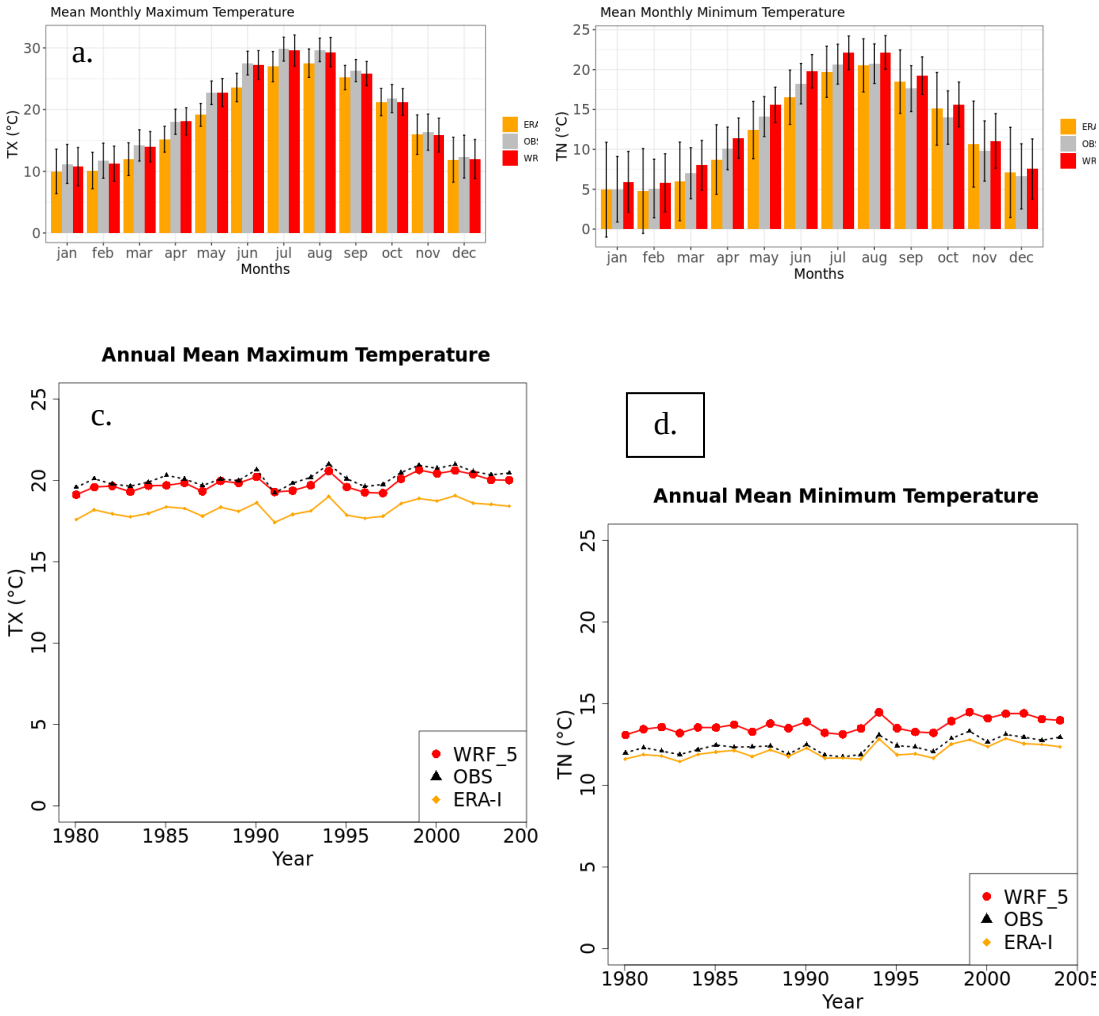

Figure 4.1 Mean annual cycle (a and b) and inter- annual variability (c and d) of maximum and minimum temperatures averaged over the historical period of 1980–2004 for the total number of stations.

Furthermore, the high-resolution domain of WRF didn't cool enough throughout the year as the results concerning the monthly cycle of TN showed a persistent overestimation (by approximately, 1°C) compared to the reanalysis and OBS data (Fig.4.1(b)). The calculated annual cycle presented the same difference, where the simulation of the reanalysis revealed closer to the observed data values than the WRF_5 (Fig.4.1(d)). The particular model's behaviour was attributed to persistently clear sky strong inversions (e.g., Soares et al. 2012) in the complex topography of Greece in conjunction with the smooth geomorphological representation of ERA-I that might allow lower values of TN, especially over mountainous regions not realistically resolved by reanalysis resolution (as illustrated in Fig.3.1(a)). Such an issue could not

be translated into canceling the ability of WRF to represent properly TN. A more extended discussion on this can be found in the statistical comparison analysis section.

Figure 4.2(a) and Figure 4.3(a) illustrate the spatial distribution of 25-years simulated (reanalysis and WRF model) mean daily TX and TN (in the same figure) with the respective one of the meteorological point observations data. The spatial patterns of the simulated WRF_5 TX and TN were in agreement with the general climatological knowledge for this area and with the observational data, where at the same time, they revealed ERA-I deficiencies in the representation of temperatures in Greece by losing important information concerning the mountainous areas.

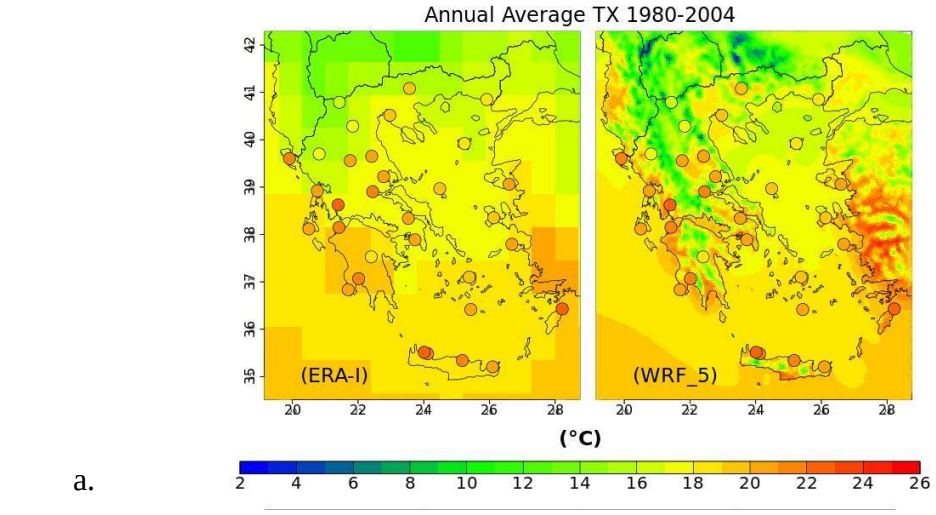

a.

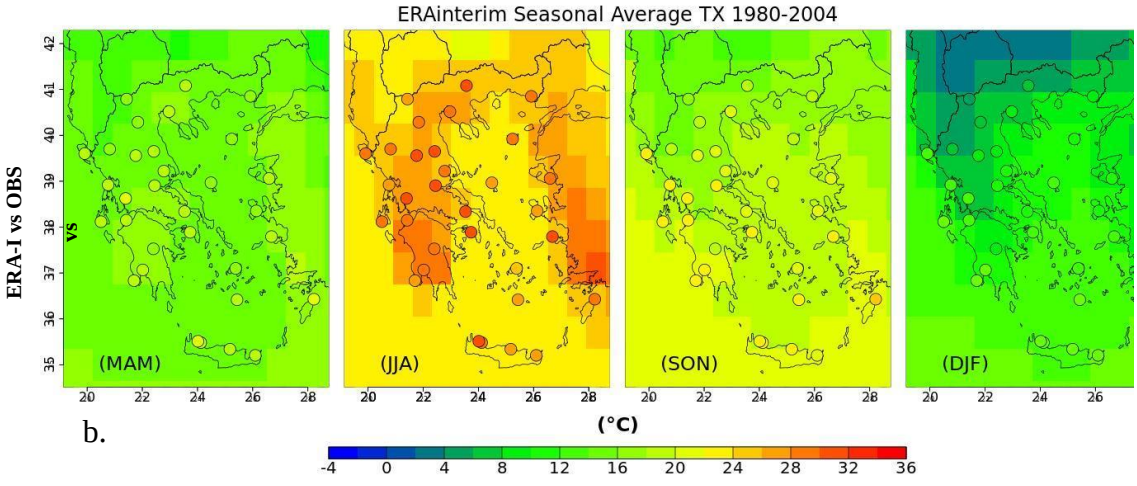

b.

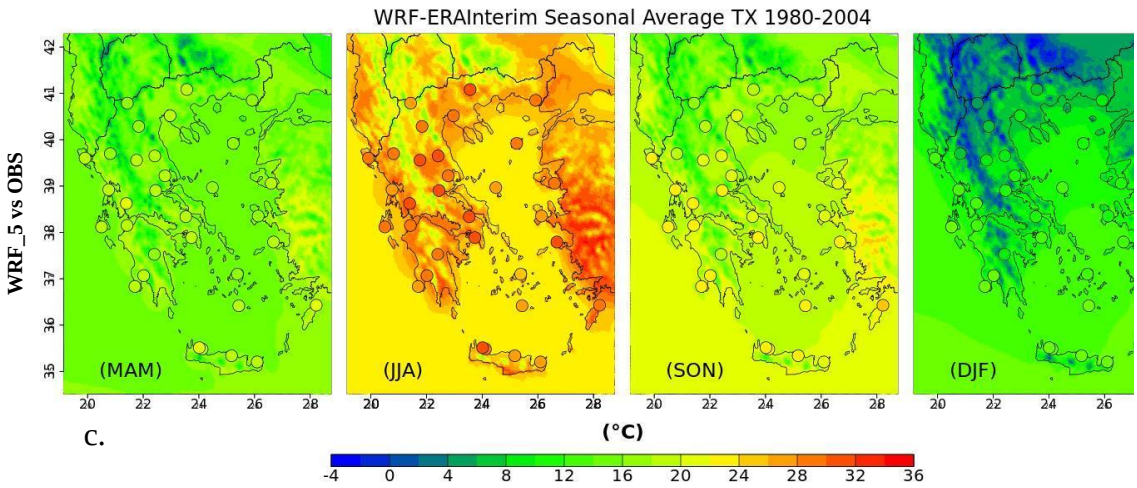

Figure 4.2 a) Spatial distribution of 25-years mean daily maximum temperature TX for ERA-I and WRF_5 compared to weather station observations (points). b) Spatial distribution of seasonal mean daily maximum temperature over the historical period of 1980–2004 for ERA-I and for c) WRF_5 in comparison to the weather station data

Figure 4.2(b and c) depicts the spatial distribution of 25 years seasonal mean daily maximum temperature derived from ERA-I and WRF_5 compared to the stations, respectively. The depiction was for winter (December, January, and February, DJF), spring (March, April, and May, MAM), summer (June, July, and August, JJA), and autumn (September, October, and November, SON). The comparison of WRF_5 with the observational data (Fig. 4.2(c)) showed that the model represented very well the geographical distribution of seasonal mean daily TX and illustrated the seasonal variation with similar ranges of temperature values among the two datasets.

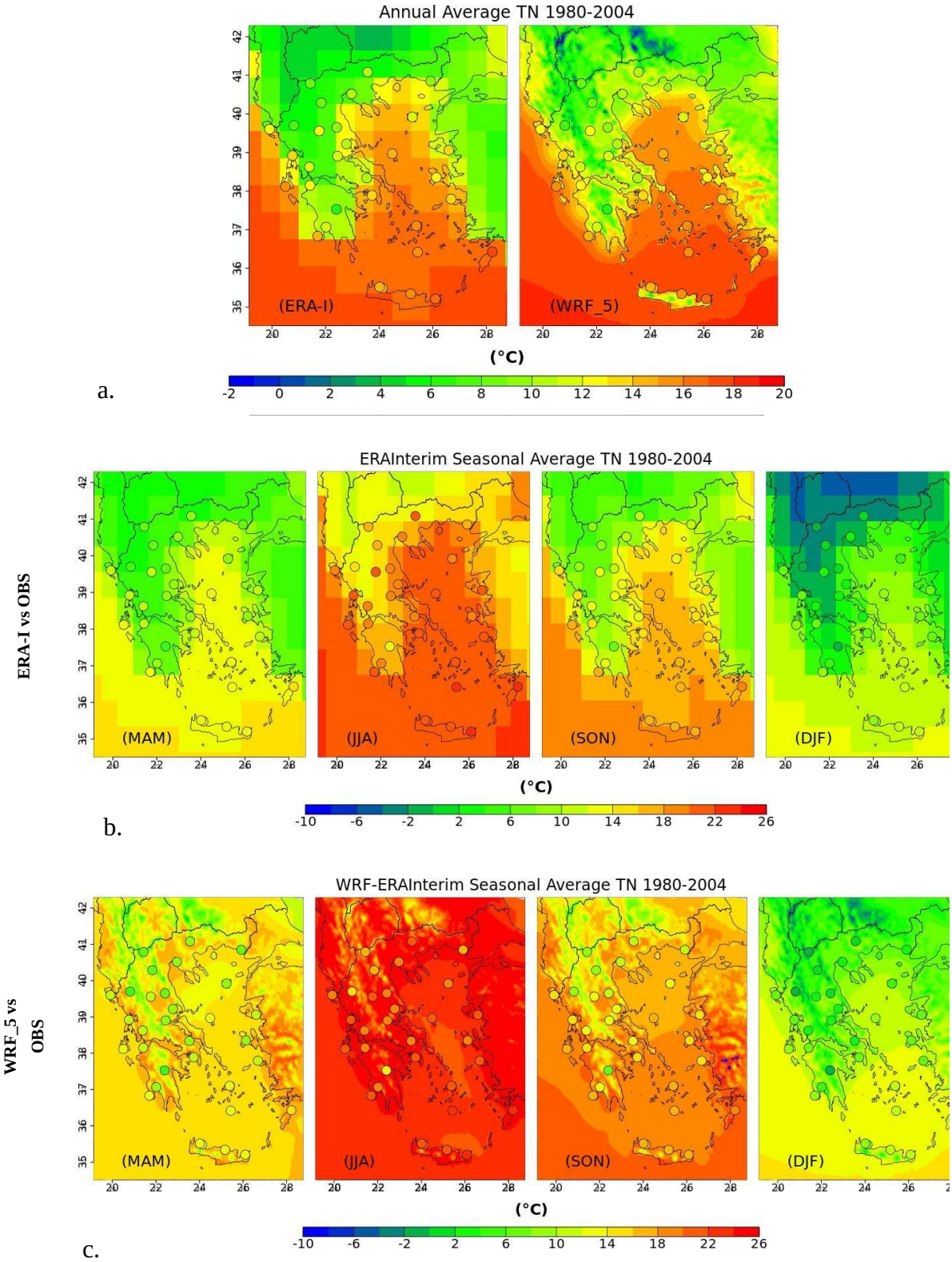

Figure 4.3 a) Spatial distribution of 25-years mean daily minimum temperature TN for ERA-I and WRF_5 compared to weather station observations (points). b) Spatial distribution of seasonal mean daily minimum temperature over the historical period of 1980–2004 for ERA-I and for c) WRF_5 in comparison to the weather station data

The higher deviations were mostly attributed to the values over altitude or steep terrain. Regarding WRF_5's spatial patterns, differences between inland and coastal areas were more intense during the summer. In the winter, mean TX varied from -4°C to 8°C, over mountainous regions, whereas in the summer, mean TX ranged from 32°C to 36°C in parts of west and south Greece. The comparison of WRF_5 TX with the observational values showed an underestimation of WRF_5 TX during the autumn season (SON, Fig 4.2(c)) as well as a more homogeneous spatial distribution of the model with values around 12-18°C. During spring, WRF_5 and observational temperatures compared very well (MAM Fig 4.2(c)) with values in the approximate range of 16°C - 24°C. The comparison revealed overall realistic seasonal TX temperature patterns for the parts of the domain of lower elevation. Moreover, it is emphasised, that there was no observational network on mountainous areas to deduce the temperature deviations based on the terrain's altitude. The seasonal distribution of reanalysis, as expected, presented a limited variation in TX values across the whole domain (Fig. 4.2b).

Similarly, the spatial pattern of the WRF_5 simulated seasonal mean daily TN compared very well to that of the observations, as illustrated in Fig. 4.3(c). The model represented TN very well across all seasons, with the most vivid variations found in the summer and winter periods with values higher than 12°C and lower than 12°C, respectively, throughout the domain. The autumn TN values tended to have a more homogenous spatial distribution over land, with values close to 12°C, while spring presented higher TN up to 15°C. Same as with TX, ERA-I did not show a realistic variation in the spatial distribution of TN values (Fig. 4.3(b)).

b) Evaluation based on statistical metrics

To assess our downscaling methodology quantitatively, it was necessary to proceed to the statistical evaluation of the simulated mean fields from WRF_5 and the driver ERA-Interim with historical observations of the examined variables. The statistical errors (as described in APPENDIX) of maximum and minimum temperatures for daily and monthly averages for WRF_5 and ERA-Interim were calculated against observational data from the weather stations over the entire domain and summarized in Table 4.2. Table 4.2 includes, also, the statistical errors for precipitation in terms of daily and monthly cumulative values. In general, the WRF model performed better than reanalysis showing improvement with the downscaling results (WRF_5). The TX daily

and monthly scale correlation coefficients for WRF_5 were 0.95 and 0.98, respectively, while the respective ones for ERA-I were much lower and equal to 0.82 and 0.8. The rather better COR values for ERA-I could be attributed to the smooth patterns of the reanalysis dataset, although their values did not unveil the heterogeneity across the domain as manifested by the observations. As was foreseeable, the errors reduce with the increasing time-averaging for WRF_5. The statistical results showed a cold bias of around -0.6 °C regarding the daily and monthly TX WRF_5 and distinctively larger values for ERA-I of -2.2°C and -3.3°C, respectively. For daily WRF_5 TX, the RMSE and MAE were of the order of 2.5°C and 1.8°C, respectively, while for monthly averaging, these errors reduced to values of 1.7°C and 1.2°C, respectively. On the other hand, for ERA-I, the statistical errors were higher than and at least twice as large as the ones for WRF_5. The efficiency metrics NSE and MIA also improved significantly with the downscaling to values approximately equal to 0.9, while for ERA-I, their values were below 0.7. The efficiency metric of MIA was improved significantly with the downscaling to values approximately equal to 0.9, while for ERA-I, their values were below 0.7.

Table 4.2 Statistical errors between model results and reanalysis against observations.

TX	**Time**	**COR**	**BIAS (°C)**	**RMSE (°C)**	**MAE (°C)**	**NSE**	**MIA**
WRF_5	**Daily**	0.95	-0.57	2.5	1.83	0.91	0.86
	Monthly	0.98	-0.57	1.7	1.21	0.95	0.90
ERA-I	**Daily**	0.82	-2.19	5.03	3.96	0.59	0.70
	Monthly	0.80	-3.25	7.66	8.27	0.67	0.46
TN							
	Daily	0.92	1.05	2.97	2.32	0.82	0.80
WRF_5	**Monthly**	0.96	1.05	2.17	1.71	0.89	0.85
	Daily	0.79	-0.49	4.71	3.67	0.55	0.69
ERA-I	**Monthly**	0.88	-0.49	3.5	2.84	0.71	0.75
PR		**COR**	**PBIAS(%)**	**RMSE(mm)**	**MAE(mm)**	**NSE**	**MIA**
	Daily	0.45	3.40	6.22	1.92	0.05	0.64
WRF_5	**Monthly**	0.67	6.60	46.87	29.31	0.40	0.65
	Daily	0.13	-12	7.06	2.44	-2.22	0.51
ERA-I	**Monthly**	0.62	-12.6	47.91	28.66	0.37	0.63

Regarding TN, correlations were found to be slightly smaller than those of TX, similarly to Zhang et al. (2009) and Soares et al. (2012), but indicated improved downscaled results compared to those of reanalysis. Overall, the other statistical errors have improved values against ERA-I except for bias. Both comparisons revealed a warm bias of about 1 °C for WRF_5 and a cold bias around -0.5°C for ERA-I. The efficiency metrics for TN showed an improved performance of the model compared to reanalysis for both temporal scales.

In what concerns precipitation statistical errors over the entire domain, relatively low correlation values were calculated between observations and WRF_5 results (around 0.5) and very much lower for the case of ERA-I (~0.13) on a daily scale. Although the WRF model improved with downscaling the results on precipitation significantly compared to ERA-I according to the error statistics, the values of COR, NSE, and MIA remained lower than those on temperatures. In general, the WRF_5 model overestimated precipitation compared to observational values but, the overall improvement over the ERA-I values was a positive outcome.

The annual cycle of the mean statistical errors calculated for the monthly maximum-minimum temperatures is presented in Figures 4.4 and 4.5, respectively, concerning WRF_5 simulations and ERA-I against observations. The best results for TX were obtained with the WRF_5 downscaling, which displayed lower BIAS than ERA-I during all the months of the year and with values below 1 °C. In particular, from May to July, ERA-I showed higher errors (BIAS, MAE, and RMSE) and a very much lower correlation compared to WRF_5 simulation. April and May presented a bias error close to zero for WRF_5. Additionally, both ERA-I and WRF_5 underestimated TX throughout the year. For some months, the acceptance criteria, defined by Emery et al. (2001) for air temperature, -0.5° C<bias< +0.5 °C, were not sufficiently met. It was also observed that MIA values for WRF_5 were higher for all the months compared to reanalysis, with only slightly lower ones in summer and autumn. NSE was overall higher for WRF_5 but it reached negative values only in June (NSE=-0.003), indicating that the mean of the observations was a better predictor than the model for that month. Similar results were obtained with the comparison of TN, where WRF_5 for all months yielded much lower statistical errors than ERA-I (Fig. 4.5). ERA-I shows constantly lower values of TN compared to observations and thus tends to yield lower values of bias error. ERA-I presents a constant cold bias during all seasons except autumn.

Consequently, the reanalysis bias in TN is much lower than that of WRF_5 due to compensation errors. At the same time, downscaled model results were characterized with remarkably higher correlations coefficients, MIA, and NSE values than the reanalysis during all months. Those NSE values of the WRF_5 indicated that the downscaled model data set was a more skillful predictor than the mean of the observations.

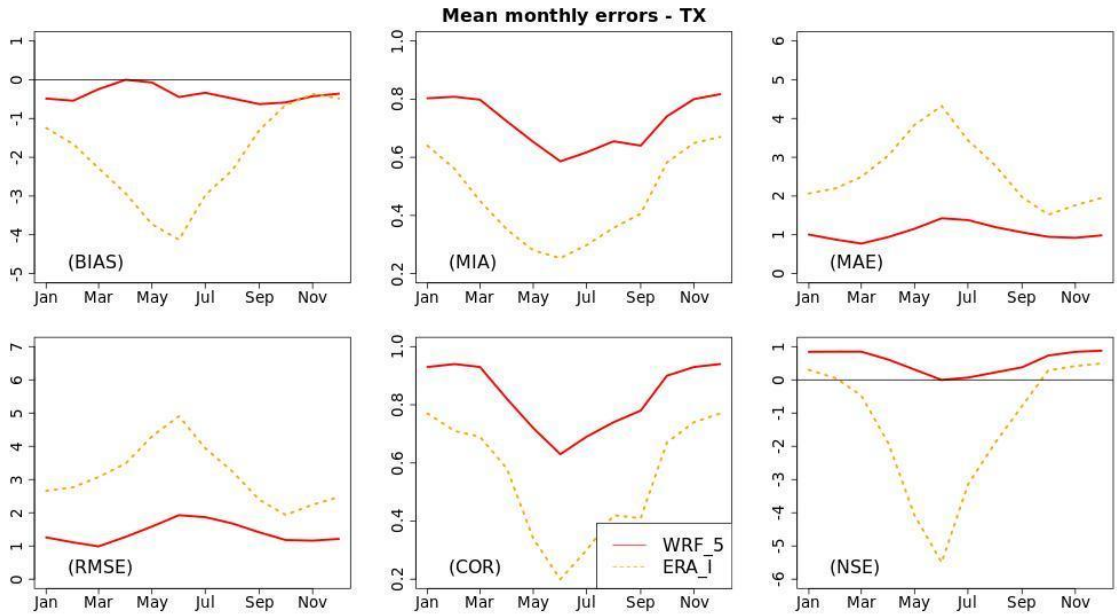

Figure 4.4 Annual cycles of mean monthly maximum temperature errors (TX) of the ERA-I (dotted orange) and 5-km WRF (solid red) simulations over the entire domain

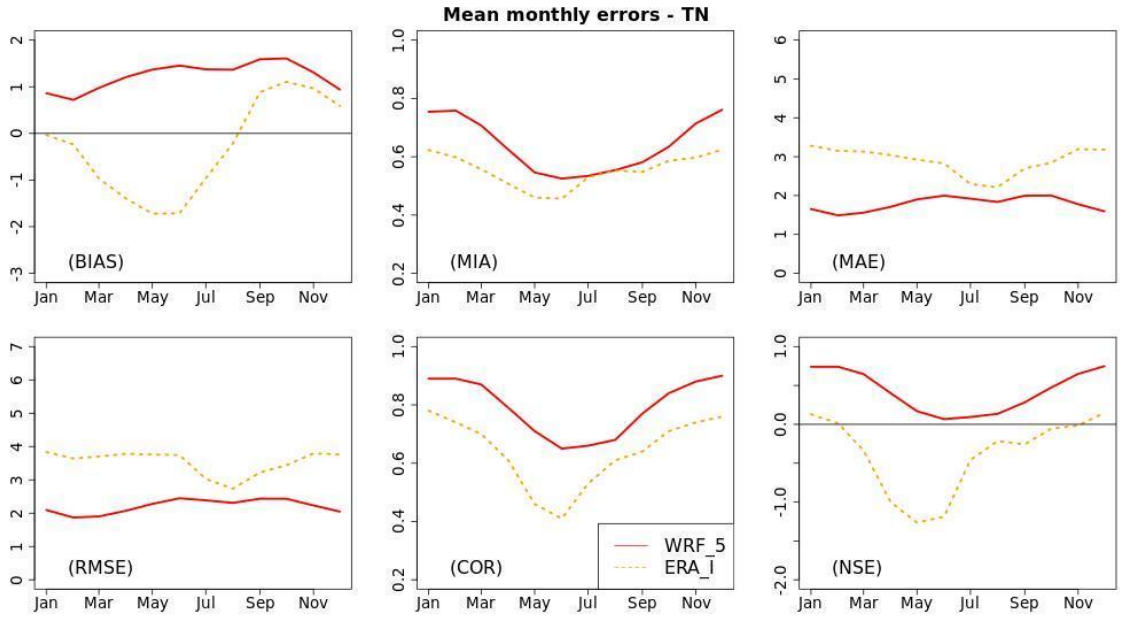

Figure 4.5 Annual cycles of mean monthly minimum temperature errors (TN) of the ERA-I (dotted orange) and 5-km WRF (solid red) simulations over the entire domain

The seasonal statistical analysis of WRF_5 and ERA-I data compared to weather stations data were calculated and summarized in Table 4.3 for TX, TN, and PR. The analysis was performed for each metric by pooling together all the points of monthly values for the four seasons for the entire domain. WRF_5 TX correlations coefficients were higher than for ERA-I in all seasons and more significantly with values around 0.95 for winter, spring, and autumn. Although the lowest value of 0.59 appeared in summer, the downscaling of the model still strongly outperformed the reanalysis value that was equal to 0.17. Furthermore, less cold bias was observed for WRF_5 TX compared to ERA-I, with remarkably improved results, especially for spring and summer seasons, as well as significantly smaller RMSE and MAE values across all seasons. ERA-I outperformed WRF_5 with a smaller warm bias of TX (0.44°C) only in SON. NSE indicated a negative skill of ERA-I during all seasons.

Table 4.3 Seasonal statistical errors of maximum temperature, minimum temperature and precipitation between model results and reanalysis for the total stations' grid points.

TX	**WRF_5**				**ERA-I**			
	MAM	**JJA**	**SON**	**DJF**	**MAM**	**JJA**	**SON**	**DJF**
COR	0.94	0.59	0.96	0.93	0.59	0.17	-0.70	0.68
BIAS (°C)	-0.29	-0.60	-0.73	-0.64	-9.47	-10.31	0.44	-6.29
RMSE(°C)	1.54	2.31	1.5	1.31	10.4	11.07	8.01	7.66
MAE(°C)	1.06	1.58	1.11	1.08	9.47	10.32	6.95	6.37
NSE	0.86	-0.1	0.91	0.83	-5.38	-24.18	-1.87	-4.87
MIA	0.97	0.75	0.98	0.96	0.46	0.25	0.62	0.53
TN								
COR	0.91	0.74	0.91	0.86	0.75	0.62	0.82	0.78
BIAS (°C)	0.99	1.21	1.32	0.66	-1.54	-1.15	0.8	-0.08
RMSE(°C)	1.97	2.2	2.31	2.19	3.75	3.18	3.36	3.68
MAE(°C)	1.59	1.82	1.82	1.59	3.01	2.44	2.79	3.13
NSE	0.76	0.32	0.75	0.69	0.12	-0.42	0.46	0.13
MIA	0.76	0.58	0.76	0.76	0.82	0.74	0.89	0.85
PR								
COR	0.59	0.47	0.62	0.56	0.49	0.54	0.58	0.52
PBIAS (%)	20.30	46.10	-3.80	1.90	8.50	39.20	-28.50	-12.90
RMSE(mm)	40.23	23.55	52.80	61.85	40.68	21.00	56.07	62.82

MAE(mm)	27.20	12.35	34.25	43.44	27.06	11.24	33.62	42.74
NSE	0.14	-0.23	0.35	0.26	0.12	0.02	0.27	0.23
MIA	0.56	0.58	0.62	0.54	0.56	0.58	0.62	0.54

Seasonal statistical errors of TN varied compared to those of TX. Seasonal correlation values between model and reanalysis were comparable though WRF_5 outperformed ERA-I in all seasons. Although a consistent warm bias was found for WRF_5 during all seasons, the reanalysis results showed a warm bias of 0.8°C only in autumn. WRF_5 turned negative bias in reanalysis into positive bias during MAM, JJA, and DJF with an improved model performance during spring. In general, the improvement was not as obvious in bias, but it was unveiled with the higher WRF_5 COR, as well as with the lower RMSE and MAE statistics of monthly TN in all seasons with values not above 2.3°C.

c) Probabilities densities and Q-Q plots

According to (Komurcu et al. 2018), the ability of a downscaling methodology to reproduce mean values of observed fields and improve upon reanalysis forecasts is significant; moreover, a worthwhile downscaling methodology should have the ability to simulate climate extremes well. In this subsection, further analysis of the meteorological variables, regarding the representation of the extremes, was performed on daily basis for the examined variables, in terms of probability density function (PDF) and quantile–quantile (Q–Q) plots. Figure 4.6 shows the seasonal probability distributions of the daily maximum temperature for WRF_5, ERA-I, and station data for the four seasons. The median temperature was underestimated by the ERA-I reanalysis in general but more significantly during the summer period and slightly in spring, showing a significant shift towards colder values. Overall, WRF_5 simulations were in excellent agreement with the observations during all seasons, with some slight shift of the median maximum temperature towards cooler values, in winter and autumn.

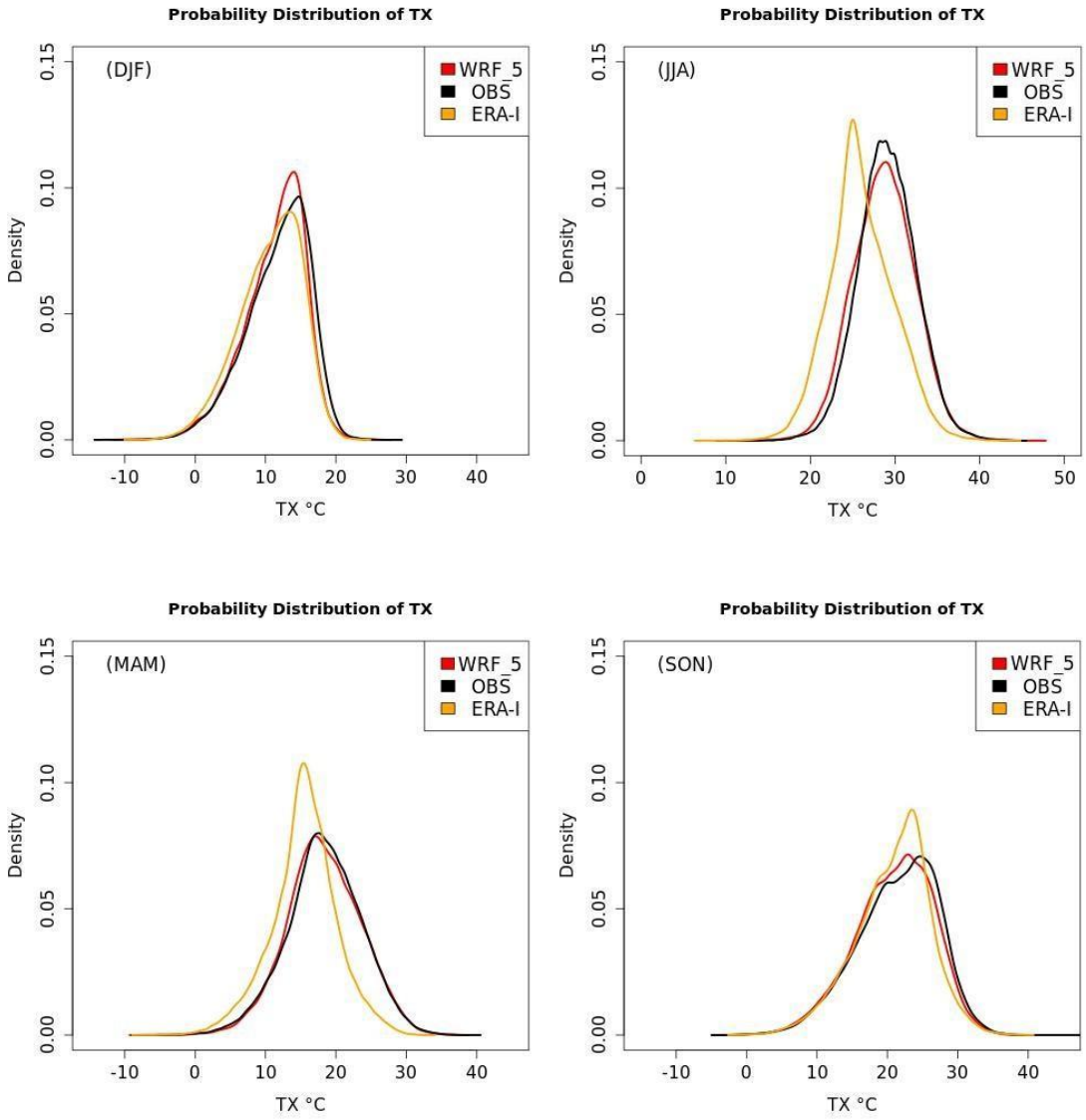

Figure 4.6 Comparison of density distributions of daily TX between WRF_5, ERA-Interim and observations for all seasons for 1980-2004

The observed and modeled quantiles, in Figure 4.7, present the calculated Q-Q probability plots of daily maximum (TX) temperature produced by WRF_5 and ERA-I for 1980-2004. The improvement in the representation of almost all quantiles, including the extreme quantiles, with the downscaled results compared to those of the reanalysis was evident for all seasons, and actually with WRF_5 marking an excellent match with the 1:1 line.

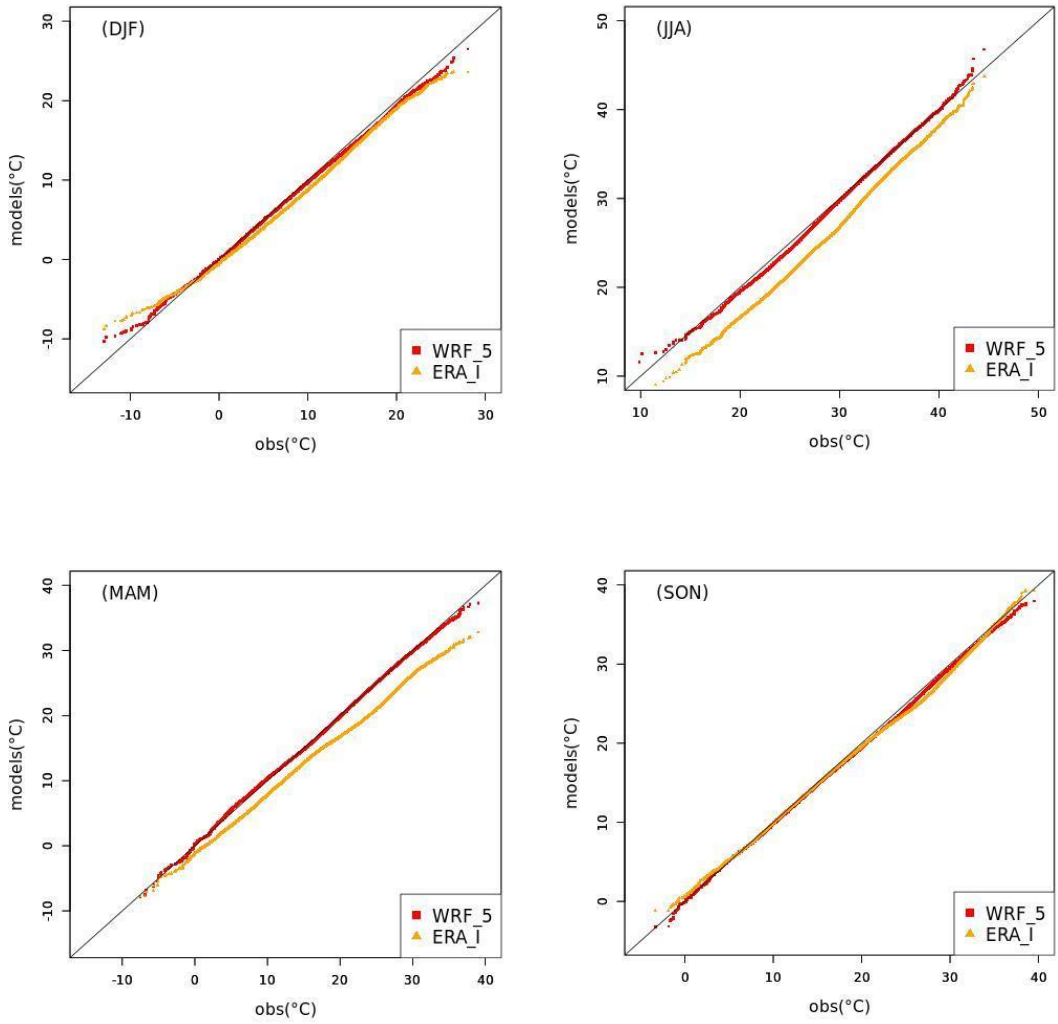

Figure 4.7 Q-Q plots of daily maximum (TX) temperature generated by WRF_5 and ERA-Interim for 1980-2004, in comparison with observations for all seasons.

Figure 4.8 depicts the density distribution of TN. The WRF_5 histogram was in line with the observations, while ERA-I indicated significantly lower density values for all seasons but with good agreement along with the distribution tails. The distribution of the WRF_5 model compared to observations showed a right shift towards higher TN values in all seasons and particularly, in the summer and autumn. In what concerns the daily minimum (TN) temperature quantiles in Figure 4.9, there was a clear improvement of WRF_5 for all seasons compared to ERA-I, particularly in winter and spring. In general, the extreme temperatures, maximum and minimum, were better reproduced by the WRF_5 simulations. Overall, those results reinforced the added value of the downscaling compared to reanalysis.

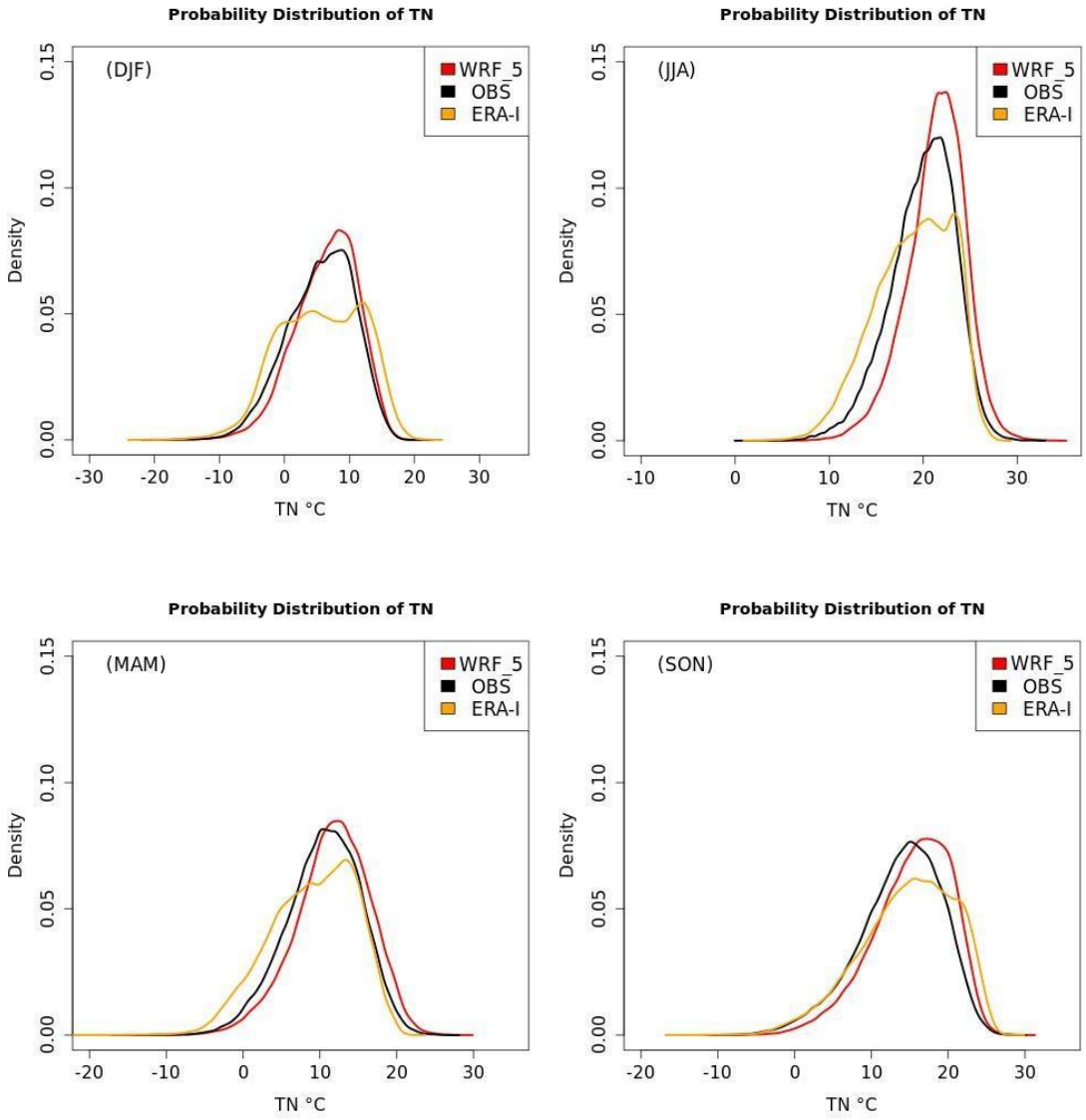

Figure 4.8 Comparison of density distributions of daily TN between WRF_5, ERA-Interim and observations for all seasons for 1980-2004

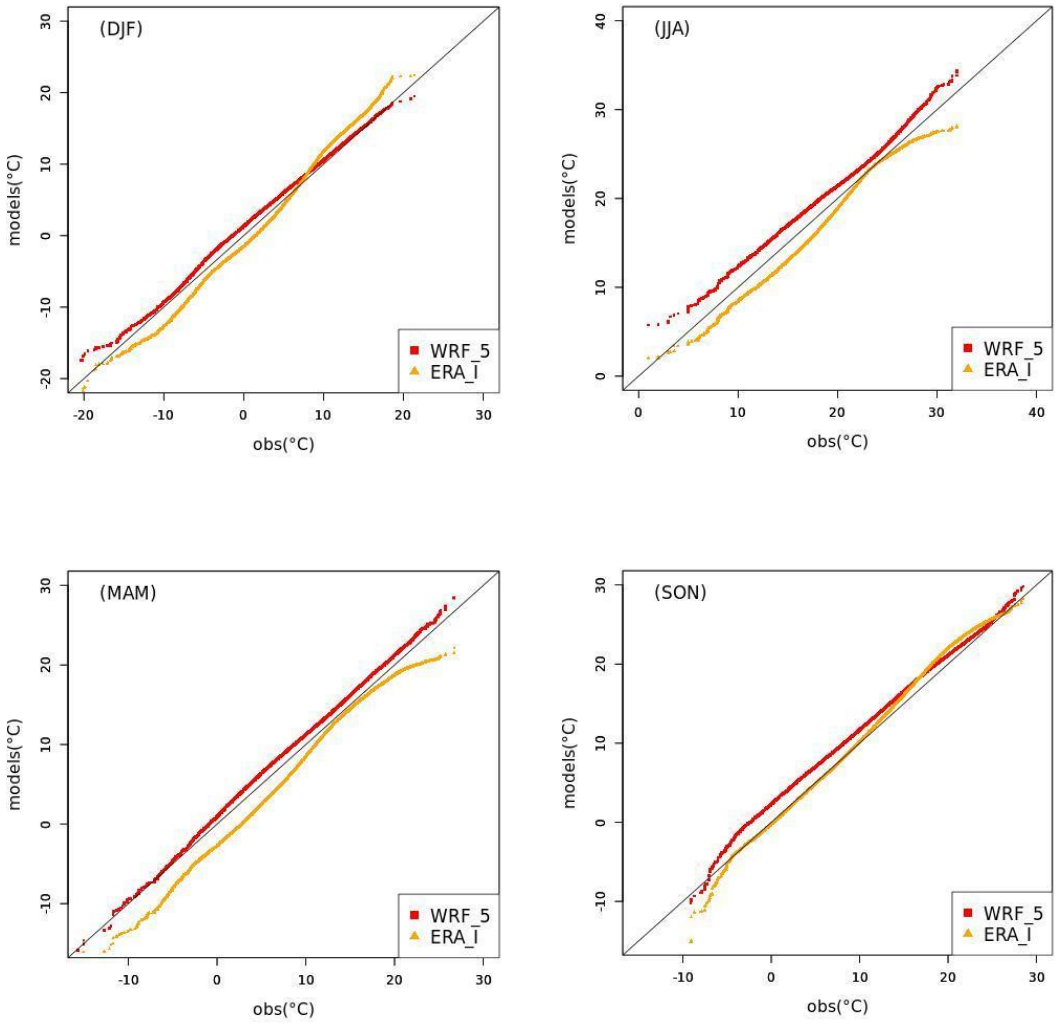

Figure 4.9 Q-Q plots of daily minimum (TN) temperature generated by WRF_5 and ERA-Interim for 1980-2004, in comparison with observations for all seasons.

Figure 4.10 presents the spatial distribution for each point station of monthly statistical errors MIA and MAE for temperatures. It would not be so safe to express an absolute conclusion regarding the minimum and maximum temperatures due to the poor sampling of the stations but, stations with lower performance were localized, such as those of Chania for TX and TN, Chania, Kalamata, and Lamia only for TN, see arrows in Figure 4.10 (a, b, c and d)).

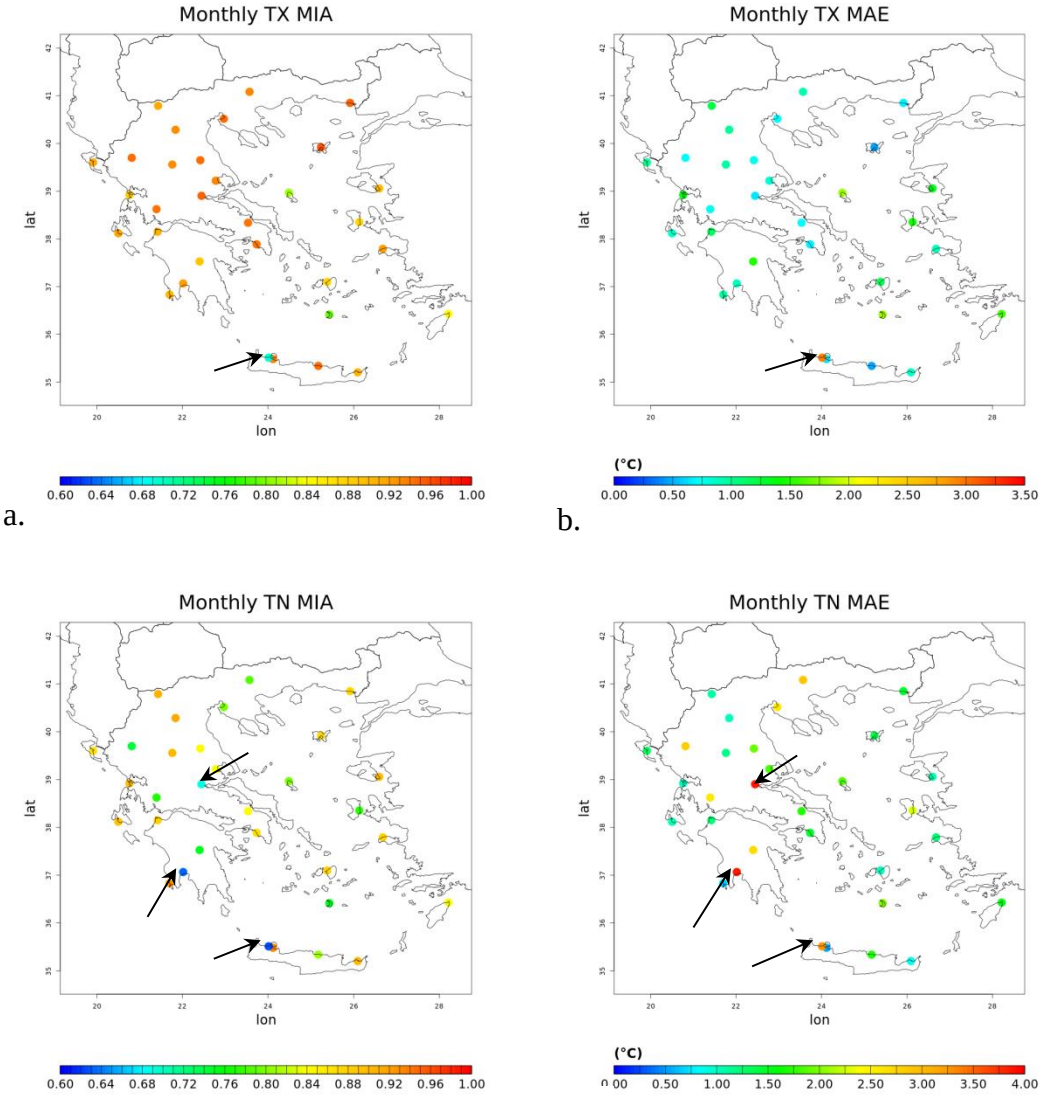

Figure 4.10 a.1980–2004 mean monthly MIA and b. MAE for TX, c. 1980–2004 mean monthly MIA and d. MAE for TN

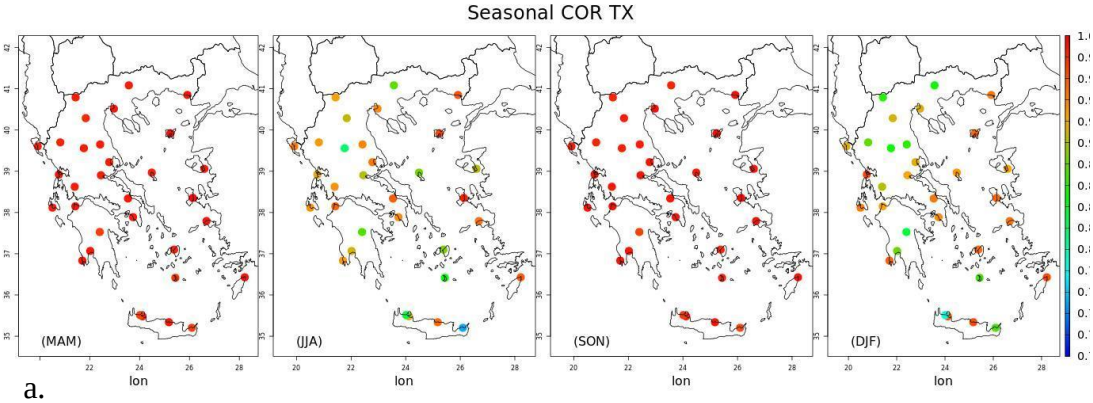

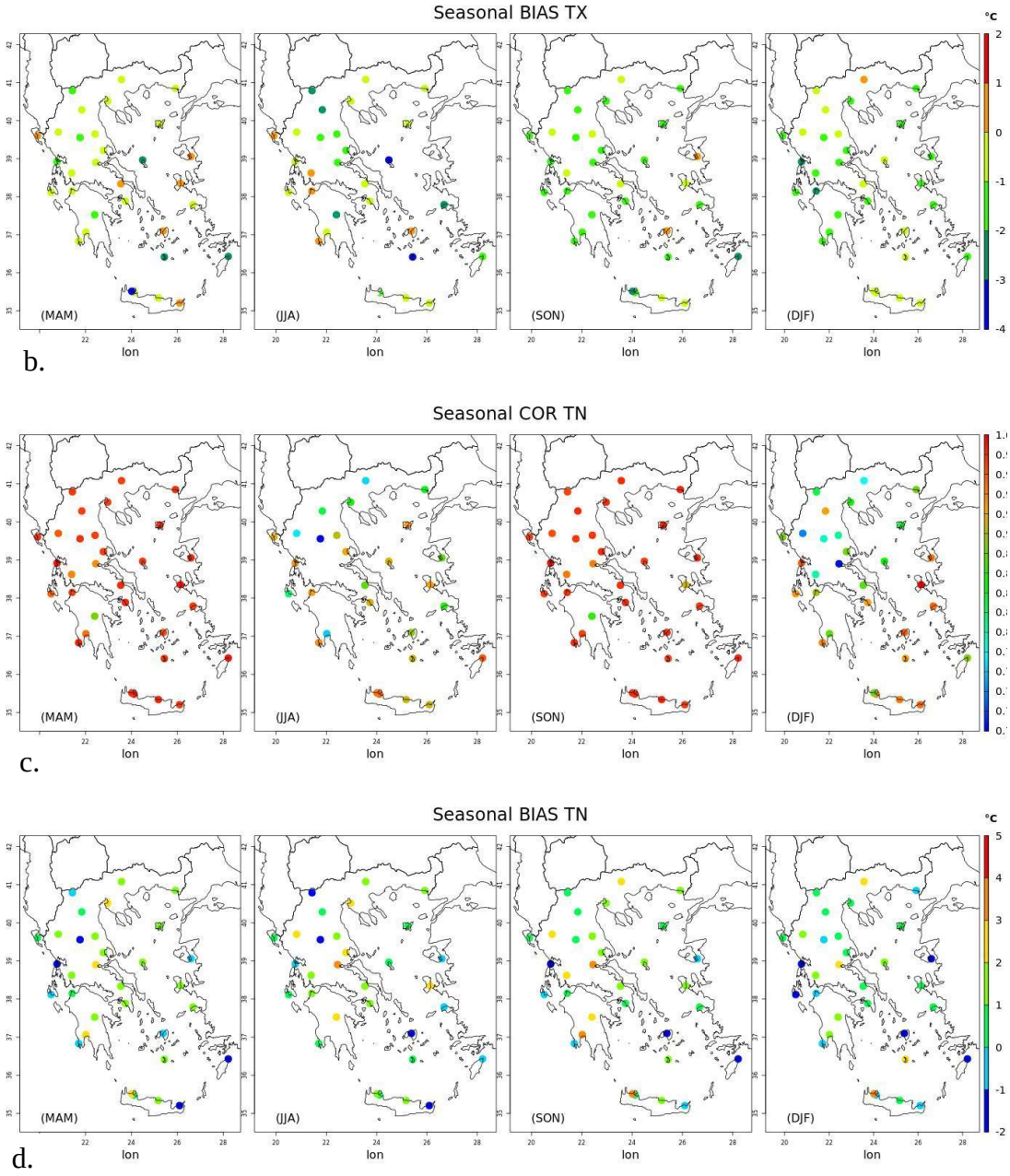

Figure 4.11 Spatial distribution for seasonal errors (COR and BIAS) for monthly maximum (a, b) and minimum (c, d) temperatures for the period 1980-2004 for WRF_5.

The spatial distribution of the COR and BIAS statistics, between WRF_5 and stations data for each season, is presented in the (Figure 4.11) for the examined meteorological variables. Regarding TX, there was a significant change in the model downscaling performance for winter and summer compared to spring and autumn. The correlation coefficient reached lower values (below 0.9) for the majority of the stations during DJF and JJA but not less than 0.8. The MAM and SON COR values were consistently high, around 0.98 for all stations. Bias error was under-predicted for all seasons in the majority of the stations, except for a few stations that slightly over-predicted TX during

mostly MAM and JJA (represented by orange to red colors dots). Similar results were found for TN concerning the seasonal correlations with values not lower than 0.9 except for a few stations during DJF and JJA where COR values varied from 0.7 to 1. A systematic warm bias was observed during all seasons except for colder bias, mainly in coastal stations, marked with blue color.

4.1.2 Evaluation of high-resolution Control-run simulations with EC-EARTH

In this section, the differences of mean annual variables between WRFEC Control Run (1980–2004) and station observations (OBS) were first presented. The individual grid point biases between the local observational stations and WRFEC simulation are shown in Fig. 4.12(a.) for TX and Fig. 4.12(b.) for TN.

TX – ANNUAL (WRFEC minus OBS) TN

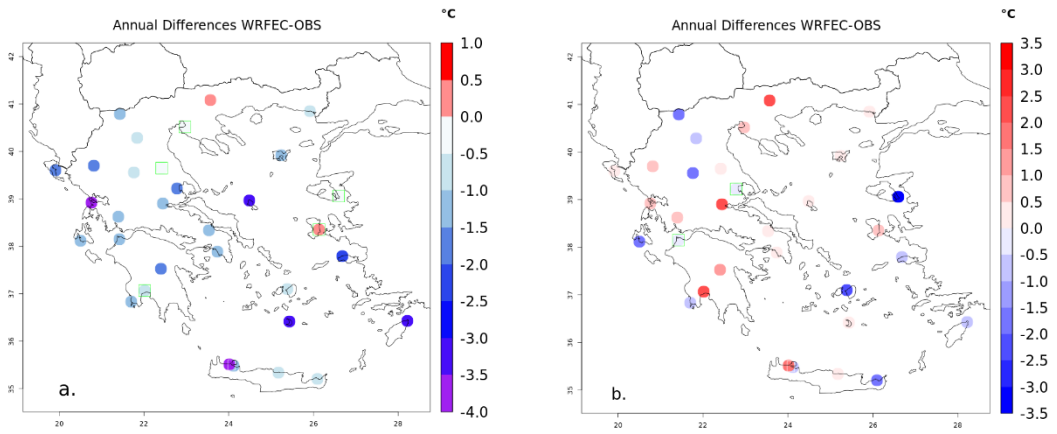

Figure 4.12 Differences of mean annual a. TX and b. TN between WRFEC Control Run (1980–2004) and station observations, (green square points specify no statistical differences between the mean distributions of annual temperatures according to Student's t test at the 95% confidence level)

It is obvious that the biases are not consistently negative or positive regarding the temperatures. WRFEC results revealed that no pattern was observed regarding the annual minimum and maximum temperature differences between model and individual station data. It was also noticed that most of the stations had differences in the range of -1.5 to 1.5°C for both temperatures. WRFEC model seems to underestimate the maximum temperatures and overestimate the minimum temperatures in the majority of the available stations. It is observed that the differences of mean annual variables

between modelled and observed variables of TX and TN are not enough relevant. Therefore, the monthly and seasonal model bias was also investigated. In Fig. 4.13 (a and b), the calculated mean maximum and mean minimum temperature monthly cycles, respectively, are depicted averaged over the historical period 1980-2004, along with the corresponding values of the standard deviation. The monthly mean values were calculated for each dataset at the grid-point location of each station and then averaged over the total number of points (stations). The monthly model results of TX show excellent agreement in the period from November to April, followed by an underestimation of the model from May to October (Fig. 4.13(a.)). On the contrary, the monthly simulated TN values agree better with observations in the period from May to October (except of June) with a slight overestimation of the model from November to May (Fig. 4.13(b.)). Overall, the monthly cycle patterns of TX and TN were well represented with WRFEC and highly correlated to the climatology of the country. The WRFEC simulation has very similar biases to the ones encountered in Politi et al. (2021), where the same model setup was forced by ERA-Interim. The higher biases are mostly associated with the warmer period months where WRFEC tends to produce lower maximum temperatures, while higher minimum temperatures are found during the colder months. The results indicate that GCMEC reproduces the observed monthly TX cycle but underestimates it. The performance of the global model improves in the case of monthly TN values, but it does not outperform the WRFEC model.

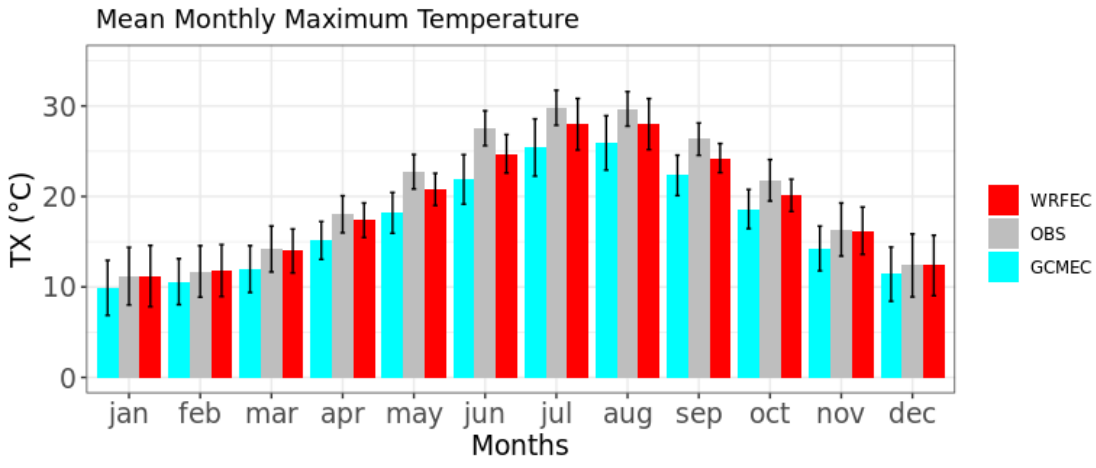

a.

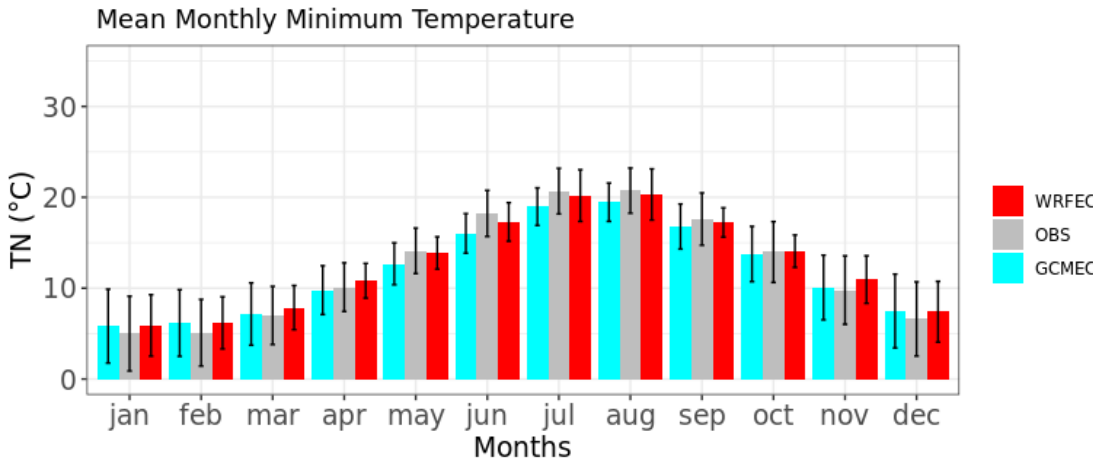

b.

Figure 4.13 Mean annual cycle of a) TX and b) TN averaged over the historical period of 1980–2004 for the total number of stations for GCMEC, WRFEC and OBS.

Figures 4.14 (a and b) depict the differences of 25 years seasonal mean maximum temperature and minimum temperature compared to the stations, respectively. The seasonal means are shown for winter (December, January, and February, DJF), spring (March, April, and May, MAM), summer (June, July, and August, JJA), and autumn (September, October, and November, SON). Smaller seasonal differences of maximum temperature are observed during the winter period in the range of -1 to 1.5°C. In particular, during winter there is a north - south gradient towards negative differences. On the other hand, the highest differences (above -5°C) are obtained during summer in a few coastal stations. Furthermore, the results showed more station locations with positive differences during spring and winter season, while negative differences are seen mainly during autumn, for the seasonal TX.

TX – (WRFEC minus OBS)

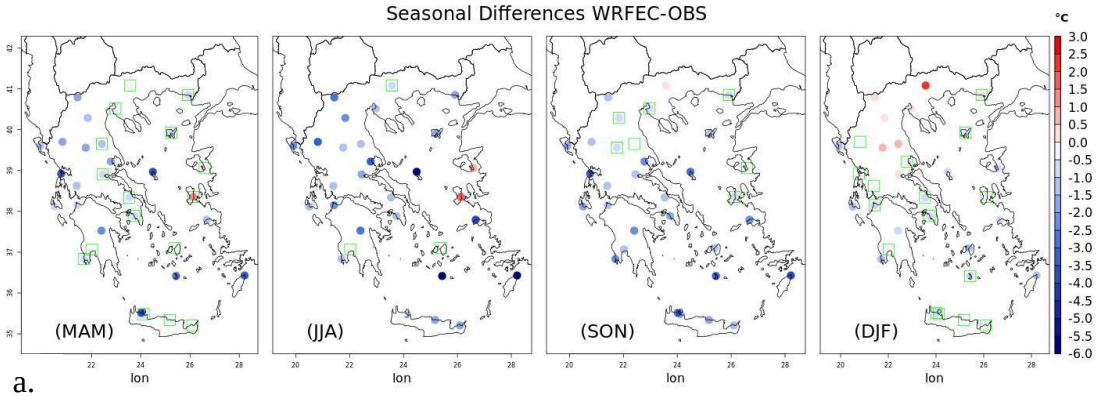

a.

TN – (WRFEC minus OBS)

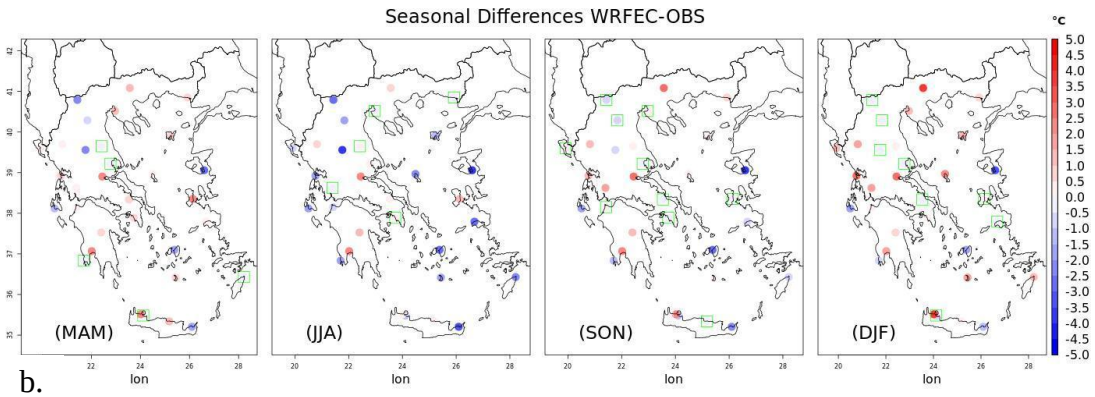

b.

Figure 4.14 Differences of mean seasonal a. maximum and b. minimum temperatures between WRFEC Control Run (1980–2004) and station observations, (green square points specify no statistical differences between the mean distributions of seasonal TX/TN according to Student's t test at the 95% confidence level)

Regarding the minimum temperatures, positive differences are found mainly during spring. The greater differences of about -2.5 to 2.5°C, are noticed during the summer period. Positive differences higher than 2°C (> 2°C) are also calculated in winter. It is observed that the majority of the stations with no statistically significant differences (green square points) in the mean values (-0.5° to 0.5°C) for TX, is observed during spring and winter seasons, while for TN during autumn and winter. The model presented also greater negative seasonal differences during summer regarding the minimum temperature in most areas, something that underlines the trend of the model to reduce minimum temperature in summer.

To assess our downscaled global model quantitatively, it was necessary to proceed to the statistical evaluation of the simulated mean fields from WRFEC with historical observations of the examined variables. The statistical errors (as described in APPENDIX) show the ability to represent the mean structure of the surface variables at different temporal scales for monthly to annual averages. The statistical analysis results of TX and TN were calculated using available observational data from the weather stations over the entire domain (Table 4.4). The approach for analysis also involved the investigation of the driver data performance of the global model EC-EARTH (GCMEC) by comparison with the observational data and WRF-EC output to showcase the added value of the downscaling methodology. Bias results of WRF-EC for all temperatures and time scales presented consistent values, which did not vary significantly between them, with cold bias around 1.1°C for maximum temperature and

a warm bias of 0.24°C for minimum temperature. The monthly, seasonal and annual scales correlation coefficients for TX and TN varied, of which seasonal values yielded the highest correlation of 0.95 and 0.94, respectively. In general, RMSE and MAE statistics progressively reduced along time scales, with the lower errors being identified on the annual scale. The efficiency scores of MIA and NSE showed an improved performance of the model on the seasonal scale with a range of values of 0.83-0.88. Furthermore, the statistical errors of WRF-EC presented improved values against GCMEC. Both temperatures of GCMEC revealed a colder bias (-2.98°C for TX and -0.4°C for TN). It is worth mentioning here, that WRF-EC produced an improved bias of TN, not only compared to GCMEC but also to the one of the downscaled reanalysis datasets with WRF in the study of (Politi et al. 2021). In addition, the RMSE and MAE metrics of the global model were larger than the ones of WRF-EC. Moreover, the efficiency metrics showed an improved performance of WRF-EC compared to the driver global model for all temporal scales. Thus, the statistical analysis of temperatures reveals a very good performance of the WRF-EC model and highlights the added value of the downscaled fields compared to those of the forcing GCM.

Table 4.4 Statistical errors of maximum and minimum temperatures and precipitation model results against observations for all grid points of available stations.

TX		COR	BIAS (°C)	RMSE (°C)	MAE (°C)	NSE	MIA
	Monthly	0.80	-1.13	2.99	2.35	0.83	0.80
WRCEC	**Seasonal**	0.95	-1.14	2.37	1.78	0.88	0.82
	Annual	0.65	-1.14	1.77	1.38	-0.37	0.5
	Monthly	0.92	-2.98	4.17	3.49	0.67	0.71
GCMEC	**Seasonal**	0.94	-2.97	3.78	3.21	0.67	0.69
	Annual	0.41	-2.98	3.33	3.06	-4	0.27
TN							
	Monthly	0.92	0.24	2.57	2.04	0.85	0.81
WRCEC	**Seasonal**	0.94	0.24	2.08	1.66	0.88	0.83
	Annual	0.83	0.23	1.6	1.26	0.67	0.72
	Monthly	0.87	-0.42	3.36	2.61	0.73	0.76
GCMEC	**Seasonal**	0.87	-0.42	3.07	2.38	0.74	0.76
	Annual	0.75	-0.42	2.76	2.02	0.10	0.76
PR		**COR**	**PBIAS (%)**	**RMSE (mm)**	**MAE (mm)**	**NSE**	**MIA**
	Monthly	0.41	-10.2	64.92	40.31	-0.16	0.54
WRFEC	**Seasonal**	0.57	-10	120.71	81.78	0.13	0.59

	Annual	0.39	2.9	292	212	-0.2	0.47
	Monthly	0.34	14.3	66.78	41.59	-0.12	0.40
GCMEC	**Seasonal**	0.49	14.2	133.17	89.83	0.2	0.45
	Annual	0.17	14.2	299.02	235.42	-0.34	0.36

Additionally, a worthwhile downscaling methodology should have the ability to simulate climate extremes well. For this reason, the quality of our downscaled results was assessed based on the realistic simulations of extremes of daily TX, TN, and RR for each season. Figure 4.15 shows the seasonal probability distributions of the daily minimum temperature for WRFEC model and station data.

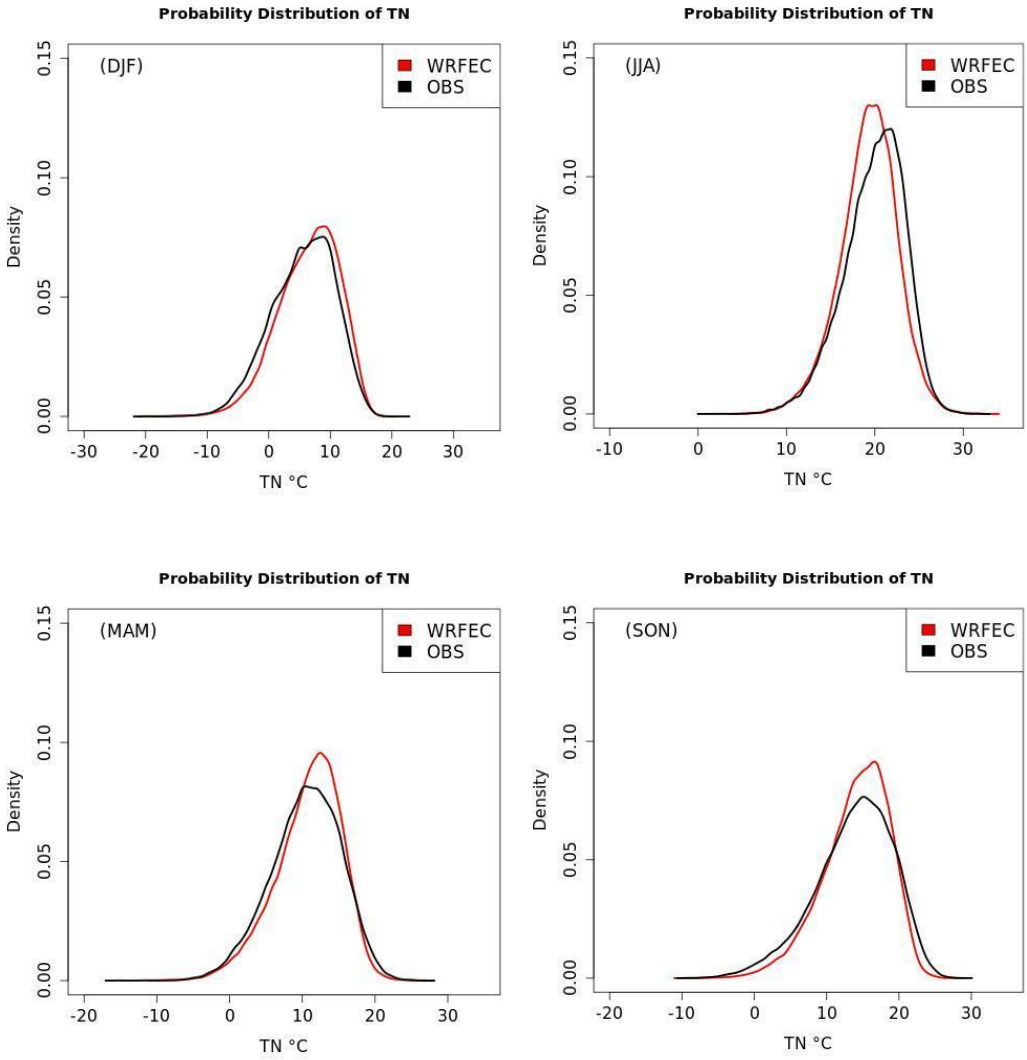

Figure 4.15 Comparison of density distributions of daily TN between WRFEC and observations for all seasons for 1980-2004

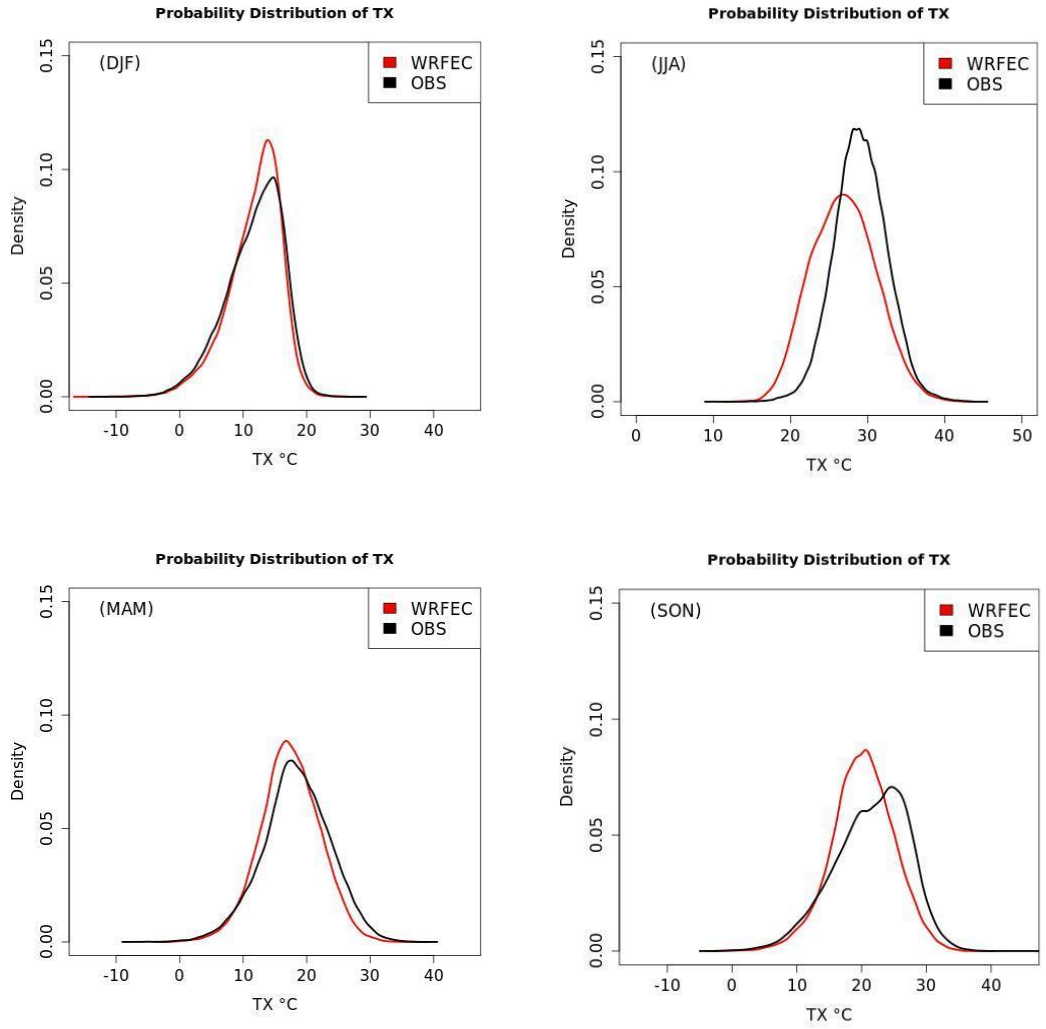

Figure 4.16 Comparison of density distributions of daily TX between WRFEC and observations for all seasons for 1980-2004

The median TN was underestimated by the model during the summer period, showing a significant shift towards colder values. Overall, the WRFEC simulations were in good agreement with the observations along with the distribution tails, during all seasons, with a very slight shift of the median TN towards warmer values, in winter, spring and autumn. Regarding the probability distribution of maximum temperature, illustrated in Figure 4.16, there was a significant shift towards lower temperature values in summer with lower density values. The median TX was also underestimated by the model during autumn but with higher density values than the observational data. A slight maximum temperature underestimation by the model compared to observations was observed for winter and spring.

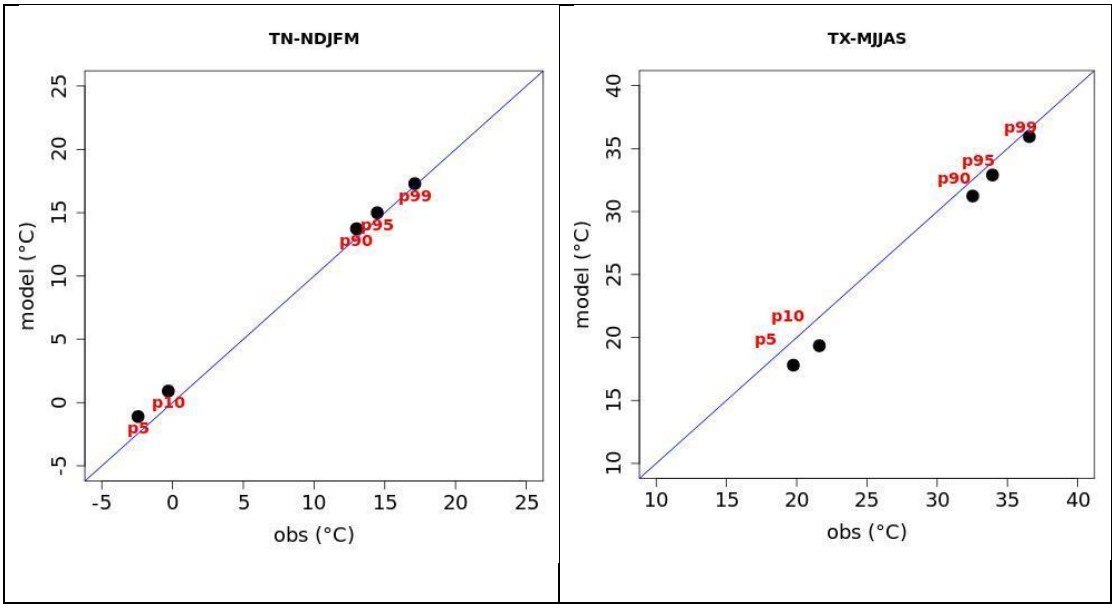

Figure 4.17 Comparison of temperature percentiles for extreme values for TN (left) and TX (right). TX was obtained from May to September (MJJAS) and TN was obtained from November to February (NDJF).

From the comparison of temperature percentiles for extreme values of model results versus observations (Fig. 4.17), a very good agreement is found in 90th, 95th and 99th percentiles of TN while a slight overestimation is obtained with the model in the coldest TN values (5th and 10th percentiles). The highest percentiles of TX (higher than 90) are slightly underestimated by the model. The two-sided Kolmogorov-Smirnov (KS) test was applied on daily data for each season and returned estimations of p-values<0.05 which rejected the null hypothesis of equal distribution between models and observations. In addition, the calculated Kolmogorov–Smirnov distances between simulated (WRFEC and CGMEC) and observed data provided a quantitative assessment of the added value of downscaling results. The comparison indicated that the high-resolution WRFEC model returned lower values of (KS) D than those of GCMEC on average for both temperatures and all seasons.

In what concerns the statistical results, Cardoso et al. (2019) reported that in the case of Portugal, EUROCORDEX models showed a cold bias regarding the maximum temperature and declared that those biases were clearly inherited from the forcing GCM since different RCM forced by the same GCM produced similar bias; on the other hand, the internal model variability played a stronger role in minimum temperature. Similarly, to the previously mentioned study, our findings of a cold GCM bias in TX are inherited also by WRF (Table 4.4). On the other hand, the sign of the TN bias changes in between

the coarse (GCMEC) and downscaled simulations (WRFEC). The slight poor performance of WRFEC for summer temperatures (a strong underestimation in summer TX and TN) could be probably related to boundary conditions deficiencies inherited by the GCM and/or due to the internal model dynamics and physics (Giorgi et al. 2001; Dasari et al. 2014).

4.2 Precipitation

4.2.1 Evaluation of high-resolution Hindcast simulations with ERA-I

a) Analysis of Spatial and Temporal Climatology

The WRF_5 mean annual cycle of monthly total precipitation (Fig. 4.18(a)) was well represented by the model concerning the maximum values in the winter and minimum ones in the summer period, with a rainier season from mid-autumn to mid-spring. According to the climatology of Greece, the precipitation patterns are generally higher during the late autumn and winter months, along with the most significant amounts of rainfall. In fact, in November and especially December, the country receives the highest amounts of monthly rainfall, which decreases towards spring (Zerefos et al. 2011). Substantially low precipitation amounts characterize the spring and summer months.

WRF_5 leads to an improvement in representing the annual cycle (Fig. 4.18(a)) in comparison with ERA-I, as it presents a better agreement with observations, except for March and the period between May and July. WRF_5 slightly overestimates the rainfall amounts between January and July; however, from August to November the WRF performance is strikingly accurate and the WRF_5 annual cycle almost overlaps with that of observational data. In November and December, the performance of the model reversed, resulting in lower precipitation values than the observations.

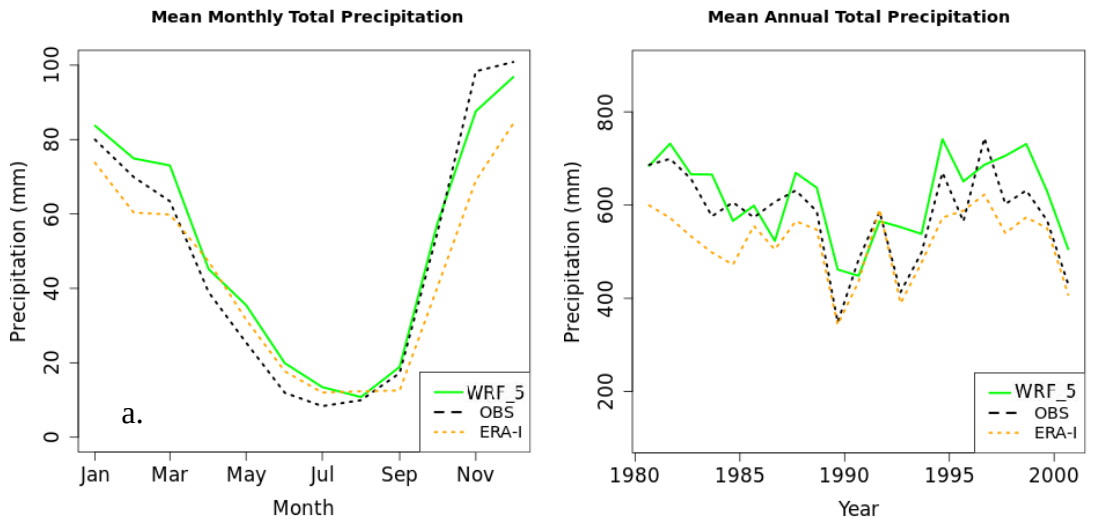

Figure 4.18 a. Mean annual cycle and b. inter-annual variability of precipitation (mm/month) averaged over the historical period of 1980–2000 for the total of stations.

The overlapping of WRF_5 annual cycle with that of observational data between August and November, is a good indicator of WRF's ability to produce rainfall correctly when nested in good-quality boundary conditions (García-Díez et al. 2015) because the model parameterizations have a higher impact on rainfall outputs when precipitation is controlled by local factors mostly during the late summer and mid-autumn (Argüeso et al. 2012).

On the other hand, the ERA-I simulations underestimated rainfall during most months of the year (August until April) but an overestimation was found between May and July. Annual precipitation can also vary considerably from year to year, as Fig. 4.18b illustrates the inter-annual cycle of the historical period from 1980-2000. WRF_5 overestimated the mean total precipitation for some years while ERA-I tended to underestimate it. ERA-I and OBS precipitation patterns have only a very close agreement between the years 1989 and 1994. Figure 4.19a shows the spatial distribution of mean annual total precipitation for ERA-I and WRF_5 in comparison to point observations (together in the same figure). The WRF_5 model captured well, in general, the observed spatial pattern of the annual precipitation fields, while it was more than evident that for ERA-I, it failed to depict the variance in the spatial distribution by smoothing the precipitation patterns in the mountainous areas. Both ERA-I and WRF_5 outputs showed that the maximum values of annual total precipitation were observed in the western part of the domain and over the mainland in a direction running from northwest-to-southeast due to the presence of high mountains. On the other hand, the annual total precipitation pattern showed smaller values over the Aegean Sea following the climatology of the country.

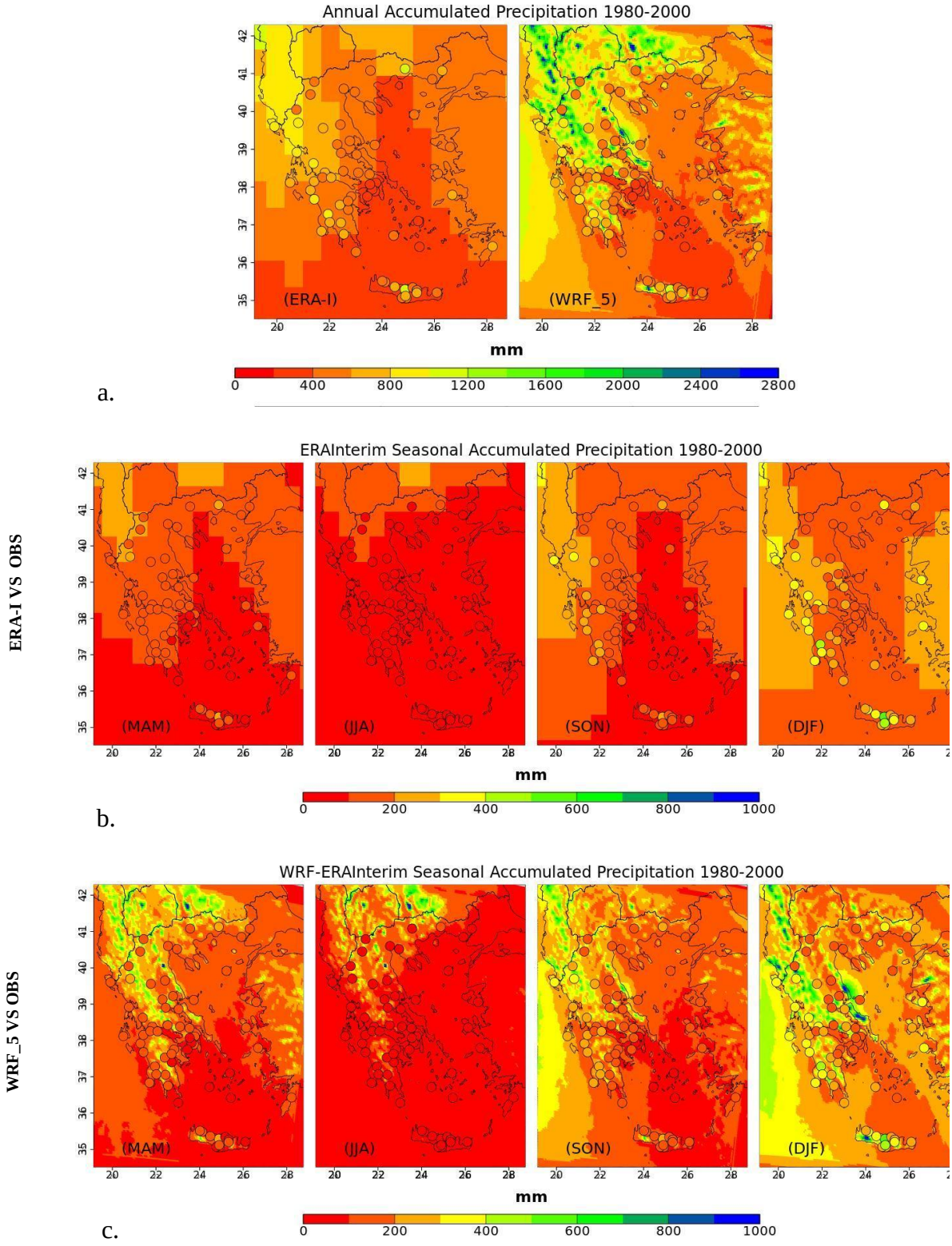

Figure 4.19 a) Annual total precipitation climatology averaged over the historical period of 1980–2001 for ERA-I and WRF_5 in comparison to weather station data (points data). b) Spatial distribution of mean seasonal accumulated precipitation over the historical period of 1980–2000 for ERA-I and for c) WRF_5 in comparison to weather station data (points data)

At this point, it should be pointed out that due to the coarse station network on mountainous areas, it was not feasible to verify the excessive and more intense rainfall amounts. For this reason, a cross-comparison was made with the mean annual precipitation provided by the climate atlas of Greece for the period 1971-2000. The climate atlas has been developed by the formal meteorological organisation of Greece, the Hellenic National Meteorological Service (HNMS) and is available at http://climatlas.hnms.gr/sdi/?lang=EN. Although there is a 10-year offset, this dataset remains the only reliable source of information on the mean climatology of Greece. The cross-comparison shows that the spatial model performance is in good agreement with the HNMS data, as large rainfall amounts above 2000mm are mainly observed on the mountains of western Greece (Pindos), the Mount Olympus and the mountains of the island of Crete, while 1200 to 2000 mm are observed on the mountainous regions of the Peloponnese. Additionally, these findings are in line with the Report of the Bank of Greece (Zerefos et al. 2011) and (Nastos et al. 2016), where the mean annual precipitation received by the Greek mountain ranges is reported to be above 2,200 mm over Pindos, 1,800 mm over the mountains of Crete, and 1,600 mm over the mountains of the Peloponnese. The lowest amounts below 400 mm are reported in the two mentioned studies, in the Saronic Gulf, the Eastern Peloponnese and the islands of the Southern Aegean (see Fig 3.1(a) – for location guidance). Furthermore, there are not available validated satellite high-resolution data that could be reliably used for model output validation because there are limitations in the evaluation of the satellite data, mostly due to the complex terrain of Greece and the data sparse mountainous regions, as acknowledged by Nastos et al. (2016). However, Tian et al. (2020) based on other studies of Herrera et al. (2010), Heikkilä et al. (2011), Argüeso et al. (2012) explained that complex terrain with high elevations (e.g., over high mountains) of more than 2,000 m are related to the highest deviations of precipitation produced by the model, suggesting that WRF at a 10 km resolution may still not capture these topographical features. Based on this and the description of the model topography (Figure 3.1, chapter 3), it could be assumed that the current deviations in precipitation amounts between the WRF_5 and OBS are due to the model horizontal resolution and the coarse network of the stations.

Figure 4.19 (b and c) depicts the spatial distribution of mean seasonal total precipitation for ERA-I, WRF_5, with point observations, respectively. WRF_5 model results were

overall in agreement with the observations for the rainier seasons of autumn and winter. They also presented higher precipitation amounts over mountainous areas and in the western parts of the country, following the known climatological patterns. Besides, the spatial pattern of precipitation in Greece is strongly associated with orography, and almost all low-pressure systems crossing the country and resulting in intense rainfall come from the west. Finally, the spatial distribution of ERA-I seasonal total precipitation did not yield a variation across the domain that could be comparable to that of the observations in autumn and spring seasons (Fig 4.19b).

b) Evaluation based on statistical metrics

The WRF_5 overestimated the rainfall during most months of the year, particularly from April to July, and underestimated it in November and December. On the other hand, ERA-I underestimated precipitation during autumn and winter months.

The annual cycle of the mean statistical errors calculated for the monthly total precipitation is depicted in Figure 4.20, concerning WRF_5 simulations and ERA-I against observations. The results obtained with the WRF_5 produced similar MAE and RMSE errors but higher correlation with the observed annual cycle compared to those of reanalysis which outperformed WRF_5 during summer months. Moreover, the annual cycle of the efficiency metric MIA showed an improved performance of the model compared to reanalysis. The NSE score for WRF_5 was negative only during May and summer. Its value for the rest of the months indicates positive model skill. Therefore, overall, the downscaled WRF_5 simulation clearly showed some added value compared with the driver reanalysis dataset ERA-Interim.

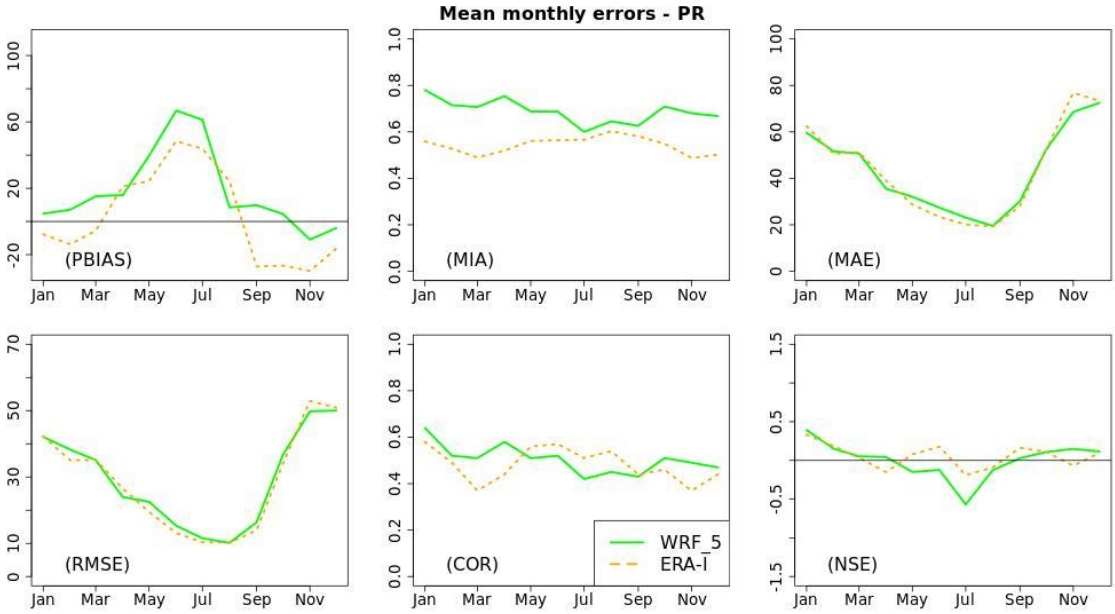

Figure 4.20 Annual cycle of mean monthly precipitation errors (PR) of the ERA-I (dotted orange) and 5-km WRF (solid green) simulations over the entire domain.

Figure 4.21 presents the spatial distribution for each point station of monthly statistical errors MIA and MAE for precipitation. Concerning the spatial pattern for precipitation, MIA values in the majority of the stations range from 0.7 to 0.9 with some exceptions in the north of the country, and some limited coastal stations with values above 0.6.

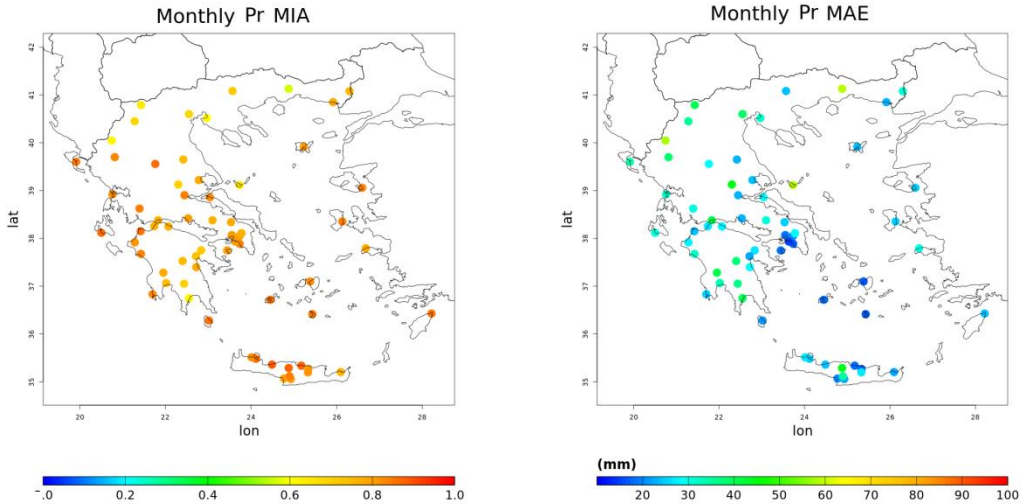

a. b.

Figure 4.21 a. 1980–2000 mean monthly MIA and b. MAE for PR, calculated for each station grid point for WRF_5

Some of these stations presented absolute errors above 30 mm (and probably related to mountainous or coastal locations), while most of them showed values between 10 and 30 mm.

Regarding the seasonal statistical errors of monthly precipitation for WRF_5 and ERA-Interim (Table 4.4, subsection 4.1.2), comparable results were found concerning the correlation, where model values were low in the range of 0.47 in summer to 0.62 in autumn but slightly better than ERA-I. Seasonal biases of WRF_5 were significantly lower compared to ERA-I, except in the spring and particularly in the summer, where a higher overestimation was noted. The amplitude of RMSE errors was also comparable for all seasons between WRF_5 and ERA-I.

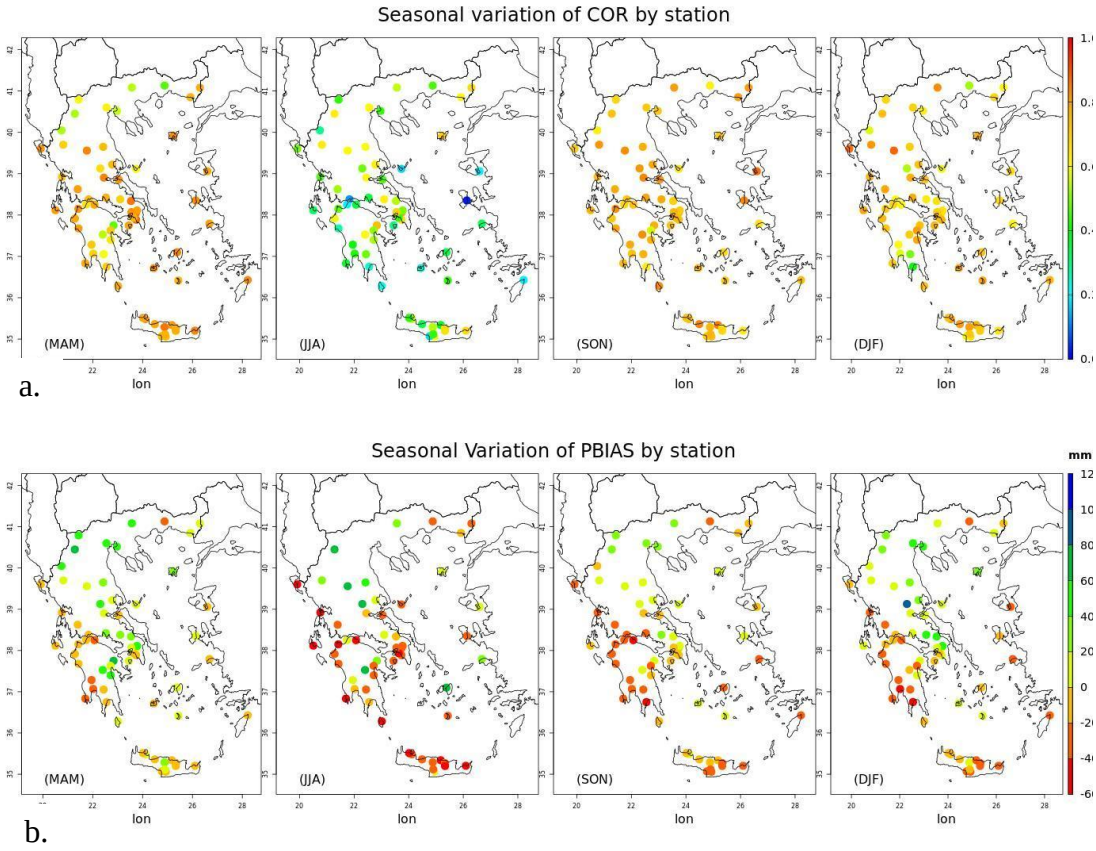

Figure 4.22 Spatial distribution for seasonal errors (COR and PBIAS) for monthly cumulative precipitation for the period 1980-2000 for WRF_5

Likewise, concerning the precipitation fields, (Figure 4.22a), the seasonal pattern of WRF_5 yielded similar correlation coefficients for all stations with a range of 0.6-0.85, showing a good ability of the downscaling process to describe the precipitation in Greece with slightly higher values specifically in autumn. However, in summer, the correlation values were smaller. This correlation pattern was in agreement with the

global seasonal precipitation. In all seasons, WRF_5 downscaled results overestimated precipitation in most parts of Greece, except in the southwest coasts as well as in the eastern coast (and islands) in the winter, where precipitation was underestimated with a range -40 to -10% (Figure 4.22b). The WRF_5 performance was regarded as outstanding because pbias rarely exceeded ±25-30% in the majority of the stations, in agreement with Argüeso et al. (2012).

c) Probabilities densities and Q-Q plots

To compute the PDF for precipitation, only the rainy days with precipitation amounts higher than 1 mm (Tank et al. 2009) were included, because the focus was placed on the examination of the probability of rainfall intensity and not of the precipitation occurrence. The seasonal frequency distribution of daily precipitation (Fig. 4.23) was plotted on a logarithmic scale with bins of 1 mm to highlight the extremely strong precipitation rates. Climate models tend to produce too much light precipitation, also verified for WRF according to our study. During all seasons, the downscaled model results improved compared to ERA-I, which presented a higher left shift with the absence of the highest precipitation bins due to the smoother fields of reanalysis. Noticeable were some cases where WRF produced excess precipitation events (above 200 mm/day) compared to observations during spring. That might be caused either by the model or by the station density that could be too low to accurately satisfy the WRF_5 resolution, especially in mountainous areas. Based on observations, the longest tails, with events close to 200 mm/day were observed for winter and particularly in autumn. Sometimes, the later season is also associated with extratropical cyclones, which produce intense extremes and flooding events in West Greece (Pytharoulis et al. 2000; Nastos et al. 2018; Emmanouil et al. 2021). These events were properly captured only with the higher resolution simulations of WRF_5.

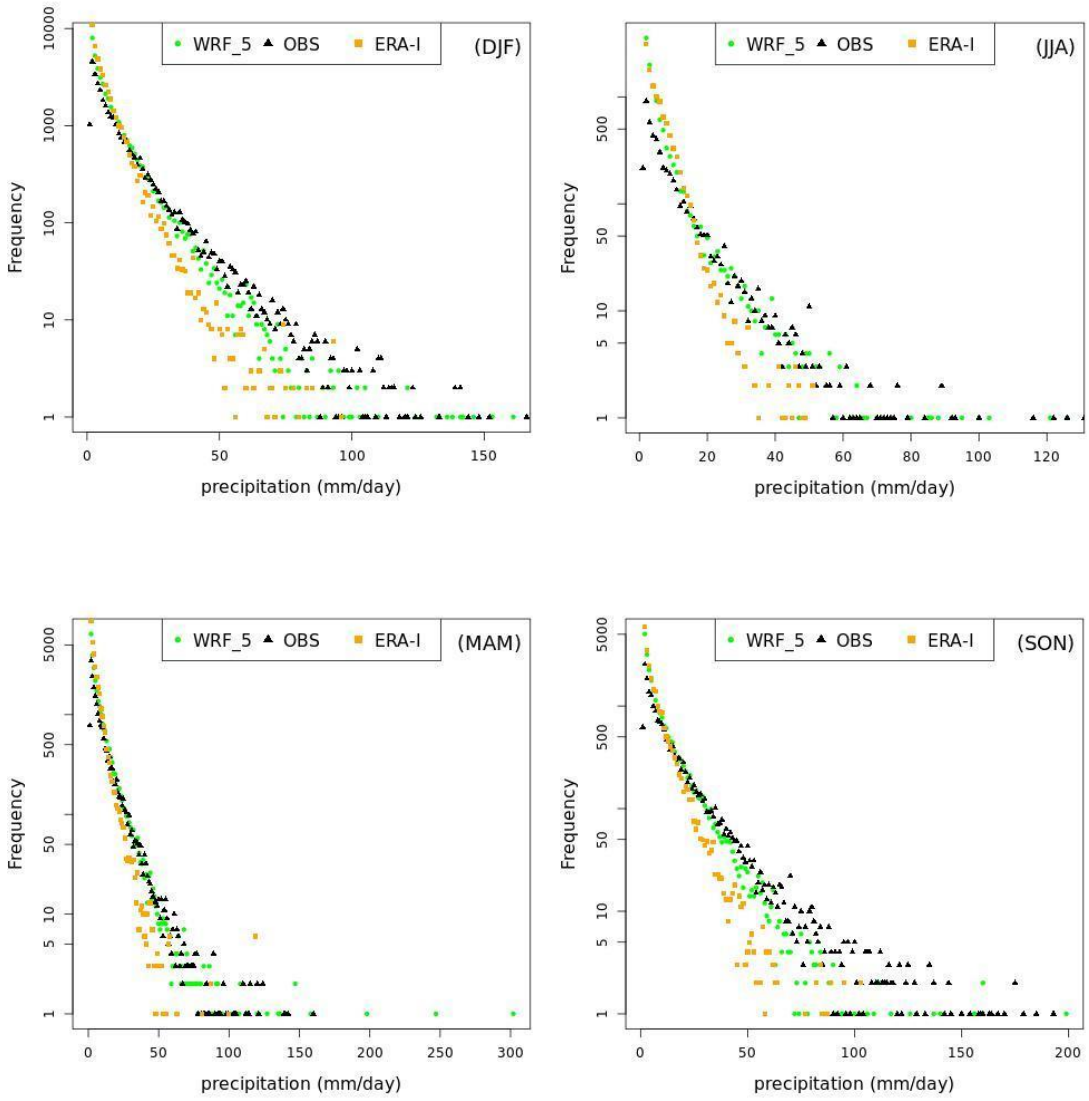

Figure 4.23 Comparison of frequency distributions of daily precipitation between WRF_5, ERA-Interim and observations for all seasons in the period 1980-2000

Figure 4.24 depicts the quantiles distribution of simulated and observed precipitation data to assess further the ability of the model to produce extremes. It was evident that WRF_5 presented more efficiently, especially the higher-ranking quantiles than ERA-I in all seasons, with the closest description of quantiles found in spring. Although during all seasons, both ERA-I and WRF_5 persistently underpredicted the strongest precipitation events, WRF_5 only presented the ability to overestimate the extreme quantiles in the spring, a fact that was also verified in the previous PDF analysis. The ERA-I dataset could not capture the high-intensity event tails in any of the cases due to the relative homogeneity induced by the coarse resolution of reanalysis.

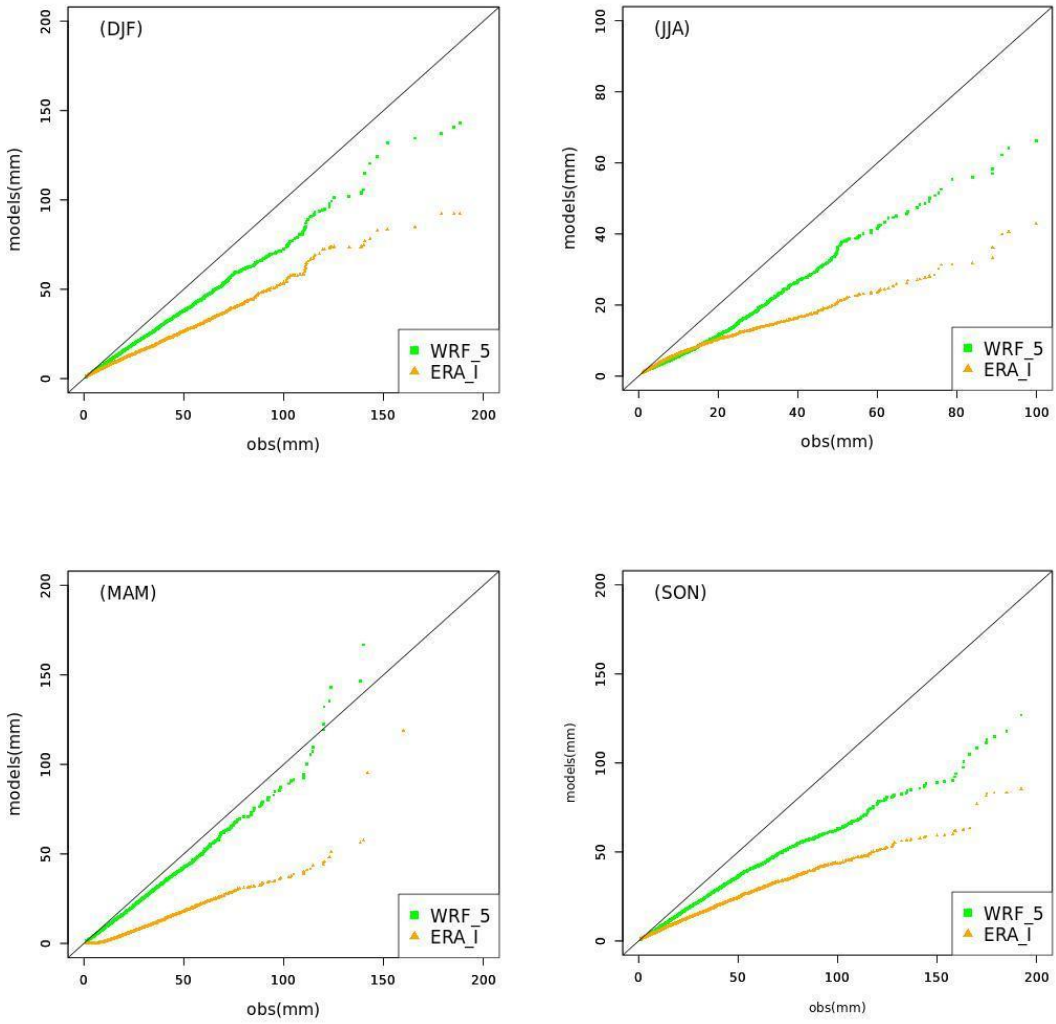

Figure 4.24 Q-Q plots of daily precipitation generated by WRF_5 and ERA-Interim for 1980-2000, in comparison with observations for all seasons.

4.2.2 Evaluation of high-resolution Control run simulations with EC-EARTH

Model results were overall in agreement with the climatology of Greece, where the precipitation patterns were generally higher during the late autumn and winter months, along with the most significant amounts of rainfall. The results also yielded higher precipitation amounts over mountainous areas and in the western parts of the country that were strongly associated with the orography, and the fact that almost all low-pressure systems crossing the country and resulting in intense rainfall come from the west. Indeed, during fall and winter prevailing westerly winds from the Ionian Sea hit the west coasts and the mountain range of central mainland (Pindos), generating precipitation all along the west region of Greece. Thus, the orographic precipitation is

an important phenomenon that affects a large portion of the west part of the country. The windward side of a mountain affected by prevailing winds is usually wetter and the leeward side of the mountain is usually dryer due to the moisture released when precipitation occurs. WRCEC results are in line with the climate atlas that has been developed by HNMS) (available at http://climatlas.hnms.gr/sdi/?lang=EN), also described in detail in the hindcast analysis by Politi et al. (2021). In the study area, the good representation of the major mountainous locations and coastline obtained with the downscaling approach allows the production of cyclogenesis and the associated orographic wind systems whatever the quality of the large-scale circulation provided at the RCM's boundaries by the global model (Politi et al. 2021).

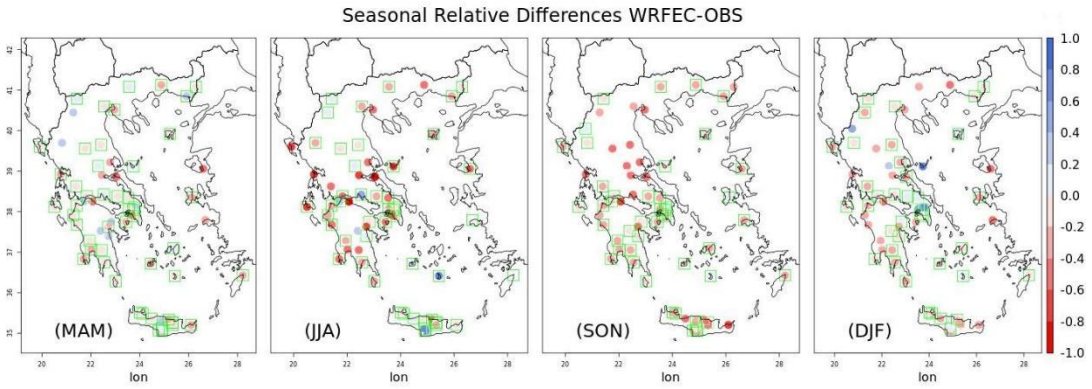

Figure 4.25 Mean seasonal total precipitation between WRFEC Control Run (1980–2004) and station observations, (green square points specify no statistical differences between the mean distributions of seasonal RR according to Student's t test at the 95% confidence level)

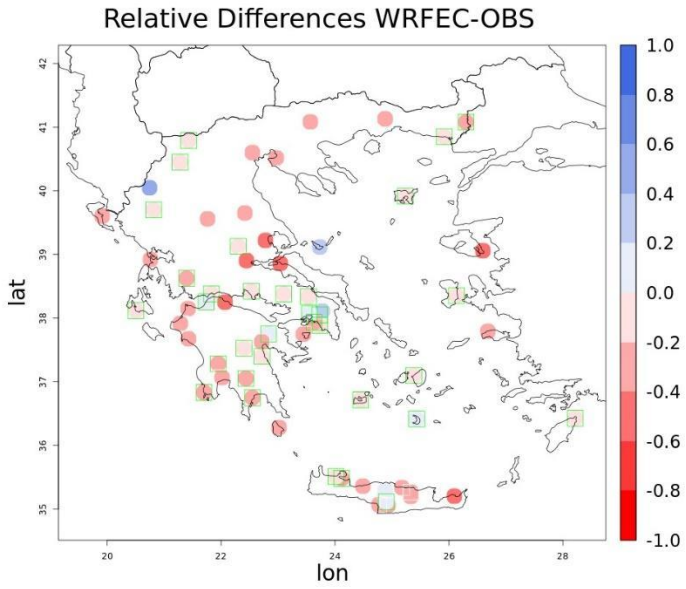

Figure 4.26 Relative differences of a. mean annual total precipitation between WRFEC Control Run (1980–2004) and station observations, (green square points specify no statistical differences between the mean distributions of seasonal RR according to Student's t test at the 95% confidence level)

The seasonal relative differences illustrated in Figure 4.25, revealed that WRFEC overall reproduced well the observations, with a general small dry bias (up to -0.4) during all seasons and a few localized exceptions of wet bias, in accordance with the results described by Soares et al. (2017). More specifically, it was found that particularly in summer and less in autumn, WRFEC underestimated slightly the precipitation in parts of the west and central Greece. The annual relative differences (in fraction) in Figure 4.26 showed a consistent pattern of underestimated annual precipitation from WRFEC in the range of 0.2 to 0.4, in the west and north stations of the country. On the seasonal scale, the majority of the station points have no statistically significant differences among observed and model mean values during all seasons (Figure 4.25). On average, only around 10 stations out of 66 present statistically significant differences with the higher number of stations found in autumn and winter seasons. On the annual temporal scale, almost half of the stations (29 out of 66) do not present statistically significant differences in the mean values between the observed and simulated points (Figure 4.26). In addition, the model showed some difficulty in describing some regions characterized by high relative differences, probably due to coarse station density which is associated with the complex topographical features. The

light seasonal rainfall under-prediction was over most parts of the country, but with a good description of the spatial precipitation pattern.

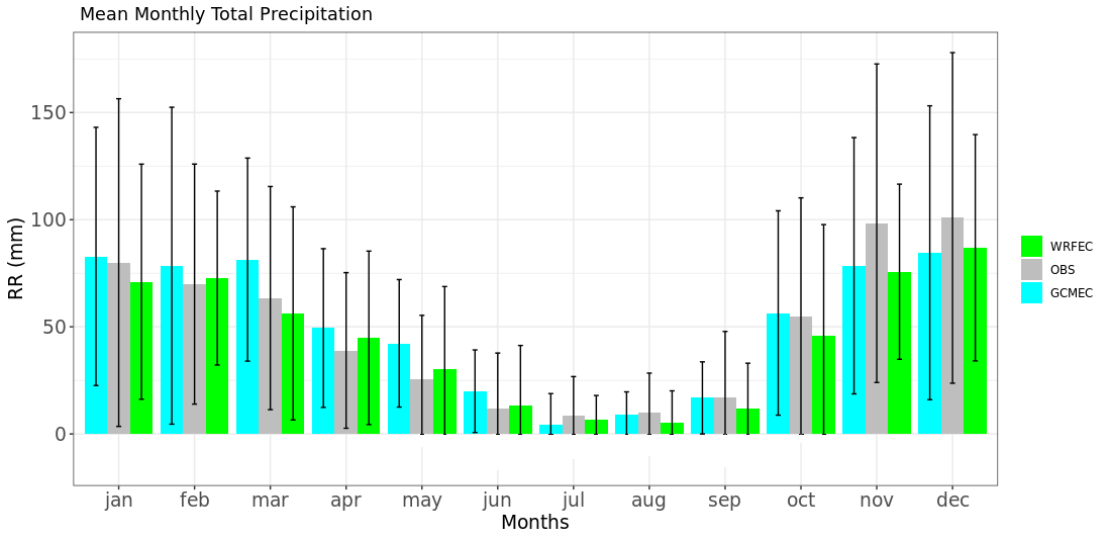

Figure 4.27 Mean annual cycle of precipitation (mm/month) averaged over the historical period of 1980–2000 for the total number of stations for GCMEC, WRFEC and OSB.

The WRFEC mean annual cycle of monthly total precipitation (Figure 4.27) was sufficiently represented by the model concerning the maximum values in the winter and minimum ones in the summer. In comparison with observations, WRFEC generally underestimated the rainfall amounts. The under-prediction was observed in January and between March and April, while from April to June the model slightly overestimated precipitation. In particular, the model's performance in June and July was strikingly accurate, however from August to December the performance of the model reversed, resulting in lower precipitation values than the observations, particularly in November and December. Yet, it should be emphasized that the rather large error bars in all datasets analyzed are due to the large spatial variability of precipitation in the study area (Hatzianastassiou et al. 2008). Overall, GCMEC tends to overestimate the values from January to July, and indicates a better performance compared to WRFEC only in January, August, September and October.

Regarding the precipitation statistical errors over the entire domain (Table 4.4, subsection 4.1.2), the values of COR, NSE, and MIA remained lower than those on temperatures. In general, the WRFEC model underestimated precipitation compared to observations on monthly and seasonal scales (less than 10%) but presented a very good performance on the annual scale with a small positive pbias of 2.9%. On the other hand,

GCMEC consistently overestimated precipitation (around 14% in all temporal scales). As in the case of temperatures, the seasonal values of WRFEC precipitation yielded the highest correlation of 0.57, larger than that of the GCMEC value (0.45). In general, the WRFEC model yielded a noticeable improvement on precipitation compared to GCMEC according to the error statistics (Table 4.4). Also, those statistics presented a very much improved agreement when compared to the study of Kotlarski et al. (2014) that reported precipitation biases in the ±40% range, regarding the EUROCORDEX ability to represent the European precipitation.

The seasonal frequency distribution of daily precipitation (Figure 4.28) was plotted on a logarithmic scale with bins of 1 mm to highlight the extremely strong precipitation rates.

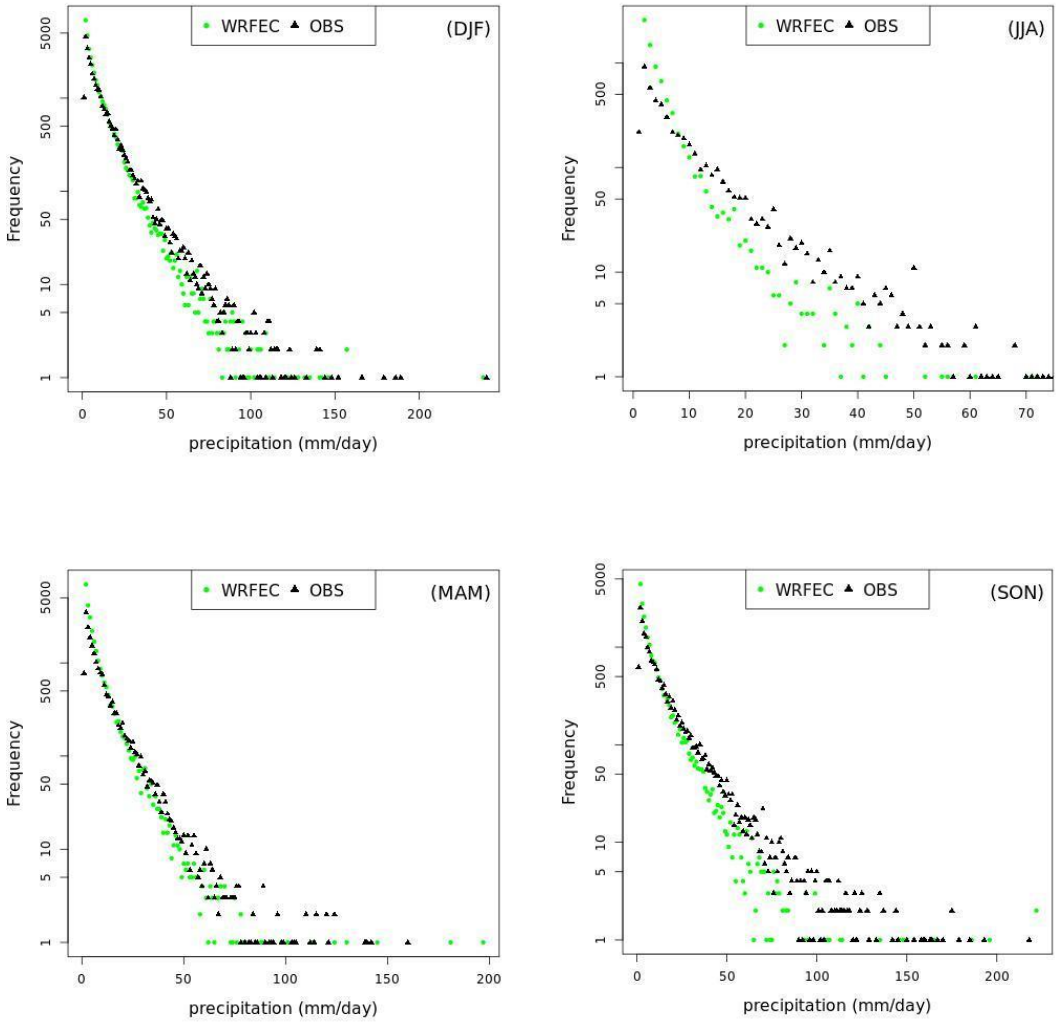

Figure 4.28 Comparison of frequency distributions of daily precipitation between WRFEC and observations for all seasons in the period 1980-2000.

Overall, the model underestimated the precipitation events below 100 mm/day in winter and autumn but could produce more extreme events during those periods. Noticeable is the case where the model produced in excess precipitation events (above 150 mm/day) compared to observations during spring. That might be caused either by the model or by the station density that could be too low to accurately satisfy the WRFEC resolution, particularly over mountainous areas.

Furthermore, for the longer-term temporal statistics (e.g., seasonal, annual), which are of interest to the present study, the added value in higher-resolution simulations is not always evident in current RCMs. Downscaling with a limited area model as WRF contributes to partly replicating the inaccurate feature of the large-scale field from the global model even in the boundary layer where small scale processes dominate its dynamics. For example, comparisons between 0.11° and 0.44° EUROCORDEX experiments indicated no systematic temperature bias reduction in the high-resolution experiments, while for precipitation, seasonal mean biases could be larger in the higher-resolution EUR-11 set of simulations (Kotlarski et al. 2014; Soares and Cardoso 2018; Zittis et al. 2019). Although our simulation has some biases in most variables, no significant departures are noticeable from observations. It is also a positive outcome that the model brings high detail in the spatial patterns and added value to the probability distributions, as the simulated frequency distribution of the precipitation and temperature extremes from the 5-km WRFEC is consistent with the observed structure and extreme values.

4.3 Main Conclusions for Hindcast and Control run

The investigation showed that the WRF model might very well represent the annual and seasonal geographical distribution of TX and TN in the study area. Also, the high-resolution model produced the seasonal differences observed with similar ranges concerning the temperature values, although there was a limited number of meteorological stations available (a network of 32 stations of continuous observations). Similar were the findings of (Kryza et al. 2017) who indicated that the spatial distribution of meteorological variables obtained with the WRF model with the same

horizontal resolution (5km x 5km) for Poland was convincingly reproduced, following the country's climatology. It was pointed out that the comparisons with similar regional climate studies should carefully be performed, as there can be quantified and qualified differences between geographical regions in terms of data availability, station network density, horizontal resolution, and driving forcings.

It is regarded as a valuable and important finding that our downscaling methodology provided a very good agreement with the observations for maximum and minimum temperatures compared to the coarse resolution ERA-Interim. More specifically, considering TX, WRF_5 reduced remarkably the daily bias from -2.19ºC of reanalysis to -0.6 ºC with a very high correlation coefficient equal to 0.96. The same range of bias error (mean surface temperature) was also found by Kryza et al. (2017) that was equal to 0.23 ºC for Poland, (but resulted from the use of twice as many stations) and Soares et al. (2012a) for Portugal with 9 km of horizontal model resolution, with the value of 0.1ºC. Another study of Heikkilä et al. (2011) using WRF at 10 km resolution and forced by ERA-40 reported a mean bias of -0.7 ºC and 0.97 correlation.

Concerning TN, although a cold bias of ERA-I was found to change to warm bias from -0.5 ºC to 1ºC, all the other statistical metrics unveiled that downscaled model results remained to present the best performance against reanalysis. Other studies did not report improved results but a similar range of bias (e.g., Soares et al. 2012) from 0.5 ºC to -0.4 ºC. Daily maximum and minimum temperature biases were between 0.06 to 1.84 ºC in the study of (Zhang et al. 2016) for the Hawaiian Islands.

Generally, improved results for WRF_5 were also found regarding the RMSE and MAE values of monthly TN in seasonal analysis, although correlation coefficients were comparable. PDF analysis and quantiles revealed an improvement of WRF_5 during spring, winter, and autumn but not for summer for the extreme quantiles compared to reanalysis.

Regarding precipitation, WRF_5 model results, as well as ERA-Interim, reproduced reasonably well the observed precipitation at monthly and inter-annual time scales, evidenced by the two more rainy seasons, spring and autumn, and the winter precipitation maximum. These results were generally in line with previous analyses (e.g., (Fantini et al. 2018)) that simulated similar regions (e.g., Italy).

Overall, WRF_5 reproduced well the spatial pattern of the observed annual and seasonal precipitation in most parts of Greece, even though there were large wet biases over the mountainous regions. These biases most likely resulted from the unrealistic simulation of rain shadow effects on precipitation caused by the high mountains (Tian et al. 2020). Precipitation results were better reproduced in our WRF-downscaled simulations compared to ERA-Interim because biases and RMSEs were significantly reduced by the downscaling.

Precipitation values satisfactorily correlated with observations from 66 stations (covering the period 1980-2000), uniformly distributed over the study area (monthly correlation coefficient mean COR = 0.67 for all stations; and seasonally COR = 0.62–0.82 for individual stations). Those findings were not as good as in the study of Cardoso et al. (2013) during summer regarding the seasonal precipitation correlation for the Iberia maybe due to the higher density network of the latter, but in agreement with Heikkilä et al. (2011) for Norway. PBIAS results were similar to other studies found by (Argüeso et al. 2012; Cardoso et al. 2013), where WRF significantly overestimated precipitation in most of Iberia during summer, while in winter and -autumn in our case- the underestimation of ERA-I turned to an improved small PBIAS for WRF. The monthly errors were similar and comparable to the other previous studies; for example, Soares et al. 2012, reported monthly values of COR, RMSE, MAE, and PBIAS of 0.89, -8.9%, 24.4 mm, and 43.4 mm, respectively. Furthermore, the WRF model performance was outstanding compared to other studies over Europe (Argüeso et al. 2012; Fantini et al. 2018) because pbias rarely exceeded ±25-30% in the majority of the stations (Argüeso et al. 2012; Fantini et al. 2018).

In q-q plots, WRF_5 simulation produced better extremes compared to the driver data that consistently underestimated most quantiles while WRF_5 showed an overprediction of higher quantiles during spring. Prein et al. (2016) in a comparison study via daily q-q plots of EU-CORDEX with observations found that the 0.11° models outperformed on the representation of extreme precipitation in all regions in MAM against 0.44°, but not for the Carpathians and the Alps regions. That behavior could be attributed to the fact that extreme precipitation events often have small spatial and temporal extents, and thus their analysis in a combination of complex topography remains very sensitive.

In general, the presented results highlight the ability of the WRF_5 model to correctly distribute precipitation all over Greece, which indicates its efficiency to reproduce the climatic characteristics of different regions and to sufficiently incorporate the effect of complex topographical features.

At this point, it is necessary to discuss an important issue in what concerns the added value of WRF model regarding the downscaled precipitation results compared to ERA-I. At a first look, comparing the statistical metrics namely MAE, RMSE, PBIAS, COR, MIA and NSE between ERA_I and OBS and between WRF_5 and OBS, the improvement in downscaled results is not entirely clear (Tables 2 and 3). On the other hand, the representation of extreme climate by RCMs is an increasingly important issue for impact assessment. The process of deeper investigation of the ability of the WRF model to simulate climate extremes in terms of probability densities and Q-Q plot revealed a clear improvement in terms of extreme values (Figs. 16 and 17). According to this analysis, WRF_5 represented in all seasons more efficiently the higher-ranking quantiles than ERA-I. These results highlight the fact that WRF_5 adds value compared to reanalysis in terms of extreme precipitation values, which is of high interest for evaluating the impact of climate change and at the same time, reinforcing the need of using dynamical downscaling. Thus, WRF_5 overcomes the problems associated with the observational dataset or even the lack of station data especially at high-altitude by yielding a significant improvement in terms of extreme values. This conclusion does not denounce the importance of the availability of high-quality observational datasets in terms of density network, long-term continuous and homogeneous data, for high-resolution model studies, to overcome any deficiencies of an RCM in representing mean values.

The presented results give confidence that the current version of the WRF model, set-up and parameterized with a high resolution of 5 km for the domain of Greece, can simulate synoptic meteorological variables and their extremes, pointing to its high potential to yield reliable information on future climate changes in extreme weather. In what concerns the ability of a GCM to reproduce the climatology of Greece at high resolution, the historical model performance evaluation showed that bias results for all temperatures and time scales presented consistent values, with cold bias around 1.1°C for TX and a warm bias of 0.24°C for TN with high correlation values with observations during monthly and seasonal time scales. The historical WRFEC generally simulated a dry bias in total precipitation, which was extended to almost the whole country with some excess of precipitation extreme events during spring and summer, but with a good description of the spatial precipitation pattern. Overall, those findings suggested that our downscaling method was able to produce results in line with the historical observations. These results are establishing confidence in the use of historical and dynamically downscaled simulations using GCM projections.

Key Remarks

- ***WRF_5 represented very well the annual and seasonal geographical distribution of TX and TN in the study area.***
- ***Downscaling methodology provided a very good agreement with the observations for maximum (-0.6 ºC) and minimum (1ºC) temperatures.***
- ***PDF analysis and quantiles revealed an improvement of WRF_5 during spring, winter, and autumn.***
- ***WRF_5 reproduced well the spatial pattern of the observed annual and seasonal precipitation in most parts of Greece.***
- ***Precipitation results were better reproduced by WRF_5 compared to ERA-Interim as concluded by the reduced statistical errors.***
- ***WRF_5 represented in all seasons more efficiently the higher-ranking quantiles than ERA-I, yielding a significant improvement in terms of extreme values.***
- ***WRF_EC bias results for all temperatures and timescales presented consistent values, with cold bias around 1.1°C for TX and a warm bias of 0.24°C for TN with high correlation values with observations during monthly and seasonal timescales.***
- ***WRF_EC described well the spatial precipitation's pattern and produced a dry bias in total precipitation.***

Chapter 5 Future Projections

This chapter describes the results of the investigation of the downscaled projected changes of the global model EC-EARTH for minimum and maximum temperatures and precipitation under two RCPs (RCP4.5 and RCP8.5) in the near future (2025-2049) and far future (2075-2099).

5.1 Future projections of minimum and maximum temperatures

WRFEC represented very well the geographical distribution of annual and seasonal mean daily TX and TN (Figs 5.1(a) -5.4(a.)) in the historical period and clearly illustrated the seasonal variation with similar ranges of temperature values also found in the previous study of Politi et al. (2021).

The annual mean and seasonal projected changes, based on delta change approach (Delta = future period- historical period) along with the spatial distribution of the historical period are depicted in Figs. 5.1, 5.2, 5.3 and 5.4. In general, the warming projections for the far future show larger changes for maximum than for minimum temperature, for both scenarios, and for the annual mean and seasonal temperatures. On the other hand, the projected changes are less intense during the near future with GCM differences under the two scenarios. According to a 2-tailed t-test, the projected changes seen in all figures are statistically significant at the 95% confidence level over the entire region. It is obvious from these figures that the mean temperatures derived from maximum and minimum temperatures increase consistently, but with different magnitudes across the regions and emission scenarios.

Because of the higher greenhouse gas emissions and radiative forcing of RCP8.5 by the end of the century, the magnitude of the mean annual maximum temperature warming for RCP8.5 is greater than that for RCP4.5 (Figure 5.1). According to the RCP4.5, the largest warming is obtained over the eastern part of the country (some northeastern inland parts and eastern coasts) reaching up to 2 °C in the period 2025-2049 and extends more towards southeastern areas up to 2.5°C in the period 2075-2099. In the case of the RCP8.5 scenario, the difference between the two future periods is remarkably more pronounced and the mean daily TX is found to increase up to 4.5 °C in the far future,

particularly in some eastern and coastal parts. It is also observed that the pattern of changes is clearly linked to the orography of central Greece and the island of Crete.

The investigation of the projected changes for the seasonal maximum temperature revealed a relative seasonality (Figure 5.2). There is a different spatial pattern of temperature (TX) change for each season. Under both RCPs, there are significant regional differences in terms of projected temperature increase in each season. Under the RCP8.5 in the far future period, WRFEC projects a robust magnitude of warming over the whole country. The model predicts maximum TX increases in the range of 2.75 and 3.75 °C in winter and autumn, but in summer and spring the changes reach values from 3 °C, near the coast, up to 5°C in some inland areas and in the north-eastern Greece. In the near future, TX increases mark a west-east gradient in spring and winter in the range of 0.75 to 2.5°C, which is profoundly linked to the orography of central mainland. The lower projected changes are observed in winter with TX increases from 0.75 to 1.5°C under both RCPs and only in the near future period.

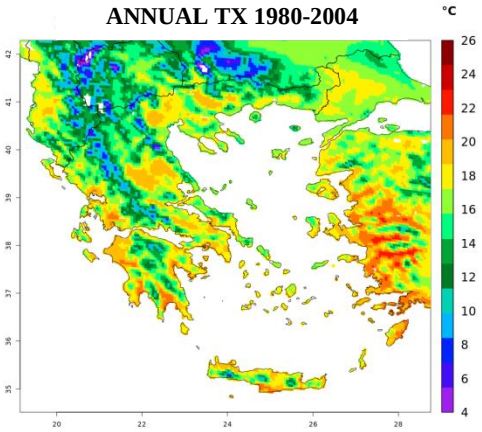

a.

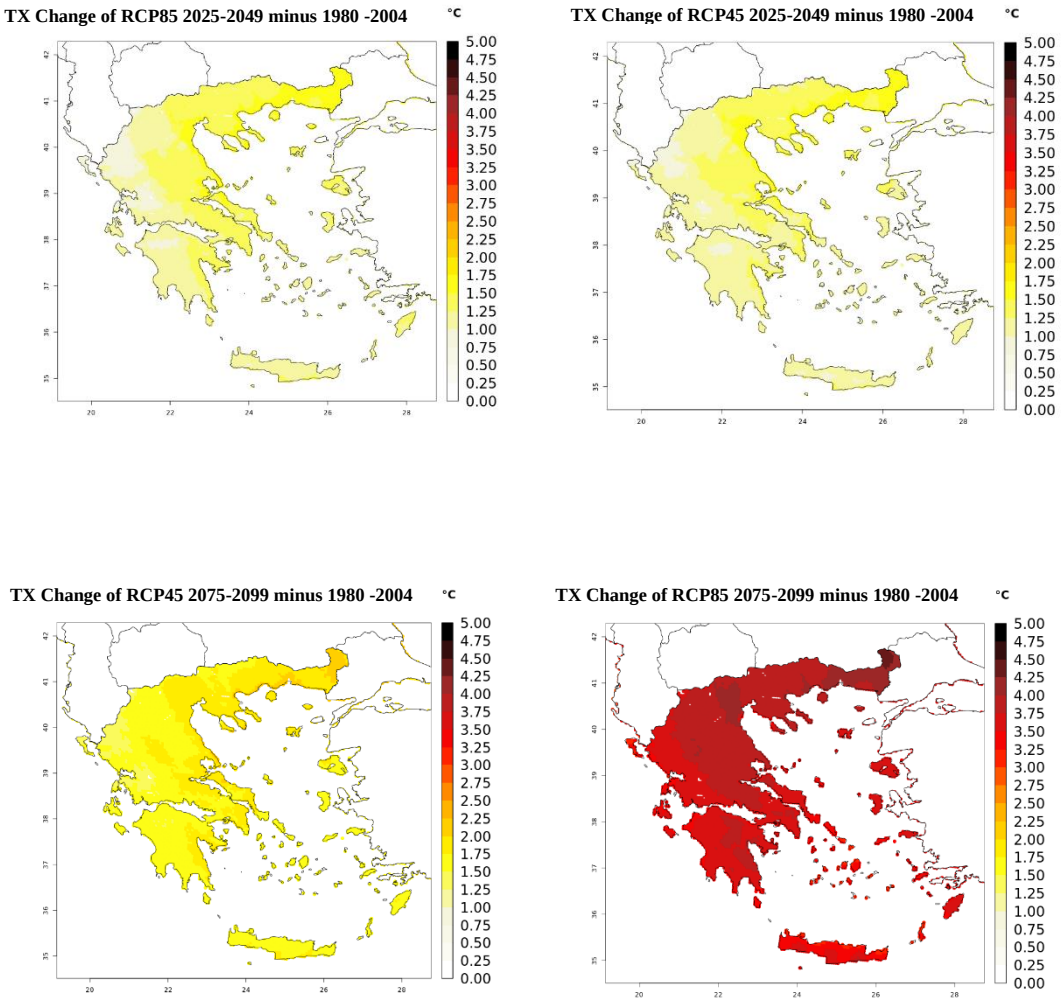

b.

Figure 5.1 a. WRFEC annual mean historical climatology, b. WRFEC climate change differences for daily maximum temperature (2025–2049 minus 1980–2004 and 2075-2099 minus 1980–2004) for RCP4.5 and RCP8.5. (Areas with no dots specify statistically significant changes using a Student's t-test at the 95% confidence level).

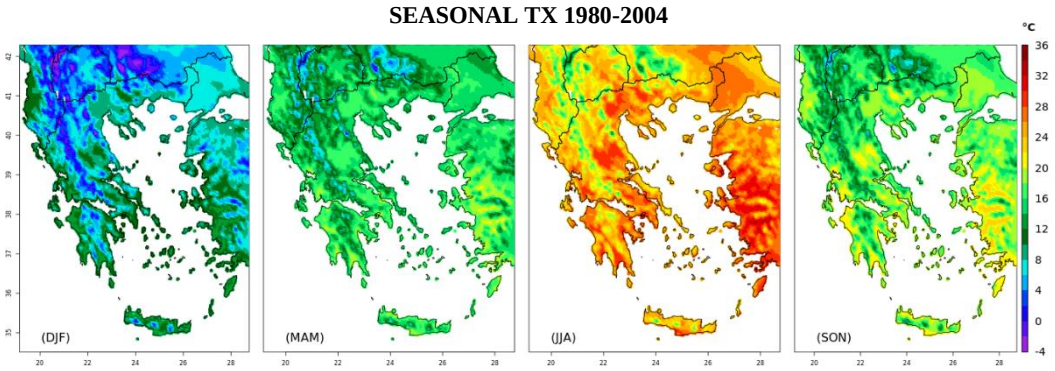

a.

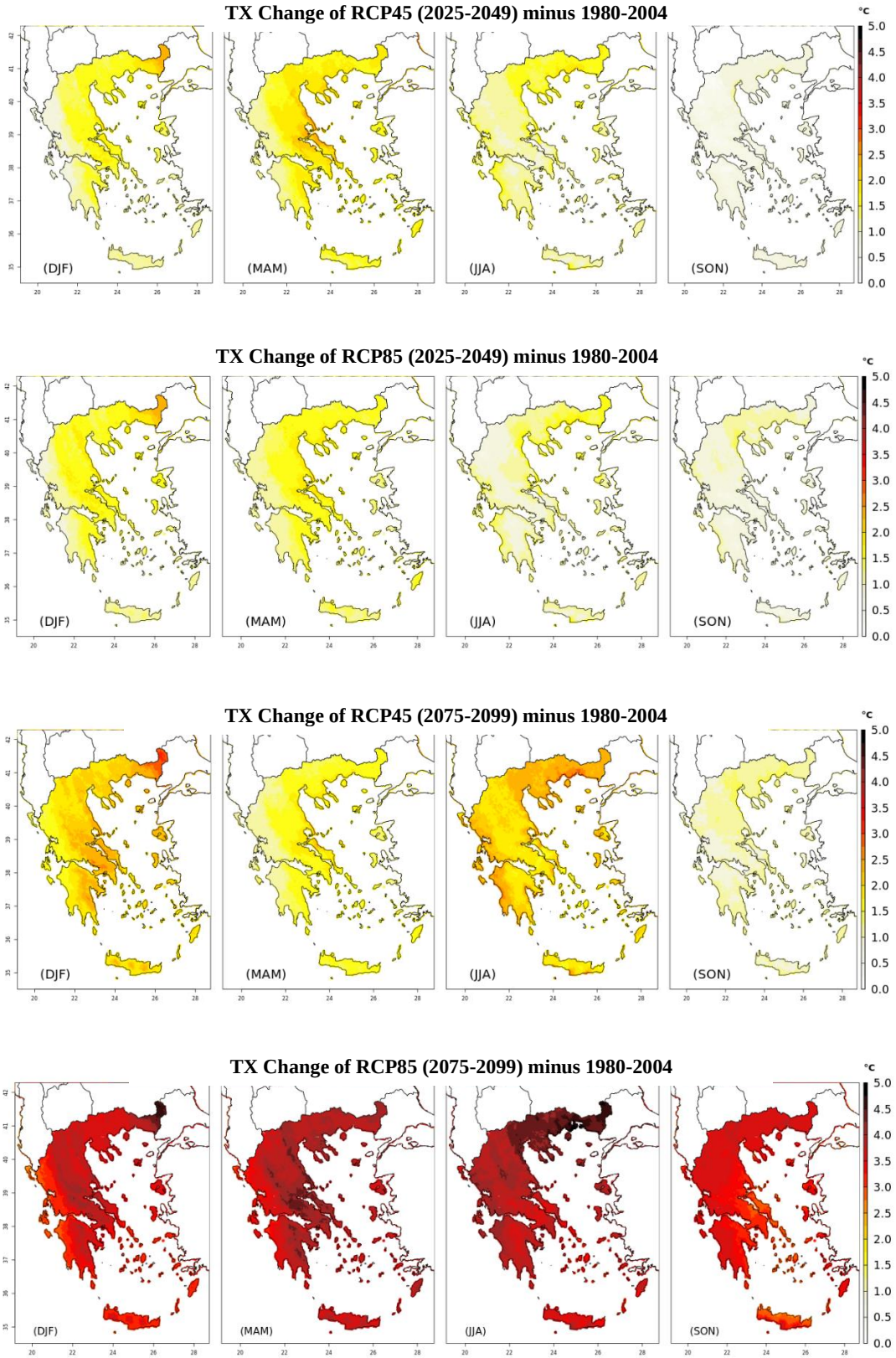

b.

Figure 5.2 a. WRFEC mean historical climatology, b. WRFEC seasonal climate change signal for daily maximum temperature (2025–2049 minus 1980–2004 and 2075-2099

minus 1980–2004) for RCP4.5 and RCP8.5. (Areas with no dots specify statistically significant changes using a Student's t-test at the 95% confidence level).

Considering the mean daily minimum temperature in RCP4.5, increases are projected up to 1.5 °C in northeastern regions in the near future and in the range between 1.75 and 2.5 °C in the far future (Figure 5.3). RCP8.5 shows a much greater warming than RCP4.5 by the end of the century with a west-east gradient, reaching values from 3°C up to 4 °C. TN is expected to increase up to 3.5 °C near the coasts and the islands of the central Aegean Sea, while the increase will be a little higher in the islands of the north and eastern Aegean area. Overall, the projected changes for the minimum temperature in the far future, according to both scenarios, are similar to the changes of the maximum temperature, but with mitigated properties; the changes are less sharp with smaller contrasts and the west-east gradient also less intense.

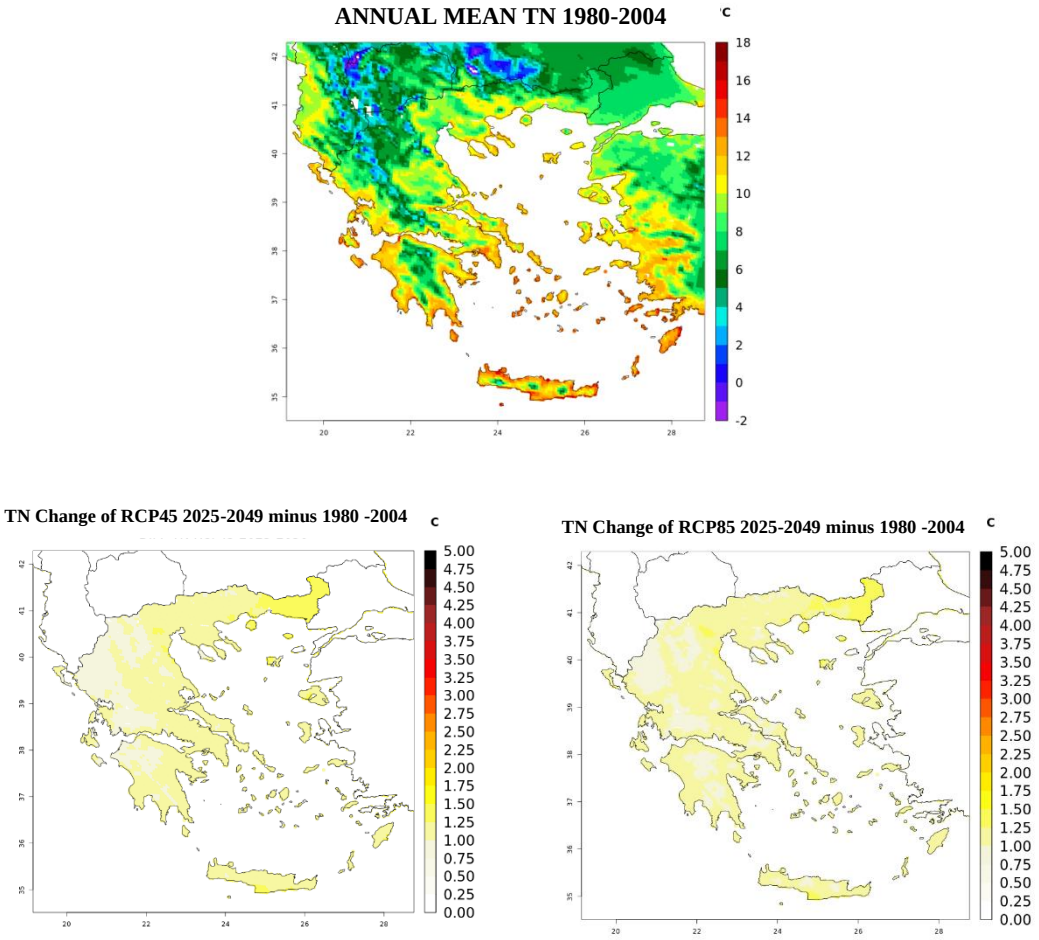

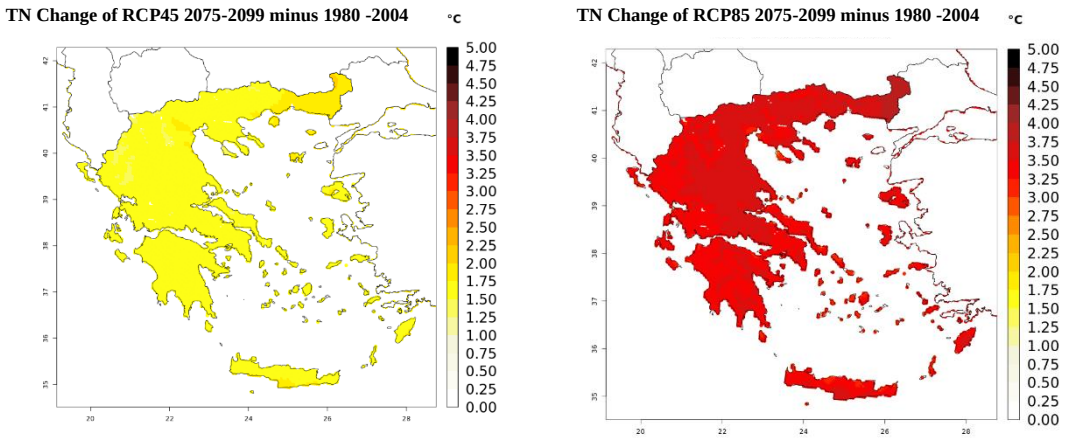

b.

Figure 5.3 a. WRFEC annual mean historical climatology, b. WRFEC climate change signal for daily minimum temperature (2025–2049 minus 1980–2004 and 2075-2099 minus 1980–2004) for RCP4.5 and RCP8.5. (Areas with no dots specify statistically significant changes using a Student's t-test at the 95% confidence level).

Under RCP4.5, the magnitude of the warming in autumn is the lowest of all seasons with values around 0.5 to 1°C (Fig. 5.4). During the summer and winter seasons of the future period 2075-2099, the WRF simulation projects a higher temperature increase of 2-2.5°C in the entire country, uniformly. During winter in the near future projection, the largest warming occurs over some inland parts and northeastern Greece. The model projects a small west-east gradient of warming in spring, for both future periods. Under RCP8.5 and during the near future projection, the model produced much milder warming (especially during autumn) in the range of 0.75 to 2.5 °C with the higher temperature increase in the northeastern part of the country and some coastal areas. However, during the far future period, the model's projection in summer predicts a larger magnitude of warming over the western part of mainland, the Ionian Islands and, in some plain parts of central and northern mainland and southern Crete. In these areas, the highest maximum temperatures are usually observed during summers. According to the projections, the high increases will impact these areas adversely. During winter, the model projects notably the most significant warming over the mountainous areas, while in spring, the temperature increases are smaller in the western than in eastern parts of the country.

SEASONAL TN 1980-2004

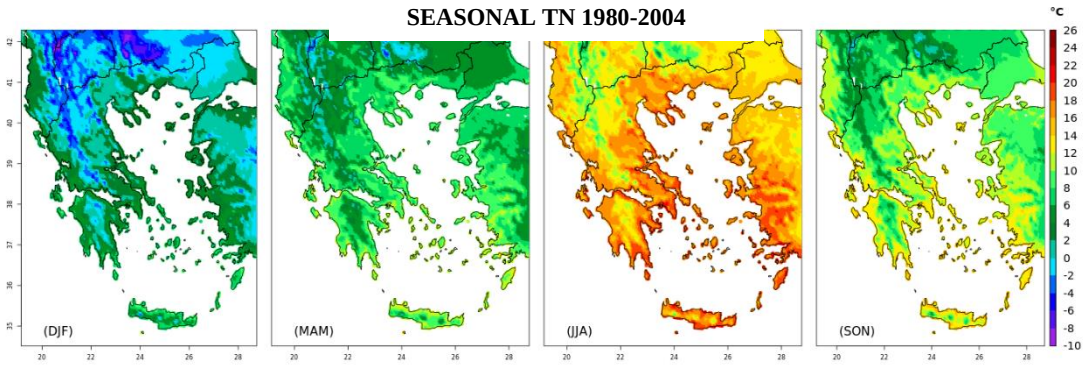

TN Change of RCP45 (2025-2049) minus 1980-2004

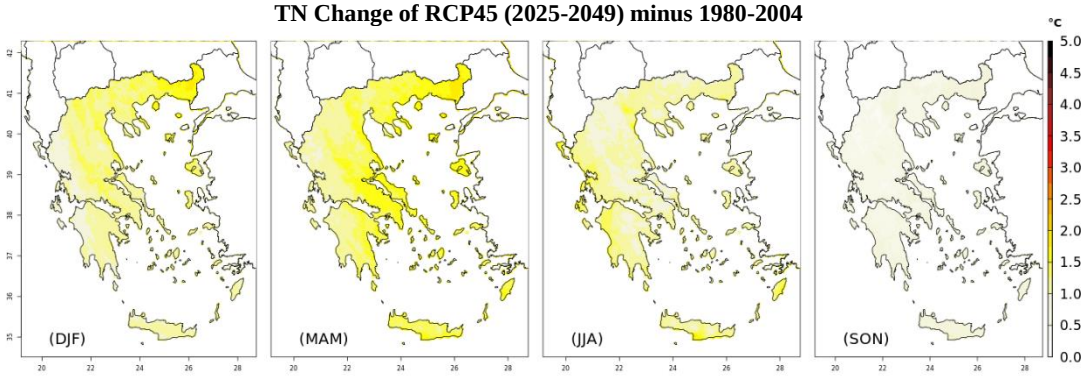

TN Change of RCP85 (2025-2049) minus 1980-2004

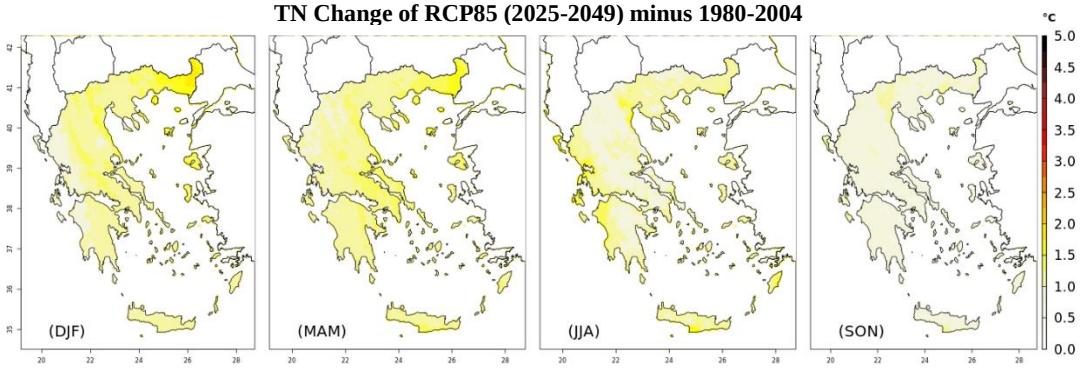

TN Change of RCP45 (2075-2099) minus 1980-2004

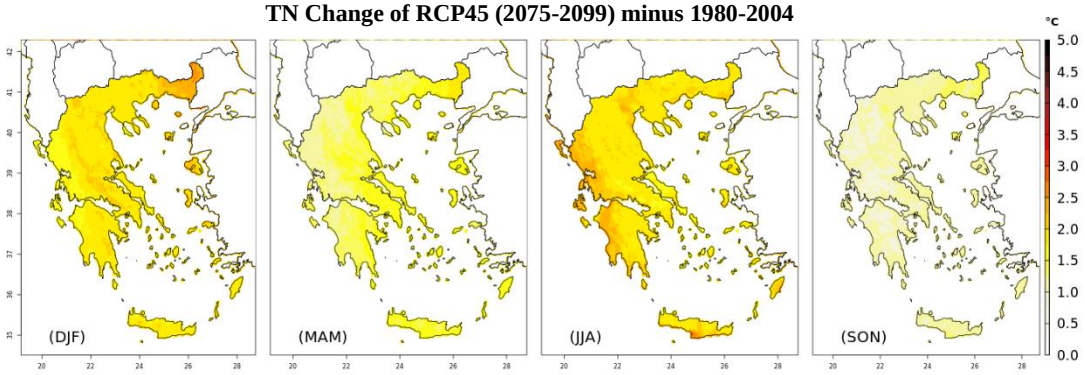

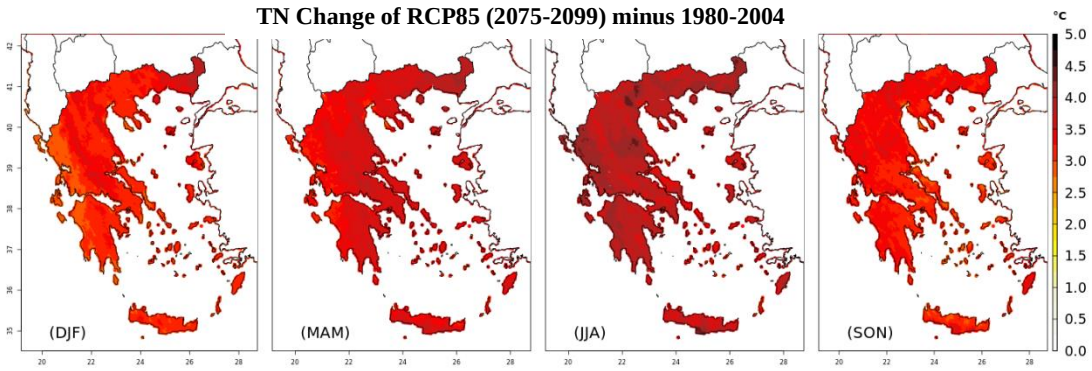

Figure 5.4 a. WRFEC mean historical climatology, b. WRFEC seasonal climate change signal for daily minimum temperature (2025–2049 minus 1980–2004 and 2075-2099 minus 1980–2004) for RCP4.5 and RCP8.5. (Areas with no dots specify statistically significant changes using a Student's t-test at the 95% confidence level).

In similar previous studies, based on global and regional models, projected changes were found to be rather uniform, as relatively small-scale climate features and feedback were smoothed due to the coarser resolution. In general, Wagner et al (2012) explained that the projected climate change signals of the coarse domain were transferred to the fine resolution without strengthening or weakening the climate change signal; but the higher resolution added some more detail in the spatial patterns as expected.

In what concerns temperature change signal, WRFEC simulation projects an annual mean warming over Greece, which is significant at the 95 % confidence interval for all grid points. In general, during the far future period, the model projects a robust magnitude of warming with most pronounced changes over the whole country under the RCP8.5 scenario. This conclusion is in accordance with (Varotsos et al. 2021a) who examined the impacts of climate change on the tourism sector from a large ensemble member of RCMs from the EUROCORDEX under three RCP emissions scenarios. Overall, the warming projections for the far future show larger changes for maximum than for minimum temperature, under both scenarios, and for the annual mean and seasonal temperatures. On the other hand, the projected changes are less intense during the near future with no significant differences under the two scenarios. The model predicts TX increases in the range of 2.75 and 3.75 °C in winter and autumn, but in summer and spring the changes may range from 3 °C, near the coast, up to 5°C in some inland areas and in north-eastern Greece. In the near future, TX increases mark a west-east gradient in spring and winter in the range of 0.75 to 2.5°C, which is profoundly

linked to the orography of central Greece. The results are generally consistent with previous studies indicating that the Mediterranean region and southern Europe will exhibit an amplified temperature increase in comparison to the rest of the continent (Giorgi et al. 2004). Our findings are also in agreement with the most recent study of (Coppola et al. 2021) that estimated for RCP8.5 during summer late century period maximum signal over the Mediterranean land regions (where Greece is included) of around 4.5°C with EUROCORDEX ensemble and 6.5°C with CMIP6. The lower projected changes are observed in the winter with TX increases from 0.75 to 1.5°C under RCP4.5 and RCP8.5 and only in the near future period. Overall, the projected changes for TN in the far future, according to both scenarios, are similar to the changes of TX, but less sharp with smaller contrasts and the west-east gradient also less intense.

5.2 Future projections of precipitation

The signal of climate change on the annual precipitation over Greece given by the WRF simulation is shown in Figure 5.5. All the results point out a general decrease of the annual precipitation all over the eastern part of the country (with islands included). However, an increase of 20% is projected in the western areas only in the near future and without statistical significance. Although in the less severe scenario (RCP4.5) the decreases of rainfall are smaller than RCP8.5, there is a significant reduction in the range of -30 to -40% in areas like the island of Evia and in small areas of the central mainland. This reduction, according to RCP8.5, becomes more extended towards the western parts of the country, particularly in the far future. More specifically, the model indicates decreases around −25% throughout most parts of the domain. Additionally, the most dramatic reductions above -30% and in some cases up to -50% are found in eastern Crete, eastern Peloponnese, central mainland and in few areas of the eastern part of the country.

The projections for the seasonal precipitation changes under RCP4.5 and RCP8.5 are depicted in Figure 5.6. Under RCP4.5, the precipitation reduction is projected to values over 30% in eastern Greece. The model also estimated statistically non-significant changes of increasing rainfall during autumn around 10% in some small areas all over the country and, only in western Greece during all the other seasons of both future periods. The most dramatic reductions (above 40%) of seasonal precipitation are

observed under RCP8.5 in the far future covering almost all the country. In all seasons, small positive and negative changes are projected of around 10%, located mostly in the western parts of the mainland, the Ionian Islands and western Crete. Nevertheless, these changes are non-significant in most areas of the country. In general, the total annual projected changes are related to the reduction of precipitation during winter, spring and autumn, since the summer precipitation contributes the minimum to the annual total.

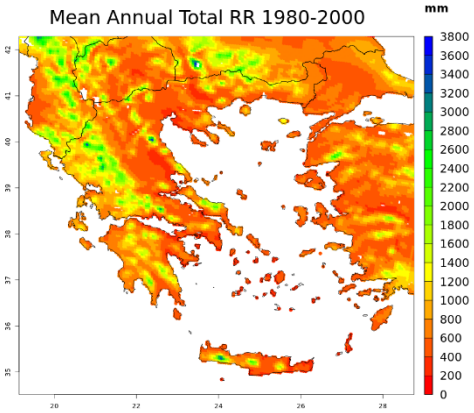

a.

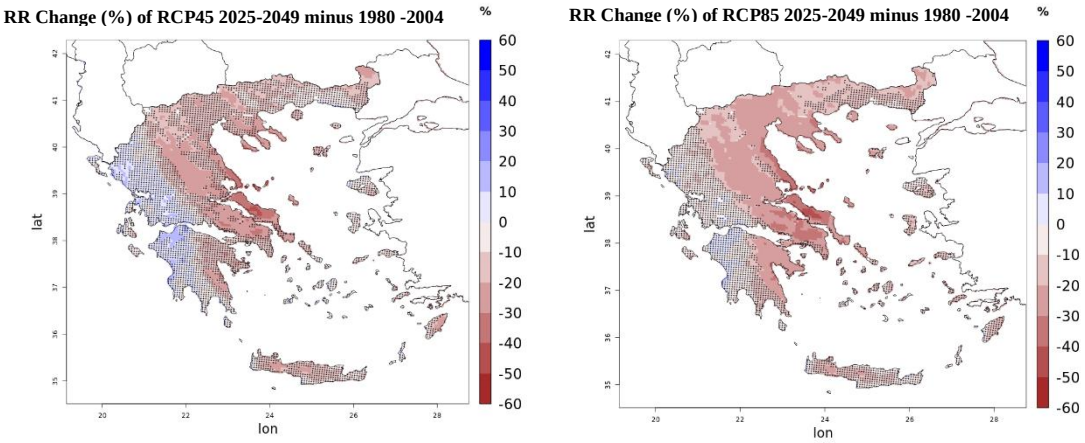

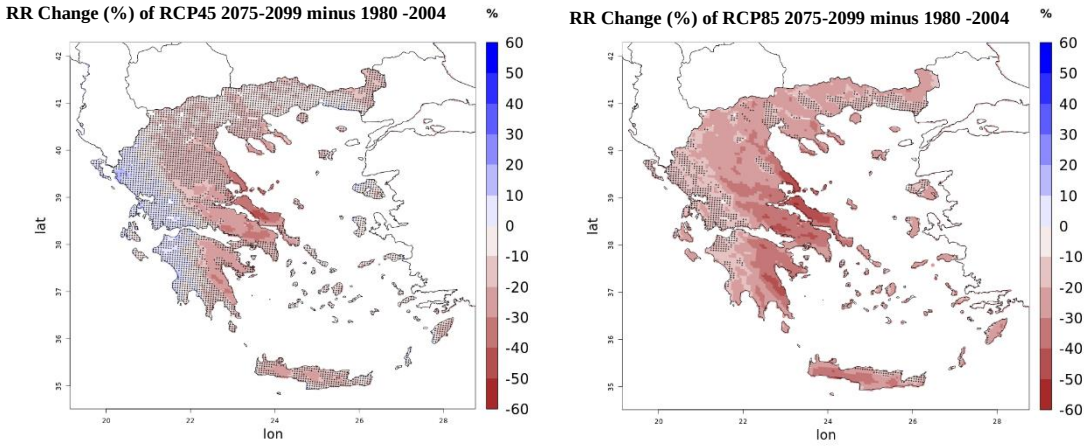

b.

Figure 5.5 a. WRFEC mean historical climatology, b. Annual mean precipitation relative changes given by WRFEC for RCP4.5 and RCP8.5 (2075–2099 minus 1980–2004) / 1980–2004. (Areas with dots specify changes not statistically significant using a Student's t test at the 95% confidence level).

a.

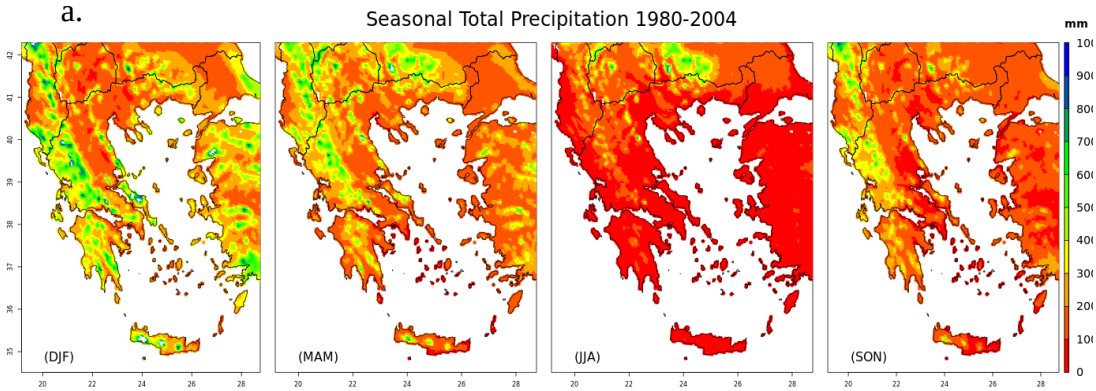

b.

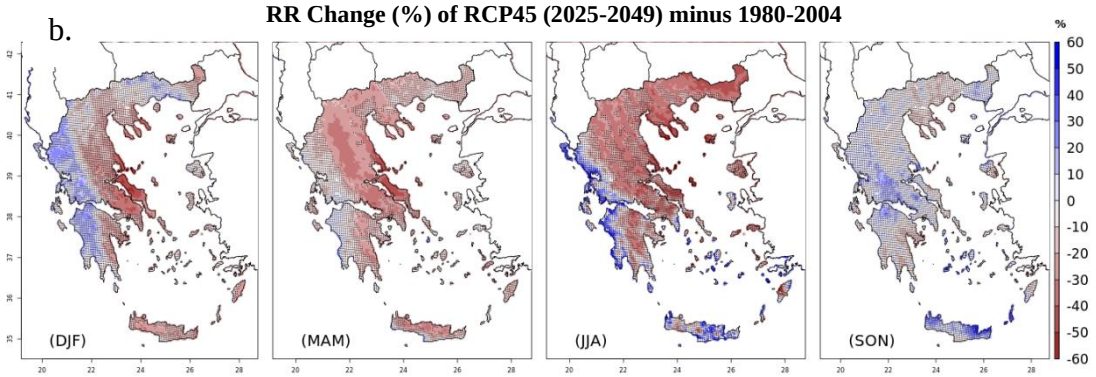

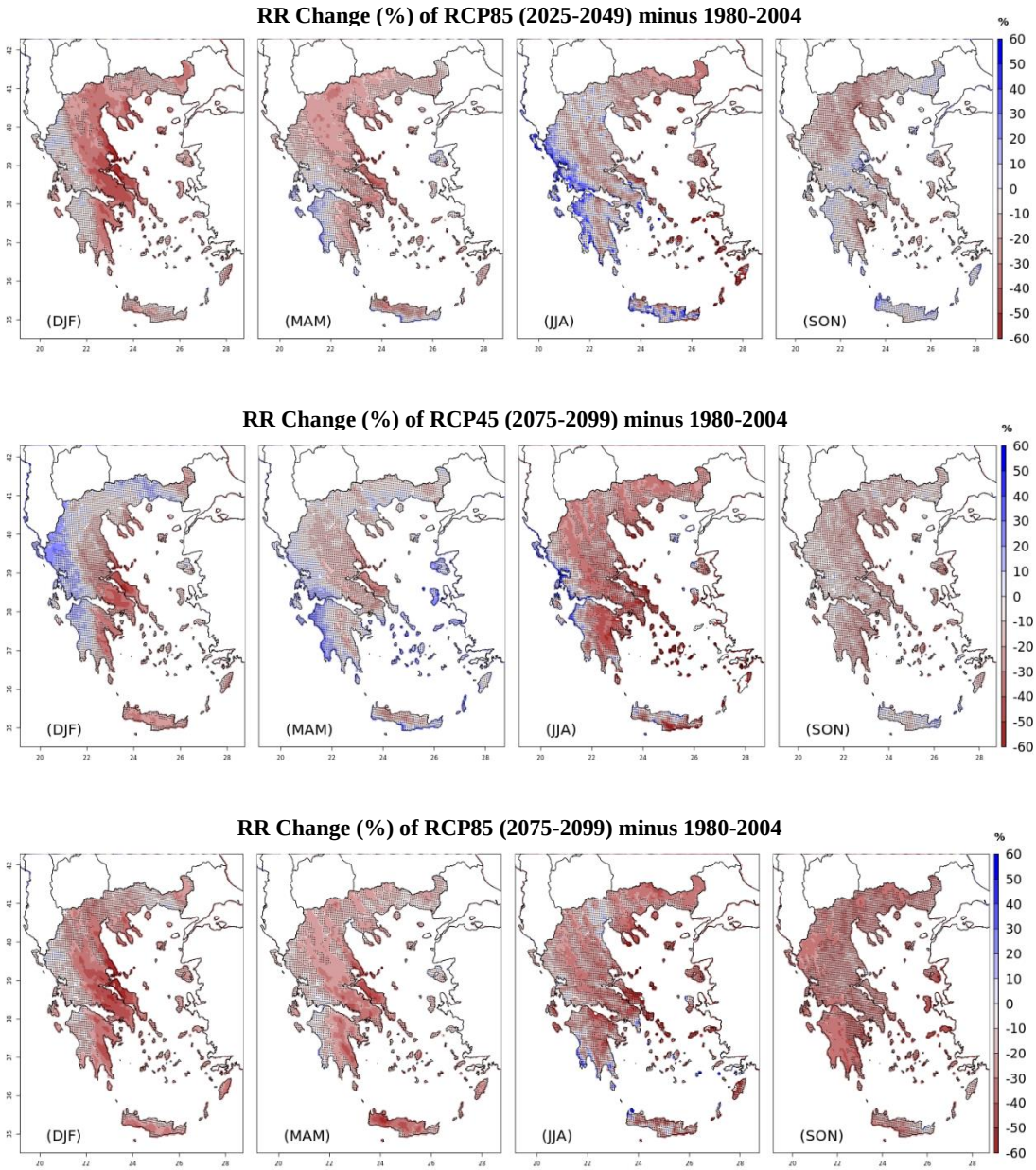

Figure 5.6 a. WRFEC mean historical climatology, b. Seasonal mean precipitation relative changes given by WRFEC for RCP4.5 and RCP8.5. (Areas with dots specify changes not statistically significant using a Student's t test at the 95% confidence level).

PDF distributions of daily precipitation intensity in the present and future climate scenarios are depicted in Figure 5.7 below. All distributions are similar to each other up to the precipitation bin of around 60 mm, where the transition between reduction and increase of frequency of extreme precipitation occurs. This rainfall amount corresponds to the 99th percentile in historical and future climate periods. An increase

of extreme rainfall amount (above ~300 mm/day) is obtained under the future scenarios with a rather low frequency of occurrence.

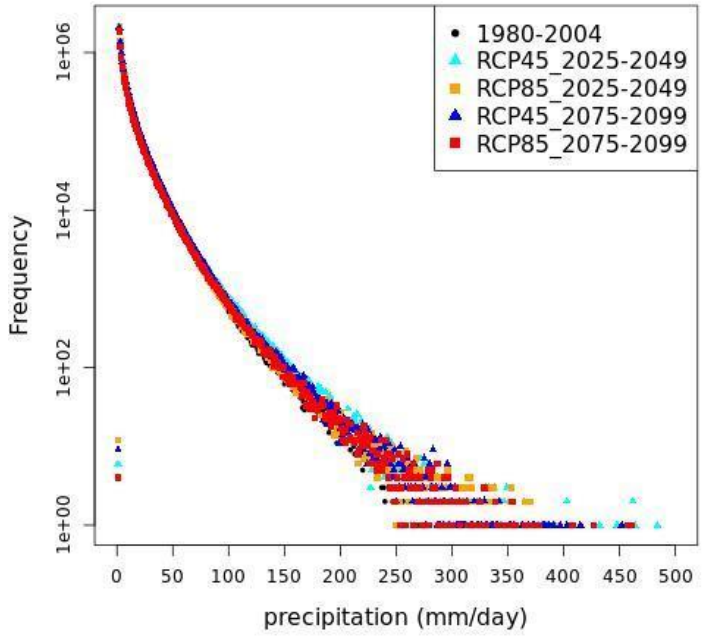

Figure 5.7 WRFEC PDFs of precipitation (mm/day) in the historical and future climate periods.

The projected changes for precipitation are in accordance with the studies of Tolika and Zanis (2012) that also reported that Greece would experience a persisting absence of rainfall. More specifically, the climate change signal of precipitation over Greece revealed a general decrease of the annual precipitation all over the eastern part of the country (with islands included) with the most dramatic reductions, above -30% and in some cases up to -50%, found in eastern Crete, eastern Peloponnese, central mainland and in few areas of the eastern part of the country. However, the large increase for summer precipitation in both scenarios in western Greece is most-probably related to a more south-westerly flow in the simulated historical period. Summertime precipitation during the historical period is considerably strong (see Figure 4.21), probably due to the convection-permitting setup and related to these isolated and usually very local events particularly in the period 2025-2049. This internal variability of simulation was also found in the study of Knist et al. (2020). Under RCP4.5, notable summer increases in the southerly flows were estimated up to 40%, which combined with large-scale subsidence, could cause a significant rise in the occurrence of heat wave events

(Karozis et al. 2021). The latter study which was part of our work revealed that estimated changes in the air mass flows under future high-emission scenarios imply changes in their associated synoptic patterns. Compared to our results, the changes in the total precipitation were found less pronounced under both the RCP4.5 and RCP8.5 in the period 2031 and 2060 over Crete in a study of (Varotsos et al. 2021b) for 5 RCM's CORDEX ensembles. The differences between the two scenarios in summer were large in eastern Greece, indicating a great natural variability over the region. For example, in some areas (Crete, eastern coastal parts of central Greece), the change was a decrease in RCP4.5 but an increase in RCP8.5. Similar findings between the two scenarios were obtained in the study of (Chen et al. 2019) for the projected changes in eastern Asia which is characterized by complex topography.

The projected changes in temperature and precipitation are related to dynamic and thermodynamic future changes. According to (Giorgi and Lionello 2008), the drying in the Mediterranean region is associated with increasing anticyclonic circulation which causes a northward shift of the mid-latitude storm track. This northward shift has a seasonal migration and it is maximum in summer and minimum in winter. Lionello and Scarascia 2018 reported that the circulation change would lead to a significant reduction of precipitation for most of the region (Greece included) due to the intensification of the Azores anticyclone in summer that causes increased advection of warm dry continental air masses towards the eastern Mediterranean. The same study concluded that in winter, the increase in barotropic sea level pressure and geopotential height at the 500 hPa level in the central Mediterranean hinders the penetration of humid air from the Atlantic towards the southern and eastern Mediterranean areas. Additionally, in the study of a comparative assessment of backward trajectories with WRCEC in the near future and both RCPs, Karozis et al. 2021 deduced for Greece a reduction of cyclones up to 45% originating from the cyclogenesis region of the central Mediterranean and the Adriatic Sea. Moreover, the same study revealed the tendency (higher probability of occurrence) of increased long-range southerly flows from Africa (circa 40%) under RCP4.5 and consequently the appearance of an increased number of heatwaves that could also result in drier conditions in the future. (Russo et al. 2014) and (Coumou et al. 2018) also reported future enhancement of mid-latitude heat waves due to non-linear interactions between Arctic teleconnections and other remote and regional feedback processes.

5.3 Main Conclusions for Future Projections

The presented study constituted a first attempt to demonstrate the benefits of a high-resolution dynamical downscaling to simulate as accurately as possible the regional climate future changes in Greece. Further to this, the study aimed to provide driving data for impact models that require high spatial details. It must be mentioned that at this stage, only one GCM and RCM have been used, limiting the quantification of the uncertainty of the results. Also, bias correction was not applied to improve the climate projections regarding the examined variables, given the lack of consistent gridded observational datasets required for such regions of complex topography and climate variation.

WRFEC results projected a noticeable magnitude of warming regarding TX with the most pronounced changes up to 5°C mostly over the eastern parts of the country under the RCP8.5 in the far future period. In addition, the model's projection in summer predicted a larger magnitude (near 5°C) of warming for TN in the far future over the western part of the mainland, the Ionian Islands, and in some plains of central and northern mainland and southern Crete. The climate change signal of precipitation revealed a general decrease of the annual precipitation all over the eastern part of the country (with islands included) with the most dramatic reductions (above 40%) in seasonal precipitation observed under RCP8.5 almost all over the country in the far future. The model also estimated statistically non-significant changes of increasing rainfall during autumn and spring, of more than 10% in some small areas of western Greece in both periods and RCPs (except of RCP8.5 in the far future).

Key Remarks

- ***Noticeable magnitude of warming regarding TX with the most pronounced changes up to 5°C mostly over the eastern parts of the country under the RCP8.5 in the far future period.***
- ***Larger magnitude (near 5°C) of warming for TN in the far future over the western part of the mainland, the Ionian Islands, and in some plains of central and northern mainland and southern Crete***
- ***Annual precipitation will reduce all over the eastern part of the country (with islands included) with the most dramatic reductions (above 40%) in seasonal precipitation observed under RCP8.5 almost all over the country in the far future.***
- ***Increased precipitation during autumn and spring, of more than 10% in some small areas of western Greece in both periods and RCPs***

Chapter 6 Climate Indices

In this chapter, the computed differences in climate indices between the two future periods and the historical period were present. The results of the statistical analysis presented in chapter 4, using the GCM coarser data and the downscaled simulations against temperature and precipitation observations, demonstrate the capability of WRFEC to capture the climate characteristics and variability Greece. This provides confidence in obtaining and using WRFEC simulations to calculate ETCCDI climate indices. Furthermore, the comparison of GCMEC and WRFEC calculated ETCCDI indices with those calculated using observational station data is carried out, to highlight the added value of using the higher resolution simulations of 5 km. The comparison with observations clearly indicates the improvement in all calculated ETCCDI indices with WRFEC, against those of GCMEC at the locations of the stations.

6.1 ETCCDI Climate Indicators

To analyze spatially the climate change signal of extreme temperature and precipitation over Greece, the extreme temperature and precipitation indices established by the Expert Team (ET) on Climate Change Detection and Indices (ETCCDI, https://www.wcrp-climate.org/etccdi) have also been calculated. Extreme climate indices unified by ETCCDI effectively promote detection and research of extreme weather and climate change, allowing for comparison between extreme weather and climate change in different regions.

Table 6.1 Definition of extreme temperature and precipitation indices

Code	Name	Definition	Unit
SU	Summer days	Annual count when daily maximum temperature >25 °C	days
HD	Hot days	Annual count when daily maximum temperature >35 °C	days
TR	Tropical nights	Annual count when daily minimum temperature >20 °C	days
FD	Frost days	Annual count when daily minimum temperature <0 °C	days
R20 mm	Very heavy precipitation days	Annual count when precipitation ≥20 mm	days
R50 mm	Extreme precipitation days	Annual count when precipitation ≥50 mm	days
CDD	Dry days	Maximum number of consecutive days when precipitation <1 mm	days

6.2 Historical presentation and Projective changes of ETCCDI

The changes in the number of days where daily TX was above 25°C (summer days, see Figure 6.1) appeared to have an increasing frequency for both scenarios and periods with less intense increase of an average of 5 to 20 days during the near future period in the mountainous and inland regions and 25 days in the coastal regions and the islands. The greater increases of around 25 days were observed all over the country in RCP4.5 in 2075-2099 while the most robust changes were obtained under RCP8.5. More specifically, the regional mean changes increase to 50-60 more days almost all over the country (around 40 days over the mountains) and up to 80 days in the coastal areas of eastern Evia, southwestern Peloponnese, north Crete and the islands. No statistically significant future changes are observed in mountainous areas under both scenarios in the near future period. Hot days (Figure 6.2), as characterized by a daily TX larger than 35°C, have a well-marked increased frequency of 30 to 45 days, especially for RCP8.5 in the far future, in specific regions such as in the central-eastern mainland (Thessaly region), Thessaloniki region (central Macedonia region), Attica, some areas in Peloponnese, southern Crete and western parts of Greece. No remarkable changes were observed under RCP4.5 during both periods. It is also obvious that the areas with non-statistically significant change are centered only in the mountainous areas of central Greece and Peloponnese in the far future period under RCP8.5.

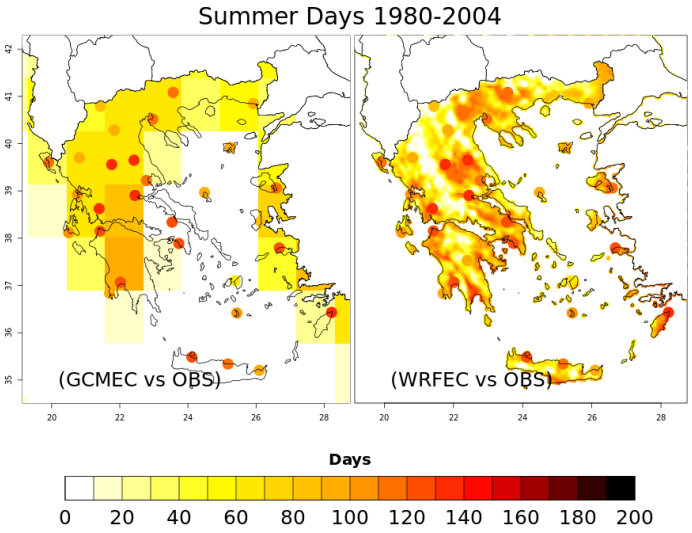

Change between scenario minus historical period

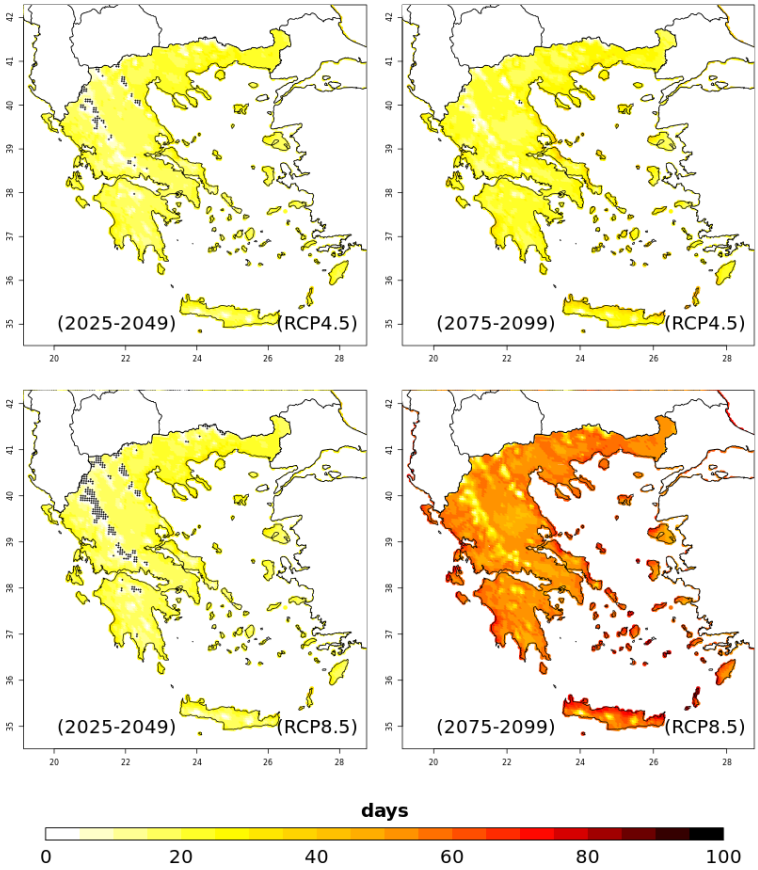

Figure 6.1 Annual mean summer days changes for 2025-2049 (near future) and 2075-2099 (far future) relative to 1980- 2004. In the top figure, the summer days index is depicted for the historical period. (Areas with dots specify changes not statistically significant using a Student's t-test at the 95% confidence level).

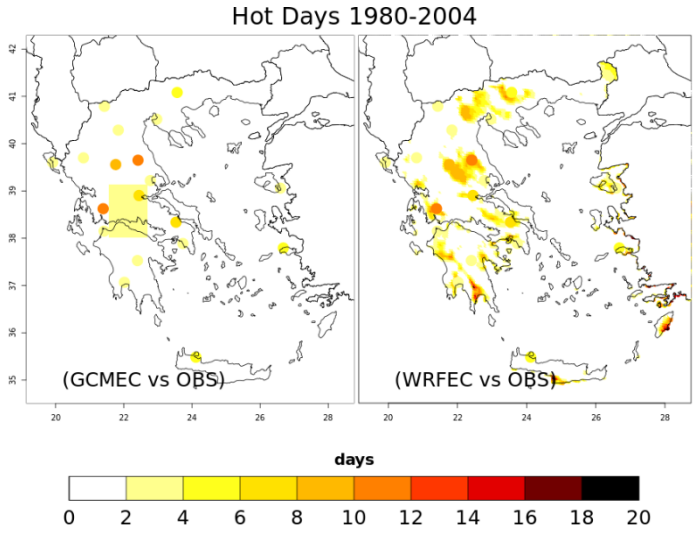

Change between scenario minus historical period

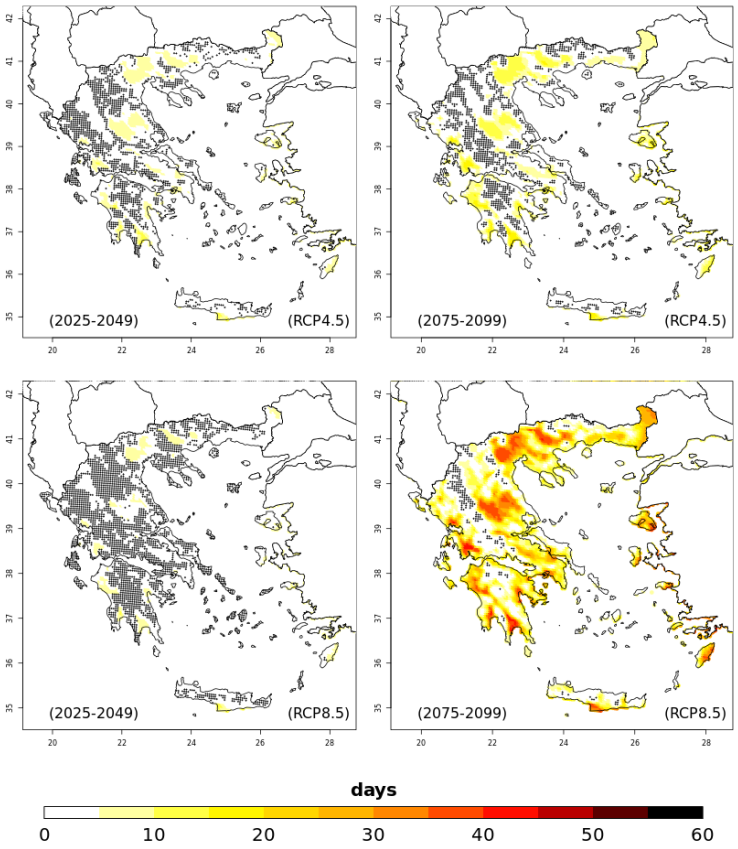

Figure 6.2 Annual mean hot days changes for 2025-2049 (near future) and 2075-2099 (far future) relative to 1980- 2004. In the top figure, the hot days index is depicted for the historical period. (Areas with dots specify changes not statistically significant using a Student's t-test at the 95% confidence level).

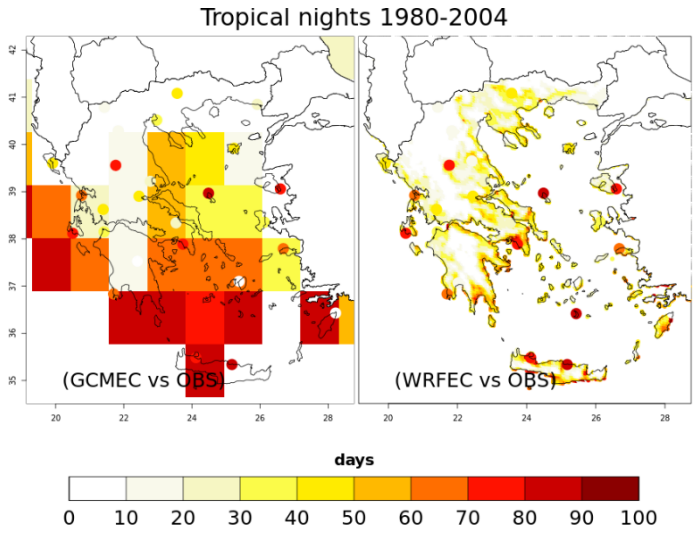

Change between scenario minus historical period

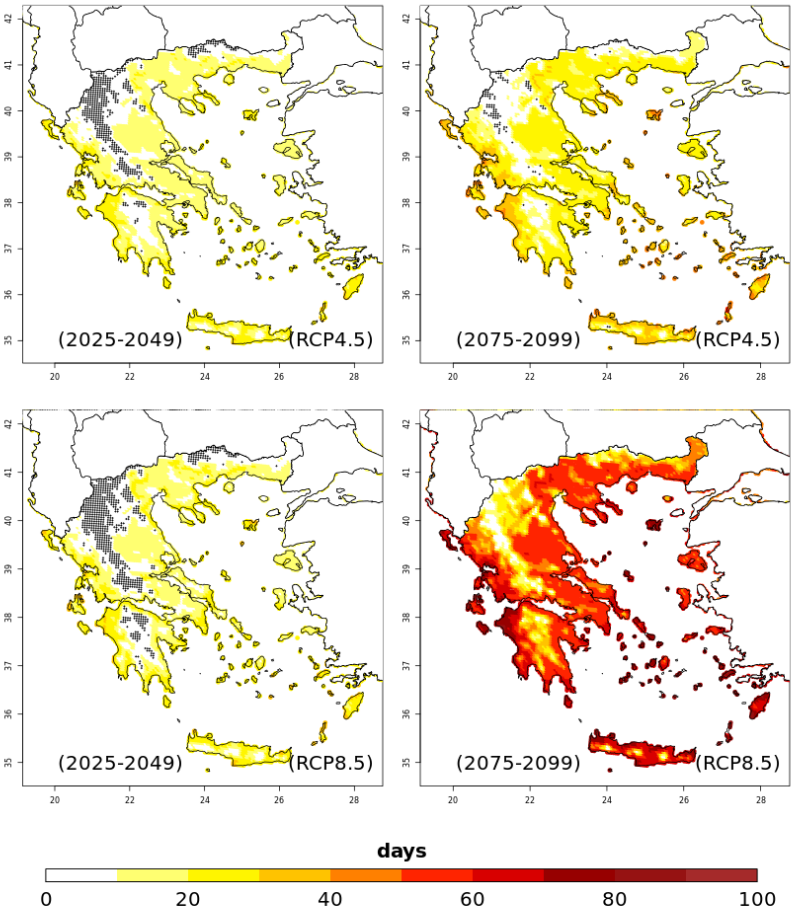

Figure 6.3 Annual mean tropical nights changes for 2025-2049 (near future) and 2075-2099 (far future) relative to 1980- 2004. In the top figure, the tropical night index is

depicted for the historical period. (Areas with dots specify changes not statistically significant using a Student's t-test at the 95% confidence level).

Regarding the tropical nights number illustrated in Figure 6.3, a general increase of about up to 30 days is found under RCP4.5 and RCP8.5 for the near future all over the country compared to the reference period. The change becomes more severe in the far future (30-40 days more) for RCP4.5 in the north-west part of Peloponnese and Crete, surpassing the 50 days under RCP8.5 and over the entire country. Only in the mountainous regions tropical nights note the lower increase, except for the period 2075-2099 in RCP8.5 (30 days of increase). It is also obvious (Fig. 6.3) that coastal areas are more affected than continental parts by increased days of tropical nights. No statistically significant changes are observed only in mountainous areas of central Greece and Peloponnese under RCP45 for both periods and under RCP8.5 in the near future.

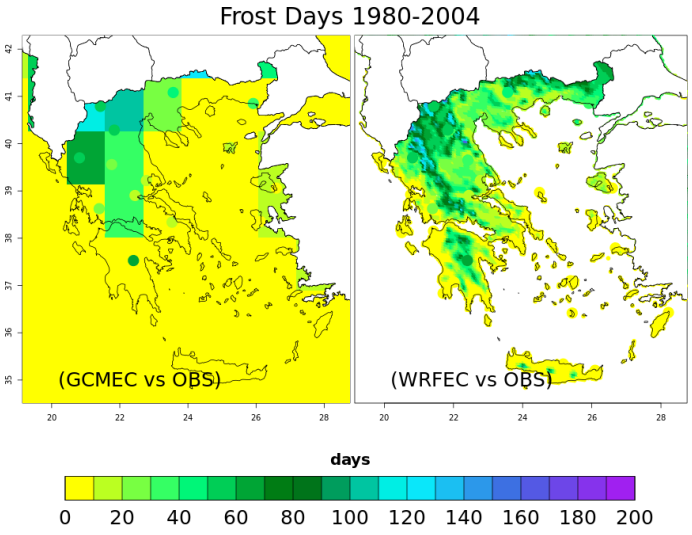

Change between scenario minus historical period

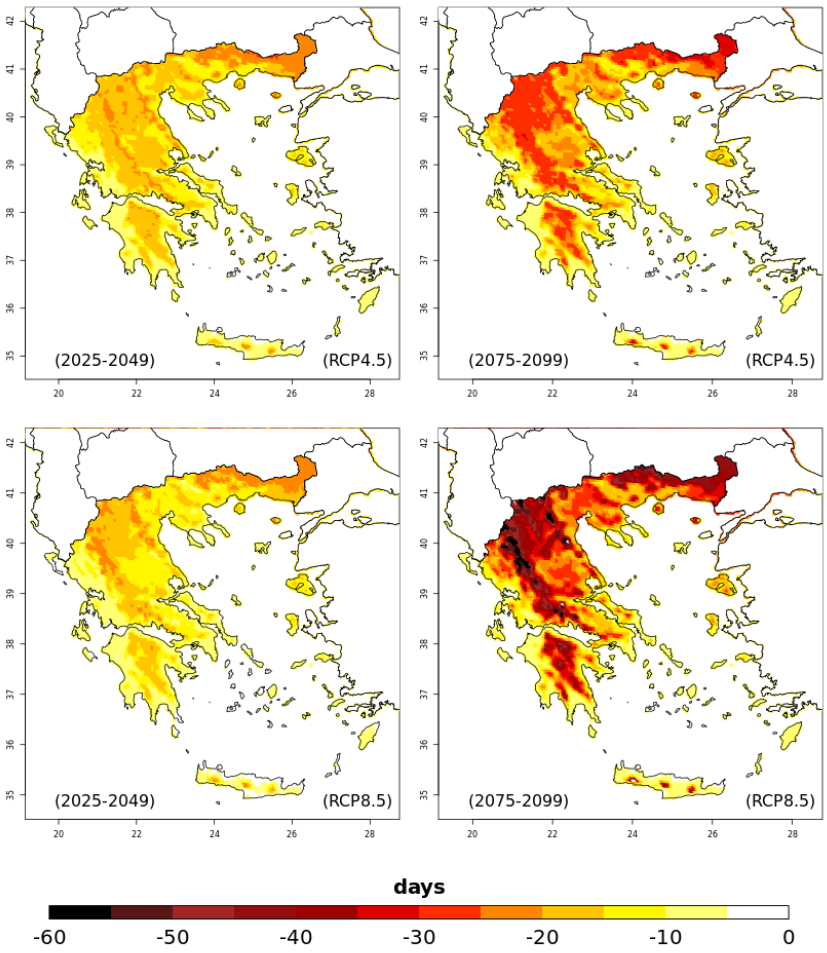

Figure 6.4 Annual mean frost days changes for 2025-2049 (near future) and 2075-2099 (near future) relative to 1980- 2004. In the top figure, the frost days index is depicted for the historical period. (Areas with dots specify changes not statistically significant using a Student's t-test at the 95% confidence level).

In Figure 6.4, a robust reduction is noted in the climate signal of frost days in the mountains, which reduces towards the coastal areas in the far future period. No noticeable differences are observed under both scenarios in the near future period. The strongest reduction of about 60 days is obtained under RCP8.5 in the far future. The calculated changes in frost days are statistically significant everywhere in the domain.

Both indices, illustrated in Figure 6.5 and Figure 6.6, show an increase in the climate change signal of extreme precipitation events, in the western part of the country for RCP4.5 in both periods and, the near future under RCP8.5 (up to 10 days). On the other hand, the highest decreases in the number of days with heavy precipitation are found mainly over the high mountainous areas of Crete and eastern mainland. This reduction

is more pronounced under RCP8.5 in the far future. The calculated changes in the number of days with heavy rainfall are statistically significant everywhere in the domain (Figure 6.5). However, the changes in the very heavy rainfall events are projected with no statistical significance in the north and eastern parts of the mainland during both periods and scenarios.

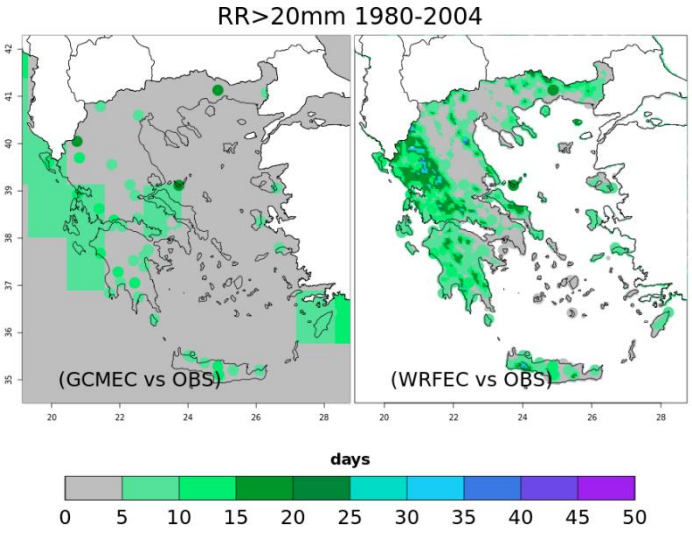

Change between scenario minus historical period

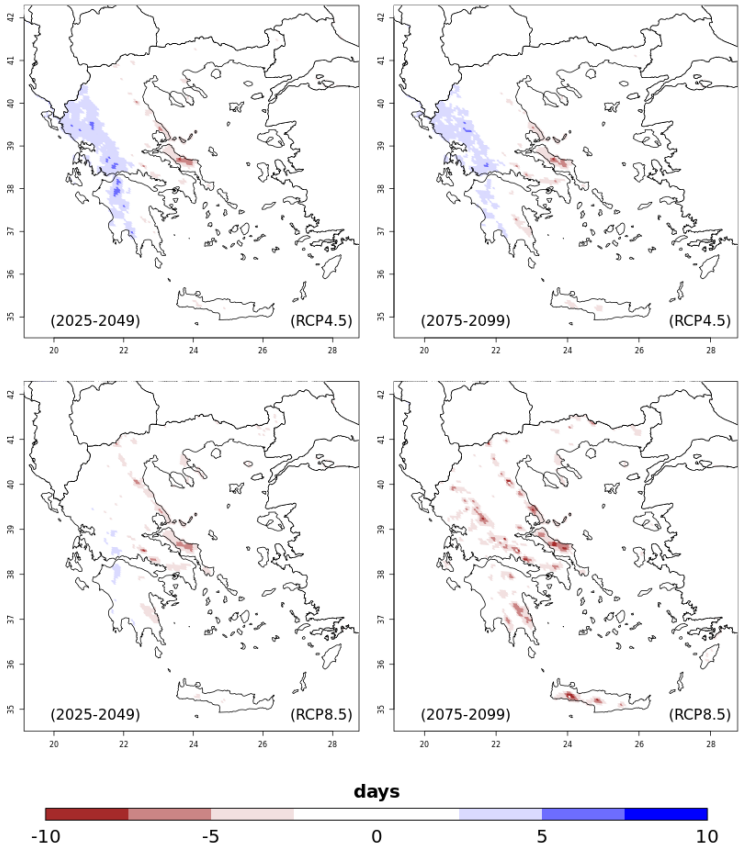

Figure 6.5 Annual mean heavy precipitation days changes for 2025-2049 (near future) and 2075-2099 (far future) relative to 1980- 2004. In the top figure, the number of heavy precipitation days (>20mm) is depicted for the historical period. (Areas with dots specify changes not statistically significant using a Student's t-test at the 95% confidence level).

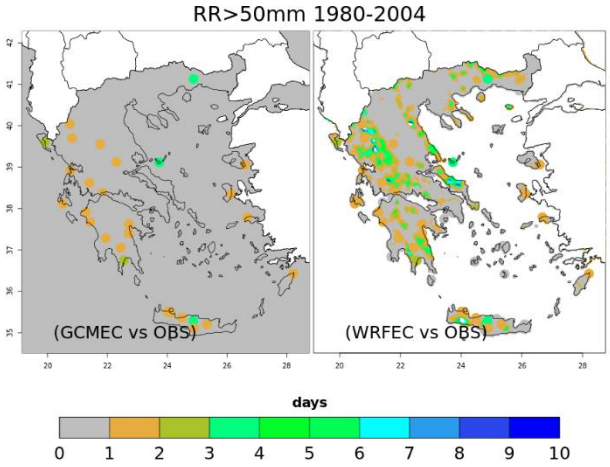

Change between scenario minus historical period

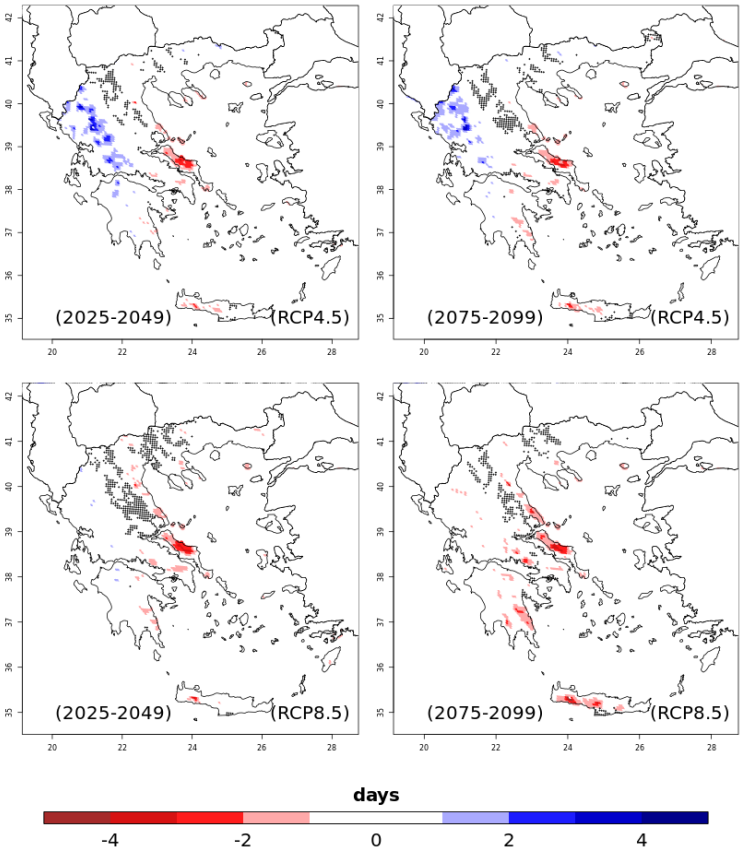

Figure 6.6 Annual mean very heavy precipitation days changes for 2025-2049 (near future) and 2075-2099 (far future) relative to 1980- 2004. In the top figure, the number of very heavy precipitation days (above 50mm) is depicted for the historical period. (Areas with dots specify changes not statistically significant using a Student's t-test at the 95% confidence level).

In what concerns dry days with daily precipitation less than 1 mm (Fig. 6.7), it is obvious that during both periods and scenarios the eastern part of the country would experience a consistent increase of dry days from 5 to 15 days. In addition, the strongest positive change is shown under RCP8.5 in the far future, all over the country with the most robust signal in the eastern parts (up to 35 days). Meanwhile, a reduction of dry days is reported up to 10 days, in the western parts of the country, the Ionian and Aegean Islands, Crete and some regions in the northeast mainland, with an exception during 2075-2099 under RCP8.5. The calculated changes in dry days are statistically significant everywhere in the domain.

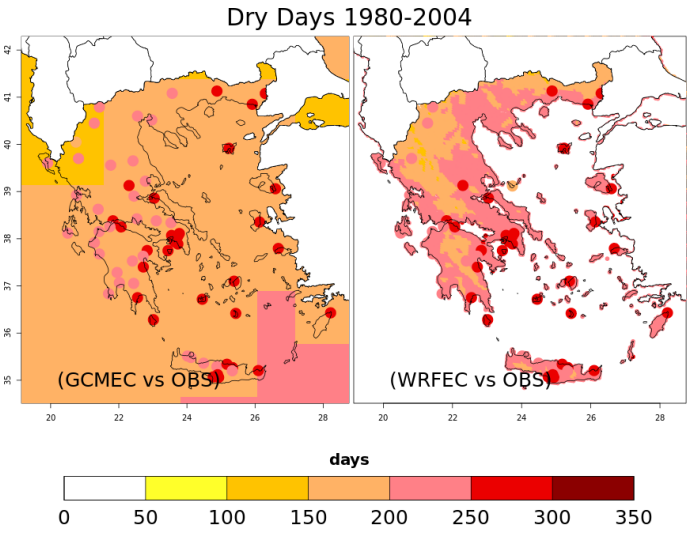

Change between scenario minus historical period

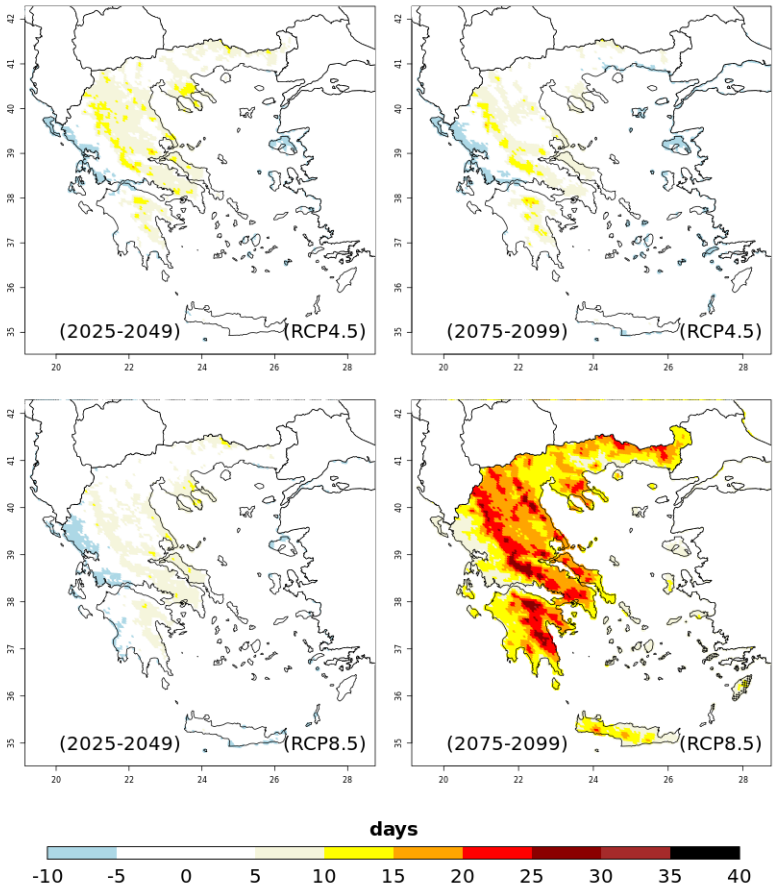

Figure 6.7 Annual mean dry days changes for 2025-2049 (near future) and 2075-2099 (far future) relative to 1980- 2004. In the top figure, the number of dry days (below 1 mm) is depicted for the historical period. (Areas with dots specify changes not statistically significant using a Student's t-test at the 95% confidence level).

Consequently, the climate change signal derived from the climate indices of extremes shows that it is clearly obvious that in both scenarios and periods extreme events would become gradually more extreme, reaching their peak in RCP8.5. These results are in good agreement with the studies of (Giannakopoulos et al. 2011; Kostopoulou et al. 2014). Leaver 2018 has also highlighted a considerable increase in the likelihood and occurrence of high temperatures based on ETCCDI climate indices based on EU-CORDEX datasets (0.44°) for the area of Greece. In agreement with our findings, another study using EU-CORDEX results (0.11°) reported future warming in Greece with the number of hot days and tropical nights in a year projected to increase significantly and the number of frost days to decrease, particularly under RCP8.5 (Georgoulias et al 2022). Moreover, our results are consistent with EU-CORDEX hot days results for the areas of Italy and the Balkans (where Greece is included) recently analysed by Coppola et al. (2020) where the number of hot days (>35°C) is robustly projected to increase by more than 50 days in the far future. Regarding precipitation, dry days become more frequent under RCP8.5 in the far future all over Greece with the eastern part of the country being highly prone to drought events. All these changes would have important impacts on agriculture production and human discomfort, as these are typical critical thresholds above which these sectors are affected.

6.3 Main Conclusions of Future Projections for ETTCDI

The climate change signal in what concerns the number of summer days is considerably increasing everywhere and particularly under RCP8.5 in the far future. The highest increases of hot days (greater than 35 days of daily TX>35°C) are observed over the plains of central-east mainland, central Macedonia, western mainland and Peloponnese under RCP8.5. Our results showed a decrease in the number of tropical nights, over the highly mountainous areas of the mainland and Crete in both periods and under both RCPs. On the other hand, their number increased elsewhere, becoming more vivid towards the coastal areas, particularly in the far future under RCP8.5 over the islands and parts of the western mainland. The number of frost days decreases everywhere in both periods and under both RCPs reaching most significant decreases over the mountainous areas and the eastern parts of the mainland under both RCPs in the far future.

Regarding precipitation climate indices, our findings revealed a reduction in the number of days with RR>20 mm everywhere apart from western Greece in both periods under RCP4.5 and in the near future under RCP8.5. The increases in the number of days of extreme precipitation (RR>50 mm) are less profound and mostly over the high altitudes of western Greece in both periods under both RCPs. Yet, the largest decreases are found over the highly mountainous areas of eastern mainland and Crete in the far future and under both RCPs. The number of dry days decreases in western Greece and the islands in both periods and under both RCPs, with an exception during 2075-2099 under RCP8.5. Significant increases are found over the mountainous areas and eastern mainland, which become more robust in the far future under RCP8.5

Key Remarks

- ***Increases in the number of hot days with more pronounced changes over the plain areas under RCP8.5 in the far future.***
- ***Decrease in the number of tropical nights, over the highly mountainous areas of the mainland and Crete in both periods and under both RCPs.***
- ***Reduction in the number days with RR>20 mm all over the country apart from western Greece in both periods under RCP4.5 and in the near future under RCP8.5***
- ***Significant increases of dry days were projected over the eastern part of the***

Chapter 7 Historical and Future Projections on Drought Characteristics

From the previous chapters, climate gridded datasets of precipitation and minimum and maximum temperatures were derived from regional climate simulations for the area of Greece, with the WRF-ARW model appropriately setup, driven by the EC-EARTH global model. This chapter, in the first section, includes a description of the applied methodology for the calculation of drought indices based on these climate gridded datasets and the overall methodology for the estimation of drought characteristics. The next section continues with the analysis and the presentation of the results associated with the impact of climate change on drought characteristics in high resolution in Greece.

7.1. SPI and SPEI

Although various definitions of drought exist, there is no universally accepted definition of drought, since there is a wide variety of sectors affected by drought, as well as due to its diverse spatial and temporal distribution (Heim, 2002). Nevertheless, by considering drought as a hazard, there is a tendency to define and classify droughts into different types, however, the relationship between the different types of droughts is complex. In international literature, three operational definitions are considered, namely meteorological or climatological, agrometeorological or agricultural and hydrological drought (Wilhite et al., 2000). As a fourth type of drought, the socioeconomic impacts of drought can also be considered.

More specifically, meteorological drought is a phenomenon associated with prolonged and abnormal moisture deficiency, characterised by a precipitation anomaly being lower than average. It is usually described by the magnitude and duration of precipitation deficit with respect to the long-term climatology, often analyzed with statistical indices like the Standardized Precipitation Index (SPI) (Mckee et al. 1993). The agricultural drought is caused by the combination of a lack of precipitation (meteorological drought) with the demand of the atmosphere for water. It is defined by the availability of soil water to support crop and forage growth and there is no direct

relationship between precipitation and infiltration of precipitation into the soil (Dalezios 2018). This type of drought is affected by both climate change and human activity on land, but also by direct human influences on the hydrological cycle. The hydrological drought refers to low flow periods with a streamflow or groundwater level deficit under "natural" conditions. Related indices often include the annual minimum of a streamflow average taken over several consecutive days. The final type of socio-economic drought is a result of water scarcity due to weather conditions, related to the water supply creating an imbalance between supply and demand for essential economic resources and affects various sectors such as food, transportation, hydropower etc.

The socio-economic impacts associated with agricultural drought can be severe. In this study, in order to identify dryness or wetness conditions that can cause drought impacts on various sectors, the Standardized Precipitation Index (SPI) [67], proposed by WMO 2010, and Standardized Precipitation Evapotranspiration Index (SPEI) (Vicente-Serrano et al. 2010) are estimated. These two indices are among the most widely used indices for drought identification and monitoring in Europe. As no single drought index alone may precisely describe all the attributes of drought conditions, their combination is a common approach in the scientific literature lately (Spinoni et al. 2015; Akbari et al. 2016; Jehanzaib et al. 2020; Dukat et al. 2022; Faye 2022).

The SPI is calculated by fitting a probability density function to a given frequency distribution of precipitation totals for a station or grid point and for an accumulation period (Faye Cheikh et al. 2019) and then the probabilities are transformed into a normalized distribution with a mean equal to zero and a variance of one, developed by Mckee et al., (1993). The SPI values can be interpreted as the number of standard deviations by which the observed anomaly deviates from the long-term mean.
SPI is calculated as follows in equation (1):

$$SPI = \frac{x_i - x_j}{\sigma} \quad (1),$$

where, xi refers to the current precipitation in the examined period, xj refers to the mean precipitation of the timeseries, and σ refers to the standard deviation of the timeseries.

SPEI is estimated using the same methodology as mentioned for SPI but includes the climatic water balance which is the difference between precipitation and

evapotranspiration. The inclusion of temperature on SPEI's calculation (through potential evapotranspiration (PET)) is suggested by European Drought Observatory (see the source link in https://edo.jrc.ec.europa.eu/edov2/php/index.php?id=1000) and the Integrated Drought Management Programme (IDMP, https://public.wmo.int/en/programmes/integrated-drought-management-programme) since it is more suitable for the study of impact of future climate change. Details of the SPEI calculation can be found in (Vicente-Serrano et al. 2010; Beguería et al. 2014). The distribution functions used for computing those indices were the 'log-Logistic' for SPEI, and 'Gamma' for SPI. The applied herein distributions are the most widely used in literature and recommended by the indices' original developers (Spinoni et al. 2019). Here, to calculate the SPEI index, the monthly potential evapotranspiration is estimated based on the Samani equation H. Hargreaves and A. Samani, 1985 (H. Hargreaves and A. Samani 1985) by estimating solar radiation from monthly minimum and maximum temperature along with the location (latitude) of the grid cell. This method is frequently used in drought studies (Vangelis et al. 2011; Vicente-Serrano et al. 2011; Spinoni et al. 2020). The comparison of SPI and SPEI is made to assess the impact of potential evapotranspiration which is a metric of the atmospheric evaporative demand (AED) to determine the drought in the study areas as well as the uncertainty in the results obtained using the SPI.

According to Wu et al., (2007) SPI values at scales up to 3-months are being non-normally distributed in arid and semi-arid regions. Furthermore, (Karavitis et al. 2014; Spinoni et al. 2019) point out in their studies that semi-arid and arid areas could give an unreliable estimation of meteorological indices computed at short accumulation periods (e.g., 3-months), especially with SPI because climatic conditions usually exhibit an extended dry period of at least a few months with a notable number of zero values that can cause statistical errors related to distribution's calculation (Cressie 2015). Thus, the SPI or SPEI values of 6- and 12-months are proposed as more appropriate for denoting not only meteorological but also agricultural droughts, applied in several studies (Karavitis et al. 2012, 2014; Stagge et al. 2017; Oikonomou et al. 2019; Tsesmelis et al. 2019) in arid and semi-arid regions. Accordingly, the SPI-6, SPEI-6, SPI-12, and SPEI-12 are selected for the drought characterization in Greece.

Both indices in the 6- and 12- months timescale are calculated over the nested domain for each grid point and all precipitation data are converted to monthly values. Also, the time series of the drought indices are calculated over the land grid cells for

each time period. Drought conditions are indicated as SPI decreases below –1.0, while increasingly severe excess rainfall is indicated as SPI increases above 1.0, as described for all drought indices values in Table 7.1. The applied classification is consistent with EU recommendations for this area which is part of the Euro-Mediterranean area (World Meteorological Organization (WMO) and Global Water Partnership (GWP) 2016; Copernicus European Drought Observatory (EDO): https://edo.jrc.ec.europa.eu/ 2020).

Table 7.1 Classification of the SPI values. The same applies to the SPEI.

SPI value	Drought class
SPI≥2.0	Extremely wet
1.5<SPI≤2	Severe Wet
1.0≤SPI<1.5	Moderate Wet
-1.0<SPI≤1.0	Normal Climate
-1.0≤SPI≤-1.5	Moderate Dry
-2.0≤SPI<-1.5	Severe Dry
SPI<-2	Extreme Dry

In this context, the characterization of a drought event is established when dry or near-normal conditions are followed by drought conditions with values of the index below −1 at least for two consecutive months. In the same way, it is considered that the event ends when the value of index corresponds to near normal/wet conditions (index values greater than 0). In order to examine the drought characteristics, three different parameters are used: (1) severity which is determined as the absolute sum of SPI and SPEI values for a drought event; (2) duration as the length of each drought event (in months); and (3) mean intensity which is calculated as the average SPI and SPEI value during a drought event or even defined by the severity divided by duration. Drought characteristics are depicted schematically in Figure 7.1.

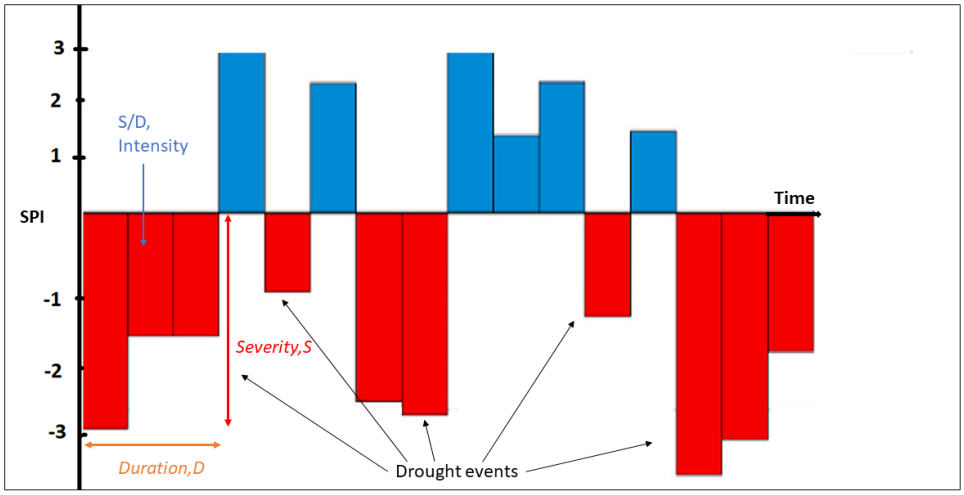

Figure 7.1 Illustration of drought duration, severity, intensity and events.

The analysis of projected changes of drought was evaluated through the Delta-Change approach (Hay et al. 2000) in terms of duration, intensity, frequency, and severity of drought events by comparing indices, their time scales, scenarios and periods. Thus, future climate changes of drought characteristics are defined as the differences (Delta change) between the projection run (near or far period) and the control run (reference period). Along with the projected changes of drought characteristics, the trends of drought characteristics were studied, as well as their significance. The linear trend is calculated based on the annual values of intensity, severity and duration of drought events. Figure 7.2 presents the regions of particular interest, as agricultural areas, based on the results.

Figure 7.2 Regions of particular interest of the country for discussion. Agricultural areas are depicted in orange color.

To calculate the SPI and SPEI, the R software was used, the "SPEI" package (Vicente-Serrano et al. 2010; Beguería et al. 2014). In addition, drought characteristics and trends have been analyzed in the R environment (http://www.r-project.org/index.html).

7.2 SPI-SPEI 6-month timescale

In this section, the results of drought characteristics and their trends derived from the SPI and SPEI values of the 6-months timescale were analyzed. The frequency (number of events), duration, severity, and intensity of the events shown in the following figures are expressed per 5 years (with an exception in the frequency of drought events that was summed only for the reference period). The historical conditions of drought characteristics are also depicted for each case.

Figure 7.3a depicts the total frequency of drought events during the 25-year reference period calculated by SPI and SPEI. Both indices yield a similar pattern of drought events, however, SPEI presents droughts of increased frequency and spatial coverage compared to SPI. The number of relatively higher frequency drought events (above 8) are found in northern Greece (parts of eastern and central Macedonia), central

mainland, the Peloponnese, Evia, and several islands (of the northern and central Aegean Sea and the Ionian Sea), and western Crete. Figure 7.3b shows the SPI and SPEI projected changes in the number of drought events (per 5 years), based on the different emission scenarios and future periods. The two indices show an overall decrease in the frequency of drought events in both future periods over the country and under both emission scenarios, apart from parts of Crete, Thessaly, western central Greece and the Peloponnese.

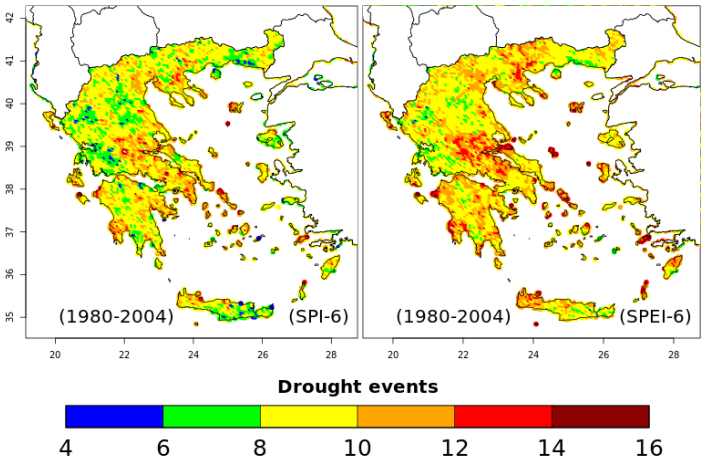

a)

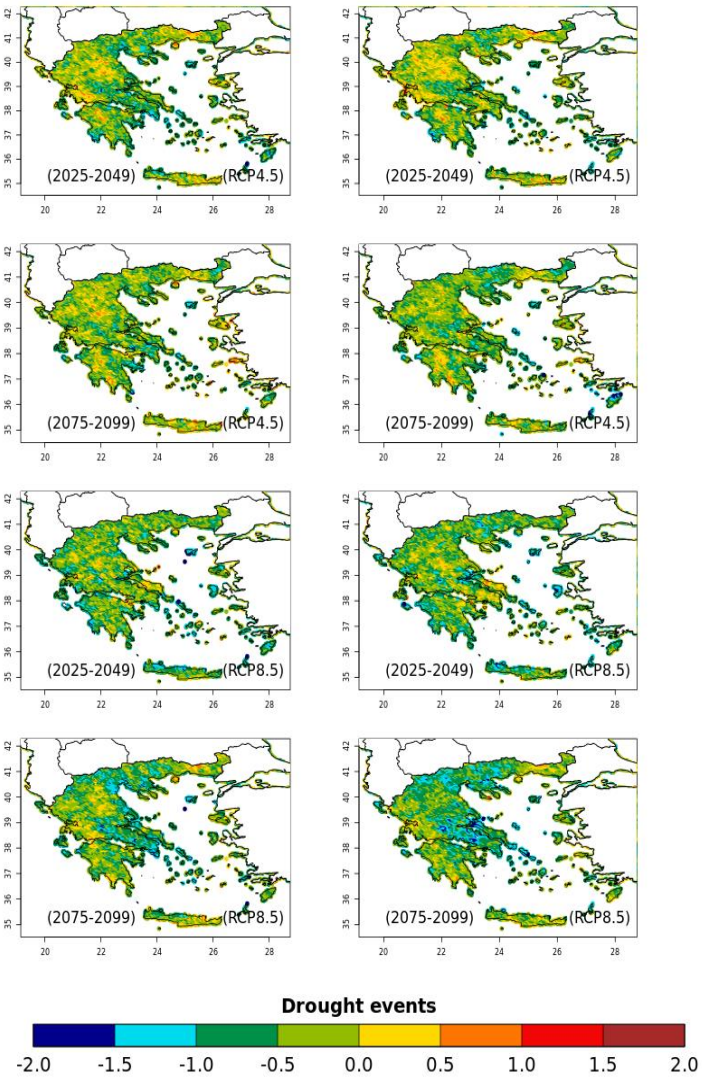

b)

Figure 7.3 a) Drought frequency as the number of events in 25 years for the reference period (1980–2004) for the SPI (left) and the SPEI (right) indices computed at 6-months timescale. b) Changes in the frequency for the 6-month SPI and SPEI for the near future period (2025–2049) and the far future (2075-2099) relative to the reference period (1980–2004) under RCP4.5 and RCP8.5.

It should be clarified that the plain areas of Crete and Thessaly exhibit an outstanding contribution to the country's agricultural sector and therefore, potential projected changes in drought frequency are of immense importance. The same holds for the areas of western and north-eastern Peloponnese.

According to SPI and SPEI, the drought events are projected to be more frequent in the near future period than in the recent past under RCP4.5 in the plain areas of Thessaly, Thrace, western-central continental Greece, central Peloponnese and eastern Crete.

Overall, changes in the far future period and under RCP4.5 yield decreased frequency of drought events in central and northern parts of the country, particularly those obtained by SPEI. On the other hand, the far future projections using both indices under RCP8.5 present a reduced signal of drought frequency over Thessaly compared to RCP4.5 results. Notably, the SPEI projected changes in the far future and under RCP8.5 showed the strongest signal of reduction in drought events compared to all other cases examined. It could also be mentioned that a reduced frequency of drought events is projected over the highly populated region of Attica except for the near-future SPEI projections under RCP8.5.

The duration of drought events attains values up to 12 months/5y for the historical period with both indices, but in the case of SPEI, the larger part of the land area is characterized from at least 6-8 months/5y duration, as it is illustrated in Figure 7.4a. Our results are in agreement with the findings of (Loukas and Vasiliades 2004) for the region of Thessaly and the historical drought investigation of (Livada and Assimakopoulos 2007) indicating severe droughts slightly increasing from north to south and from west to east.

Regarding the projected duration (Figure 7.4b), under RCP4.5 and according to both indices, the drought events are projected to be longer in the near future than in the past in Thessaly (~4months/5y), in north-eastern Greece (Macedonia), western-central Greece and north-western Peloponnese, eastern Crete and eastern Aegean (islands). Shorter drought events are observed in Epirus, the mountainous parts of the mainland, eastern parts of central Greece, and northeastern Peloponnese. Some of these areas like western Macedonia, and Epirus show in the far future an increased duration of drought events and a reduced one in Evia.

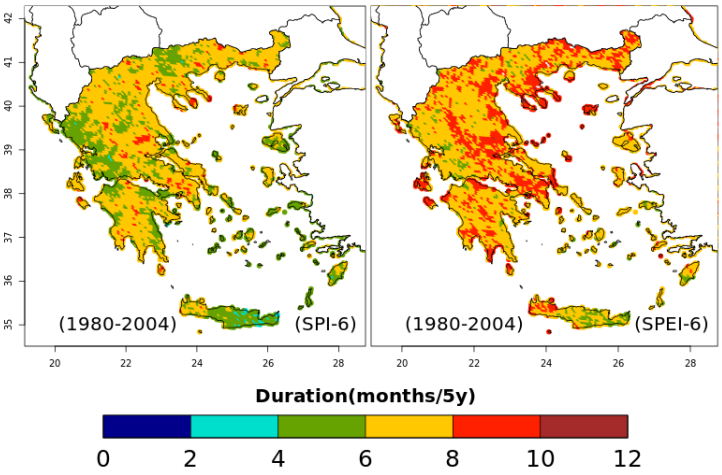
(1980-2004) (SPI-6)
(1980-2004) (SPEI-6)
Duration(months/5y)
0 2 4 6 8 10 12

a)

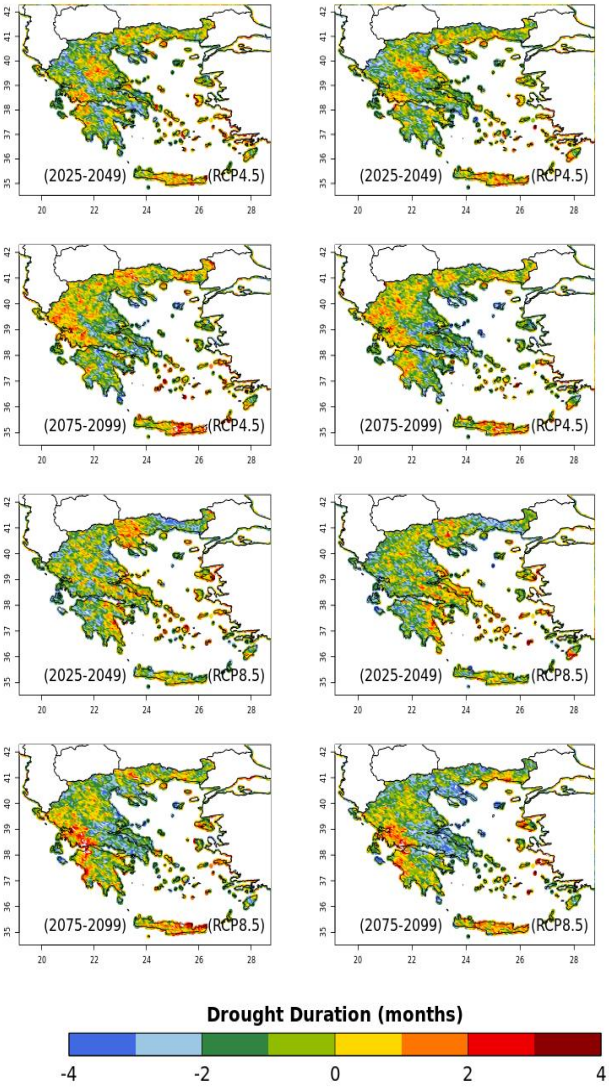
(2025-2049) (RCP4.5)
(2025-2049) (RCP4.5)
(2075-2099) (RCP4.5)
(2075-2099) (RCP4.5)
(2025-2049) (RCP8.5)
(2025-2049) (RCP8.5)
(2075-2099) (RCP8.5)
(2075-2099) (RCP8.5)
Drought Duration (months)
-4 -2 0 2 4

b)

Figure 7.4 a) Drought Duration as the averaged values obtained for the entire reference period (1980–2004) for the SPI and the SPEI indices computed at 6-months timescale. b) Changes in the duration for the 6-month SPI and SPEI for the near future period (2025–2025–2049) and the far future (2075-2099) relative to the reference period (1980–2004) under RCP4.5 and RCP8.5

In the near future period and under RCP8.5, the increase of drought length is more intense in the eastern parts of the country (with the Aegean islands included), with both indices and less intense in Crete. However, in the far future, the projected RCP8.5 change of increased duration of drought events is more intense and shifted to the western parts of the country (Epirus/western Greece and western Peloponnese) and Crete, with almost the same spatial patterns for the two indices. On the other hand, a notable reduction in the signal of drought duration is observed over the larger part of the central and eastern mainland with Attica included.

Concerning the severity (Figure 7.5) and the duration of drought events, the drought events are projected according to both indices to follow, on average, the same spatial patterns, while the spatial patterns of the drought intensity (Figure 7.6) are less homogeneous and this remark is also made in the study of (Christel et al. 2014). The intensity of drought events using both indices, as illustrated in Figure 7.6a, shows that SPI yields higher values and spatial coverage compared to SPEI. The intensity is projected to be higher and more extended with SPI than SPEI (see Figure 7.6b), for all periods and RCPs, and particularly for the northern and eastern parts of the country and Crete, with the additional inclusion of the western mainland during the far future under both RCPs.

a.

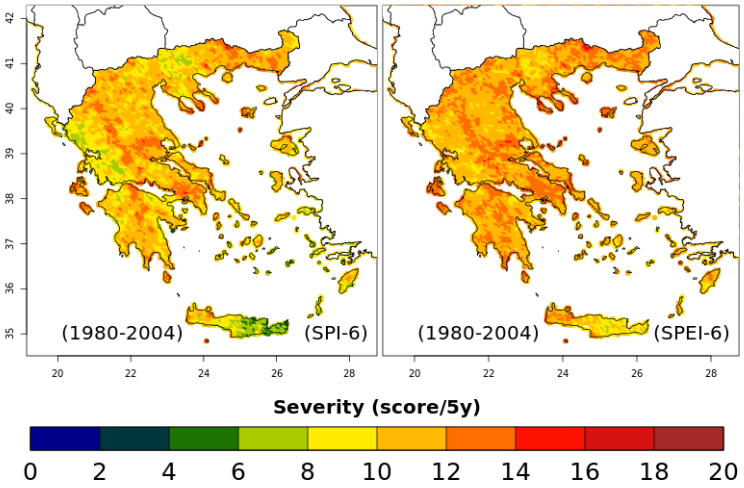

b.

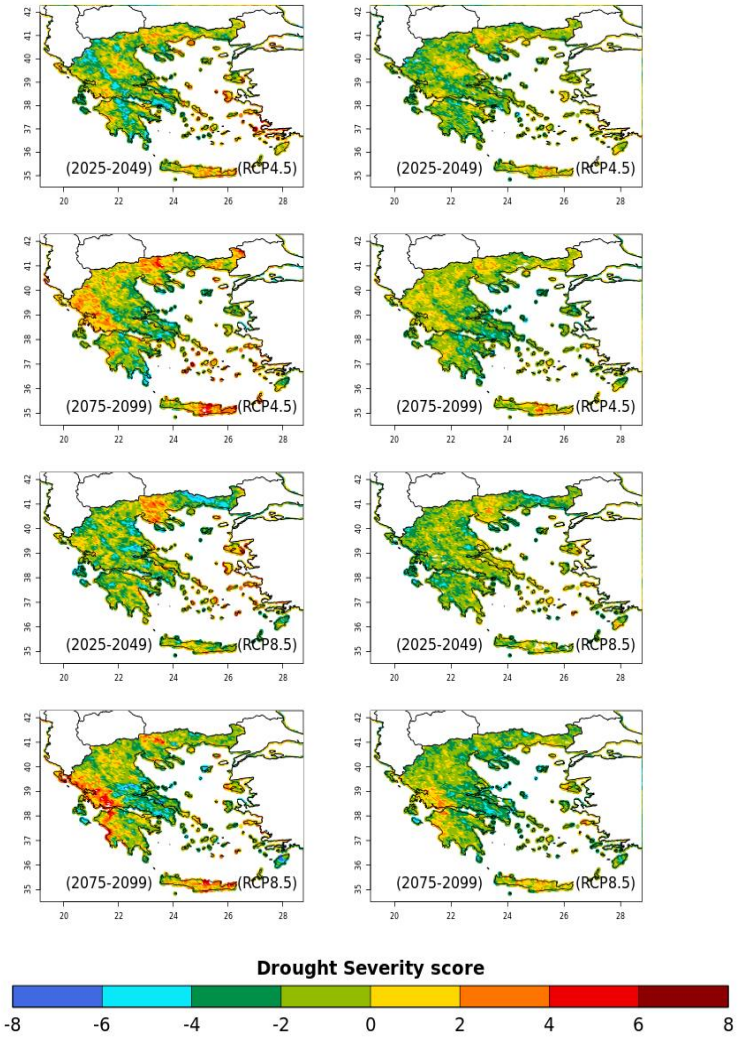

Figure 7.5 a) Drought Severity as the averaged values obtained for the entire reference period (1980–2004) for the SPI and the SPEI indices computed at 6-months timescale. b) Changes in the severity for the 6-month SPI and SPEI for the near future period (2025–2049) and the far future (2075-2099) relative to the reference period (1980–2004) under RCP4.5 and RCP8.5

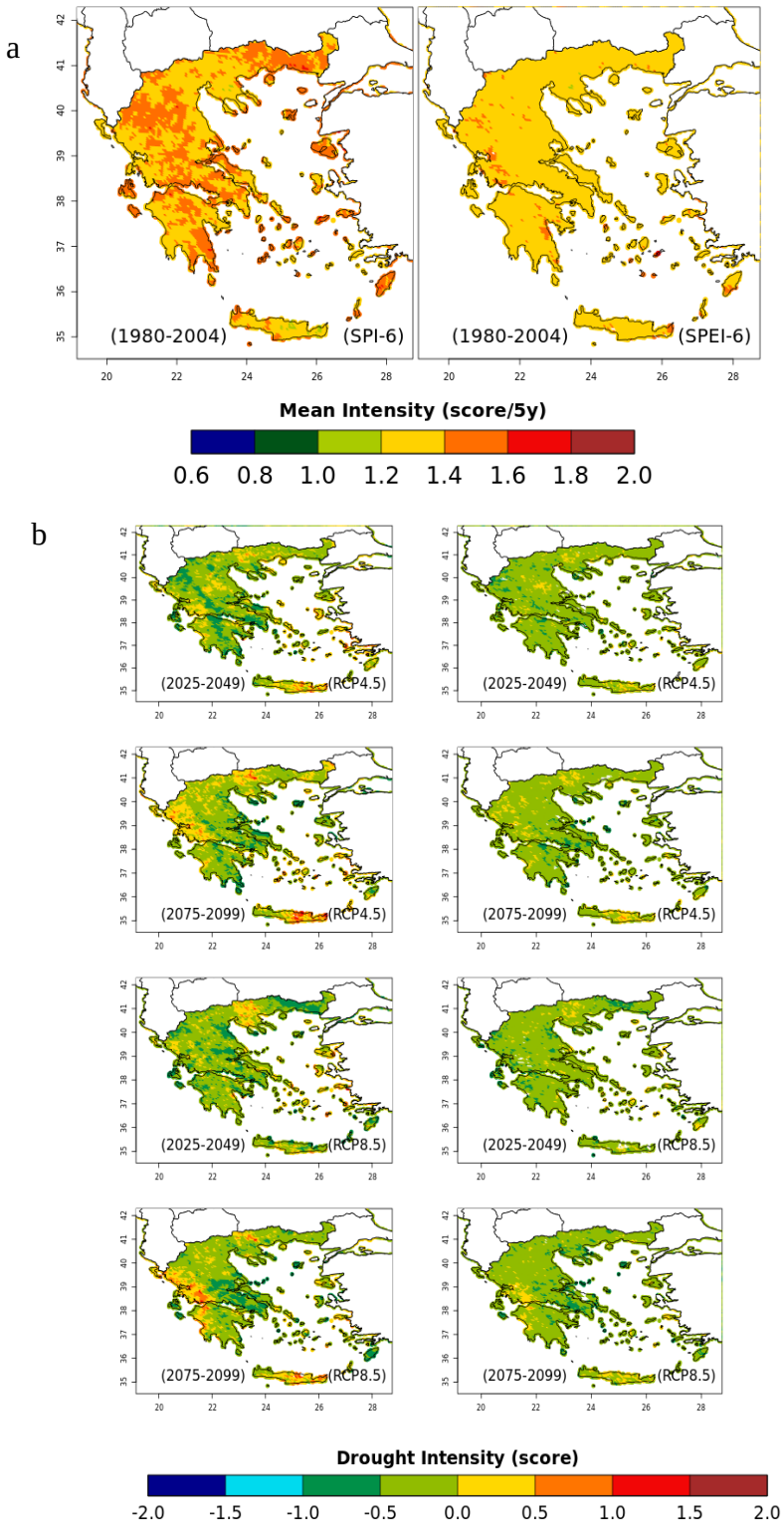

Figure 7.6 a) Drought Intensity as the averaged values obtained for the entire reference period (1980–2004) for the SPI and the SPEI indices computed at 6-months timescale. b) Changes in the intensity for the 6-month SPI and SPEI for the near future period (2025–

2049) and the far future (2075-2099) relative to the reference period (1980–2004) under RCP4.5 and RCP8.5

The analysis of drought characteristics is also studied in terms of spatial trends for the area of Greece, for the two periods, RCPs and indices to examine their differences along with the representation of their statistical significance. Severity and duration trends, as illustrated in Figure 7.7 and Figure 7.8, show similar spatial patterns for both scenarios over Greece. In general, the projected results show both positive and negative trends, with larger areas presenting a strong positive (of which in many areas statistically significant) trend by using both indices mainly under RCP8.5 due to a combination of both warming and drying climate change signal (see (Politi et al. 2022)

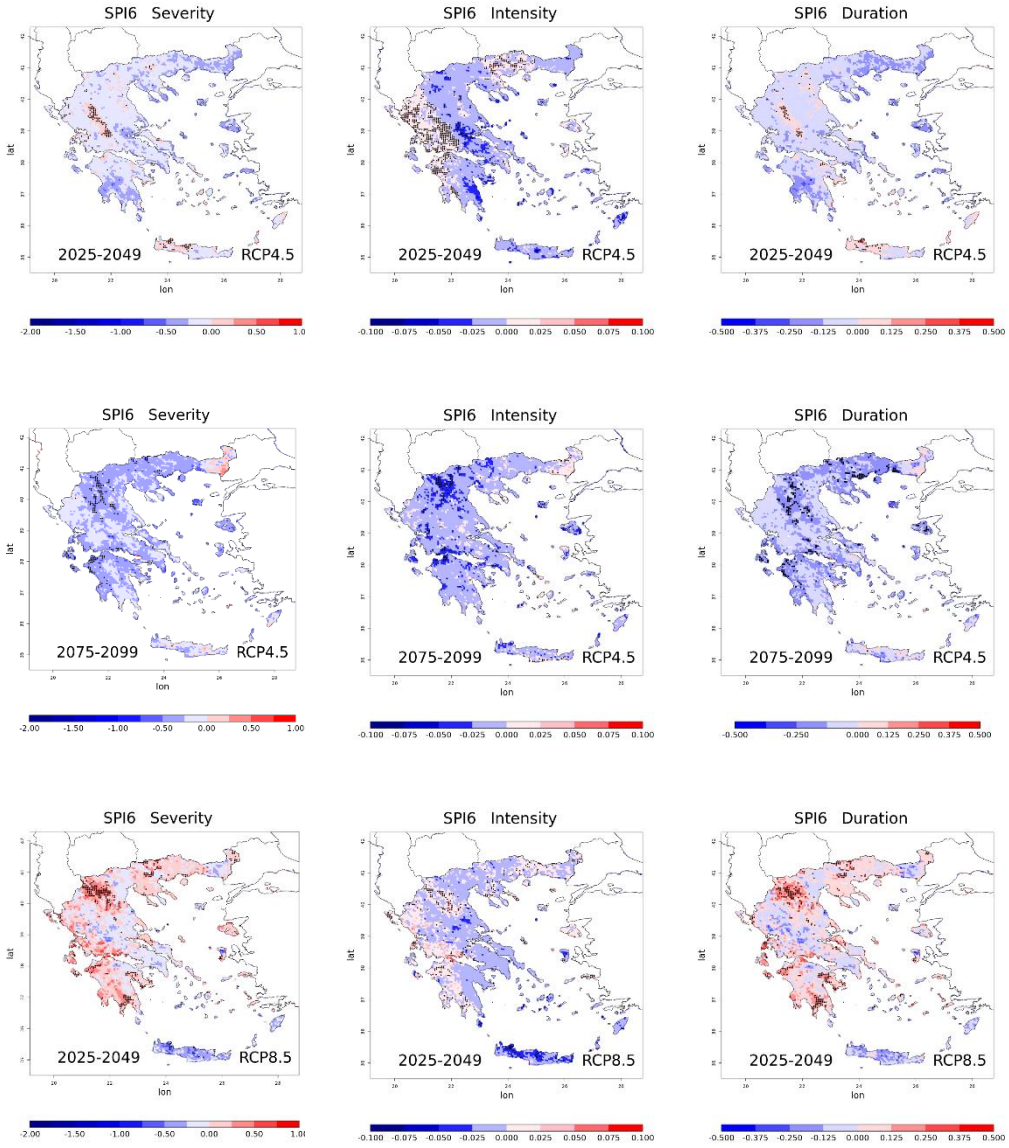

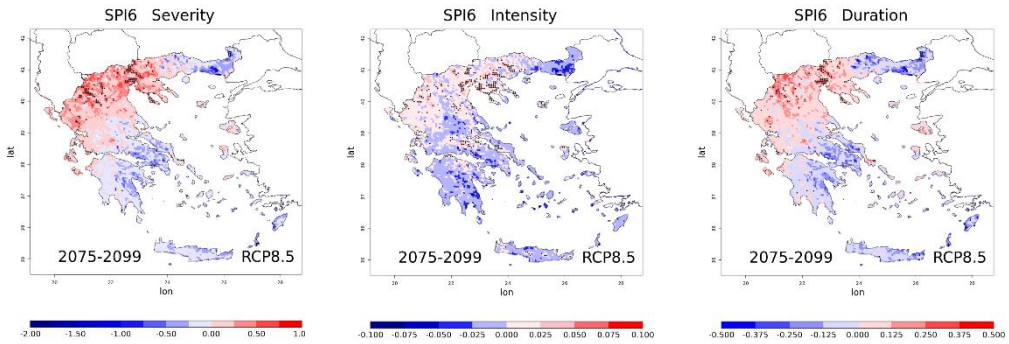

Figure 7.7 Trends of Severity, Intensity and Duration for the 6-months SPI under RCP4.5 and RCP8.5 for the period 2025-2049 and 2075-2099. The black dotted areas show significant changes in the drought characteristics at the 5% significance level

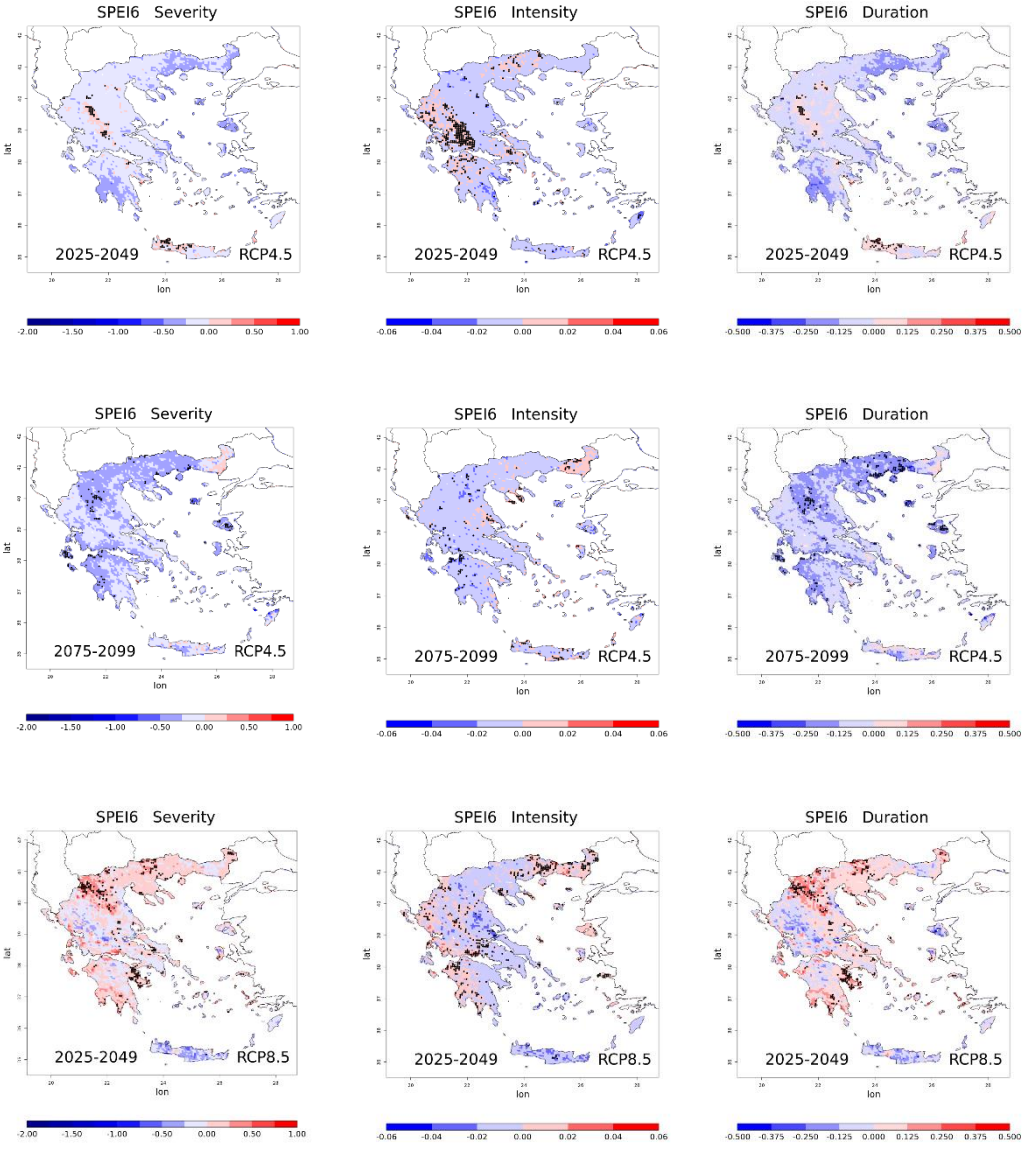

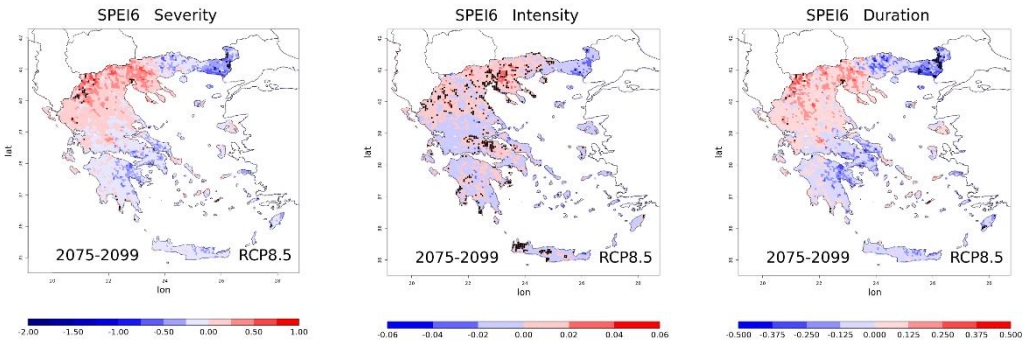

Figure 7.8 Trends of Severity, Intensity and Duration for the 6-months SPEI under RCP4.5 and RCP8.5 for the period 2025-2049 and 2075-2099. The black dotted areas show significant changes in the drought characteristics at the 5% significance level

On the other hand, both indices revealed a negative trend under RPC4.5 mainly during the far future period all over the country with a statistically significant trend in some areas in the northern part of the country, western Peloponnese and the Ionian islands. Yet, there are some exceptions, where statistically significant positive trends are noticed with SPEI resulting in more intense drought events, for example in areas of Thessaly, Thrace, Chalkidiki and Crete but at the same time these drought events are less severe and/or of shorter duration (Figure. 7.8).

Under RPC4.5 and in the near future, statistically significant positive trends are observed with intense drought events in western mainland and eastern Macedonia, with an also statistically significant positive trend in severity and duration in western mountainous parts and western Crete.

Finally, it is also worthy to report that under RCP8.5 for both periods there is a northeast to southwest gradient towards negative trends in some areas of central-eastern Greece, eastern Peloponnese, the Aegean Islands, Crete and Thrace, without being statistically significant though. In the far future and in both emission scenarios, a decrease in the mean duration and severity is observed locally on the eastern coasts of the mainland, probably related to the extreme rainfall events that only persist there in the far future, as it has been indicated in the study of (Vlachogiannis et al. 2022). This outcome is associated with the Arctic amplification and possible connection to the weakening of mid-latitude storm tracks (Chang et al. 2016). A profound positive statistically significant trend in changes in drought characteristics is found mainly locally over areas in Macedonia, Thrace, Thessaly and Peloponnese using both indices and under both

periods. The high spatial resolution of the simulations gives the opportunity to determine the specific areas of a rather small extent prone to drought, e.g., northern parts of the island of Rhodes under RCP4.5 in the near future (Figure 7.7) and the islands of Lesvos and Chios in eastern Aegean Sea under RCP8.5 in the near future (Figure 7.8). However, when averaged over the whole area of Greece, it was necessary to proceed with the investigation of the general response to drought tendency.

In this context, boxplots illustrate the trends of the total land area of drought characteristics during each period and emission scenario (Figure 7.9). The drought characteristics are calculated by spatial and temporal averaging (over five years). Drought intensity, duration and severity follow similar patterns, showing positive trends using both indices in the near future period under both scenarios and only in the far future under RCP8.5. It is deduced that RCP8.5 drought characteristics with SPI-6 and SPEI-6 present a stronger positive trend than those obtained under RCP4.5. The negative projected trend in the far future period under RCP4.5 is probably related to the negative projected trend of maximum temperature and simultaneously the positive projected trend of precipitation (particularly in the west parts of the country for both variables) during the same period (not shown), leading to wetter and milder conditions.

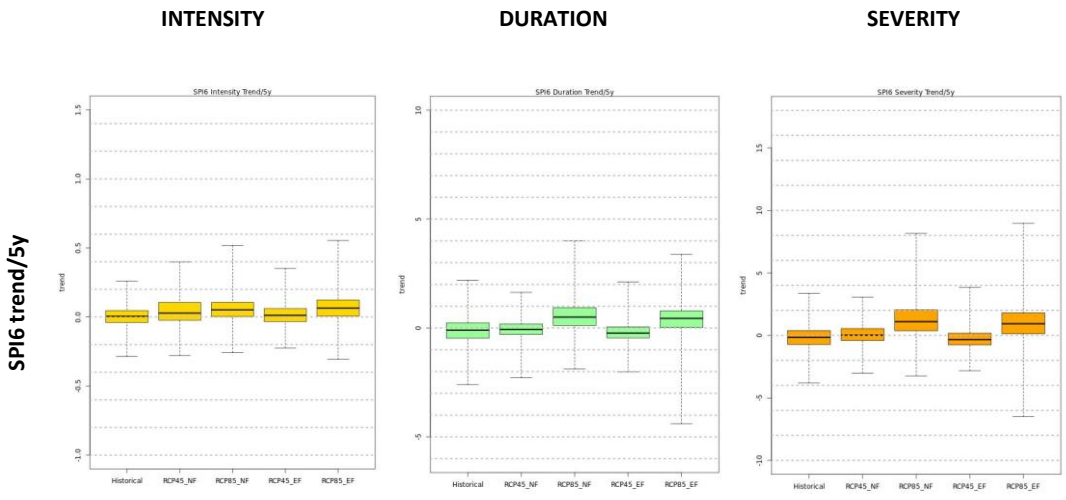

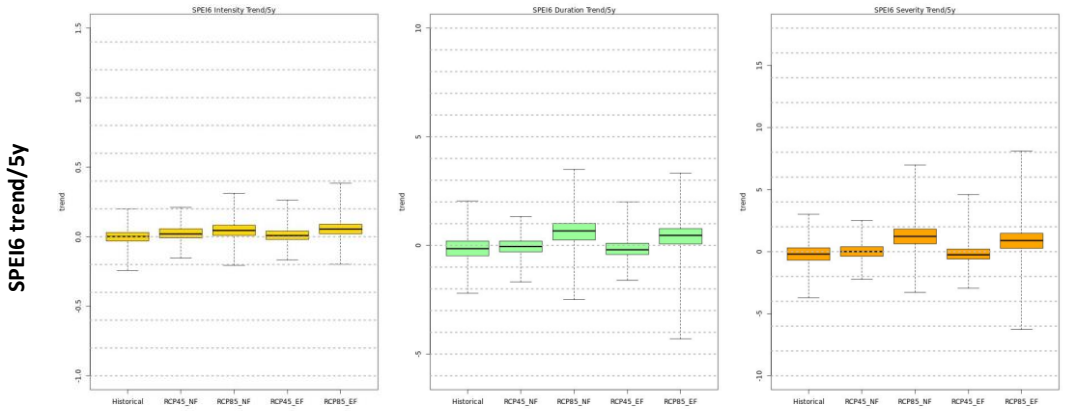

Figure 7.9 5-years mean trends of drought severity, intensity and duration averaged over land area, for the 6-months SPI/SPEI under RCP4.5 and RCP8.5 for the period 2025-2049 and 2075-2099 and the reference period (1980-2004)

7.3 SPI-SPEI 12-month timescale

As depicted in Figure 10a, historical simulations with SPI and SPEI illustrate similar spatial patterns of drought event, with an exception in some areas of western Peloponnese where SPEI presents droughts of increased frequency and spatial coverage compared to SPI. Moreover, the two indices agree on the projected decrease or increase in drought frequency (per 5 years) with a higher number of drought events being observed under RCP4.5 during both time periods (Figure 7.10b).

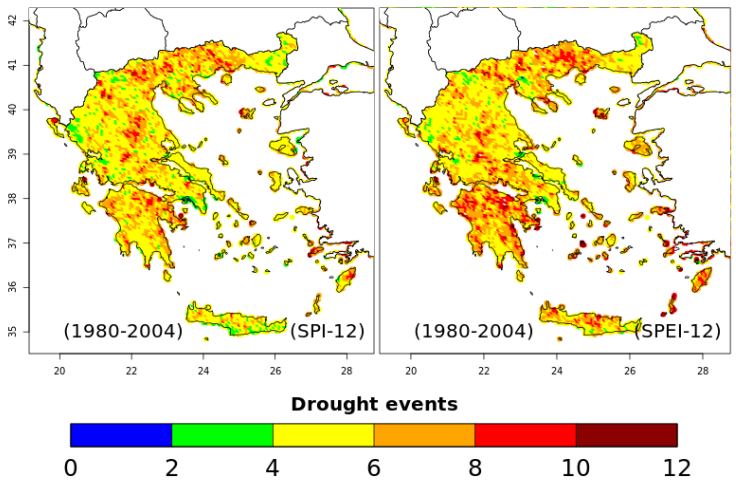

a)

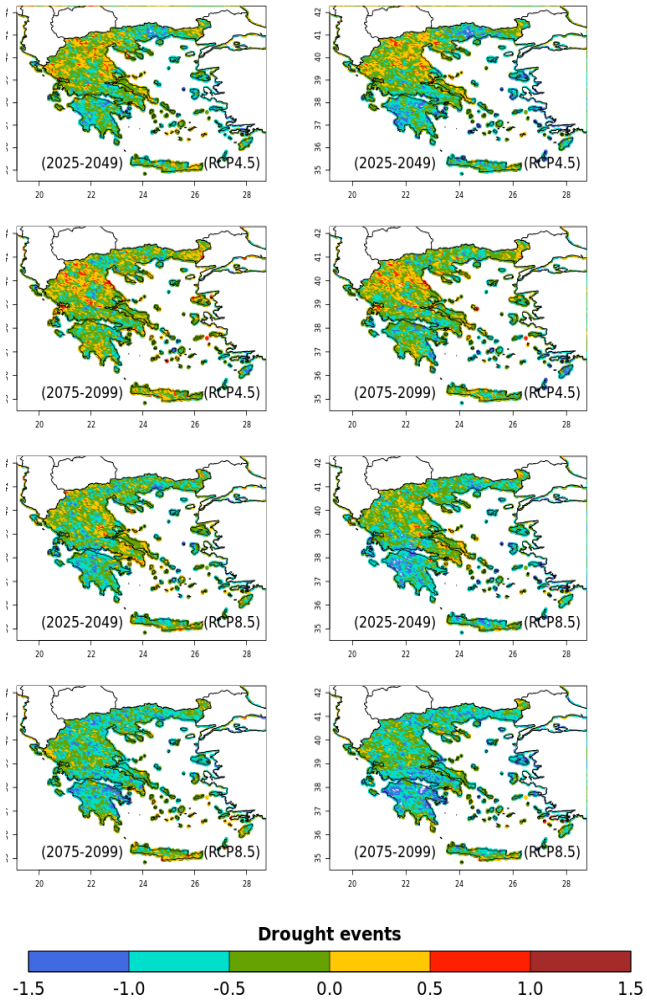

b)

Figure 7.10 a) Drought frequency as the number of events in 25 years for the reference period (1980–2004) for the SPI and the SPEI indices computed at 12-months timescale. b) Changes in the frequency for the 12-months SPI and SPEI for the near future period (2025–2049) and the far future (2075-2099) relative to the reference period (1980–2004) under RCP4.5 and RCP8.5

Drought duration for the historical period shows that SPEI covers more extended areas of longer duration all over the country than the SPI, mainly in eastern Macedonia, Thrace, Epirus, Central Greece (with Attica and Evia included) and northern Peloponnese (Figure 7.11a). Increases in projected drought duration under RCP4.5 affect many plain areas all over Greece, with maximum values of duration of ~8 months/5y occurring in Macedonia and in local areas in Thessaly, northern Evia, central Greece, the Ionian and Aegean islands, Crete and the Peloponnese (Figure 7.11b). In the near future, only Epirus and northeast Peloponnese are the regions with reduced duration of drought events. While, in the far future, only the eastern Peloponnese,

Attica, south Evia, and eastern Rhodes will experience drought events of shorter duration. These results are deduced with both indices. Under RCP8.5, the duration will be longer in some parts of the eastern country and Crete in the near future. Nevertheless, the signal will change in the far future with a longer duration in the southern and western Peloponnese, central-west continental parts and Epirus, central Macedonia and Thrace. Thus, the regions of north-east Peloponnese, northern Evia and Thessaly are projected to experience the strongest decrease in drought duration in the far future. Overall, the differences between SPI and SPEI in duration are almost negligible.

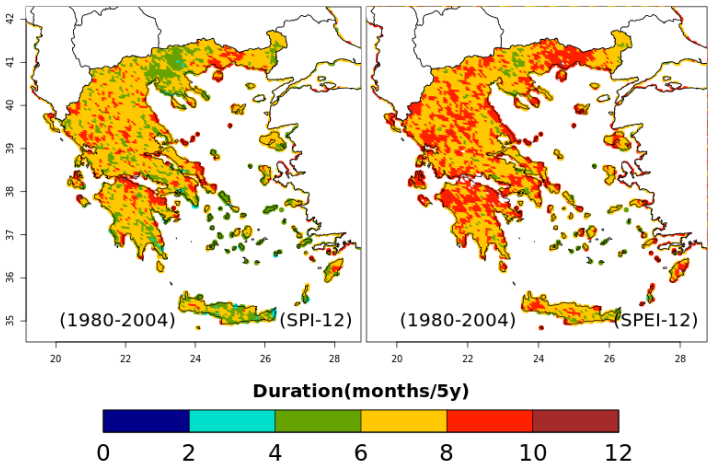

a)

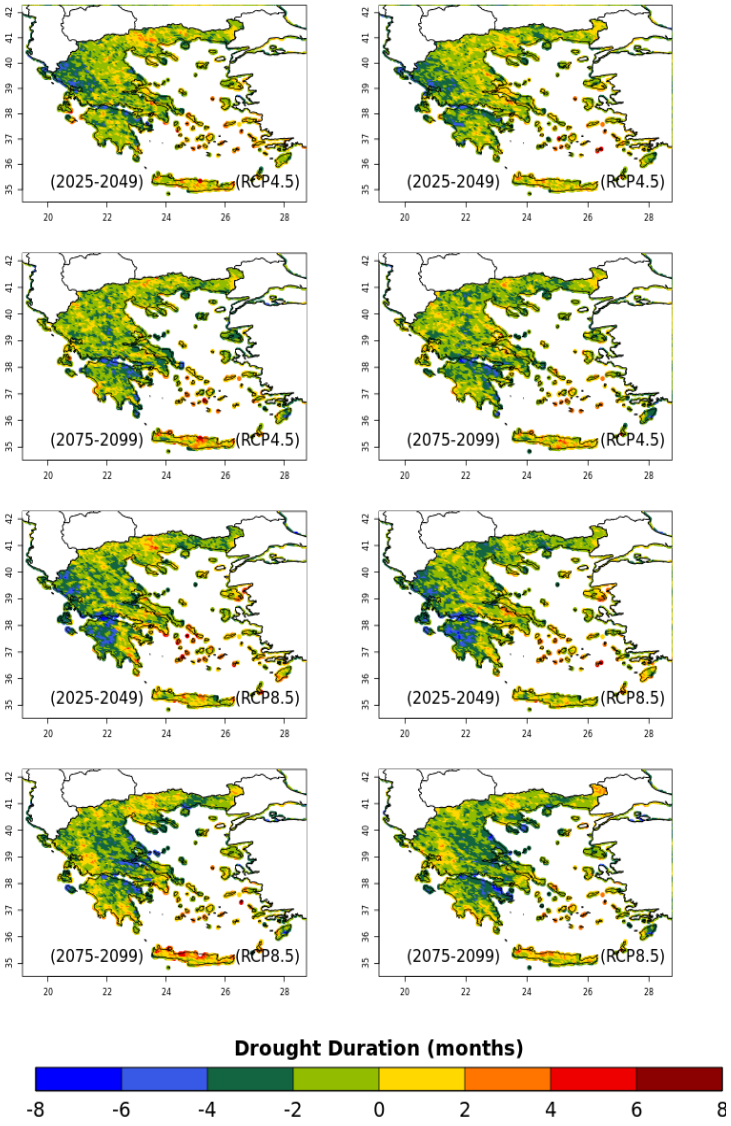

b)

Figure 7.11 a) Drought duration as the number of events in 25 years for the reference period (1980–2004) for the SPI and the SPEI indices computed at 12-months timescale. b) Changes in the duration for the 12-months SPI and SPEI for the near future period (2025–2049) and the far future (2075-2099) relative to the reference period (1980–2004) under RCP4.5 and RCP8.5

In what concerns the increase in drought duration (e.g. Figure. 7.11a) and severity (e.g. Figures 7.12a) for the historical period for the region of Thessaly, our results are in agreement with the findings of Loukas and Vasiliades (2004). Furthermore, our findings agree with the historical drought investigation of Livada and Assimakopoulos (2007) indicating severe droughts slightly increasing from north to south and from west to east (e.g. Figures 7.4a and 7.10a).

In general, the overall area projected to be impacted by more severe drought events in the future is much larger according to SPI than the SPEI as depicted in Figure 7.12b. However, in some locations, the opposite signal in severity is detected between the two indices (e.g. central Macedonia, Attica) in the near future, particularly under RCP8.5. This finding concerning Attica and SPI is consistent with the results of (Karozis et al. 2021) that indicated a reduction of air mass origin up to 45% originating from the cyclogenesis region of the central Mediterranean and the Adriatic Sea. Over the island of Crete and the northern and eastern parts of the country, the drought severity is projected to increase under both RCPs and future periods, but more prominent increases are found with the SPI index. Moreover, both indices indicate more notable increases in drought severity in the south-western parts of the country in the far future, under RCP8.5.

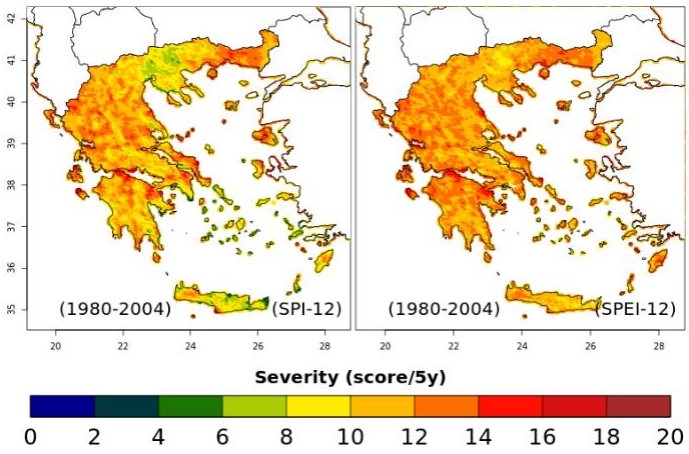

a)

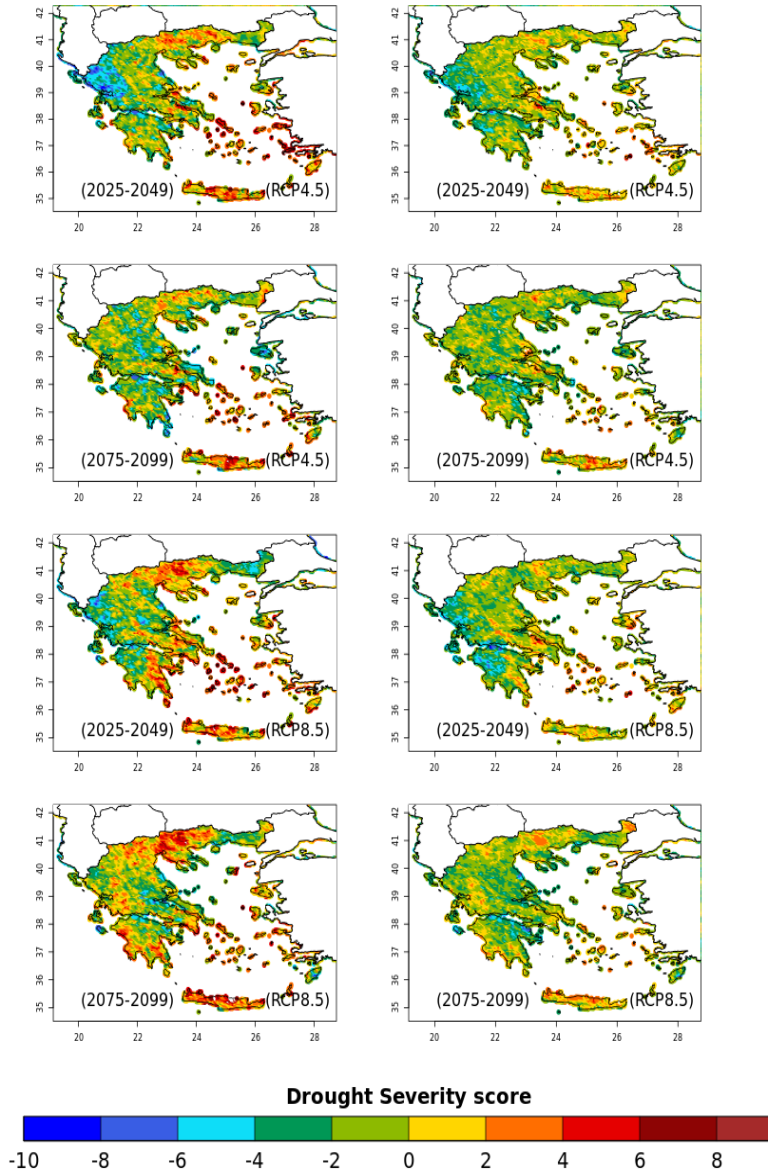

b)

Figure 7.12 a) Drought severity as the number of events in 25 years for the reference period (1980–2004) for the SPI and the SPEI indices computed at 12-month timescale. b) Changes in the duration for the 12-months SPI and SPEI for the near future period (2025–2049) and the far future (2075-2099) relative to the reference period (1980–2004) under RCP4.5 and RCP8.5

The climate change signal of reduced drought conditions in several western parts of the country and over some locations in the central and northern mainland (e.g. Thrace) is associated with the increased precipitation as derived in the study of (Politi et al. 2022), during both periods under RCP4.5 and in the near future under RCP8.5. Additionally, in these areas, the increase in precipitation is strong enough to outweigh the effect of increasing temperature (and, thus, the evapotranspiration), explaining why the drought

variables decrease according to SPI. Those areas will be characterized by a hot and wet future, potentially being exposed to even more weather precipitation extremes (Spinoni et al. 2020).

Regarding drought intensity under RCP4.5, there is a clear climate change signal for more intense drought events derived from SPI in the areas of central and eastern Macedonia, northern Evia, some locations in central Greece and the Aegean islands and Crete, in both future periods (Figure 7.13). High intensity of drought events under RCP8.5 will additionally impact several locations of western Greece and Peloponnese in the far future. However, using the SPEI index, the climate signal of drought intensity becomes overall significantly weaker, locally more limited, which yields future droughts of reduced intensity under both RCPs.

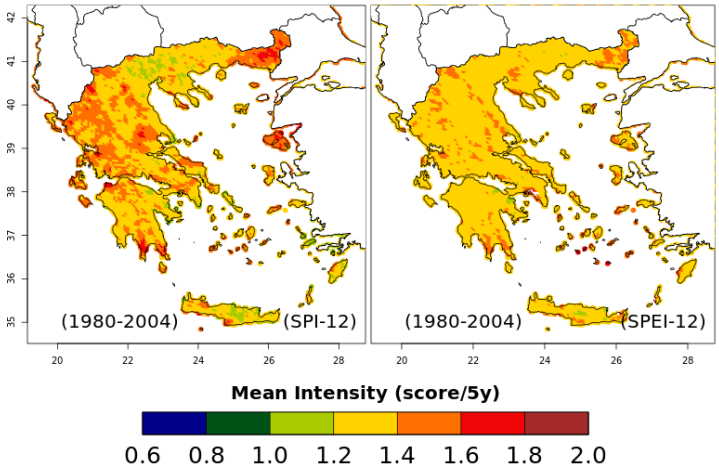

a)

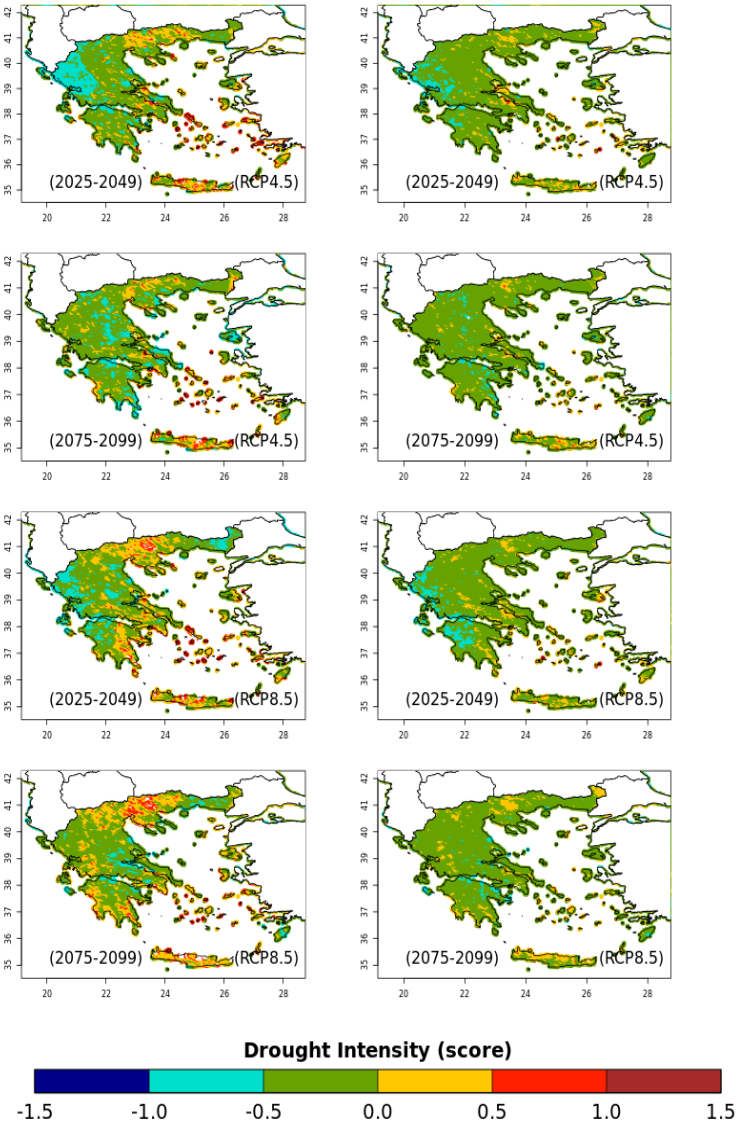

b)

Figure 7.13 a) Drought intensity as the number of events in 25 years for the reference period (1980–2004) for the SPI and the SPEI indices computed at 12-month timescale. b) Changes in the duration for the 12-months SPI and SPEI for the near future period (2025–2049) and the far future (2075-2099) relative to the reference period (1980–2004) under RCP4.5 and RCP8.5

Similar patterns are observed regarding the spatial trends of corresponding drought characteristics derived from the 12-months SPI and SPEI, as presented in figures 7.14 and 7.15 respectively, however, the results obtained with SPI show higher positive trends. Regarding the far future, the two scenarios show different tendencies of projected drought conditions, with larger areas of strong positive trends under RCP8.5. In particular, the projections with both indices reveal longer and more intense and

severe drought events under RCP8.5. However, the results indicate, with spatially limited statistical significance, an amplified signal for Crete with less intense and severe droughts of shorter duration, in the near future and under RCP8.5.

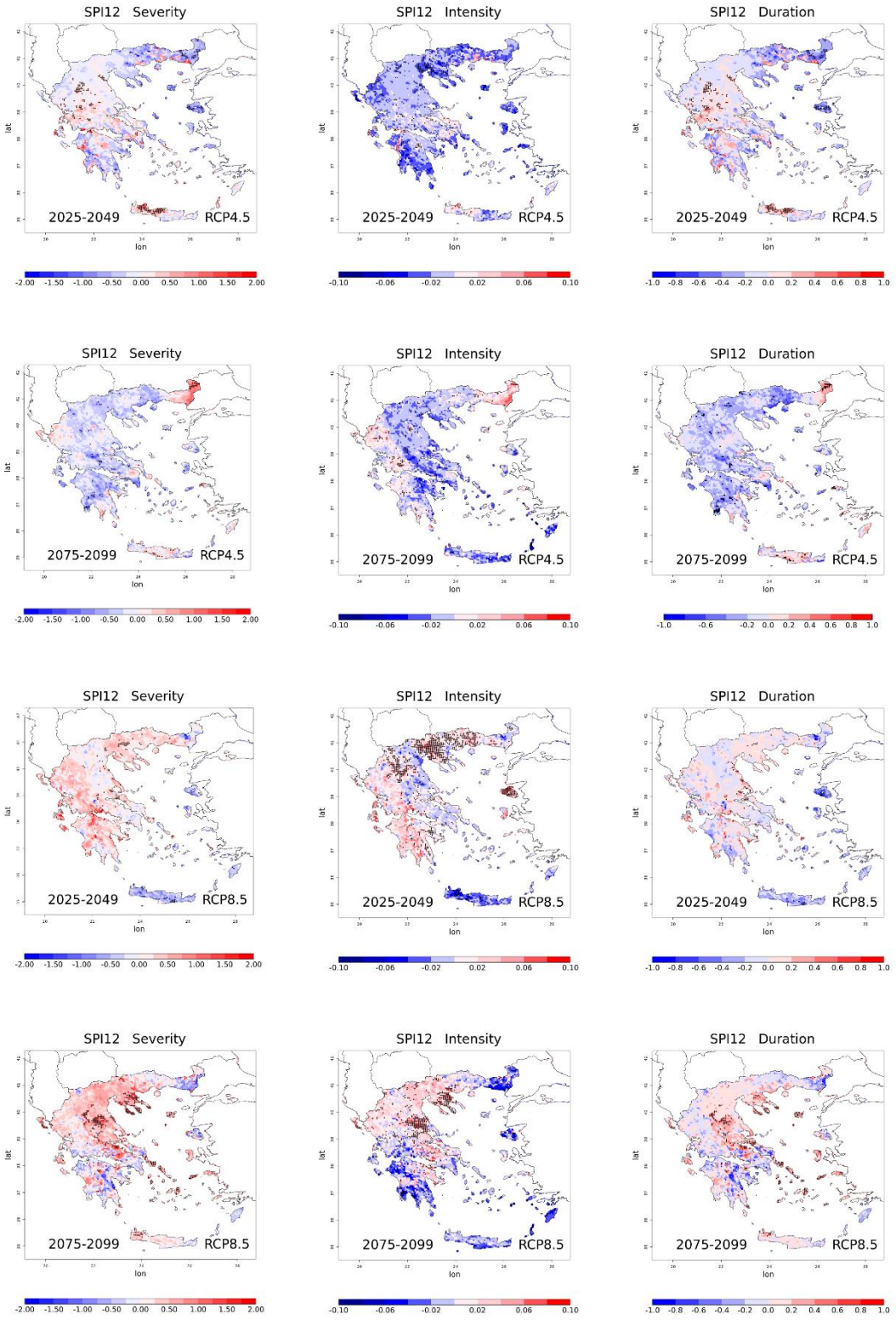

Figure 7.14 Trends of Severity, Intensity and Duration for the 12-months SPI under RCP4.5 and RCP8.5 for the period 2025-2049 and 2075-2099 over the area of Greece. The black dotted areas show significant changes in the drought characteristics at the 5% significance level.

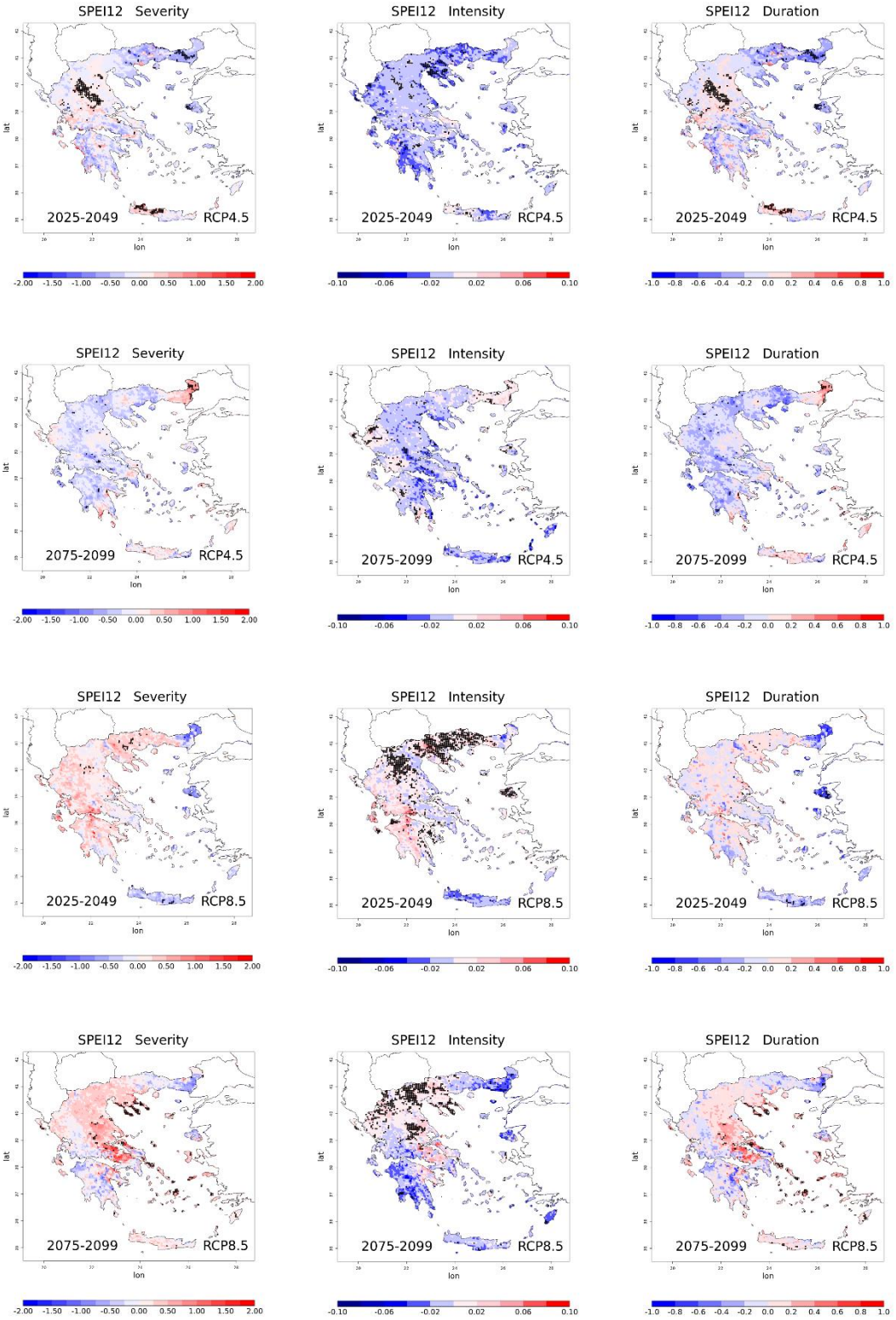

Figure 7.15 Trends (per year) of Severity, Intensity and Duration for the 12-months SPEI under RCP4.5 and RCP8.5 for the period 2025-2049 and 2075-2099 over the area of Greece. The black dotted areas show significant changes in the drought characteristics at the 5% significance level.

Under RCP.4.5, projected changes of drought characteristics are milder than those under RCP8.5 for both periods but indicate some notable remarks where some areas are prone to longer and more severe and intense droughts. In the near future and under RCP4.5, statistically significant drought characteristics over western Crete are projected to increase resulting in longer and more intense and severe events. The majority of the country tends to be exposed to more severe and longer drought events, except for Macedonia, Thrace, islands of north-eastern Aegean and some local areas in southern Peloponnese. It should be mentioned that areas in the central mainland with a positive trend of statistical significance in drought duration and severity become more spatially extended with the SPEI index under RCP4.5 in the near future. In addition, under RCP4.5, some areas of western Greece and Thrace are prone to a positive statistically significant trend on projected changes in drought intensity in the far future.

On the other hand, a profound positive statistically significant trend in changes in drought intensity is found using both indices mainly over the areas of Macedonia and Lesvos in the near future, under RCP8.5. Also, in the far future and under RCP8.5, a positive statistically significant trend in drought intensity is obtained with both indices for some areas of central Macedonia and Thessaly. Moreover, a noteworthy positive trend of statistical significance in severity and duration is revealed with SPI only in large parts of Thessaly. In general, drought conditions are related to the local climate conditions which are characterized by low precipitation with high variability. According to the two indices, RCP8.5 drought characteristics, as illustrated in Figure 7.16, present a stronger positive 5-years trend than those obtained under RCP4.5, similarly as in the study of 6-months indices.

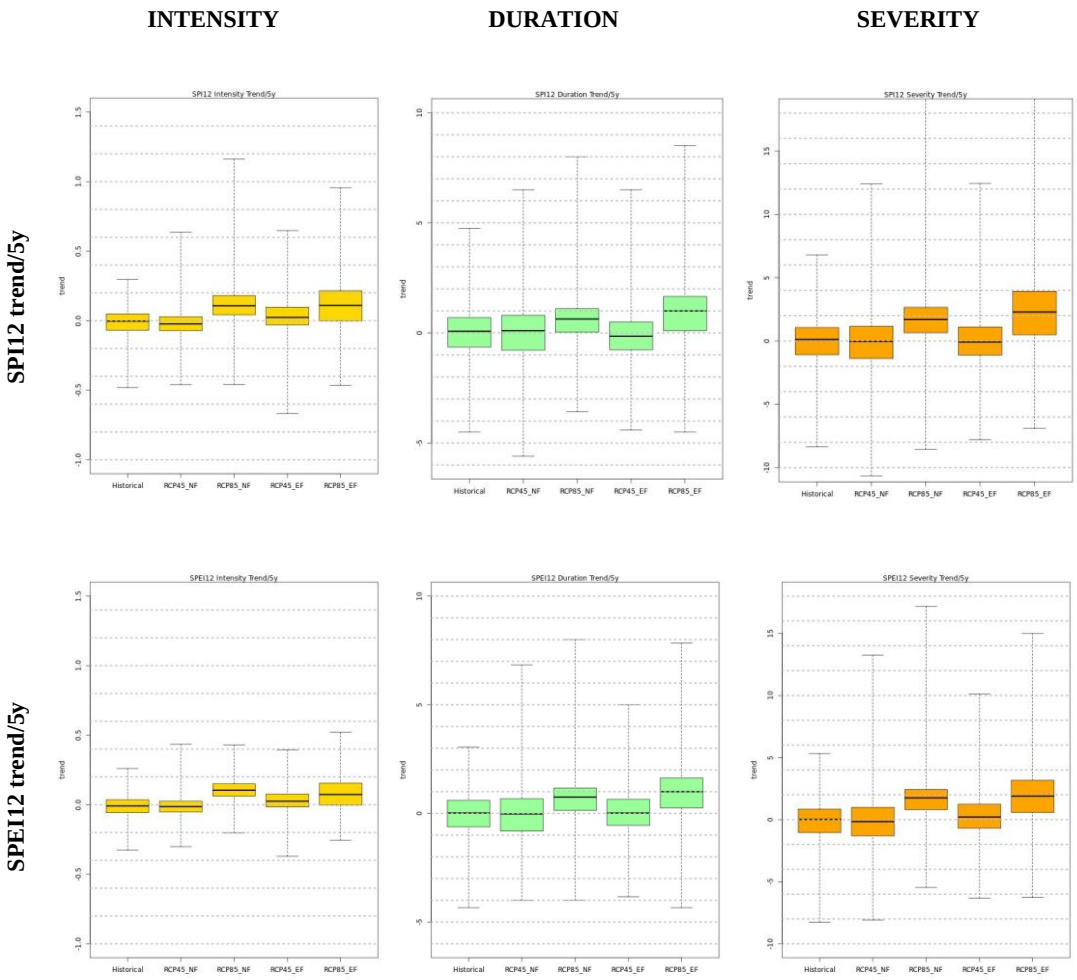

Figure 7.16 5-years mean trends of drought severity, intensity and duration averaged over land area, for the 12-months SPI/SPEI under RCP4.5 and RCP8.5 for the period 2025-2049 and 2075-2099 and the reference period (1980-2004).

7.4. Discussion and conclusions

The presented results based on these two drought indices showed that Greece will experience an increasingly severe climate with increasing drought severity and duration under moderate (RCP4.5) and extreme (RCP8.5) global emission scenarios in almost all parts of the country.

In general, previous works that indicate an increase in the frequency, duration and severity of drought events, conducted for local areas of Greece under different periods and/or IPCC scenarios, are in agreement with our findings in the context of future projections; Vasiliades et al. (2009) for Karla Lake in Thessaly, Zerefos et al. (2011) for the eastern part of the mainland (from Thrace down to the Peloponnese), Nastos et

al. (2013) for eastern Greece and northern Aegean Islands, Vrochidou et al. (2013) for Crete, Anagnostopoulou 2017 and Paparrizos et al. 2018 for Ardas and Sperchios river basins in north-eastern and central Greece. Similar reports are included on the critical review of water resources in Greece by Kourgialas (2021). More recently, Georgoulias et al. 2022 found that the number of consecutive dry days in a year will increase by 15.4 days (30%) at the end of the century for central-southern Aegean Sea and continental areas around based on an ensemble of EURO-CORDEX regional climate simulations. Kairis et al. 2022 indicated that desertification risk in the future is expected to increase in a study of future land degradation for Thessaly, using the RCA4 / MPI-ESM-LR models from EURO-CORDEX. The study of Spinoni et al. 2018, based on an ensemble of 11 bias-adjusted simulations from the EURO-CORDEX datasets using a composite index (combination of SPI, SPEI, and RDI), showed that an increasing drought trend is projected to continue and grow stronger until the end of the 21st century over southern Europe for both scenarios investigated (RCP4.5 and 8.5). In general, a composite drought index takes into account multiple drought characteristics which have been successfully applied for drought detection (Ziese et al., 2014), monitoring (Sepulcre-Cantò et al., 2012; Cammalleri et al., 2017), and prediction (Hao et al., 2016).

The positive trends observed in drought intensity, severity and duration on 12 months' timescale analysis, are also consistent with the tendency (higher probability of occurrence) of increased long-range southerly flows (40%) under RCP4.5 and hence more heatwaves, that can result in drier conditions in the future, as reported by Karozis et al. 2021 in a study of a comparative assessment of backward trajectories in the near future and both RCPs. It also observed that the drought tendencies of the two indices revealed for some areas contradicting values. The interpretation of these cases (not only for 6-months indices but 12-months as well) is more complicated since it must be considered the climate change signal of precipitation (SPI) and temperature (SPEI) and consequently evapotranspiration or both variables in these areas. In some cases, drought characteristics increase with increasing temperature and/or decreasing precipitation, while in other parts of Greece they may remain the same or even decrease. Each region or river basin may have its own unique response to climate change. Consequently, the sensitivity to continued climate warming becomes very region-specific.

Furthermore, the results derived by both indices enhance the importance of using their combination for studying drought projections since by excluding temperature could

lead to an incomplete interpretation of the situation. Projections of drought events using SPI show more moderate/robust changes or trends than those from the SPEI or the opposite, according to the area, topography, etc. This is because an index based solely on precipitation cannot explain the full magnitude or spatial extent of drying reflected by the SPEI (Cook et al. 2016). In fact, (Ault et al. 2016) has pointed out that as the temperature increases in the future, the evapotranspiration increases also (because of the greater moisture demand by the atmosphere) which is possible to result in even more profound impact than precipitation deficits in a warmer world. Hence, the use of SPEI is imperative in the investigation of climate change impacts on drought. On the other hand, droughts can also be caused by changes in rainfall characteristics in terms of seasonality, dry spells and precipitation intensity. That causes of drying depend on the season and are probably linked to the dominant seasonal precipitation formation mechanisms in winter (synoptic processes, NAO anomalies) and summer (local phenomena due to convection), as suggested by Brogli et al. (2019). Thus, it would also be of great importance to investigate with regard to observed climate change, in general, the possibility of positive trends particularly occurring in case of wet periods in areas prone to drought.

The impact of global warming and reduced precipitation on the country will become more evident in the far future, as the extreme maximum temperature will become the most significant hazard, particularly under RCP8.5 (Vlachogiannis et al. 2022). This fact can lead to a remarkable increase in evaporative demand resulting in a shift toward more arid climates. In this context and considering that the projected climate change is likely to result in more frequent and severe weather-related extremes (Ali et al. 2022), it is of the highest importance to investigate over which areas meteorological or agricultural droughts are likely to become more frequent, more intense and/or severe.

The present study indicated that Greece will face relatively severe drought conditions in the upcoming years. Moreover, our findings are comparable with those in other studies conducted for the Mediterranean region (García-Valdecasas Ojeda et al. 2017; Guerreiro et al. 2018; Spinoni et al. 2018). Overall, our results point towards a warmer and drier future, particularly under RCP8.5 in agreement with the latest IPCC report on the Mediterranean region by Ali et al. 2022. It is also observed that both SPI and SPEI followed similar patterns in what concerns the spatial distribution of drought severity, intensity, and duration. This fact declares an agreement at local level in spatiotemporal

resolution; however, a weaker signal is found in the case of SPEI that in some cases minimizes the effect of drought characteristics, particularly at the 12-months timescale.

The results of this study could be used for estimating the impacts of future drought events, and consequently, for the development of adequate mitigation and adaptation strategies for water management under climate change in Greece. In addition, the importance of these results lies in the calculation of two drought indices to estimate the projected changes on drought characteristics in high resolution that takes into consideration the complex topography of Greece, and how the results can differentiate based on the parameter that is probably most dominant in future change between temperature (potential evapotranspiration) and precipitation in the future. However, the complex topography of the domain or parts of it may imply the requirement of further impact drought assessment studies by downscaling the climate data to even higher than a 5 km resolution. It was found that the drought conditions will be more severe in the lowland areas (plain areas), such as Thessaly, Crete, etc. where all the agricultural activity takes place. Sordo-Ward et al. (2017) who studied past and future SPEI droughts in the La Plata Basin suggested the need for a potential relocation of certain crops from the exposed vulnerable regions towards cooler and wetter regions. This conclusion is reinforced by the increased statistical significance calculated in those areas. The results also point out that special attention needs to be given to avoid water scarcity problems that will have a great impact on the local population and agricultural activities.

Summarising, the investigation of drought characteristics focused on projected changes in temperature and precipitation in Greece, which can provide a comprehensive attribution of drought events. It is deduced that the study of drought events is not a straightforward task for areas of complex topography that present climatic variations and the corresponding spatial and temporal characteristics may depend on the choice of the index. Some limitations are related to the fact only one GCM and RCM have been used in this study and no bias correction was applied to improve the climate projections regarding the examined variables, given the lack of consistent gridded observational datasets required for such regions of complex topography and climate variation. In general, the future changes in drought characteristics are expected to have a significant impact on the country's ecosystems, as well as on a number of human activity sectors (e.g. health, agriculture, tourism, forest fire risk, loss of biodiversity, etc.). In any case,

the produced high resolution projected changes of the present study can serve as a firm and reliable basis for climate change impact assessments based on drought characteristics for the area of Greece.

Key Remarks

- ***Both SPI and SPEI followed similar patterns in what concerns the spatial distribution of drought severity, intensity, and duration.***
- ***12-months SPI and SPEI for the period 2075- 2099 and under RCP8.5 have shown a profound increase in the mean duration of drought events along with increased severity for the areas of Crete, central Aegean islands (Cyclades), southern Peloponnese, western continental Greece, Attica, central Macedonia and Thrace.***
- ***A positive statistically significant trend in drought intensity is also observed with both indices for some areas of central Macedonia and Thessaly***
- ***Drought events with the 12-months analysis are projected to be more frequent locally in the central to northern parts of the country, under RCP4.5 than RCP8.5, in both future periods.***
- ***6-months SPI and SPEI yield that a more extended area is affected by drought conditions and more severe and prolonged drought events are expected under both scenarios (particularly, in areas of central and eastern part of the country in the near future, and areas of the western parts in the far future).***
- ***Central and eastern mainland will experience a notable reduction in the signal of drought duration along with decreased frequency of drought events in the far future under RCP8.5.***
- ***Thessaly, a region of high agricultural interest, will experience more frequent and longer drought events in the near future under RCP4.5.***
- ***Crete (and mainly the eastern part) is projected to experience increasingly more prolonged and severe drought events under both scenarios and periods.***
- ***Reduced frequency of drought events is projected over the highly populated region of Attica, except for the near-future SPEI projections under RCP8.5***
- ***RCP8.5 drought characteristics with both indices present a stronger positive trend than those obtained under RCP4.5***

Chapter 8 Conclusions

8.1 Key Findings

The motivation for this work lay in the necessity of gathering reliable climate future information on the primary climate variables associated with the phenomenon of drought, such as maximum and minimum temperatures and precipitation to calculate and evaluate future drought characteristics for Greece. Accordingly, this research included WRF simulations duly performed to analyze the projections of drought characteristics due to climate change using two drought indices over the whole country of Greece with a spatial resolution of 5 km, which to the best of our knowledge is the highest used so far (higher-resolution data are available only for very few basins). The The model simulations were carried out with the dynamical downscaling technique for the area of interest under RCP4.5 and RCP8.5. Consequently, the state-of the art extended high-resolution climate datasets derived for the region to 5 km for this area are unique so far. In particular, the 5km horizontal resolution allowed better understanding of subscales phenomena and how climate change can affect them. In addition, the application of this high-resolution dynamical downscaling methodology could be applied in areas characterized by complex topography as dynamical downscaling provides added value in such cases.

The suitability of the WRF model, to simulate the climate characteristics of the study area, required initially the appropriate configuration of the model through sensitivity tests. For this purpose, at first a set of seven different combinations of physics schemes were compared with observational datasets for one year in terms of extreme temperatures and precipitation to derive the four best performing set ups. Using these set ups, more sensitivity tests were applied to 5-year periods to obtain the most effective set of parameterization schemes. In addition, the model sensitivity to reinitialisation was investigated following three different types of time integration approaches to conclude the optimal model configuration. This procedure requested the evaluation of the downscaled results and ERA-I reanalysis datasets with the historical observations from the HNMS network based on statistical metrics. The procedure and the selection of the optimal setup were analysed in Chapter 3.

Following the optimal model configuration, WRF simulations were performed for the climatological period of 25 years (1980-2004) owing to observational data availability. The model performance at 5 km spatial resolution (WRF_5) was evaluated with statistical tools using observational data from the HNMS network. In addition, the coarse resolution ERA_I data were compared with observations. The research work resulted in the proof of the added value of the high-resolution downscaling (5 km) methodology using the reanalysis fields of ERA-Interim and secondly validated high resolution historical climatological downscaled datasets driven by the EC-EARTH global model from 1980 to 2004. The main findings were reported in Chapter 4.

This work aimed also to provide projected climatological datasets for impact models that require high spatial details. To that end, downscaled fields with WRF driven by the GCMEC model for two different future emission scenarios (RCP4.5 and RCP8.5) and two 25-year future time slices (2025–2049 and 2075–2099) were obtained. This was regarded as a great achievement and it involved a detailed assessment of future changes in minimum and maximum temperatures and precipitation for Greece, along with the spatial and temporal change of climate indices based on ETTCDI. The high spatial detail of climatological variables in Greece pointed out distinct and vulnerable areas prone to climate change, as described in Chapters 5 and 6 and highlighted in the final remarks of those chapters.

In the Chapter 7, projected spatial and temporal changes of drought characteristics (severity, duration, and intensity of drought events) were thoroughly investigated using two drought indices, the Standardized Precipitation Index (SPI) and the Standardized Precipitation Evapotranspiration Index (SPEI) in different timescales (6 and 12 months). The high spatial resolution identified in high detail the areas that will face less or more drought in the future. Overall, our results pointed toward a warmer and drier future, particularly under RCP8.5. It was also shown that both SPI and SPEI followed similar patterns in what concerns the spatial distribution of drought severity, intensity, and duration. That fact declared an agreement at a local level in spatiotemporal resolution; however, a weaker signal was found in the case of SPEI that in some cases minimized the effect of drought characteristics, particularly at the 12-month timescale. The projected higher frequency and longer duration meant the stabilization in drier conditions. In this context, the 12-month indices represented more suitably the prolonged duration of drought events. Moreover, owing to the high spatial resolution

used, substantial differences in drought characteristics were found in future projections between areas, highly varying in temporal and spatial terms under the two emission scenarios.

8.2 Future recommendations

Future work could consider trend analysis and calculation of return periods following differentiation between wet and dry seasons, the analysis of moisture transport impacting selected regions during extreme conditions, or studies based on analysis of other factors influenced by drought, such as the characteristics of soils, hydrology, production of different types of crops, etc. Also, further research could include drought impacts using other drought indices or hydrological parameters and soil parameters in the most affected areas of agricultural or tourism interest (e.g., Thessaly, Crete, Islands) as already identified in our study, to investigate extensively water resource availability for agricultural production and fire risk assessment. In the context of climate change studies and services, future work could consider applications of the WRF model datasets to other economic sectors such as tourism, energy etc. In addition, since the dynamical downscaling technique with the WRF model is a valuable tool to study future climatology in high spatial resolution, especially in areas with complex topography, its application should be included in research works using CMIP6 data and new SSPs scenarios, which has been the focus of interest in the research community nowadays. The SSPs are based on five narratives describing broad socioeconomic trends that could shape future society. Thus, these scenarios look at five different ways in which the world might evolve in the absence of climate policy and how different levels of climate change mitigation could be achieved when the mitigation targets of RCPs are combined with the SSPs.

It must be mentioned that at this stage, only one GCM and RCM have been used, limiting the quantification of the uncertainty of the results. Also, bias correction was not applied to improve the climate projections regarding the examined variables, given the lack of consistent gridded observational datasets required for such regions of complex topography and climate variation. In summary, uncertainties still exist in projecting future climate changes in Greece—a region with a complex topography and unique weather and climate systems, thus, the importance of in-depth analyses of model

simulations and large ensembles of high resolution should be emphasized. A natural follow-up would also be to investigate the use of an ensemble of different bias corrected methods results with observational data to quantify the uncertainty of the dynamical downscaling results in the past and future periods for climate indices and particularly for specific areas which are projected to be more affected by extreme events in the future.

Finally, as extreme weather becomes increasingly frequent and changes in the climate more pronounced, the finer spatial resolution of such gridded products could contribute to enhancing the potential of digital modelling of the Earth systems to provide better capabilities for the assessment and prediction of environmental extremes in support of risk assessment and management. Through richer observation datasets and increased simulation capabilities, humanity will be better prepared to respond to major natural disasters, adapt to climate change and predict with higher confidence the socioeconomic impacts.

Publications

Peer reviewed papers in Scientific Journals

Politi, N.; Nastos, P.T.; Sfetsos, A.; Vlachogiannis, D.; Dalezios, N.R. Evaluation of the AWR-WRF Model Configuration at High Resolution over the Domain of Greece. *Atmos Res* **2018**, doi:10.1016/J.ATMOSRES.2017.10.019.

Politi, N.; Sfetsos, A.; Vlachogiannis, D.; Nastos, P.T.; Karozis, S. A Sensitivity Study of High-Resolution Climate Simulations for Greece. *Climate* **2020**, *8*, 1–28, doi:10.3390/cli8030044.

Politi, N.; Vlachogiannis, D.; Sfetsos, A.; Nastos, P.T. High-Resolution Dynamical Downscaling of ERA-Interim Temperature and Precipitation Using WRF Model for Greece. Climate Dynamics 2021 *57:3* **2021**, *57*, 799–825, doi:10.1007/S00382-021-05741-9.

Politi, Nadia, · D Vlachogiannis, · A Sfetsos, and · P T Nastos. 2022. "High Resolution Projections for Extreme Temperatures and Precipitation over Greece." Climate Dynamics **2022**, 1–35. https://doi.org/10.1007/S00382-022-06590-W.

Politi, N.; Vlachogiannis, D.; Sfetsos, A.; Nastos, P.T.; Dalezios, N.R. High Resolution Future Projections of Drought Characteristics in Greece Based on SPI and SPEI Indices. *Atmosphere (Basel)* **2022**, *13*, doi:10.3390/atmos13091468.

Presentations in scientific Conferences and peer reviewed papers in Conferences proceedings

Politi, N.; Nastos, P.T.; Sfetsos, A.; Vlachogiannis, D.; Dalezios, N.R.; Gounaris, N.; Cardoso, M.R.; Soares, M.M.P.; Sfetsos, Á.A.; Vlachogiannis, Á.D.; et al. Comparison and Validation of WRF Model Physics Parameterizations Over the Domain of Greece. In Proceedings of the Perspectives on Atmospheric Sciences; Springer, Cham, 2017; pp. 55–61.

N Politi, D Vlachogiannis A Sfetsos, and P T Nastos, Investigation of SPI and SPEI trends for wet and dry periods under climate change in Greece, Morocco, MEDCLIVAR CONF, 4-8 October 2022

Politi N., Markantonis I., Karozis S, Sfetsos A, Nastos P. and Vlachogiannis D., 26-29 September 2021, Validation of WRF high resolution climatic simulation of temperatures over Greece, Ioannina, 15th International Conference on Meteorology, Climatology and Atmospheric Physics, COMECAP 2021

Nadia Politi, Athanasios Sfetsos, Diamando Vlachogiannis and Panagiotis Nastos, Sensitivity of WRF model initialization for regional climate dynamical downscaling in the domain of Greece, October 15-17, Alexandroupolis, 14th International Conference on Meteorology, Climatology and Atmospheric Physics, COMECAP 2018

A. Sfetsos, N. Politi, N. Gounaris, S. N Karozis, D. Vlachogiannis, "Investigation of the AWR-WRF model configuration at high resolution over the domain of Greece", Zagreb, Croatia, 6th International Conference on Meteorology and Climatology of the Mediterranean & Challenges in Meteorology 5 (MetMed), February 20 - 22, 2017

Politi N., Nastos P. T., Sfetsos A., Vlachogiannis D., Dalezios N. R., Gounaris N., Kapsomenakis J. "Evaluation of high-resolution dynamical downscaling over Greece", Athens, Greece, MEDCLIVAR CONF, 26-30 September 2016.

Nadia Politi, Panagiotis T. Nastos, Athanasios Sfetsos, Diamando Vlachogiannis, Nikolaos Gounaris, Pedro M.M. Soares and Rita M. Cardoso, "Comparison and validation of WRF Model Physics parameterizations over the Domain of Greece", Thessaloniki, 13th International Conference on Meteorology, Climatology and Atmospheric Physics, COMECAP 2016.

Exploitation of key PhD outcomes and data products

Politi, Nadia, Diamando Vlachogiannis, Athanasios Sfetsos, Nikolaos Gounaris, and Vassiliki Varela. 2023. "Investigation of Fire Weather Danger under a Changing Climate at High Resolution in Greece" Sustainability 15, no. 3: 2498. https://doi.org/10.3390/su15032498

Vlachogiannis, D.; Sfetsos, A.; Markantonis, I.; Politi, N.; Karozis, S.; Gounaris, N. Quantifying the Occurrence of Multi-Hazards Due to Climate Change. *Applied Sciences* **2022**, *3*, doi:10.3390/app12031218.

Katopodis, T.; Markantonis, I.; Vlachogiannis, D.; Politi, N.; Sfetsos, A. Assessing Climate Change Impacts on Wind Characteristics in Greece through High Resolution Regional Climate Modelling. Renew Energy 2021, 179, 427–444, doi:https://doi.org/10.1016/j.renene.2021.07.061.

Katopodis, T., Markantonis, I., Politi, N., Vlachogiannis, D., & Sfetsos, A. (2020). High-resolution solar climate atlas for greece under climate change using the weather research and forecasting (WRF) model. Atmosphere, 11(7). https://doi.org/10.3390/ATMOS11070761

APPENDIX

A.1 Statistical metrics

The following standard errors statistics, with formulae described in Table A.1 (where "o" is the value of the observational data, "f" is the simulated data) were estimated: the BIAS, the root mean square error (RMSE) that gives an overview of the accuracy of simulations, the mean absolute error (MAE), a measure of the absolute values of the model errors, the Pearson's correlation coefficient (COR), the modified Index of Agreement (MIA), developed by (Willmott 1981; Legates and McCabe Jr. 1999) as a standardized measure of the degree of model prediction error, and finally the Nash–Sutcliffe efficiency (Nash and Sutcliffe 1970), NSE, which is a normalized skill score that determines an overall performance and can vary between 1 for perfect agreement and $-\infty$ for complete disagreement. While the NSE has traditionally been used in hydrological applications, it can also be applied to any type of model data with paired observations of the same quantities (Lee et al. 2018). According to Bieniek et al. (2016), station and reanalysis data contain their uncertainties; however, the term BIAS is used only to denote the differences between the WRF model output and observational data and not to imply that the differences are errors entirely born in the model results. The model error was calculated as the difference between the modeled and observed values. The total error was then found by pooling together all the points of meteorological stations and not by averaging.

The statistical indices used in the present study are given in the table below:

Table A.1 Summary of statistical formulas calculated for model evaluation in this study:

Parameter	Formula	Range	Ideal value
Mean Bias Error	$BIAS = \frac{1}{N}\sum_{i=0}^{n}(f_i - o_i) = \bar{f} - \bar{o}$	$(-\infty,\infty)$	0
Root Mean Square Error	$RMSE = \sqrt{\frac{\sum_{i=0}^{n}(f-o)^2}{N}}$	$(0,\infty)$	0
Mean Absolute Error	$MAE = \frac{1}{N}\sum_{i=0}^{n}\lvert f_i - o_i\rvert$	$(0,\infty)$	0

Pearson Correlation Coefficient	$COR = \frac{\sum_{i=1}^{n}(f_i - \bar{f})(o_i - \bar{o})}{\sqrt{\sum_{i=0}^{n}(f_i - \bar{f})^2}\sqrt{\sum_{i=0}^{n}(o_i - \bar{o})^2}}$	(-1,1)	1
Modified Index of Agreement	$MIA = 1 - \frac{\sum_{i=1}^{n}\lvert(o_i - f_i)\rvert}{\sum_{i=1}^{n}\lvert(f_i - \bar{o})\rvert + \sum_{i=1}^{n}\lvert(o_i - \bar{o})\rvert}$	(0,1)	1
Nash-Sutcliffe efficiency	$NSE = 1 - \frac{\sum_{i=1}^{n}(o_i - f_i)^2}{\sum_{i=1}^{n}(o_i - \bar{o})^2}$	(-Inf,1)	1

A.2 Taylor diagrams

Taylor diagrams are used in addition to provide a comprehensive statistical and graphical verification of how well observed and simulated patterns match each other in terms of their correlation and normalized standard deviation (Taylor 2001). Taylor diagrams were computed through R scripts with "plotrix" package.

A.3 Contingency tables

Categorical (CAT) verification statistics measure the agreement between the estimated and observed occurrence of P events. The capability of the model to distinguish dichotomous (yes/no) P events.

In the case of sensitivity test 2, the accuracy of the simulated precipitation was determined by statistical scores of a contingency table (Table A.2): probability of detection (POD), critical success index (CSI) and false alarm ratio (FAR). In this study for four distinct threshold values of precipitation was used for low rainfall (>1mm), medium rainfall (>2.5 mm), heavy rainfall (>10 mm) and extremely heavy rainfall days (>20 mm) to evaluate small and large rainfall events, for the location of each station separately.

Table A.2 Contingency table and statistics. The counts a, b, c and d are the total number of hits, false alarms, misses and correct rejections.

	Event observed		**POD**	**FAR**	**CSI**
Event forecast	YES	NO	**(Perfect score: 1)**	**(Perfect score: 0)**	**(Perfect score: 1)**

YES	a	b	a/(a+c)	b/(a+b)	a/(a+b+c)
NO	c	d			

For sensitivity test 3, the accuracy of the simulated precipitation was also determined by the previous measures based on contingency tables, described on Table A.3, for 3 thresholds (0.1mm, 1mm, and 10mm), calculated for each station separately.

Table A.3 Contingency table and statistics.

	Event observed		POD	SR	Bias	CSI
Event forecast	YES	NO				
YES	a	b	a/(a+c)	1-(b(a+b))	(a+b)/(a+c)	a/(a+b+c)
NO	c	d				

A.4 Stations HNMS

Precipitation's stations provided by HNMS

ID	NAME	ELEVATION	LON	LAT
16606	Serres	32	23.567	41.083
16609	Xanthi	43	24.88	41.13
16611	Soufli_Palios	15	26.3	41.0794
16613	Florina	695	21.43	40.79
16614	Kastoria-Airport	660.95	21.28	40.45
16619	Trikala_Imatheias	1	22.55	40.6
16622	Thessaloniki/Mikra	2	22.967	40.517
16627	Alexandroupolis	4	25.917	40.85
16628	Konitsa	530	20.74462	40.04807
16641	Kerkyra	1	19.912	39.603
16642	Ioannina	483	20.817	39.7
16643	Aktio	3	20.7613	38.9214
16645	Trikala_Thessalias	163	21.76247	39.55857
16648	Larisa	73	22.417	39.65
16650	Limnos	4	25.2333	39.9167
16655	Astros	25	22.72	37.4
16657	Domokos	570	22.3002	39.12756
16662	Skopelos_Palios	11	23.7333	39.1167
16665	Aghialos	15.3	22.78	39.22
16667	Mytilini	4	26.596	39.059
16672	Agrinio	72	21.39458	38.6241

16673	Nafpaktos	15	21.83	38.38
16674	Aliartos	110	23.1	38.38
16675	Lamia	107	22.44613	38.90364
16681	Edipsos	2	23.04	38.86
16682	Andravida	14	21.2833	37.9167
16685	Argostoli	25	20.503	38.118
16687	Araxos	15	21.42	38.15
16688	Diabolitsi	108	21.95	37.2833
16689	Patra	1	21.7375	38.25556
16692	Aigio	64	22.06889	38.25
16693	Desfina	585	22.52981	38.42082
16699	Tanagra	138	23.533	38.339
16701	Nea_Filadelfia	136	23.73	38.05
16706	Chios	23	26.13172	38.35341
16707	Pyrgos	12	21.42667	37.67667
16710	Tripoli	651	22.401	37.527
16711	Stephani(Korinthia)	960	22.833	37.75
16715	Tatoi	225	23.776	38.11
16716	Elliniko_Airport	10	23.7333	37.8877
16717	Pireus	29	23.63167	37.93556
16718	Elefsis	31	23.55	38.07
16723	Samos	10	26.68199	37.79368
16724	Argos	38	22.71355	37.62824
16725	Sparti	204	22.43638	37.05306
16726	Kalamata	6	22.017	37.067
16732	Naxos	9	25.383	37.1
16734	Methoni	34	21.7	36.8333
16736	Aigina_Palios	7	23.44364	37.74813
16737	Githeio	2.7	22.55	36.75
16738	Milos	183	24.45	36.7167
16743	Kythira	167	23.0167	36.2833
16744	Thira	36	25.433	36.4167
16746	Souda	151	24.1167	35.4833
16747	Chania	7	24.0148	35.51303
16749	Rodos	95	28.21661	36.42896
16752	Anogeia	801	24.88	35.29
16753	Gortis	182	24.93	35.06
16754	Heraklion	39	25.174	35.339
16755	Fourni	316	25.333	35.2667
16756	Ierapetra	5	25.333	35.2667
16757	Siteia	30	26.095	35.205
16758	Rethymno	50	24.48904	35.3612
16759	Timpaki	6.7	24.77	35.07
16760	Kasteli	336	25.33	35.2
16761	Zaros	343	24.9	35.11667

Temperature’s stations

NAME	ELEVATION	LON	LAT
SERRES	32	23.567	41.083
FLORINA	695	21.43	40.79
THESSALONIKI/MIKRA	2	22.967	40.517
ALEXANDROUPOLIS	4	25.917	40.85
KOZANI	621	21.839	40.287
KERKYRA	1	19.912	39.603
IOANNINA	483	20.817	39.7
AKTIO	3	20.7613	38.9214
TRIKALA_THESSALIAS	163	21.76247	39.55857
LARISA	73	22.417	39.65
LIMNOS	4	25.239	39.92
AGHIALOS	15	22.78	39.22
MYTILINI	4	26.596	39.059
AGRINIO	72	21.39458	38.6241
LAMIA	107	22.44613	38.90364
SKYROS	12	24.4872	38.9676
ARGOSTOLI	25	20.503	38.118
ARAXOS	15	21.42	38.15
TANAGRA	138	23.533	38.339
CHIOS	23	26.13172	38.35341
TRIPOLI	651	22.401	37.527
ELLINIKO_AIRPORT	10	23.7333	37.8877
SAMOS	10	26.68199	37.79368
KALAMATA	6	22.017	37.067
NAXOS	9	25.383	37.1
METHONI	34	21.7	36.8333
THIRA	36	25.433	36.4167
SOUDA	151	24.1167	35.4833
RODOS	95	28.21661	36.42896
HERAKLION	39	25.174	35.339
SITEIA	30	26.095	35.205
CHANIA	7	24.0148	35.51303

References

Akbari M, Ownegh M, Asgari H, et al (2016) Drought Monitoring Based on the SPI and RDI Indices under Climate Change Scenarios (Case Study: Semi-Arid Areas of West Golestan Province). https://doi.org/10.18869/modares.Ecopersia.4.4.1585

Ali E, Cramer W, Carnicer J, et al (2022) Cross-Chapter Paper 4: Mediterranean Region. In: Climate Change 2022: Impacts, Adaptation, and Vulnerability. Contribution of Working Group II to the Sixth Assessment Report of the Intergovernmental Panel on Climate Change [H.-O. Pörtner, D.C. Roberts, M. Tignor, E.S. Poloczanska, K. Mintenbeck, A. Alegría, M. Craig, S. Langsdorf, S. Löschke, V. Möller, A. Okem, B. Rama (eds.)]. Cambridge University Press. In Press

Alpanakis Nikolaos, Giannis Faraslis, Nicolas R. Dalezios and Konstantinos Perakis, 2022. Analysis of Drought using the satellite based SPI index for the spatial variability in the semi-arid region of Thessaly. Proceedings, 15 the International Conference of the Hellenic Hydrotechnical Association, AUTH, Thessaloniki,1-3 June 2022 (in Greek).

Anagnostopoulou C (2017) FUTURE DROUGHT PROJECTION FOR THE GREEK REGION. Bulletin of the Geological Society of Greece 50:1038. https://doi.org/10.12681/bgsg.11808

Anagnostopoulou C, Maheras P, Karacostas T, Vafiadis M (2003) Spatial and temporal analysis of dry spells in Greece. Theoretical and Applied Climatology 2002 74:1 74:77–91. https://doi.org/10.1007/S00704-002-0713-5

Argüeso D, Hidalgo-Muñoz JM, Gámiz-Fortis SR, et al (2011) Evaluation of WRF parameterizations for climate studies over southern Spain using a multistep regionalization. J Clim 24:5633–5651. https://doi.org/10.1175/JCLI-D-11-00073.1

Argüeso D, Hidalgo-Muñoz JM, Gámiz-Fortis SR, et al (2012) Evaluation of WRF Mean and Extreme Precipitation over Spain: Present Climate (1970–99). J Clim 25:4883–4897. https://doi.org/10.1175/JCLI-D-11-00276.1

Ault TR, Mankin JS, Cook BI, Smerdon JE (2016) Relative impacts of mitigation, temperature, and precipitation on 21st-century megadrought risk in the American Southwest. Sci Adv 2:. https://doi.org/10.1126/SCIADV.1600873/SUPPL_FILE/1600873_SM.PDF

Barcikowska MJ, Kapnick SB, Feser F (2018) Impact of large-scale circulation changes in the North Atlantic sector on the current and future Mediterranean winter hydroclimate. Clim Dyn 50:2039–2059. https://doi.org/10.1007/s00382-017-3735-5

Barros V (ed) (2014) Climate change 2014: impacts, adaptation, and vulnerability. part b: regional aspects. contribution of working group ii to the fifth assessment. Cambridge University Press

Barstad I, Sorteberg A, Flatøy F, Déqué M (2009) Precipitation, temperature and wind in Norway: dynamical downscaling of ERA40. Clim Dyn 33:769–776. https://doi.org/10.1007/s00382-008-0476-5

Bartók B, Wild M, Folini D, et al (2017) Projected changes in surface solar radiation in CMIP5 global climate models and in EURO-CORDEX regional climate models for Europe. Clim Dyn 49:2665–2683. https://doi.org/10.1007/s00382-016-3471-2

Basharin D, Polonsky A, Stankūnavičius G (2015) Projected precipitation and air temperature over Europe using a performance-based selection method of CMIP5 GCMs. Journal of Water and Climate Change 7:103–113. https://doi.org/10.2166/wcc.2015.081

Beguería S, Vicente-Serrano SM, Reig F, Latorre B (2014) Standardized precipitation evapotranspiration index (SPEI) revisited: parameter fitting, evapotranspiration models, tools, datasets and drought monitoring. International Journal of Climatology 34:3001–3023. https://doi.org/https://doi.org/10.1002/joc.3887

Berg P, Christensen OB, Klehmet K, et al (2019) Summertime precipitation extremes in a EURO-CORDEX 0.11° ensemble at an hourly resolution. Natural Hazards and Earth System Sciences 19:957–971. https://doi.org/10.5194/nhess-19-957-2019

Berg P, Wagner S, Kunstmann H, Schädler G (2013) High resolution regional climate model simulations for Germany: part I—validation. Clim Dyn 40:401–414. https://doi.org/10.1007/s00382-012-1508-8

Berrisford P, Dee D, Fielding K, et al (2009) The ERA-Interim Archive

Bieniek PA, Bhatt US, Walsh JE, et al (2016) Dynamical Downscaling of ERA-Interim Temperature and Precipitation for Alaska. J Appl Meteorol Climatol 55:635–654. https://doi.org/10.1175/JAMC-D-15-0153.1

Boberg F, Berg P, Thejll P, et al (2010) Improved confidence in climate change projections of precipitation further evaluated using daily statistics from ENSEMBLES models. Clim Dyn 35:1509–1520. https://doi.org/10.1007/s00382-009-0683-8

Brogli R, Gauthier S, Keane CJ, et al (2019) Causes of future Mediterranean precipitation decline depend on the season. Environmental Research Letters 14:114017. https://doi.org/10.1088/1748-9326/AB4438

Caldwell P (2010) California Wintertime Precipitation Bias in Regional and Global Climate Models. J Appl Meteorol Climatol 49:2147–2158. https://doi.org/10.1175/2010JAMC2388.1

Cammalleri C, Vogt J, Salamon P. 2017. Development of an operational low-flow index for hydrological drought monitoring over Europe. Hydrol. Sci. J. 62(3): 346– 358.

Cardoso RM, Soares PMM, Lima DCA, Miranda PMA (2019) Mean and extreme temperatures in a warming climate: EURO CORDEX and WRF regional climate high-resolution projections for Portugal. Clim Dyn 52:129–157. https://doi.org/10.1007/s00382-018-4124-4

Cardoso RM, Soares PMM, Miranda PMA, Belo-Pereira M (2013a) WRF high resolution simulation of Iberian mean and extreme precipitation climate. International Journal of Climatology 33:2591–2608. https://doi.org/10.1002/joc.3616

Cardoso RM, Soares PMM, Miranda PMA, Belo-Pereira M (2013b) WRF high resolution simulation of Iberian mean and extreme precipitation climate. International Journal of Climatology 33:2591–2608. https://doi.org/10.1002/joc.3616

Cattiaux J, Douville H, Peings Y (2013) European temperatures in CMIP5: Origins of present-day biases and future uncertainties. Clim Dyn 41:2889–2907. https://doi.org/10.1007/S00382-013-1731-Y/FIGURES/12

Cavan G, Hare PO (2016) (Climate Change Management) Walter Leal Filho Climate Change Adaptation, Resilience and Hazards.pdf. 225–240. https://doi.org/10.1007/978-3-319-39880-8

Cavicchia L, Scoccimarro E, Gualdi S, et al (2018) Mediterranean extreme precipitation: a multi-model assessment. Clim Dyn 51:901–913. https://doi.org/10.1007/s00382-016-3245-x

Chang EKM, Ma C-G, Zheng C, Yau AMW (2016) Observed and projected decrease in Northern Hemisphere extratropical cyclone activity in summer and its impacts on maximum temperature. Geophys Res Lett 43:2200–2208. https://doi.org/https://doi.org/10.1002/2016GL068172

Chen F, Dudhia J, Chen F, Dudhia J (2001) Coupling an Advanced Land Surface–Hydrology Model with the Penn State–NCAR MM5 Modeling System. Part I: Model Implementation and Sensitivity. Mon Weather Rev 129:569–585. https://doi.org/10.1175/1520-0493(2001)129<0569:CAALSH>2.0.CO;2

Chen F, Mitchell K, Schaake J, et al (1996) Modeling of land surface evaporation by four schemes and comparison with FIFE observations. Journal of Geophysical Research: Atmospheres 101:7251–7268. https://doi.org/10.1029/95JD02165

Chen N, Gao X, Nan C, Xuejie G (2019) Climate change in the twenty-first century over China: projections by an RCM and the driving GCM. New pub: KeAi 12:270–277. https://doi.org/10.1080/16742834.2019.1612695

Christel P, Ignazio G, L RE, et al (2014) Hydrological droughts in the 21st century, hotspots and uncertainties from a global multimodel ensemble experiment.

Proceedings of the National Academy of Sciences 111:3262–3267. https://doi.org/10.1073/pnas.1222473110

Christensen JH, Carter TR, Rummukainen M, Amanatidis G (2007) Evaluating the performance and utility of regional climate models: the PRUDENCE project. Clim Change 81:1–6. https://doi.org/10.1007/s10584-006-9211-6

Christensen JH, Christensen OB (2007) A summary of the PRUDENCE model projections of changes in European climate by the end of this century. Clim Change 81:7–30. https://doi.org/10.1007/s10584-006-9210-7

Clarke L., Edmonds J., Jacoby H., et al (2007) Scenarios of Greenhouse Gas Emissions and Atmospheric Concentrations: Report - Climate Change Science Program (U.S.) - Βιβλία Google

Colmet-Daage A, Sanchez-Gomez E, Ricci S, et al (2018) Evaluation of uncertainties in mean and extreme precipitation under climate change for northwestern Mediterranean watersheds from high-resolution Med and Euro-CORDEX ensembles. Hydrol Earth Syst Sci 22:673–687. https://doi.org/10.5194/hess-22-673-2018

Cook BI, Anchukaitis KJ, Touchan R, et al (2016) Spatiotemporal drought variability in the Mediterranean over the last 900 years. J Geophys Res Atmos 121:2060–2074. https://doi.org/10.1002/2015JD023929

Cook BI, Smerdon JE, Seager R, Coats S (2014) Global warming and 21st century drying. Clim Dyn 43:2607–2627. https://doi.org/10.1007/S00382-014-2075-Y/FIGURES/16

Copernicus European Drought Observatory (EDO): https://edo.jrc.ec.europa.eu/ (2020) Standardized Precipitation Index (SPI). In: European Commission. https://edo.jrc.ec.europa.eu/documents/factsheets/factsheet_spi.pdf. Accessed 24 Aug 2022

Coppola E, Nogherotto R, Ciarlo' JM, et al (2021) Assessment of the European Climate Projections as Simulated by the Large EURO-CORDEX Regional and Global Climate Model Ensemble. Journal of Geophysical Research: Atmospheres 126:e2019JD032356. https://doi.org/10.1029/2019JD032356

Coppola E, Sobolowski S, Pichelli E, et al (2020) A first-of-its-kind multi-model convection permitting ensemble for investigating convective phenomena over Europe and the Mediterranean. Clim Dyn 55:3–34. https://doi.org/10.1007/s00382-018-4521-8

Coumou D, Di Capua G, Vavrus S, et al (2018) The influence of Arctic amplification on mid-latitude summer circulation. Nature Communications 2018 9:1 9:1–12. https://doi.org/10.1038/s41467-018-05256-8

Cressie NAC (2015) Statistics for Spatial Data. John Wiley & Sons

Dai A (2011) Drought under global warming: a review. Wiley Interdiscip Rev Clim Change 2:45–65. https://doi.org/10.1002/WCC.81

Dalezios, N.R., 2021. Remote Sensing Applications in Environmental and Earth System Sciences. Chapter 6: Environmental Hazards p177-222, Publisher: Taylor& Francis, CRC group, ISBN: 978-1-138-05456-1, 368 pages.

Dalezios, N.R., A.N. Angelakis and S. Eslamian, 2018a. Water Scarcity Management: Part 1: Methodological Framework. I.J.G.E.I, Volume 17, No 1, 1-40.

Dalezios, N.R., N. Dercas and S. Eslamian, 2018b. Water Scarcity Management: Part 2: Satellite-based Composite Drought Analysis. I.J.G.E.I., Vol. 17, No 2/3, 267-295.

Dalezios, N.R., 2018c: Drought and Remote Sensing: An Overview. Book chapter 1, In: Remote Sensing of Hydrometeorological Hazards. Editors: Prof. G.P. Petropoulos and T. Islam, Publisher: Taylor and Francis, 3-32.

Dalezios, N.R., N.V. Spyropoulos and S. Eslamian, 2017a: Remote Sensing in Drought Quantification and Assessment. Book chapter 21 in Vol. 1 of 3- Volume Handbook of Drought and Water Scarcity (HDWS). Editor: Prof. S. Eslamian. Publisher: Taylor and Francis, 377-396.

Dalezios, N.R., A.M. Tarquis and S. Eslamian, 2017b: Drought Assessment and Risk Analysis. Book chapter 18 in Vol. 1 of 3-Volume Handbook of Drought and Water Scarcity (HDWS). Editor: Prof. S. Eslamian. Publisher: Taylor and Francis, 323-343.

Dalezios, N.R., A. Gobin, A.M. Tarquis and S. Eslamian, 2017c: Agricultural Drought Indices: Combining Crop, Climate and Soil Factors. Book chapter 5 in Vol. 1 of 3-Volume Handbook of Drought and Water Scarcity (HDWS). Editor: Prof. S. Eslamian. Publisher: Taylor and Francis Group, 73-89.

Dalezios, N.R., A.Blanta, N.V.Spyropoulos and A.M. Tarquis, 2014. Risk Identification of Agricultural Drought in Sustainable Agroecosystems. NHESS: 14, 2435-2448.

Dalezios, N.R., A. Blanta, and N. V. Spyropoulos, 2012. “Assessment of remotely sensed drought features in vulnerable agriculture”. NHESS, 12, 3139-3150.

Dalezios NR, Loukas A, Vasiliades L, Liakopoulos E (2000) Severity-duration-frequency analysis of droughts and wet periods in Greece. Hydrological Sciences Journal 45:751–769. https://doi.org/10.1080/02626660009492375

Dalezios NR, Papazafiriou ZG, Papamichail DM, Karacostas TS (1991) Drought assessment for the potential of precipitation enhancement in northern Greece. Theoretical and Applied Climatology 1991 44:2 44:75–88. https://doi.org/10.1007/BF00867995

Daliakopoulos IN, Panagea IS, Tsanis IK, et al (2017) Yield Response of Mediterranean Rangelands under a Changing Climate. Land Degrad Dev 28:1962–1972. https://doi.org/10.1002/LDR.2717

Dasari HP, Challa VS (2015) A Study of Precipitation Climatology and Its Variability over Europe Using an Advanced Regional Model (WRF). Am J Clim Change 04:22–39. https://doi.org/10.4236/ajcc.2015.41003

Dee DP, Uppala SM, Simmons AJ, et al (2011) The ERA-Interim reanalysis: Configuration and performance of the data assimilation system. Quarterly Journal of the Royal Meteorological Society 137:553–597. https://doi.org/10.1002/qj.828

Déqué M, Rowell DP, Lüthi D, et al (2007) An intercomparison of regional climate simulations for Europe: assessing uncertainties in model projections. Clim Change 81:53–70. https://doi.org/10.1007/s10584-006-9228-x

Dosio A (2016) Projections of climate change indices of temperature and precipitation from an ensemble of bias-adjusted high-resolution EURO-CORDEX regional climate models. Journal of Geophysical Research: Atmospheres 121:5488–5511. https://doi.org/10.1002/2015JD024411

Droutsa KG, Kontoyiannidis S, Balaras CA, et al (2021) Climate Change Scenarios and Their Implications on the Energy Performance of Hellenic Non-Residential Buildings. Sustainability 2021, Vol 13, Page 13005 13:13005. https://doi.org/10.3390/SU132313005

Duan, Z. και συν., 2016. Evaluation of eight high spatial resolution gridded precipitation products in Adige Basin (Italy) at multiple temporal and spatial scales. Science of the Total Environment, Τόμος 573, p. 1536–1553.

Dukat P, Bednorz E, Ziemblińska K, Urbaniak M (2022) Trends in drought occurrence and severity at mid-latitude European stations (1951–2015) estimated using standardized precipitation (SPI) and precipitation and evapotranspiration (SPEI) indices. Meteorology and Atmospheric Physics 134:1–21. https://doi.org/10.1007/S00703-022-00858-W/FIGURES/13

Dulière VR, Zhang Y, Salathé EP (2011) Extreme precipitation and temperature over the U.S. Pacific Northwest: A comparison between observations, reanalysis data, and regional models. J Clim 24:1950–1964. https://doi.org/10.1175/2010JCLI3224.1

Efstathiou GA, Zoumakis NM, Melas D, et al (2013) Sensitivity of WRF to boundary layer parameterizations in simulating a heavy rainfall event using different microphysical schemes. Effect on large-scale processes. Atmos Res 132–133:125–143. https://doi.org/10.1016/j.atmosres.2013.05.004

Ek MB (2003) Implementation of Noah land surface model advances in the National Centers for Environmental Prediction operational mesoscale Eta model. J Geophys Res 108:8851. https://doi.org/10.1029/2002JD003296

Eleftheriadou A, Sfetsos A, Gounaris N (2016) The suitability of high resolution downscaled seasonal models for the energy assessment of the building sector. Energy Build 111:176–183. https://doi.org/10.1016/j.enbuild.2015.09.034

Eleftheriou D, Kiachidis K, Kalmintzis G, et al (2018) Determination of annual and seasonal daytime and nighttime trends of MODIS LST over Greece - climate change implications. Science of The Total Environment 616–617:937–947. https://doi.org/https://doi.org/10.1016/j.scitotenv.2017.10.226

El-Samra R, Bou-Zeid E, El-Fadel M (2018) To what extent does high-resolution dynamical downscaling improve the representation of climatic extremes over an orographically complex terrain? Theor Appl Climatol 134:265–282. https://doi.org/10.1007/s00704-017-2273-8

Emmanouil G, Vlachogiannis D, Sfetsos A (2021) Exploring the ability of the WRF-ARW atmospheric model to simulate different meteorological conditions in Greece. Atmos Res 247:105226. https://doi.org/https://doi.org/10.1016/j.atmosres.2020.105226

Evans JP, Oglesby RJ, Lapenta WM (2005) Time series analysis of regional climate model performance. Journal of Geophysical Research D: Atmospheres 110:1–23. https://doi.org/10.1029/2004JD005046

Expósito FJ, González A, Pérez JC, et al (2015) High-resolution future projections of temperature and precipitation in the Canary Islands. J Clim 28:7846–7856. https://doi.org/10.1175/JCLI-D-15-0030.1

Fantini A, Raffaele F, Torma C, et al (2018) Assessment of multiple daily precipitation statistics in ERA-Interim driven Med-CORDEX and EURO-CORDEX experiments against high resolution observations. Clim Dyn 51:877–900. https://doi.org/10.1007/s00382-016-3453-4

Faye C (2022) Comparative Analysis of Meteorological Drought based on the SPI and SPEI Indices. HighTech and Innovation Journal 3:15–27. https://doi.org/10.28991/hij-sp2022-03-02

Faye Cheikh, Grippa Manuela, Wood Stephen (2019) Use of the Standardized Precipitation and Evapotranspiration Index (SPEI) from 1950 to 2018 to determine drought trends in the Senegalese territory. Climate Change 327–341

Feng X, Sahoo A, Arsenault K, et al (2008) The Impact of Snow Model Complexity at Three CLPX Sites. J Hydrometeorol 9:1464–1481. https://doi.org/10.1175/2008jhm860.1

Fernández J, Montávez JP, Sáenz J, et al (2007) Sensitivity of the MM5 mesoscale model to physical parameterizations for regional climate studies: Annual cycle. J Geophys Res 112:D04101. https://doi.org/10.1029/2005JD006649

Forster PM, Maycock AC, McKenna CM, Smith CJ (2019) Latest climate models confirm need for urgent mitigation. Nature Climate Change 2019 10:1 10:7–10. https://doi.org/10.1038/s41558-019-0660-0

Founda D, Papadopoulos KH, Petrakis M, et al (2004) Analysis of mean, maximum, and minimum temperature in Athens from 1897 to 2001 with emphasis on the last decade: trends, warm events, and cold events. Glob Planet Change 44:27–38. https://doi.org/https://doi.org/10.1016/j.gloplacha.2004.06.003

Founda D, Varotsos K V, Pierros F, Giannakopoulos C (2019) Observed and projected shifts in hot extremes' season in the Eastern Mediterranean. Glob Planet Change 175:190–200. https://doi.org/https://doi.org/10.1016/j.gloplacha.2019.02.012

Frei C, Christensen JH, Déqué M, et al (2003) Daily precipitation statistics in regional climate models: Evaluation and intercomparison for the European Alps. Journal of Geophysical Research: Atmospheres 108:n/a-n/a. https://doi.org/10.1029/2002JD002287

Gao Y, Xu J, Chen D (2015) Evaluation of WRF Mesoscale Climate Simulations over the Tibetan Plateau during 1979–2011. J Clim 28:2823–2841. https://doi.org/10.1175/JCLI-D-14-00300.1

García-Díez M, Fernández J, Fita L, Yagüe C (2013) Seasonal dependence of WRF model biases and sensitivity to PBL schemes over Europe. Quarterly Journal of the Royal Meteorological Society 139:501–514. https://doi.org/10.1002/qj.1976

García-Díez M, Fernández J, Vautard R (2015) An RCM multi-physics ensemble over Europe: multi-variable evaluation to avoid error compensation. Clim Dyn 45:3141–3156. https://doi.org/10.1007/s00382-015-2529-x

García-Valdecasas Ojeda M, Gámiz-Fortis SR, Castro-Díez Y, Esteban-Parra MJ (2017) Evaluation of WRF capability to detect dry and wet periods in Spain using drought indices. Journal of Geophysical Research: Atmospheres 122:1569–1594. https://doi.org/10.1002/2016JD025683

García-Valdecasas Ojeda M, Gámiz-Fortis SR, Romero-Jiménez E, et al (2021) Projected changes in the Iberian Peninsula drought characteristics. Science of the Total Environment 757:. https://doi.org/10.1016/j.scitotenv.2020.143702

García-Valdecasas Ojeda M, Raquel Gámiz-Fortis S, Manuel Hidalgo-Muñoz J, et al (2015) Regional Climate Model sesitivity to different parameterizations schemes with WRF over Spain. Geophysical Research Abstracts EGU General Assembly 17:2015–11640

Georgoulias AK, Akritidis D, Kalisoras A, et al (2022) Climate change projections for Greece in the 21st century from high-resolution EURO-CORDEX RCM simulations. Atmos Res 271:. https://doi.org/10.1016/j.atmosres.2022.106049

Gerber F, Besic N, Sharma V, et al (2018) Spatial variability in snow precipitation and accumulation in COSMO-WRF simulations and radar estimations over complex terrain. Cryosphere 12:3137–3160. https://doi.org/10.5194/tc-12-3137-2018

Giannakopoulos C, Kostopoulou E, Varotsos K V., et al (2011) An integrated assessment of climate change impacts for Greece in the near future. Reg Environ Change 11:829–843. https://doi.org/10.1007/S10113-011-0219-8/TABLES/5

Giannaros TM, Kotroni V, Lagouvardos K (2016) WRF-LTNGDA: A lightning data assimilation technique implemented in the WRF model for improving

precipitation forecasts. Environmental Modelling & Software 76:54–68. https://doi.org/10.1016/j.envsoft.2015.11.017

Giannaros TM, Melas D, Daglis IA, et al (2013) Numerical study of the urban heat island over Athens (Greece) with the WRF model. Atmos Environ 73:103–111. https://doi.org/10.1016/j.atmosenv.2013.02.055

Giorgi F (2006) Climate change hot-spots. Geophys Res Lett 33:L08707. https://doi.org/10.1029/2006GL025734

Giorgi F, Bi X, Pal J (2004) Mean, interannual variability and trends in a regional climate change experiment over Europe. II: Climate change scenarios (2071-2100). Clim Dyn 23:839–858. https://doi.org/10.1007/S00382-004-0467-0/FIGURES/14

Giorgi F, Gutowski WJ (2015) Regional Dynamical Downscaling and the CORDEX Initiative. Annu Rev Environ Resour 40:467–490. https://doi.org/10.1146/annurev-environ-102014-021217

Giorgi F, Lead BH, Christensen J, et al (2001) Regional Climate Information-Evaluation and Projections

Giorgi F, Lionello P (2008) Climate change projections for the Mediterranean region. Glob Planet Change 63:90–104. https://doi.org/10.1016/j.gloplacha.2007.09.005

Guerreiro SB, Dawson RJ, Kilsby C, et al (2018) Future heat-waves, droughts and floods in 571 European cities. Environmental Research Letters 13:034009. https://doi.org/10.1088/1748-9326/AAAAD3

Guo D-L, Sun J-Q, Yu E-T (2018) Evaluation of CORDEX regional climate models in simulating temperature and precipitation over the Tibetan Plateau. Atmospheric and Oceanic Science Letters 11:219–227. https://doi.org/10.1080/16742834.2018.1451725

Gutowski Jr WJ, Ullrich PA, Hall A, et al (2020) The Ongoing Need for High-Resolution Regional Climate Models: Process Understanding and Stakeholder Information. Bull Am Meteorol Soc 101:E664–E683. https://doi.org/10.1175/BAMS-D-19-0113.1

H. Hargreaves G, A. Samani Z (1985) Reference Crop Evapotranspiration from Temperature. Appl Eng Agric 1:96–99. https://doi.org/https://doi.org/10.13031/2013.26773

Hatzianastassiou N, Katsoulis B, Pnevmatikos J, Antakis V (2008) Spatial and Temporal Variation of Precipitation in Greece and Surrounding Regions Based on Global Precipitation Climatology Project Data. J Clim 21:1349–1370. https://doi.org/10.1175/2007JCLI1682.1

Hay LE, Wilby RL, Leavesley GH (2000) A Comparison of Delta Change and Downscaled GCM Scenarios for Three Mountainous Basins in the United States. JAWRA Journal of the American Water Resources Association 36:387–397

Hao Z, Hao F, Singh VP. 2016. A general framework for multivariate multi-index drought prediction based on multivariate ensemble streamflow prediction (MESP). J. Hydrol. 539: 1– 10.

Hazeleger W, Severijns C, Semmler T, et al (2010) EC-Earth: A Seamless Earth-System Prediction Approach in Action. Bull Am Meteorol Soc 91:1357–1364. https://doi.org/10.1175/2010BAMS2877.1

Hazeleger W, Wouters B, Van Oldenborgh GJ, et al (2013) Predicting multiyear North Atlantic Ocean variability. J Geophys Res Oceans 118:1087–1098. https://doi.org/10.1002/JGRC.20117

Heikkilä U, Sandvik A, Sorteberg A (2011) Dynamical downscaling of ERA-40 in complex terrain using the WRF regional climate model. Clim Dyn 37:1551–1564. https://doi.org/10.1007/s00382-010-0928-6

Heim, R. R. Jr., 2002: A Review of Twentieth-Century Drought Indices Used in the United States. Bulletin of the American Meteorological Society, 83(8), 1149-1165.

Henderson-Sellers A, Pitman AJ, Love PK, et al (1995) The Project for Intercomparison of Land Surface Parameterization Schemes (PILPS): Phases 2 and 3. Bull Am Meteorol Soc 76:489–503

Hewitt C (2005) The ENSEMBLES Project Providing ensemble-based predictions of climate changes and their impacts. In: EGGS newsletter. http://ensembles-eu.metoffice.com/docs/EGGS_subm.pdf. Accessed 31 Mar 2017

Hong S-Y, Lim J-O (2006) The {WRF} Single-Moment 6-Class Microphysics Scheme {(WSM6)}. J Korean Meteor Soc 42:

Hong S-Y, Noh Y, Dudhia J, et al (2006) A New Vertical Diffusion Package with an Explicit Treatment of Entrainment Processes. Mon Weather Rev 134:2318–2341. https://doi.org/10.1175/MWR3199.1

Horton DE, Johnson NC, Singh D, et al (2015) Contribution of changes in atmospheric circulation patterns to extreme temperature trends. Nature 522:465–469. https://doi.org/10.1038/nature14550

Hu X-M, Xue M, McPherson RA, et al (2018) Precipitation Dynamical Downscaling Over the Great Plains. J Adv Model Earth Syst 10:421–447. https://doi.org/10.1002/2017MS001154

Iacono MJ, Delamere JS, Mlawer EJ, et al (2008) Radiative forcing by long-lived greenhouse gases: Calculations with the AER radiative transfer models. J Geophys Res 113:D13103. https://doi.org/10.1029/2008JD009944

Im E-S, Coppola E, Giorgi F, Bi X (2010) Validation of a High-Resolution Regional Climate Model for the Alpine Region and Effects of a Subgrid-Scale Topography and Land Use Representation. J Clim 23:1854–1873. https://doi.org/10.1175/2009JCLI3262.1

IPCC (2014) AR5 Climate Change 2014: Impacts, Adaptation, and Vulnerability — IPCC. https://www.ipcc.ch/report/ar5/wg2/. Accessed 11 May 2022

IPCC, Pörtner HO, Roberts DC, et al (2022) Summary for Policymakers:Climate Change 2022: Impacts, Adaptation, and Vulnerability. Contribution of Working Group II to the Sixth Assessment Report of the Intergovernmental Panel on Climate Change. Cambridge University Press, Cambridge, UK

Jacob D, Petersen J, Eggert B, et al (2014) EURO-CORDEX: new high-resolution climate change projections for European impact research. Reg Environ Change 14:563–578. https://doi.org/10.1007/s10113-013-0499-2

Jacob D, Teichmann C, Sobolowski S, et al (2020) Regional climate downscaling over Europe: perspectives from the EURO-CORDEX community. Reg Environ Change 20:1–20. https://doi.org/10.1007/S10113-020-01606-9/FIGURES/3

Janjić ZI (2001) Nonsingular Implementation of the Mellor-Yamada Level 2.5 Scheme in the NCEP Meso model

Jehanzaib M, Sattar MN, Lee JH, Kim TW (2020) Investigating effect of climate change on drought propagation from meteorological to hydrological drought using multi-model ensemble projections. Stochastic Environmental Research and Risk Assessment 34:7–21. https://doi.org/10.1007/S00477-019-01760-5/FIGURES/7

Jung G (2006) Regional Climate Change and the Impact on Hydrology in the Volta Basin of West Africa. PHD Thiss 150–157

Kain JS, Kain JS (2004) The Kain–Fritsch Convective Parameterization: An Update. Journal of Applied Meteorology 43:170–181. https://doi.org/10.1175/1520-0450(2004)043<0170:TKCPAU>2.0.CO;2

Kairis O, Karamanos A, Voloudakis D, et al (2022) Identifying Degraded and Sensitive to Desertification Agricultural Soils in Thessaly, Greece, under Simulated Future Climate Scenarios. Land (Basel) 11:395. https://doi.org/10.3390/land11030395

Kalnay E, Kanamitsu M, Kistler R, et al (1996) The NCEP/NCAR 40-Year Reanalysis Project. Bull Am Meteorol Soc 77:437–471. https://doi.org/10.1175/1520-0477(1996)077<0437:TNYRP>2.0.CO;2

Kambezidis HD, Psiloglou BE, Varotsos K V, Giannakopoulos C (2021) Climate Change and Thermal Comfort in Greece. Climate 9:. https://doi.org/10.3390/cli9010010

Karavitis CA, Alexandris S, Tsesmelis DE, Athanasopoulos G (2011) Application of the Standardized Precipitation Index (SPI) in Greece. Water 2011, Vol 3, Pages 787-805 3:787–805. https://doi.org/10.3390/W3030787

Karavitis CA, Chortaria C, Alexandris S, et al (2012) Development of the standardised precipitation index for Greece.

http://dx.doi.org/101080/1573062X2012690431 9:401–417. https://doi.org/10.1080/1573062X.2012.690431

Karavitis CA, Tsesmelis DE, Skondras NA, et al (2014) Linking drought characteristics to impacts on a spatial and temporal scale. Water Policy 16:1172–1197. https://doi.org/10.2166/wp.2014.205

Karozis S, Sfetsos A, Gounaris N, Vlachogiannis D (2021) An assessment of climate change impact on air masses arriving in Athens, Greece. Theoretical and Applied Climatology 2021 145:1 145:501–517. https://doi.org/10.1007/S00704-021-03624-X

Kartsios S, Kotsopoulos S, Karacostas TS, et al (2015) Statistical evaluation of the simulated convective activity over Central Greece. Geophysical Research Abstracts EGU General Assembly 17:2015–8418

Katavoutas G, Founda D, Kitsara G, Giannakopoulos C (2021) Climate Change and Thermal Comfort in Top Tourist Destinations—The Case of Santorini (Greece). Sustainability 2021, Vol 13, Page 9107 13:9107. https://doi.org/10.3390/SU13169107

Katopodis T, Vlachogiannis D, Politi N, et al (2019) Assessment of climate change impacts on wind resource characteristics and wind energy potential in Greece. Journal of Renewable and Sustainable Energy 11:066502. https://doi.org/10.1063/1.5118878

Katragkou E, Garciá-Diéz M, Vautard R, et al (2015) Regional climate hindcast simulations within EURO-CORDEX: Evaluation of a WRF multi-physics ensemble. Geosci Model Dev 8:603–618. https://doi.org/10.5194/gmd-8-603-2015

Ke Y, Leung LR, Huang M, Li H (2013) Enhancing the representation of subgrid land surface characteristics in land surface models. Geosci Model Dev 6:1609–1622. https://doi.org/10.5194/gmd-6-1609-2013

Khodayar S, Kalthoff N, Kottmeier C (2016) Atmospheric conditions associated with heavy precipitation events in comparison to seasonal means in the western mediterranean region. Clim Dyn 1–17. https://doi.org/10.1007/s00382-016-3058-y

Kioutsioukis I, de Meij A, Jakobs H, et al (2016) High resolution WRF ensemble forecasting for irrigation: Multi-variable evaluation. Atmos Res 167:156–174. https://doi.org/10.1016/j.atmosres.2015.07.015

Knist S, Goergen K, Simmer C (2016) Added value and land-atmosphere coupling in convection-permitting WRF climate simulations over a Middle European domain. EGU General Assembly 2016, held 17-22 April, 2016 in Vienna Austria, p4808 18:4808

Knist S, Goergen K, Simmer C (2020) Evaluation and projected changes of precipitation statistics in convection-permitting WRF climate simulations over

Central Europe. Clim Dyn 55:325–341. https://doi.org/10.1007/s00382-018-4147-x

Koenigk T, Brodeau L, Graversen RG, et al (2013) Arctic climate change in 21st century CMIP5 simulations with EC-Earth. Clim Dyn 40:2719–2743. https://doi.org/10.1007/S00382-012-1505-Y/FIGURES/18

Komurcu M, Emanuel KA, Huber M, Acosta RP (2018) High-Resolution Climate Projections for the Northeastern United States Using Dynamical Downscaling at Convection-Permitting Scales. Earth and Space Science 5:801–826. https://doi.org/10.1029/2018EA000426

Kostopoulou E, Giannakopoulos C, Hatzaki M, et al (2014) Spatio-temporal patterns of recent and future climate extremes in the eastern Mediterranean and Middle East region. Natural Hazards and Earth System Sciences 14:1565–1577. https://doi.org/10.5194/nhess-14-1565-2014

Kostopoulou E, Jones PD (2005) Assessment of climate extremes in the Eastern Mediterranean. Meteorology and Atmospheric Physics 89:69–85. https://doi.org/10.1007/s00703-005-0122-2

Kotlarski S, Keuler K, Christensen OB, et al (2014) Regional climate modeling on European scales: a joint standard evaluation of the EURO-CORDEX RCM ensemble. Geosci Model Dev 7:1297–1333. https://doi.org/10.5194/gmd-7-1297-2014

Kotroni V, Lagouvardos K (2004) Evaluation of MM5 High-Resolution Real-Time Forecasts over the Urban Area of Athens, Greece. Journal of Applied Meteorology 43:1666–1678. https://doi.org/10.1175/JAM2170.1

Kourgialas NN (2021) A critical review of water resources in Greece: The key role of agricultural adaptation to climate-water effects. Science of The Total Environment 775:145857. https://doi.org/https://doi.org/10.1016/j.scitotenv.2021.145857

Kryza M, Wałaszek K, Ojrzyńska H, et al (2017) High-Resolution Dynamical Downscaling of ERA-Interim Using the WRF Regional Climate Model for the Area of Poland. Part 1: Model Configuration and Statistical Evaluation for the 1981–2010 Period. Pure Appl Geophys 174:511–526. https://doi.org/10.1007/s00024-016-1272-5

Kryza M, Werner M, Wałaszek K, Dore AJ (2013) Application and evaluation of the WRF model for high-resolution forecasting of rainfall - A case study of SW Poland. Meteorologische Zeitschrift 22:595–601. https://doi.org/10.1127/0941-2948/2013/0444

Lagouvardos K, Kotroni V (2005) Improvement of high-resolution weather forecasts through humidity adjustment based on satellite data. Quarterly Journal of the Royal Meteorological Society 131:2695–2712. https://doi.org/10.1256/qj.04.112

Laprise R (2008) Regional climate modelling. J Comput Phys 227:3641–3666. https://doi.org/10.1016/j.jcp.2006.10.024

Legates DR, McCabe Jr. GJ (1999) Evaluating the use of "goodness-of-fit" Measures in hydrologic and hydroclimatic model validation. Water Resour Res 35:233–241. https://doi.org/10.1029/1998WR900018

Leung LR, Mearns LO, Giorgi F, et al (2003) Regional Climate Research. Bull Am Meteorol Soc 84:89–95. https://doi.org/10.1175/BAMS-84-1-89

Level M, Closure T (1998) Mellor-Yamada Level 2.5 Turbulence Closure 1. Ocean Model (Oxf) 5–7

Lhotka O, Kyselý J, Plavcová E (2018) Evaluation of major heat waves' mechanisms in EURO-CORDEX RCMs over Central Europe. Clim Dyn 50:4249–4262. https://doi.org/10.1007/s00382-017-3873-9

Li H, Li Z, Chen Y, et al (2021) Drylands face potential threat of robust drought in the CMIP6 SSPs scenarios. Environmental Research Letters 16:. https://doi.org/10.1088/1748-9326/ac2bce

Lionello P, Scarascia L (2018) The relation between climate change in the Mediterranean region and global warming. Reg Environ Change 18:1481–1493. https://doi.org/https://doi.org/10.1007/s10113-018-1290-1

Livada I, Assimakopoulos VD (2007) Spatial and temporal analysis of drought in Greece using the Standardized Precipitation Index (SPI). Theor Appl Climatol 89:143–153. https://doi.org/10.1007/s00704-005-0227-z

Lo JC-F, Yang Z-L, Pielke RA (2008) Assessment of three dynamical climate downscaling methods using the Weather Research and Forecasting (WRF) model. J Geophys Res 113:D09112. https://doi.org/10.1029/2007JD009216

Loukas A, Vasiliades L (2004) Probabilistic analysis of drought spatiotemporal characteristics in Thessaly region, Greece

Loukas A, Vasiliades L, Tzabiras J (2007) Evaluation of Climate Change on Drought Impulses in Thessaly, Greece. European Water 17:17–28

Marcos R, Llasat MC, Quintana-Seguí P, Turco M (2017) Seasonal predictability of water resources in a Mediterranean freshwater reservoir and assessment of its utility for end-users. Science of The Total Environment 575:681–691. https://doi.org/10.1016/J.SCITOTENV.2016.09.080

Mariotti A, Dell'Aquila A (2012) Decadal climate variability in the Mediterranean region: Roles of large-scale forcings and regional processes. Clim Dyn 38:1129–1145. https://doi.org/10.1007/S00382-011-1056-7/FIGURES/10

Marta-Almeida M, Teixeira JC, Carvalho MJ, et al (2016) High resolution WRF climatic simulations for the Iberian Peninsula: Model validation. Physics and Chemistry of the Earth 94:94–105. https://doi.org/10.1016/j.pce.2016.03.010

Mathbout S, Lopez-Bustins JA, Royé D, Martin-Vide J (2021) Mediterranean-scale drought: Regional datasets for exceptional meteorological drought events during 1975-2019. Atmosphere (Basel) 12:. https://doi.org/10.3390/atmos12080941

Matsangouras IT, Nastos PT, Pytharoulis I (2011) Synoptic-mesoscale analysis and numerical modeling of a tornado event on 12 February 2010 in northern Greece. Advances in Science and Research 6:187–194. https://doi.org/10.5194/asr-6-187-2011

Mavromatis T, Georgoulias AK, Akritidis D, et al (2022) Spatiotemporal Evolution of Seasonal Crop-Specific Climatic Indices under Climate Change in Greece Based on EURO-CORDEX RCM Simulations. Sustainability 14:. https://doi.org/10.3390/su142417048

Mazarakis N, Kotroni V, Lagouvardos K, Argiriou AA (2009) The sensitivity of numerical forecasts to convective parameterization during the warm period and the use of lightning data as an indicator for convective occurrence. Atmos Res 94:704–714. https://doi.org/10.1016/j.atmosres.2009.03.002

Mckee TB, Doesken NJ, Kleist J (1993) The relationship of drought frequency and duration to time scale. In: Eighth Conference on Applied Climatology. pp 17–22

Menendez M, García-Díez M, Fita L, et al (2014) High-resolution sea wind hindcasts over the Mediterranean area. Clim Dyn 42:1857–1872. https://doi.org/10.1007/s00382-013-1912-8

Moss RH, Edmonds JA, Hibbard KA, et al (2010) The next generation of scenarios for climate change research and assessment. Nature 2010 463:7282 463:747–756. https://doi.org/10.1038/nature08823

Nakicenovic N, Alcamo J, Grubler A, et al (2000) Special Report on Emissions Scenarios (SRES), A Special Report of Working Group III of the Intergovernmental Panel on Climate Change

Nash JE, Sutcliffe J V (1970) River flow forecasting through conceptual models part I — A discussion of principles. J Hydrol (Amst) 10:282–290. https://doi.org/https://doi.org/10.1016/0022-1694(70)90255-6

Nastos PT, Kapsomenakis J, Douvis KC (2013a) Analysis of precipitation extremes based on satellite and high-resolution gridded data set over Mediterranean basin. Atmos Res 131:46–59. https://doi.org/10.1016/j.atmosres.2013.04.009

Nastos PT, Kapsomenakis J, Philandras KM (2016) Evaluation of the TRMM 3B43 gridded precipitation estimates over Greece. Atmos Res 169:497–514. https://doi.org/10.1016/j.atmosres.2015.08.008

Nastos PT, Karavana Papadimou K, Matsangouras IT (2018) Mediterranean tropical-like cyclones: Impacts and composite daily means and anomalies of synoptic patterns. Atmos Res 208:156–166. https://doi.org/https://doi.org/10.1016/j.atmosres.2017.10.023

Nastos PT, Matzarakis A (2019) Present and Future Climate—Tourism Conditions in Milos Island, Greece. Atmosphere 2019, Vol 10, Page 145 10:145. https://doi.org/10.3390/ATMOS10030145

Nastos PT, Politi N, Kapsomenakis J (2013b) Spatial and temporal variability of the Aridity Index in Greece. Atmos Res 119:140–152. https://doi.org/10.1016/j.atmosres.2011.06.017

Nastos PT, Zerefos CS (2008) Decadal changes in extreme daily precipitation in Greece. Advances in Geosciences 16:55–62. https://doi.org/10.5194/adgeo-16-55-2008

Nastos PT, Zerefos CS (2009) Spatial and temporal variability of consecutive dry and wet days in Greece. Atmos Res 94:616–628. https://doi.org/10.1016/j.atmosres.2009.03.009

Oikonomou PD, Tsesmelis DE, Waskom RM, et al (2019) Enhancing the standardized drought vulnerability index by integrating spatiotemporal information from satellite and in situ data. J Hydrol (Amst) 569:265–277. https://doi.org/https://doi.org/10.1016/j.jhydrol.2018.11.058

Ojrzyńska H, Kryza M, Wałaszek K, et al (2017) High-Resolution Dynamical Downscaling of ERA-Interim Using the WRF Regional Climate Model for the Area of Poland. Part 2: Model Performance with Respect to Automatically Derived Circulation Types. Pure Appl Geophys 174:527–550. https://doi.org/10.1007/s00024-016-1273-4

Olsson J, Berg P, Kawamura A (2015) Impact of RCM Spatial Resolution on the Reproduction of Local, Subdaily Precipitation. J Hydrometeorol 16:534–547. https://doi.org/10.1175/JHM-D-14-0007.1

Orlowsky B, Seneviratne SI (2012) Global changes in extreme events: regional and seasonal dimension. Clim Change 110:669–696. https://doi.org/10.1007/s10584-011-0122-9

Ozturk T, Ceber ZP, Türkeş M, Kurnaz ML (2015) Projections of climate change in the Mediterranean Basin by using downscaled global climate model outputs. International Journal of Climatology 35:4276–4292. https://doi.org/10.1002/JOC.4285

Palmer TN (2013) Climate extremes and the role of dynamics. Proc Natl Acad Sci U S A 110:5281–5282. https://doi.org/10.1073/pnas.1303295110

Paparrizos S, Maris F, Matzarakis A (2016) INTEGRATED ANALYSIS AND MAPPING OF ARIDITY OVER GREEK AREAS WITH DIFFERENT CLIMATE CONDITIONS

Paparrizos S, Maris F, Weiler M, Matzarakis A (2018) Analysis and mapping of present and future drought conditions over Greek areas with different climate conditions. Theor Appl Climatol 131:259–270. https://doi.org/10.1007/s00704-016-1964-x

Pérez JC, Díaz JP, González A, et al (2014) Evaluation of WRF Parameterizations for dynamical downscaling in the Canary Islands. J Clim 27:5611–5631. https://doi.org/10.1175/JCLI-D-13-00458.1

Pieri AB, von Hardenberg J, Parodi A, Provenzale A (2015) Sensitivity of Precipitation Statistics to Resolution, Microphysics, and Convective Parameterization: A Case Study with the High-Resolution WRF Climate Model over Europe. J Hydrometeorol 16:1857–1872. https://doi.org/10.1175/jhm-d-14-0221.1

Plexousakis M (2013) The utilization of WRF for the study of extreme weather events over Greece Modeling and Computations in Atmospheric Sciences

Polade SD, Gershunov A, Cayan DR, et al (2017) Precipitation in a warming world: Assessing projected hydro-climate changes in California and other Mediterranean climate regions. Scientific Reports 2017 7:1 7:1–10. https://doi.org/10.1038/s41598-017-11285-y

Politi N, Nastos PT, Sfetsos A, et al (2018) Evaluation of the AWR-WRF model configuration at high resolution over the domain of Greece. Atmos Res. https://doi.org/10.1016/J.ATMOSRES.2017.10.019

Politi N, Sfetsos A, Vlachogiannis D, et al (2020) A sensitivity study of high-resolution climate simulations for Greece. Climate 8:1–28. https://doi.org/10.3390/cli8030044

Politi N, Vlachogiannis D, Sfetsos A, Nastos PT (2021) High-resolution dynamical downscaling of ERA-Interim temperature and precipitation using WRF model for Greece. Climate Dynamics 2021 57:3 57:799–825. https://doi.org/10.1007/S00382-021-05741-9

Politi N, Vlachogiannis D, Sfetsos A, Nastos PT (2022) High resolution projections for extreme temperatures and precipitation over Greece. Clim Dyn. https://doi.org/10.1007/s00382-022-06590-w

Prein AF, Gobiet A, Truhetz H, et al (2016) Precipitation in the EURO-CORDEX 0.11◦ and 0.44◦ simulations: high resolution, high benefits. Clim Dyn 46:383–412. https://doi.org/10.1007/s00382-015-2589-y

Prein AF, Holland GJ, Rasmussen RM, et al (2013) Importance of regional climate model grid spacing for the simulation of heavy precipitation in the colorado headwaters. J Clim 26:4848–4857. https://doi.org/10.1175/JCLI-D-12-00727.1

Prein AF, Rasmussen RM, Ikeda K, et al (2017) The future intensification of hourly precipitation extremes. Nat Clim Chang 7:48–52. https://doi.org/10.1038/nclimate3168

Pytharoulis I, Craig GC, Ballard SP (2000) The hurricane-like Mediterranean cyclone of January 1995. Meteorological Applications 7:261–279. https://doi.org/10.1017/S1350482700001511

Pytharoulis I, Tegoulias I, Kotsopoulos S, et al (2014) High-Resolution WRF Hindcasts over the central Greece: Characteristics of simulated convective activity and model evaluation. In: 15th Annual WRF Users' Workshop. Boulder, Colorado, USA

Rauscher SA, Coppola E, Piani C, Giorgi F (2010) Resolution effects on regional climate model simulations of seasonal precipitation over Europe. Clim Dyn 35:685–711. https://doi.org/10.1007/s00382-009-0607-7

Raymond F, Ullmann A, Tramblay Y, et al (2019) Evolution of Mediterranean extreme dry spells during the wet season under climate change. Reg Environ Change 19:2339–2351. https://doi.org/10.1007/S10113-019-01526-3/FIGURES/4

Riahi K, Rao S, Krey V, et al (2011) RCP 8.5-A scenario of comparatively high greenhouse gas emissions. Clim Change 109:33–57. https://doi.org/10.1007/S10584-011-0149-Y/FIGURES/12

Rovithakis A, Grillakis MG, Seiradakis KD, et al (2022) Future climate change impact on wildfire danger over the Mediterranean: The case of Greece. Environmental Research Letters 17:. https://doi.org/10.1088/1748-9326/ac5f94

Russo S, Dosio A, Graversen RG, et al (2014) Magnitude of extreme heat waves in present climate and their projection in a warming world. Journal of Geophysical Research: Atmospheres 119:12,500-12,512. https://doi.org/10.1002/2014JD022098

Ruti PM, Somot S, Giorgi F, et al (2016) Med-CORDEX Initiative for Mediterranean Climate Studies. Bull Am Meteorol Soc 97:1187–1208. https://doi.org/10.1175/BAMS-D-14-00176.1

Qian JH, Seth A and Zebiak S (2003) Reinitialized versus Continuous Simulations for Regional Climate Downscaling, Mon. Wea. Rev., 131, 2857–2874, https://doi.org/10.1175/15200493(2003)

Salman SA, Shahid S, Sharafati A, et al (2021) Projection of Agricultural Water Stress for Climate Change Scenarios: A Regional Case Study of Iraq. Agriculture 2021, Vol 11, Page 1288 11:1288. https://doi.org/10.3390/AGRICULTURE11121288

Schwartz CS, Kain JS, Weiss SJ, et al (2010) Toward Improved Convection-Allowing Ensembles: Model Physics Sensitivities and Optimizing Probabilistic Guidance with Small Ensemble Membership. Weather Forecast 25:263–280. https://doi.org/10.1175/2009waf2222267.1

Sepulcre-Cantò G, Horion SMAF, Singleton A, Carrao H, Vogt J. 2012. Development of a combined drought indicator to detect agricultural drought in Europe. Nat. Hazards Earth Syst. Sci. 12(11): 3519– 3531.

Sharafati A, Pezeshki E, Shahid S, Motta D (2020) Quantification and uncertainty of the impact of climate change on river discharge and sediment yield in the Dehbar river basin in Iran. J Soils Sediments 20:2977–2996. https://doi.org/10.1007/S11368-020-02632-0/FIGURES/11

Sindosi OA, Bartzokas A, Kotroni V, Lagouvardos K (2012) Verification of precipitation forecasts of MM5 model over Epirus, NW Greece, for various

convective parameterization schemes. Natural Hazards and Earth System Science 12:1393–1405. https://doi.org/10.5194/nhess-12-1393-2012

Skamarock B, Dudhia J (2011) The Advanced Research WRF (ARW) Dynamics Solver. Power Point Slides presented at the November 2011 NCAS Tutorial 1–42

Skamarock WC, Skamarock WC, Klemp JB, et al (2008) A description of the Advanced Research WRF version 3. NCAR Technical note -475+STR

Soares PMM, Cardoso RM (2018) A simple method to assess the added value using high-resolution climate distributions: application to the EURO-CORDEX daily precipitation. International Journal of Climatology 38:1484–1498. https://doi.org/10.1002/JOC.5261

Soares PMM, Cardoso RM, Lima DCA, Miranda PMA (2017) Future precipitation in Portugal: high-resolution projections using WRF model and EURO-CORDEX multi-model ensembles. Clim Dyn 49:2503–2530. https://doi.org/10.1007/s00382-016-3455-2

Soares PMM, Cardoso RM, Miranda PMA, et al (2012) WRF high resolution dynamical downscaling of ERA-Interim for Portugal. Clim Dyn 39:2497–2522. https://doi.org/10.1007/s00382-012-1315-2

Sordo-Ward A, Bejarano MD, Iglesias A, et al (2017) Analysis of Current and Future SPEI Droughts in the La Plata Basin Based on Results from the Regional Eta Climate Model. Water 2017, Vol 9, Page 857 9:857. https://doi.org/10.3390/W9110857

Sørland SL, Schär C, Lüthi D, Kjellström E (2018) Bias patterns and climate change signals in GCM-RCM model chains. Environmental Research Letters 13:. https://doi.org/10.1088/1748-9326/aacc77

Spinoni J, Barbosa P, Bucchignani E, et al (2020) Future global meteorological drought hot spots: A study based on CORDEX data. J Clim 33:3635–3661. https://doi.org/10.1175/JCLI-D-19-0084.1

Spinoni J, Barbosa P, De Jager A, et al (2019) A new global database of meteorological drought events from 1951 to 2016. J Hydrol Reg Stud 22:. https://doi.org/10.1016/j.ejrh.2019.100593

Spinoni J, Naumann G, Vogt J (2015) Spatial patterns of European droughts under a moderate emission scenario. Advances in Science and Research 12:179–186. https://doi.org/10.5194/ASR-12-179-2015

Spinoni J, Vogt J V., Naumann G, et al (2018) Will drought events become more frequent and severe in Europe? International Journal of Climatology 38:1718–1736. https://doi.org/10.1002/joc.5291

Spyridi, Dimitra, Vlachokostas C, Michailidou V. A, Sioutas C, Moussiopoulos N (2015) Strategic planning for climate change mitigation and adaptation: the case of Greece. Int J Clim Chang Strateg Manag 7:272–289. https://doi.org/10.1108/IJCCSM-02-2014-0027

Stagge JH, Kingston DG, Tallaksen LM, Hannah DM (2017) Observed drought indices show increasing divergence across Europe. Sci Rep 7:14045. https://doi.org/10.1038/s41598-017-14283-2

Sun X, Xue M, Brotzge J, et al (2016) An evaluation of dynamical downscaling of Central Plains summer precipitation using a WRF-based regional climate model at a convection-permitting 4 km resolution. Journal of Geophysical Research: Atmospheres 121:13,801-813,825. https://doi.org/10.1002/2016JD024796

Sunyer MA, Luchner J, Onof C, et al (2017) Assessing the importance of spatio-temporal RCM resolution when estimating sub-daily extreme precipitation under current and future climate conditions. International Journal of Climatology 37:688–705. https://doi.org/10.1002/joc.4733

Sylla MB, Coppola E, Mariotti L, et al (2010) Multiyear simulation of the African climate using a regional climate model (RegCM3) with the high resolution ERA-interim reanalysis. Clim Dyn 35:231–247. https://doi.org/10.1007/s00382-009-0613-9

Tank AMGK, Zwiers FW, Zhang X (2009) WMO Guidelines on Analysis of extremes in a changing climate in support of informed decisions. Climate Data and Monitoring 52

Tapiador FJ, Moreno R, Navarro A, et al (2019) Climate classifications from regional and global climate models: Performances for present climate estimates and expected changes in the future at high spatial resolution. Atmos Res 228:107–121. https://doi.org/https://doi.org/10.1016/j.atmosres.2019.05.022

Taylor KE (2001) Summarizing multiple aspects of model performance in a single diagram. Journal of Geophysical Research: Atmospheres 106:7183–7192. https://doi.org/10.1029/2000JD900719

Thompson G, Field PR, Rasmussen RM, et al (2008) Explicit Forecasts of Winter Precipitation Using an Improved Bulk Microphysics Scheme. Part II: Implementation of a New Snow Parameterization. Mon Weather Rev 136:5095–5115. https://doi.org/10.1175/2008MWR2387.1

Tian L, Jin J, Wu P, et al (2020) High-resolution simulations of mean and extreme precipitation with WRF for the soil-erosive Loess Plateau. Clim Dyn 54:3489–3506. https://doi.org/10.1007/s00382-020-05178-6

Tolika CK, Zanis P (2012) Regional climate change scenarios for Greece: Future temperature and precipitation projections from ensembles of RCMs. Global NEST Journal 14:407–421

Touma D, Ashfaq M, Nayak MA, et al (2015) A multi-model and multi-index evaluation of drought characteristics in the 21st century. J Hydrol (Amst) 526:196–207. https://doi.org/10.1016/J.JHYDROL.2014.12.011

Tramblay Y, Ruelland D, Somot S, et al (2013) High-resolution Med-CORDEX regional climate model simulations for hydrological impact studies: A first

evaluation of the ALADIN-Climate model in Morocco. Hydrol Earth Syst Sci 17:3721–3739. https://doi.org/10.5194/hess-17-3721-2013

Tsakiris, G., Pangalou, D. & Vangelis, H. Regional Drought Assessment Based on the Reconnaissance Drought Index (RDI). Water Resour Manage 21, 821–833 (2007). https://doi.org/10.1007/s11269-006-9105-4

Tsakiris G, Vangelis H (2004) Towards a Drought Watch System based on Spatial SPI. Water Resources Management 2004 18:1 18:1–12. https://doi.org/10.1023/B:WARM.0000015410.47014.A4

Tsesmelis DE, Oikonomou PD, Vasilakou CG, et al (2019) Assessing structural uncertainty caused by different weighting methods on the Standardized Drought Vulnerability Index (SDVI). Stochastic Environmental Research and Risk Assessment 33:515–533. https://doi.org/10.1007/s00477-019-01648-4

Tsesmelis DE, Vasilakou CG, Kalogeropoulos K, et al (2022) Drought assessment using the standardized precipitation index (SPI) in GIS environment in Greece. Computers in Earth and Environmental Sciences 619–633. https://doi.org/10.1016/B978-0-323-89861-4.00025-7

Turkes M, Tufan Turp M, An N, et al (2020) Impacts of Climate Change on Precipitation Climatology and Variability in Turkey. 467–491. https://doi.org/10.1007/978-3-030-11729-0_14

Ukkola AM, Pitman AJ, Kauwe MG De, et al (2018) Evaluating CMIP5 Model Agreement for Multiple Drought Metrics. J Hydrometeorol 19:969–988. https://doi.org/10.1175/JHM-D-17-0099.1

van der Schriek T, Varotsos K V., Giannakopoulos C, Founda D (2020) Projected Future Temporal Trends of Two Different Urban Heat Islands in Athens (Greece) under Three Climate Change Scenarios: A Statistical Approach. Atmosphere 2020, Vol 11, Page 637 11:637. https://doi.org/10.3390/ATMOS11060637

van Vuuren DP, Edmonds J, Kainuma M, et al (2011) The representative concentration pathways: an overview. Clim Change 109:5. https://doi.org/10.1007/s10584-011-0148-z

Vangelis H, Spiliotis M, Tsakiris G, et al (2011) Drought Severity Assessment Based on Bivariate Probability Analysis. https://doi.org/10.1007/s11269-010-9704-y

Vangelis H, Tigkas D, Tsakiris G (2013) The effect of PET method on Reconnaissance Drought Index (RDI) calculation. J Arid Environ 88:130–140. https://doi.org/10.1016/J.JARIDENV.2012.07.020

Varela V, Vlachogiannis D, Sfetsos A, et al (2020) Methodology for the study of near-future changes of fire weather patterns with emphasis on archaeological and protected touristic areas in greece. Forests 11:1–18. https://doi.org/10.3390/f11111168

Varotsos K V., Karali A, Kitsara G, Giannakopoulos C (2021a) Climate change impacts on the Greek tourism sector. EMS2021. https://doi.org/10.5194/EMS2021-324

Varotsos K V, Karali A, Lemesios G, et al (2021b) Near future climate change projections with implications for the agricultural sector of three major Mediterranean islands. Reg Environ Change 21:16. https://doi.org/10.1007/s10113-020-01736-0

Vasiliades L, Loukas A, Patsonas G (2009) Evaluation of a statistical downscaling procedure for the estimation of climate change impacts on droughts. Natural Hazards and Earth System Science 9:879–894. https://doi.org/10.5194/NHESS-9-879-2009

Vautard R, Kadygrov N, Iles C, et al (2021) Evaluation of the Large EURO-CORDEX Regional Climate Model Ensemble. Journal of Geophysical Research: Atmospheres 126:e2019JD032344. https://doi.org/10.1029/2019JD032344

Vergara-Temprado J, Ban N, Panosetti D, et al (2020) Climate Models Permit Convection at Much Coarser Resolutions Than Previously Considered. J Clim 33:1915–1933. https://doi.org/10.1175/JCLI-D-19-0286.1

Vicente-Serrano SM, Beguería S, López-Moreno JI (2010) A Multiscalar Drought Index Sensitive to Global Warming: The Standardized Precipitation Evapotranspiration Index. J Clim 23:1696–1718. https://doi.org/10.1175/2009JCLI2909.1

Vicente-Serrano SM, López-Moreno JI, Drumond A, et al (2011) Effects of warming processes on droughts and water resources in the NW Iberian Peninsula (1930−2006). Clim Res 48:203–212

Vicente-Serrano SM, Quiring SM, Peña-Gallardo M, et al (2020) A review of environmental droughts: Increased risk under global warming? Earth Sci Rev 201:102953. https://doi.org/10.1016/J.EARSCIREV.2019.102953

Vigaud N, Pohl B, Crétat J (2012) Tropical-temperate interactions over southern Africa simulated by a regional climate model. Clim Dyn 39:2895–2916. https://doi.org/10.1007/s00382-012-1314-3

Vlachogiannis D, Sfetsos A, Karozis SN, et al (2013) Mesoscale Simulation of hot weather eventsduring august 2012 in Greece. In: Int. Conf. on Harmonisation within Atmospheric Dispersion Modelling for Regulatory Purposes. Madrid, Spain

Vlachogiannis D, Sfetsos A, Markantonis I, et al (2022) Quantifying the Occurrence of Multi-Hazards Due to Climate Change. Applied Sciences 3:. https://doi.org/10.3390/app12031218

Vrochidou AEK, Grillakis MG, Tsanis IK (2013a) Drought Assessment Based on Multi-Model Precipitation Projections for the Island of Crete. Journal of Earth Science & Climatic Change 2013 4:6 4:1–7. https://doi.org/10.4172/2157-7617.1000158

Vrochidou AEK, Tsanis IK, Grillakis MG, Koutroulis AG (2013b) The impact of climate change on hydrometeorological droughts at a basin scale. J Hydrol (Amst) 476:290–301. https://doi.org/10.1016/J.JHYDROL.2012.10.046

Wagner S, Berg P, Schädler G, Kunstmann H (2013) High resolution regional climate model simulations for Germany: Part II—projected climate changes. Clim Dyn 40:415–427. https://doi.org/10.1007/s00382-012-1510-1

Wang J, Kotamarthi VR (2015) High-resolution dynamically downscaled projections of precipitation in the mid and late 21st century over North America. Earths Future 3:268–288. https://doi.org/10.1002/2015EF000304

Wang Y, Leung LR, Mcgregor JL, et al (2004) Regional Climate Modeling: Progress, Challenges, and Prospects. Journal of the Meteorological Society of Japan 82:1599–1628

Warrach-Sagi K, Schwitalla T, Wulfmeyer V, Bauer HS (2013) Evaluation of a climate simulation in Europe based on the WRF-NOAH model system: Precipitation in Germany. Clim Dyn 41:755–774. https://doi.org/10.1007/s00382-013-1727-7

Warscher M, Wagner S, Marke T, et al (2019) A 5 km resolution regional climate simulation for Central Europe: Performance in high mountain areas and seasonal, regional and elevation-dependent variations. Atmosphere (Basel) 10:. https://doi.org/10.3390/atmos10110682

White BA, Buchanan AM, Birch CE, et al (2018) Quantifying the Effects of Horizontal Grid Length and Parameterized Convection on the Degree of Convective Organization Using a Metric of the Potential for Convective Interaction. J Atmos Sci 75:425–450. https://doi.org/10.1175/JAS-D-16-0307.1

Wilhite DA, Pulwarty RS (2017) National drought management policy guidelines: A template for action. CRC Press

Wilhite, D.A., Hayes, M.J., Kinutson C., and K.H. Smith, 2000: Planning for drought: moving from crisis to risk management. J. Amer. Water Res. Assoc., 36(4), 697-710.

Willmott CJ (1981) ON THE VALIDATION OF MODELS. Phys Geogr 2:184–194. https://doi.org/10.1080/02723646.1981.10642213

World Meteorological Organization (WMO), Global Water Partnership (GWP) (2016) Handbook of Drought Indicators and Indices (M. Svoboda and B.A. Fuchs). Integrated Drought Management Programme (IDMP),), Integrated Drought Management Tools and Guidelines Series 2, Geneva

Xu Z, Han Y, Yang Z (2019) Dynamical downscaling of regional climate: A review of methods and limitations. Sci China Earth Sci 62:365–375. https://doi.org/10.1007/s11430-018-9261-5

Xu Z, Yang ZL (2015) A new dynamical downscaling approach with GCM bias corrections and spectral nudging. J Geophys Res 120:3063–3084. https://doi.org/10.1002/2014JD022958

Zanis P, Kapsomenakis I, Philandras C, et al (2009) Analysis of an ensemble of present day and future regional climate simulations for Greece. International Journal of Climatology 29:1614–1633. https://doi.org/10.1002/JOC.1809

Zanis P, Katragkou E, Ntogras C, et al (2015) Transient high-resolution regional climate simulation for Greece over the period 1960-2100: Evaluation and future projections. Clim Res 64:123–140. https://doi.org/10.3354/cr01304

Zelinka MD, Myers TA, McCoy DT, et al (2020) Causes of Higher Climate Sensitivity in CMIP6 Models. Geophys Res Lett 47:e2019GL085782. https://doi.org/10.1029/2019GL085782

Zerefos CS, Repapis C, Giannakopoulos C, et al (2011) The climate of the Eastern Mediterranean and Greece: past, present and future. The environmental, economic and social impacts of climate change in Greece 1–126

Zhang C, Wang Y, Hamilton K, Lauer A (2016) Dynamical Downscaling of the Climate for the Hawaiian Islands. Part I: Present Day. J Clim 29:3027–3048. https://doi.org/10.1175/jcli-d-15-0432.1

Zhang C, Wang Y, Lauer A, Hamilton K (2012) Configuration and Evaluation of the WRF Model for the Study of Hawaiian Regional Climate. Mon Weather Rev 140:3259–3277. https://doi.org/10.1175/MWR-D-11-00260.1

Zhang Y, Dulière V, Mote PW, et al (2009) Evaluation of WRF and HadRM Mesoscale Climate Simulations over the U.S. Pacific Northwest*. J Clim 22:5511–5526. https://doi.org/10.1175/2009JCLI2875.1

Zhou C, Chen D, Wang K, et al (2020) Conditional Attribution of the 2018 Summer Extreme Heat over Northeast China: Roles of Urbanization, Global Warming, and Warming-Induced Circulation Changes. Bull Am Meteorol Soc 101:S71–S76. https://doi.org/10.1175/BAMS-D-19-0197.1

Ziese M, Schneider U, Meyer-Christoffer A, Schamm K, Vido J, Finger P, Bissolli P, Pietzsch S, Becker A. 2014. The GPCC drought index – a new, combined and gridded global drought index. Earth Syst. Sci. Data 6(2): 285– 295.

Zittis G, Hadjinicolaou P, Fnais M, Lelieveld J (2016) Projected changes in heat wave characteristics in the eastern Mediterranean and the Middle East. Reg Environ Change 16:1863–1876. https://doi.org/10.1007/s10113-014-0753-2

Zittis G, Hadjinicolaou P, Klangidou M, et al (2019) A multi-model, multi-scenario, and multi-domain analysis of regional climate projections for the Mediterranean. Reg Environ Change 19:2621–2635. https://doi.org/10.1007/S10113-019-01565-W/FIGURES/6

Zittis G, Hadjinicolaou P, Lelieveld J (2014) Comparison of WRF Model Physics Parameterizations over the MENA-CORDEX Domain. Am J Clim Change 03:490–511. https://doi.org/10.4236/ajcc.2014.35042